

An Analytical Model for the Colorimetric Characterization of Color CRTs

by

Ricardo J. Motta

A thesis submitted in partial fulfillment
of the requirements for the degree of
Master of Science Degree in the Center for
Imaging Science in the College of
Graphic Arts and Photography of the
Rochester Institute of Technology

April 1991

Signature of the Author _____
Ricardo J. Motta

Accepted by _____
Mehdi Vaez-Iravani _____
Coordinator, M.S. Degree Program

College of Graphic Arts and Photography
Rochester Institute of Technology
Rochester, New York

CERTIFICATE OF APPROVAL

M.S. DEGREE THESIS

The M.S. Degree Thesis of Ricardo J. Motta
has been examined and approved by the thesis
committee as satisfactory for the thesis requirement for the
Master of Science Degree

Dr. Roy S. Berns, Thesis Advisor

Ms. Paula Alessi

Mr. Leroy DeMarsh

Date

April 1991



R0006040867

THESIS RELEASE PERMISSION FORM

Rochester Institute of Technology
College of Graphic Arts and Photography

Title of Thesis : An Analytical Model for the Colorimetric Characterization of Color CRTs

I, Ricardo J. Motta , hereby grant permission to the Wallace Memorial Library of R. I. T. to reproduce my thesis in whole or in part. Any reproduction will not be for commercial use or profit.

Date :

April 1991

An Analytical Model for the Colorimetric Characterization of Color CRTs

by

Ricardo J. Motta

A thesis submitted in partial fulfillment
of the requirements for the degree of
Master of Science Degree in the Center for
Imaging Science in the College of
Graphic Arts and Photography of the
Rochester Institute of Technology

Abstract

To be a viable instrument for color appearance research, the color Cathode Ray Tube has to be very well calibrated and characterized. The purpose of this research was to develop the techniques and methods used to carry out such characterization, and also to evaluate to what degree of precision and accuracy can such a characterization be performed. A new model for predicting the CRT behavior is presented along with the experimental results that validate it.

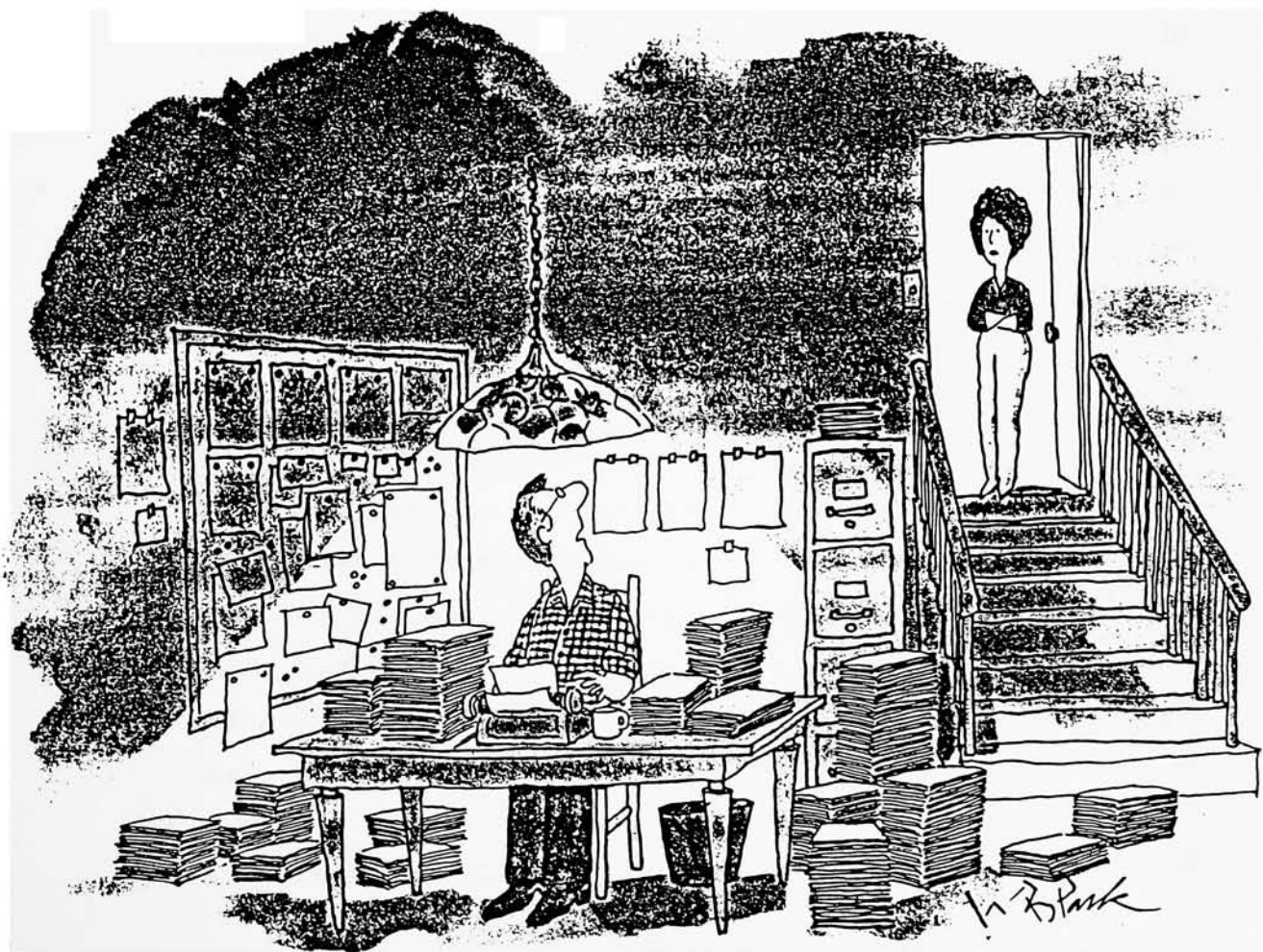
Acknowledgements

I wish to express my gratitude to a number of individuals and institutions that made this work possible. Dr. Roy Berns has guided me with a generous and firm hand. Through his enthusiasm and his teachings I have learned the fundamentals of color science and found myself engaged in this field. I also want to thank my board of advisors, Leroy DeMarsh and Paula Alessi, for their good advise and patience. Their suggestions and support were crucial for the success of this work. At the Center for Imaging Science I have found generous help and friendship. I especially wish to thank Tim Gallagher and Dick Norman for technical support, and Peter Engeldrum, Mark Fairchild, Mark Gorzynski and Dennis Daoust for the many long and enlightening conversations. I have especially fond memories of the late Dr. Ronald Francis. His guidance and example through my early years at CIS had a lasting impact on my character and intellectual horizons.

The Xerox Corporation has provided me with help in the form of a stipend and equipment. This crucial help is sincerely appreciated. Key contributions in form of equipment and good advise were also provided by the Eastman Kodak Co., Minolta Corp., the Photo-Research division of Kollmorgen Corp., and Tektronix Corp. I also want to gratefully acknowledge the Brazilian Government for a two year scholarship (CNPq.202070.84).

Finally, I wish to thank my parents. It was through their love and generosity that I found the means to grow.

Para Marcia,
com amor.



"Finish it? Why would I want to finish it?"

Contents

1	INTRODUCTION	1
1.1	Research Objectives	7
2	THEORETICAL MODEL	10
2.1	Introduction	10
2.1.1	A Simple Model	12
2.1.2	Failures of the Simple Model	12
2.2	Predicting the CRT <i>RGB</i> Tristimulus Values	14
2.2.1	Digital Image Data	16
2.2.2	Look-Up-Table	16
2.2.3	Video Generator	17
2.2.4	Video Amplifier	18
2.2.5	Electron Gun	18
2.2.6	Phosphors	19
2.2.7	Screen Radiance	20
2.2.8	Ambient Light	21
2.2.9	Total Radiance	22
2.2.10	CRT Tristimulus Values	22
2.2.11	Normalizing the Transfer Function Equation	23
2.3	A Model for CRT Calibration	25
2.3.1	Evaluating Gamma	26

2.3.2 Simplified Transfer Function Model	29
3 THE CALIBRATION OF A CRT	31
3.1 Characterization Method	31
3.1.1 Permanent Characteristics	32
CRT stability and latency time	32
Phosphor constancy	32
Gonio properties	33
Phosphor Chromaticities	33
3.1.2 Transitory characteristics	34
Setup	34
Viewing conditions	35
Screen uniformity	36
Load dependency	36
Transfer function and White point	36
3.2 Characterizing the Transfer Functions	37
3.2.1 Setup	37
3.2.2 Algorithm	38
3.2.3 Results	39
3.3 Estimating the Model Parameters	40
3.3.1 A Nonlinear Algorithm	40
3.3.2 Results	42
3.4 Verifying the Model	43
4 CONCLUSIONS	47
4.1 Recommendations	49
A DERIVATION	52
A.1 Computer Image Formation	52
A.1.1 Digital Images	52

A.1.2	The LUT	55
A.1.3	The Video Generator	58
A.1.3.1	The RS-170 Signal	58
A.1.3.2	The Frame Rate	60
A.1.3.3	Voltage Levels	64
A.1.3.4	The Effect of the Modulation Transfer Function	66
A.1.4	The Video Equation	70
A.2	The Cathode Ray Tube Display	71
A.2.1	The Video Amplifier	73
A.2.2	The Cathode Ray Tube	75
A.2.3	The Electron Gun	78
A.2.4	Phosphor Screen	83
A.2.5	The Energy Conversion	84
A.2.6	Phosphor Efficiency	86
A.2.7	Deviations from Linearity	88
A.2.8	Phosphor Decay and Dwell Time	90
A.2.9	Flicker	94
A.2.10	Composition of the Phosphors	96
A.2.11	Screen Radiance	98
A.2.12	Phosphor Constancy	102
A.2.13	<i>RGB</i> CRT Tristimulus Values	104
A.3	The CRT Color	105
A.3.1	CRT Color Mosaic	106
A.3.1.1	Hexagonal array, circular phosphor dots	110
A.3.1.2	Linear array, striped phosphors	111
A.3.1.3	Hexagonal array, rectangular phosphor dots	111
A.3.2	Additive Color Synthesis	112

B Experimental Techniques	122
B.1 Introduction	122
B.2 Apparatus	123
B.2.1 Location	123
B.2.2 Computers	124
B.2.3 Software	124
B.2.4 Video Generator	124
B.2.5 CRT's	124
B.2.6 Detectors	125
B.2.7 Measurement Instruments	126
B.3 Procedures	126
B.3.1 CRT Areas	126
B.3.2 Data Collection	127
B.3.2.1 PR703A/PC	127
B.3.2.2 TV-2160	128
B.3.3 Placement of the TV-2160 Probe	129
C Tristimulus Measurements	130
C.1 Introduction	130
C.1.1 Precision	130
C.1.2 Accuracy	131
C.2 Repeatability	132
C.3 Integration Time, Area and Noise	132
C.3.1 Detection of single emissions	135
C.3.2 Integration of several emissions	137
C.3.2.1 Integration of noise	137
C.3.2.2 Synchronization of measurement	138
C.4 Minolta Repeatability	140
C.4.1 Experimental	141

C.4.2 Results	142
C.5 CRT Repeatability	144
C.5.1 Introduction	144
C.5.2 Long term stability	145
C.5.3 Short term repeatability	146
C.5.3.1 Experimental	146
C.5.4 Results	147
D Minolta Linearity Correction	151
D.1 Photometric Scale	151
D.1.1 Inverse Square Law	153
D.1.2 Experimental	155
D.1.3 Results	156
E Load Dependency	161
E.1 Introduction	161
E.2 Additivity Failure	163
E.2.1 Measuring the additivity failure	164
E.2.1.1 Additivity of the phosphor screen	166
E.2.1.2 Measuring v_{G1}	167
E.2.2 Modeling the Additivity Failure	169
E.3 Accounting for the Deviations	171
F Goniocolorimetric Properties	174
F.1 Introduction	174
F.2 Experimental	177
F.3 Results	184
F.4 Conclusions	186
G Screen Uniformity	190

G.1	Introduction	190
G.2	Qualitative view	196
G.2.1	Experimental	196
G.2.2	Results	196
G.3	Quantitative view	201
G.3.1	Experimental	201
G.3.2	Estimating variance	202
G.3.3	Results	205
G.4	Discussion	208
H	Uniformity Measurements	212
I	Tables of Goniocolorimetric Properties	219
J	Program crtCAL.c	224
K	Program crtCALC.c	226

List of Figures

1.1	Typical 25 kV, 90° shadow mask color cathode ray tube.	2
1.2	Schematic of Robertson's "future visual colorimeter".	3
1.3	Diagram of CRT based color psychophysics laboratory at MCSL.	8
2.1	Transfer function of a computer driven CRT monitor.	11
2.2	The γ obtained by a simple model is not always the same over the entire range of radiances.	13
2.3	Block diagram of the CRT image formation process.	15
2.4	Estimating gamma for fixed gain a and different offsets b	27
2.5	Estimating gamma for fixed offsets b and different gains a	28
3.1	Histogram of CRT model ΔE_{ab}^* errors over entire CRT gamut.	44
3.2	Histogram of ΔE_{ab}^* color difference due to errors of 1 digital count.	45
3.3	ΔE_{ab}^* model errors for only the red and green channels	46
A.1	Block diagram of the Number 9 512x32 graphics board.	54
A.2	A LUT where 4 bits are mapped to 24 bits.	56
A.3	Different features of the RS-170 video signal.	59
A.4	Interlaced path of scanning electron beam.	61
A.5	Typical synchronization pulses.	62
A.6	Blanking and display periods of the RS-170 video signal.	65

A.7 Downward and upward paths of the electron beam when scanning and interlaced image.	66
A.8 Voltage values of a single line of the RS-170 signal.	67
A.9 Typical CRT circuit.	72
A.10 The video generator and the video amplifier.	74
A.11 Some of the different kinds of CRT available.	76
A.12 The CRT divided into five regions.	77
A.13 Electron guns commonly used in shadow mask tubes.	78
A.14 In-line gun with single main-focus lens.	79
A.15 Triode and tetrode structures.	80
A.16 The relationship between the voltage v_{G1} and the beam current.	81
A.17 List of selected phosphors.	85
A.18 Internal reflections on the phosphor screen.	89
A.19 Temporal profile of exciting electron pulse and phosphor decay.	90
A.20 Luminance buildup with repeated excitation.	91
A.21 Relation between the dwell time and phosphor output.	92
A.22 Chromaticities of different compositions of (ZnS,CdS):Ag phosphors.	97
A.23 Phosphors and activators listed in chronological order of commercial use.	98
A.24 Chronological evolution of phosphors chromaticities.	99
A.25 Data from the previous table plotted on the CIE 1931 chromaticity diagram.	100
A.26 SPD of Tektronix 690 SR red phosphor.	101
A.27 SPD of Tektronix 690 SR green phosphor.	102
A.28 SPD of Tektronix 690 SR blue phosphor.	103
A.29 Delta and precision-in-line arrangements.	107
A.30 In-line gun. Trinitron arrangement.	108
A.31 Four-stud leaf-spring arrangement to secure the shadow mask.	109
A.32 Bimetal element to compensate for mask expansion when heated.	110
B.1 25 different areas used on many measurements.	127

C.1	The same energy, but with different temporal distributions, will be collected by the three areas.	134
C.2	Temporal responses of two different kinds of detector.	136
C.3	Periodic signal with constant background noise.	138
C.4	Frequency spectrum of CRT signal and noise.	139
C.5	Same detection period will collect different number of spikes.	140
C.6	Luminous output of a CRT during the first hour of operation.	148
C.7	Luminous output of a CRT during the first six hours of operation.	149
D.1	Diagram illustrating the inverse square law.	154
D.2	φ , correction term for photometric linearity of the X tristimulus value.	157
D.3	φ , correction term for photometric linearity of the Y tristimulus value.	158
D.4	φ , correction term for photometric linearity of the Z tristimulus value.	159
D.5	All three correction terms plotted with a logarithmic horizontal axis.	160
E.1	Picture of set-up for testing the screen additivity.	166
E.2	Two channel load dependency is the square of the three channel case.	171
F.1	Goniophotometric curve of a black and white CRT.	175
F.2	Geometry of the faceplate and viewing.	176
F.3	Large bench to support the CRT and provide lateral movement.	178
F.4	A rotation stage was placed close to the bench and under the CRT faceplate.	179
F.5	A light-weight arm served as support for the detection lens and the optical fiber.	180
F.6	CRT gonio bench assembled.	181
F.7	Picture of apparatus in use.	182
F.8	Diagram of the diffuse light source.	183
F.9	The detected luminance of the near-Lambertian surface increase with angle.	184
F.10	Difference in collection angles at the edges of the detection cone.	185
F.11	Goniocolorimetric indicatrix of area 10	187

F.12 Goniocolorimetric indicatrix of area 13	188
F.13 Goniocolorimetric indicatrix of area 15	189
G.1 Distribution of color difference vectors.	191
G.2 Pin-cushion and barrel distortions.	192
G.3 Maximum screen output for the red, green and blue channels on 25 different positions on the CRT.	197
G.4 Gamma (γ) of the red, green and blue channels on 25 different positions on the CRT.	198
G.5 The system offset (K_1) of the red, green and blue channels on 25 different positions on the CRT.	199
G.6 Scattergram of the green channel intensity (Y_{max}) and estimated γ (gamma) for 29 repeated measurements of an area near the center of the CRT.	203
G.7 Scattergram of the green channel intensity (Y_{max}) and estimated system gain (K_1) for 29 repeated measurements of an area near the center of the CRT.. .	204
G.8 Scattergram of the system gain (K_1) and estimated γ (gamma) for 29 repeated measurements of an area near the center of the CRT.	204
G.9 Scattergram of the green channel intensity (Y_{max}) and estimated γ (gamma) for 32 measurements made on different areas of the CRT.	205
G.10 Scattergram of the green channel intensity (Y_{max}) and estimated system gain (K_1) for 32 measurements made on different areas of the CRT.	206
G.11 Scattergram of the system gain (K_1) and estimated γ (gamma) for 32 measurements made on different areas of the CRT.	206
G.12 Scattergrams of the green channel intensity (L_{max}) plotted against the system gain (K_1) and γ (gamma) with 95% confidence intervals	207
G.13 Definition of modulation. $M = \frac{a-b}{a+b}$	209
G.14 Low frequency modulation and the correction by counter-modulating d'	211

List of Tables

3.1	CIE 1931 chromaticity coordinates of CRT phosphors.	38
3.2	8 combinations of the three CRT primaries.	39
3.3	CRT transfer function measured over 25 steps of d	41
3.4	Estimated CRT model parameters, normal setup.	42
3.5	Estimated CRT model parameters, low brightness.	42
3.6	Estimated CRT model parameters, high brightness.	43
A.1	Timing of the RS-170 video signal generated by the Number 9 display buffer.	63
C.1	Uncertainty on the value of $L_{d'}$ determined by generating sequential series of d' on the Tektronix 650 HR.	143
C.2	Uncertainty on the value of $L_{d'}$ determined by generating random levels of d' on the Tektronix 650 HR.	150
E.1	Ratio between predicted and measured “white” luminance for the Barco CD33HR	165
H.1	Variation of the basic properties of the red channel of the Tektronix 650 HR over 25 regularly spaced areas accross the screen.	213
H.2	Variation of the basic properties of the red channel of the Tektronix 650 HR over 25 regularly spaced areas accross the screen.	214
H.3	Variation of the basic properties of the red channel of the Tektronix 650 HR over 25 regularly spaced areas accross the screen.	215

H.4	Colorimetric variations of a homogeneous white field displayed over 25 regularly spaced areas accross the screen of the Tektronix 650 HR.	216
H.5	29 repeated calibrations performed on the greeen channel in a fixed position on the screen of the Tektronix 650 HR CRT.	217
H.6	32 calibrations performed on the greeen channel for randomly chosen positions on the screen of the Tektronix 650 HR CRT.	218
I.1	Goniocolorimetric properties of lambertian diffuser	220
I.2	Goniocolorimetric properties at center of screen.	221
I.3	Goniocolorimetric properties at the left of screen.	222
I.4	Goniocolorimetric properties at 3 positions of screen.	223

List of Symbols

α, β	scalars
a, b	video amplifier gain and offset
(A_p/A_T)	fraction of screen irradiating the flux
C	any of R, G , and B
$d_{w,h}$	value of pixel at position w, h
d_r, d_g, d_b	red, green and blue values of pixel
d'	LUT entry corresponding to pixel value d
d'_{max}	$= 2^N - 1$, maximum pixel value where N is number of bits/pixel
$\eta_{e,\lambda}$	phosphor efficiency, nm^{-1}
η_v	phosphor luminous efficiency, Lumens/Watt nanometers
γ	an exponent
k_p	constant associated with the video path resistance
k_j	constant associated with the beam current
k_g	constant associated with the goniocolorimetric properties of the screen
k_f	constant associated with the screen radiant flux
$k_{\lambda,t}$	spectral constant associated with the CRT model
K	luminous efficacy, Lumens/Watt
K_m	$= 683$, maximum luminous efficacy, Lumens/Watt
K_1	- system gain
K_2	system offset

j	beam current, Amps
p	beam power, Watts
l	load dependency coefficient
L_λ	spectral radiance, Watts/m ² sr nm
L_v	luminance, [Lumens/m ² sr nm] or [cd/m ²]
M_λ	spectral radiant exitance, Watts/m ² nm
n	a scalar
Φ_λ	spectral radiant flux , Watts/nm
Φ_e	total radiant flux , Watts
Φ_v	luminous flux , Lumens
R, G, B	relative CRT tristimulus values
$\mathcal{R}, \mathcal{G}, \mathcal{B}$	CRT primaries
t	time
$(1 - t_b/t_f)$	- fraction of time the beam is blanked
T_m	shadow mask transmittance
T_λ	transmittance, nm ⁻¹
$T_{s,\lambda}$	screen transmittance, nm ⁻¹
v	voltage
v_s	voltage at the screen
v_0	“dead” potential of the screen
$(v_s - v_0)$	screen potential
v_d	video voltage
v_{G1}	first grid voltage
v_C	voltage cut-off
v_D	driving voltage
v_{min}	black level video voltage
v_{max}	white level video voltage
Δv	= $v_{max} - v_{min}$, amplitude of image portion of video signal
$< w, h >$	position of pixel
X, Y, Z	CIE tristimulus values

Illustration Credits

Several of the illustrations in this thesis have been copied from other sources. They are listed here in alphabetical order.

From Beson [8], figure 2.16. From Fink [71], figures 2.7, 2.10. From Harshbarguer [86], figure 2.8. From Hewlett-Packard Corp., figure 2.5. From Kamler [97], figures 2.22, 2.25. From Leher [116], figures 2.12, 2.15, 2.18, 2.20, 2.21. From Poole [146], figures 2.14, 2.23, 2.24. From Morrel [133], figures 1.1, 2.17, 2.26, 2.32, 2.33, 2.34, 2.35. From Moss [134], figure 2.19. From Number Nine Corp., figure 2.4. From Robertson [156], figure 1.2.

Chapter 1

INTRODUCTION

Cathode Ray Tubes (CRTs, figure 1.1) have become the dominating imaging media in our world. They are able to produce in real time a color image at very little expense and with reasonably good quality.

Radars, televisions and oscilloscopes are some of the devices that first profited from the use of CRTs for information display. Lately, the ability to drive a CRT from computer generated signals has opened new possibilities for image manipulation and display. One of the many areas that has benefited is vision and color appearance research, for which the CRT can be used as a visual colorimeter. The flexibility and speed typical of the interactions between man and computer have brought within the reach of most experimenters what Robertson [158] has envisioned as the *future visual colorimeter* (figure 1.2), a system which should allow the experimenter free choice of how the reactions of the subject of the experiment are translated into changes of appearance of stimuli.

The basic requirement for a machine to generate a video signal (the signal that drives the raster scan CRT) is the ability to modulate a voltage very quickly (a more detailed discussion of the video signal follows). The required speed of modulation increases as we increase the number of scan lines or the length of the lines. Higher speeds are also needed to increase the modulation transfer function (MTF) at high frequencies (i.e., to be able to have high contrast patterns with short spatial separation) or to generate a color image.

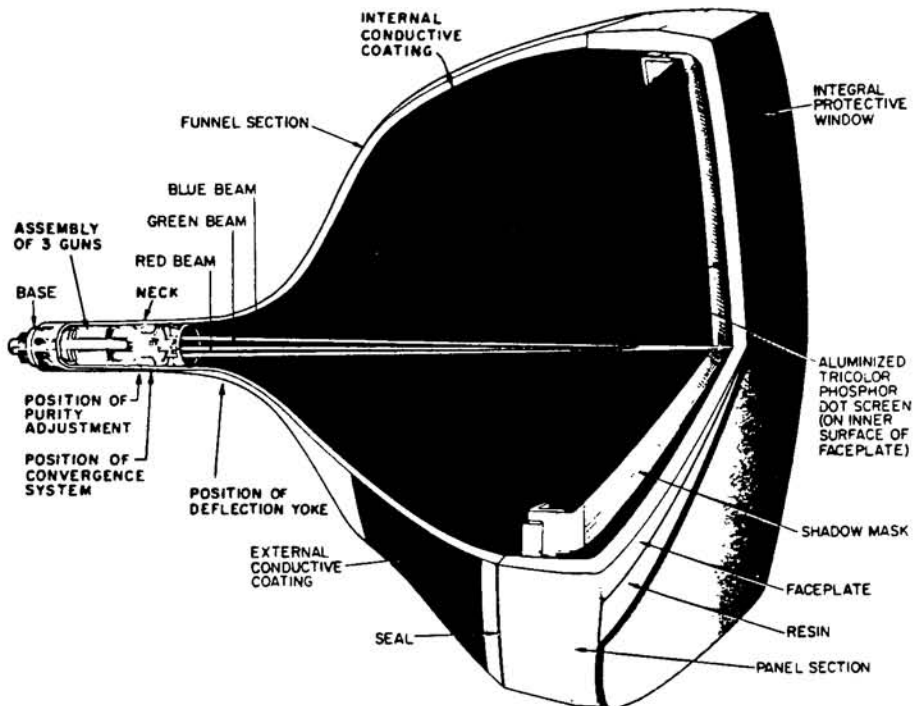


Figure 1.1: Typical 25 kV, 90° shadow mask color cathode ray tube.

Initially, the small bandwidth of the computing machinery available, and the high cost of components were the limiting factors. This has dramatically changed to a situation where even small microcomputers are able to generate high quality video signals. For a while, the limitation has switched to the CRT. Since early 1987 color CRTs have been available with bandwidths of more than two hundred megahertz (MHz), switching the limitations back to the signal generating electronics.

The problem that faces the color scientist who attempts to make a viable colorimeter out of a CRT system is that he or she will require levels of performance which are beyond that required for most applications, e.g., television, computer graphics and information display.

Television engineers were the first to make extensive use of CRTs for research in vision, though their research was aimed primarily at solving technical problems related to television

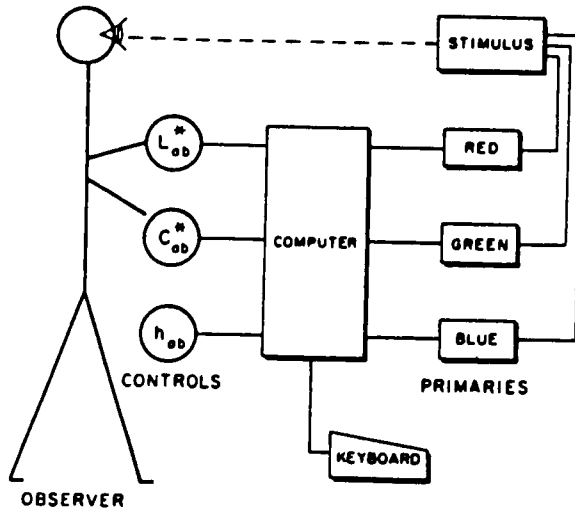


Figure 1.2: Schematic of Robertson’s “future visual colorimeter”.

itself. Part of the problem is that television engineers had to focus on the preferred, and not colorimetric, color reproduction of scenes, mostly because of constraints that originate from the typical viewing situation [86, 90, 91, 93, 117, 123]. Such constraints are similar to those described by Breneman and Bartleson for photography [5, 6, 22], and by DeMarsh for color television [62, 63], but will in reality be compounded by conditions such as flicker [81, 193], the actual set up of the CRT monitor [24, 167, 176], and the variability of the chromaticities of the phosphors used [84, 152]. All of these contribute to the deviation from colorimetric reproduction. Also, in television, the CRT is only one end of a long and complex chain of processes. The major concern of the TV engineer has been the coding of the color signals and their broadcast (see for instance [8, 21, 65, 165, 182]), which must conform to the standards developed by the NTSC in 1953 [142]. Although the adoption of a standard for the HDTV (High-Definition Television) still seems to be a remote reality, it holds the promise of incorporating significant improvements due to our better understanding of the psychophysics of the visual system [35, 166, 172] and the availability of improved color

spaces and associated formulae [37, 171].

From the perspective of computer graphics, the CRT is usually viewed as a work space for viewing images, with no need, until recently, to have its appearance correlated with some other media [184, 185]. The emphasis is on speed, resolution and ergonomics, with usually little concern paid to the colorimetric properties of the CRT per se. The research integrating color science and appearance to computer graphics [82, 131, 132] has been aimed mostly at the modeling of gonio-colorimetric properties of surfaces for the generation of synthetic realities by means of ray tracing techniques [74] and the determination of suitable hardware oriented color spaces [96, 130, 178]. Unfortunately, the characteristics of the image when displayed on the CRT are usually overlooked. There are no standards for the display of CRT imagery, and the evaluation of digital image processing algorithms is often done haphazardly, with the user playing with the “contrast” and “brightness” controls of the CRT until the results please him. One of the largest contributions towards improving the computer scientist’s understanding of CRT colorimetry has come from William Cowan of the NRC, whose contributions on the calibration of CRTs have had a large impact [54, 56].

Display engineers using computer graphics to generate avionics, medical and other information displays have created an entire new set of requirements and expectations for the CRT performance, and encountered difficulties that include the visual fatigue caused by CRT viewing [9, 42, 59, 119, 113], the determination of the actual brightness of the display colors [111, 112, 140, 151, 189], heterochromatic brightness matches [31, 39, 53, 160, 179], and determining sets of the most distinguishable colors when viewed under different conditions [36, 50, 51, 52, 175, 197]. These problems are all basic to colorimetry and date back to the establishment of the CIE (Commission International de l’Eclairage) when there was great concern about the colors of traffic lights and other light signals [41]. For instance, color coded information displays used in avionics have to use a very distinguishable set of colors within constraints that vary from cockpit to cockpit [198]; e.g., military cockpits should not have any infrared or near-infrared emitters to avoid detection [133], nor should blues be used for small letters over a black background because of small field tritanopia

[196] and the strain in the eyes caused by the need to accomodate to a large depth of focus [139, 161].

Despite the unsolved problems, computer generated CRT imagery is an extremely attractive way of generating stimuli for performing color appearance research. This kind of stimulus generator can be extremely flexible and modulated interactively. The existence of a computer in the cycle makes it possible to collect the data, control and monitor the signal, and interface with the user. All of this accomplished with simplified and somewhat modular equipment. According to Vingrys [195, 110] and King-Smith, there are seven degrees of freedom for the circular test spot used on their visual threshold experiments that can be produced in a color CRT (using their terminology) amplitude, red-green angle, blue-yellow angle, duration, diameter, eccentricity and meridian. Obviously, these are not all the degrees of freedom for the CRT imagery, but this illustrates the flexibility of such a system.

Such flexibility has been well exploited by many researchers. Schade [169] has used a television based system to build an analog of the eye for simulation purposes. Mackworth and Mackworth[124] have used a CRT based system to study eye fixation patterns for different kinds of scenes. Granger and Heurtley [78, 77] have used the CRT to create sinusoidal gratings for the determination of the visual chromaticity transfer function. Harmon [85] used a CRT combined with image processing hardware to investigate the relation between information content of images and their recognition. Snyder [179] used a CRT to investigate heterochromatic brightness matches against achromatic reference stimuli. Sekuler and Levison [173] reported several experiments on the perception of moving targets that were performed on CRTs. Brou, *et al* [26] reported some interesting but naive experiments performed on color CRTs about the importance of edges for color perception. Arend and Reeves [2] investigated color constancy mechanisms by generating “Mondrian” displays. Fuchida, *et al* [76] investigated the effect of the chromaticity of surrounds when matching large color differences. McCormick, *et al* [128] presented an improved method for presenting red-green gratings on oscilloscope tubes. Anstis, *et al* [1] have devised a clever way of

screening newborns for color vision defects. Held [58] has used CRTs for testing infants on several aspects of their visual development at MIT's Infant Vision Lab. King-Smith [109, 195, 40] and coworkers have published several papers on the investigation of visual thresholds using a CRT to generate the already mentioned luminous spots. Kelly [105] has used CRTs on his investigations of contrast and flicker sensitivity.

In the proceedings of a conference on Colour Vision, which took place in Cambridge in 1982 [134], there were several references to work performed with the aid of CRTs. Rodieck ([134], p.131) used a color CRT to perform color exchange experiments to isolate the rod and cone contributions of cat ganglion cells. Tansley, *et al* ([134], p.445) used a computer controlled CRT to study chromatic and achromatic border perception by creating squares with different spacings and controlling their intensity through a keyboard. Switkes and De Valois ([134], p.465) used the CRT to create red and green sinusoidal gratings to study the interaction between luminance and chromaticity in spatial vision. Van Esch, *et al* ([134], p.425) used a color CRT with a wave function generator to create temporal and spatial sine wave patterns in the CRT and study the sensitivity to spatiotemporal color contrast. McCann and Houston ([134], p.535) studied color constancy by displaying complex scenes on a color CRT and asking the observer to match a test patch (also displayed on the CRT). De Weert and Szada ([134], p.553) investigated why stereopsis is absent in isoluminant random dot displays if it can be achieved in isoluminant displays containing a strong figure ground relationship. Derrington, *et al* ([134], p.245) used a color CRT to display sinusoidal gratings and studied the chromatic response of neurons in the macaque lateral geniculate nucleus. As we see the CRT has found use in many kinds of visual research. Boynton [18] predicts that by the next decade most of color vision research will be carried out with raster displays.

One area where CRTs have the greatest potential is the research of color constancy and chromatic adaptation mechanisms. With a CRT, one would be able to display a complex scene and insert a color patch for assessment by an observer with respect to its appearance. This kind of work would be similar to the one carried out by Breneman [23], with the added

advantage of great flexibility. A CRT based system combined with a controlled viewing environment would be suitable for investigating the passage from related color to unrelated color, and to what extent each is affected, or not affected, by the state of adaptation. Also, within the limited gamut of colors offered by the CRT, color discrimination ellipsoids could be evaluated under different states of chromatic adaptation for the development of better color difference formulae [157]. On the more practical side of colorimetry, computer graphics with image processing and appearance data on materials can be combined to generate synthetic realities where different illuminating sources could be tested for visual assessment of their color rendering properties; commercial color matching systems could display on CRTs the measured color differences, permitting visual evaluation of the quality of the match without physically producing any samples. Finally, color proofing systems that are used by the graphic arts industry could use the CRT as a real soft-copy display, and not just as a rough approximation [25, 144, 190, 126, 125, 106, 153].

Figure 1.3 illustrates diagrammatically the system that has been implemented at the Munsell Color Science Laboratory (MCSL) in the course of the research reported here. The different parts of this system will be described throughout the text.

1.1 Research Objectives

Underlying the above discussion and suggested work is the assumption that a CRT can be made to generate whatever stimulus is desired. This, unfortunately, is not such a trivial task. Therefore, the characterization of a color CRT system and the development of a general model which will enable the accurate control of the CRT output are the purposes of this research.

The problem of calibrating and characterizing a CRT system can be divided into two independent parts :

- Control Characterization of the relation between the CRT output and factors affecting it.

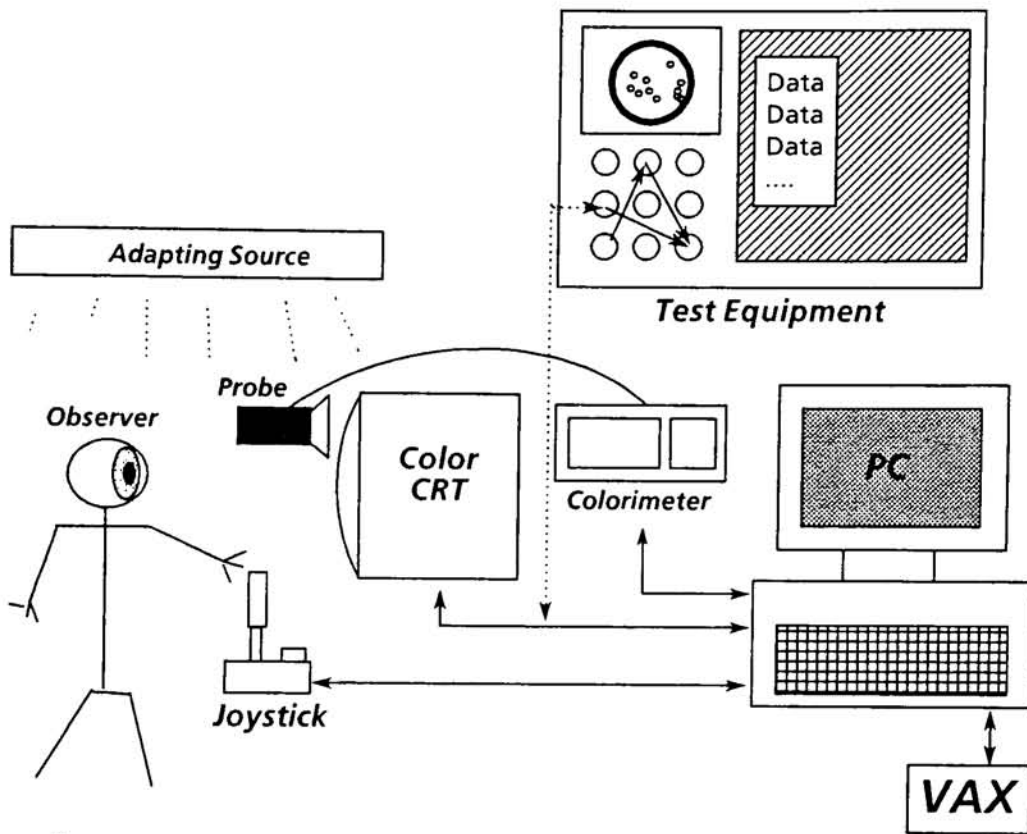


Figure 1.3: Diagram of CRT based color psychophysics laboratory at MCSL.

- Appearance Characterization of the appearance of the CRT output.

The research described herein is concentrated in the control aspect of the CRT calibration. Colorimetric parameters will be only discussed to the extent that they are used as a conventional way of describing the CRT output, and not its appearance.

In the process of calibrating and measuring the CRT output, the following problems have to be dealt with:

- Methodology
 - Acquisition and Specification of Apparatus
 - Procedures and Management of Data

- Software Writing and Acquisition
- Experimental Setups
- Radiometry
 - Calibration of Detectors
 - Integration Time and SNR
 - Detector Coverage and SNR
- Control
 - Long and Short Term Stability
 - Repeatability
 - Screen Uniformity
 - Goniophotometric Properties
 - Load Dependency

Some of the spatial and temporal parameters that affect appearance and were not investigated are :

- Convergence
- Resolution
- Flicker

The following discussion will introduce an extended theoretical model so that the rationale of the above division can be put in perspective. The detailed derivation of the theoretical model is available in appendix A along with the reports on some of the experiments performed.

Chapter 2

THEORETICAL MODEL

2.1 Introduction

A parametric solution to the problem of predicting the state of the CRT output from a limited set of system parameters would be very useful, not only for its intrinsic elegance, but also because it should be more efficient computationally. Parametric forms can be added, differentiated, and in general, subject to all operations of mathematical analysis.

The CRT and electron tube literature [72, 122, 135, 136, 146, 147, 148, 174, 180, 186] has provided many parametric forms applicable to diverse color image formation problems such as CRT to film transfer [38, 162], television [11, 12, 92, 121, 143, 145, 183, 199] and computer graphics [64, 74, 129, 184]. Of special importance is the CRT transfer function, which accounts for the non-linearities found in this class of devices. Figure 2.1 illustrates a transfer function typical of a computer driven CRT monitor. The transfer function describes the relationship between the data in the computer, specified in digital counts, and the luminous output of the CRT.

To describe it, some authors, such as Foley [74], Cowan [56], and Hartmann [88], have presented models that attempt to predict the display intensities directly from the memory digital counts or video voltages with no other parameters included. These and many other published articles have used the CRT parametric forms in ways that violate some of the basic

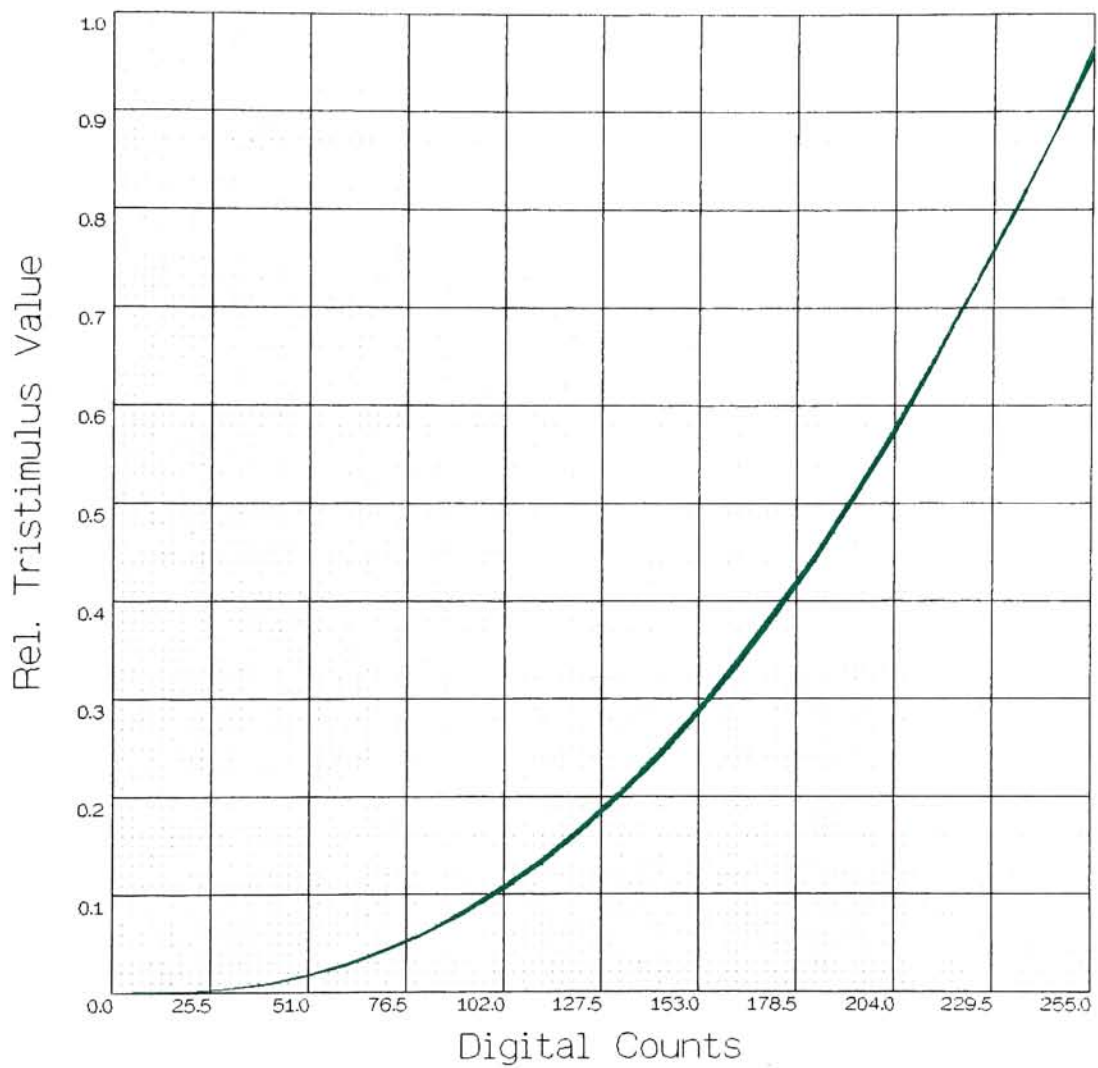


Figure 2.1: Transfer function of a computer driven CRT monitor.

assumptions originally built into those forms. To contrast with a more rigorous approach to be presented later, a simple parametric form of the CRT transfer function is presented next.

2.1.1 A Simple Model

Let v be a computer generated video voltage that drives the CRT monitor, and L the resulting displayed luminance, both related by the function $L(v)$. We define the normalized values of v and L as

$$v_n = \frac{v}{v_{max}} \quad (2.1)$$

and

$$L_n = \frac{L}{L_{max}} \quad (2.2)$$

The popular parametric form of the CRT transfer function is expressed as

$$L_n = v_n^\gamma \quad (2.3)$$

where γ is a scalar usually called gamma and the subscript n indicates that the values are normalized. Under these conditions, γ could be determined in a straight forward way by

$$\gamma = \frac{\ln(L_n)}{\ln(v_n)} \quad (2.4)$$

Thus, given the knowledge of γ , of L_{max} (which only requires one measurement) and equations 2.2 and 2.3, the actual value of L is

$$L(v_n) = L_{max} v_n^\gamma \quad (2.5)$$

2.1.2 Failures of the Simple Model

We will return to these forms later and discuss them more carefully. For the time being, it is important to notice that this model will not take into account a number of variables that are usually found in any CRT monitor, and that determine the final transfer function of the CRT system. The effect of parameters such as the “contrast” and “brightness” (gain

and offset) settings on the CRT monitor, room illumination and screen uniformity are not easily predictable at the signal generation stage, but have a very definitive effect on the final image appearance. This has been recognized by some authors. Catmull [38] and Brainard [20] for instance, suggested that look-up-tables built from actual intensity data might be a better descriptor of screen intensities.

When γ is calculated according to equation 2.5, we usually obtain a result such as displayed on figure 2.2. Depending on the CRT set-up the values might deviate over the lower or upper part of the range. The direction of the deviation also depends on the set-up.

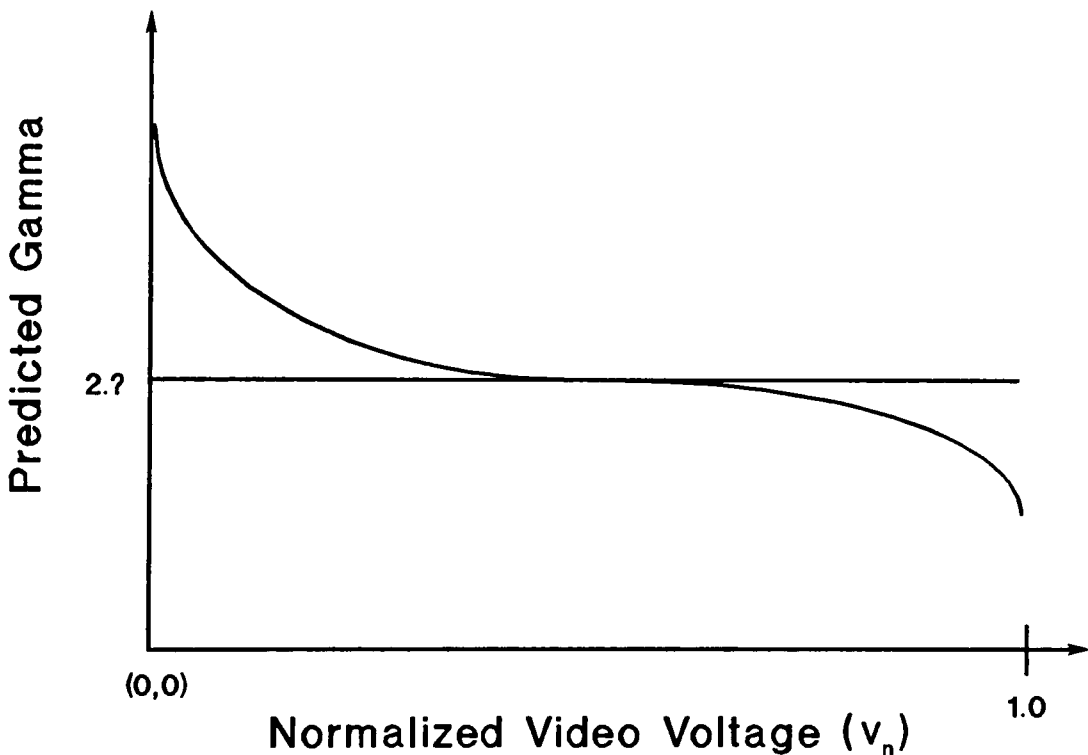


Figure 2.2: The γ obtained by a simple model is not always the same over the entire range of radiances.

With respect to such deviations, Cowan [56] stated that “the .. [gamma] .. ranges between 2.75 at the highest values of gun voltage and 4.0 at the lowest values. This range is well above the often-quoted value of 2.5”. As a way around this he suggested a two

parameter fit to equation 2.4 which can be expressed as

$$\ln(L(v_n)) = \alpha \ln(v_n) + \beta \ln(v_n)^2 \quad (2.6)$$

where α and β are two constants. It has also been suggested [88, 56] that the problem should be avoided by not attempting to calibrate the entire CRT gamut at once.

In the next section, we will present a more rigorous model of the CRT image formation process, with emphasis on modeling the transfer function of the CRT. The discussion is based on the specific system available at the Munsell Color Science Laboratory (MCSL) at RIT. Figure 2.3 is a block diagram of the CRT color image formation process and corresponds roughly to the topical division of the next sections. The derivation will migrate from the computer to the eye, following the same path as the image. The boundary between the CRT and the eye also indicates the scope of this thesis. This derivation is described in detail in appendix A.

2.2 Predicting the CRT *RGB* Tristimulus Values

Suppose one wants to calibrate a certain area of the CRT, i.e. predict what will be the chromaticity and luminance of the pixel at position $< w, h >$ on the screen. What follows is a list of the steps and assumptions leading to a model for the process. The discussion in appendix A contains the principal facts and formulae that have to be taken into account when predicting the CRT color output. The derivation is presented here in the form of a summary, with directions to the sections in the appendix where the relevant references and detailed discussions are located.

Notice that the assumptions made here are not necessarily truisms, they just reflect the variables that were built into the model and the operation of a quasi-ideal CRT color imaging system. The actual implementation of this model may differ in many ways from the one exemplified here, mostly because, in a real system, there are deviations that have to be accommodated. In later sections, the deviations from the predicted behavior will be discussed and the consequences of such deviations analyzed.

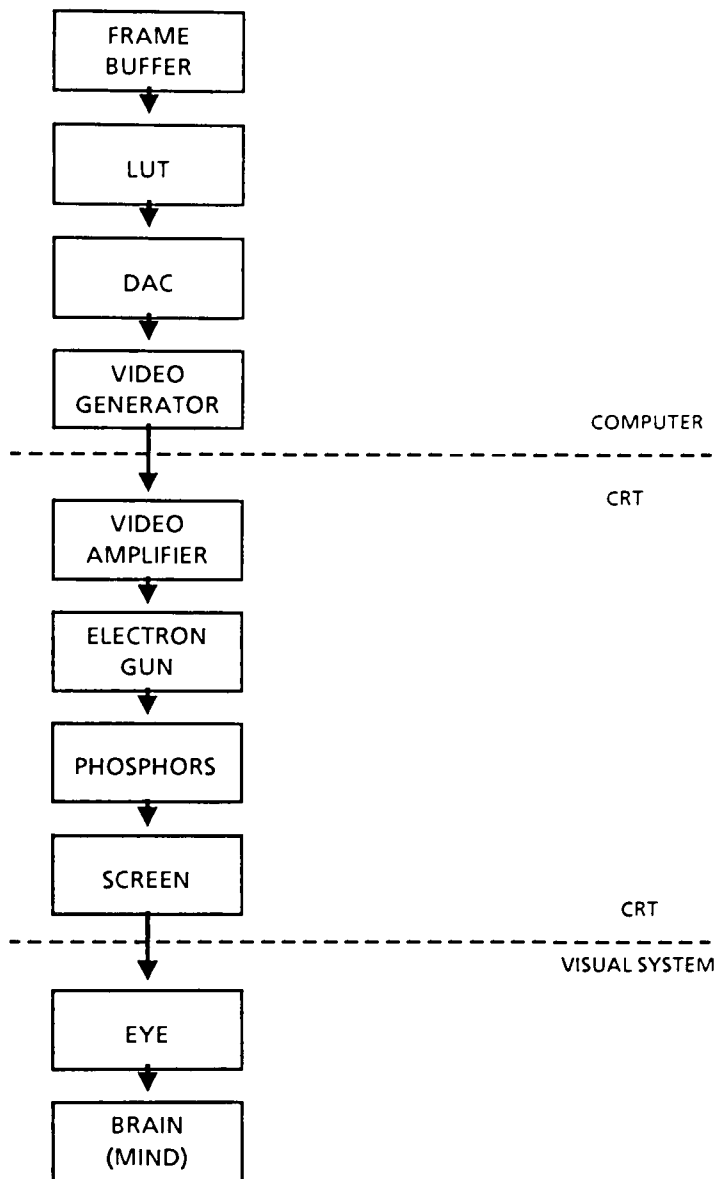


Figure 2.3: Block diagram of the CRT image formation process.

2.2.1 Digital Image Data

In a digital image, we represent the value of the pixel at position $\langle w, h \rangle$ by:

$$\mathbf{d}_{w,h} = \begin{bmatrix} d_r \\ d_g \\ d_b \end{bmatrix} \quad (2.7)$$

See section A.1.1

Assumptions:

1. The frame buffer has same amount of memory allocated for the red, green and blue memory planes.¹
2. The range of values of $d_{w,h}$ will be

$$0 \rightarrow (2^{N_{mem}} - 1) \quad (2.8)$$

where N_{mem} is the number of bits per plane in the image memory.

2.2.2 Look-Up-Table

The LUT entry for value d :

$$d' = LUT(d) \quad (2.9)$$

See section A.1.2

Assumptions:

1. Entries in the LUT can be manipulated individually.
2. The operation is independent of position.

¹To avoid the unnecessary multiplication of subscripts the remainder of this derivation is presented without distinguishing the red, green and blue signal paths. The reader should assume that unless specifically indicated, all constants and variables have three different (i.e. red, green and blue) versions.

3. The range of values of d' will be

$$0 \rightarrow d'_{max}, \quad (2.10)$$

where

$$d'_{max} = 2^{N_{LUT}} - 1, \quad (2.11)$$

and N_{LUT} is the number of bits to which the LUT can map.

2.2.3 Video Generator

The DAC and the Video Generator will transform the digital value into a video voltage v_d :

$$v_d = \Delta v \left[\frac{d'}{d'_{max}} \right] + v_{min} \quad (2.12)$$

where

$$\Delta v = v_{max} - v_{min} \quad (2.13)$$

See sections A.1.3 and A.1.4

Assumptions:

1. The range of voltages is

v_{max} = reference white level, 100 IRE,

v_{min} = reference black level, 7.5 IRE.

2. The voltages generated by the DAC will be quantized and linearly related to d' .
3. The value of v_d is independent of the contents of the image, the position within the image and the value of the pixels preceding and following it.
4. The video signal follows the RS-170 format.
5. The red, green and blue video signals have the same gain (e.g. 92.5 IRE) and offset (e.g. 7.5 IRE).

2.2.4 Video Amplifier

The video amplifier will transform the positive valued v_d into a negative valued v_{G1} which will drive the first grid (G1) on the electron gun.

$$v_{G1} = a k_p v_d + b \quad (2.14)$$

where

a - amplifier gain,

b - amplifier offset,

k_p - a constant accounting for the voltage drop due to the resistance of the transmission path (subscript p stands for path).

See section A.2.1

Assumptions:

1. Individual control of a and b are available for each color channel, as well as overall control through the display “contrast and brightness” controls.
2. The value of a and b for each channel is independent of the values on the other channels, image content and position on the screen.

Note that a , b and k_p are unknown.

2.2.5 Electron Gun

v_{G1} will modulate the first grid in the electron gun and will result in an electron beam with current j .

$$j = \begin{cases} 0, & \text{if } v_{G1} - v_C \leq 0 \\ k_j v_D^\gamma, & \text{if } v_{G1} - v_C > 0 \end{cases} \quad (2.15)$$

where

v_C - the cutoff voltage,

γ gamma, an exponent.

k_j - a constant, where j stands for current, accounting for various characteristics of the electron gun.

See sections A.2.2 and A.2.3

Assumptions :

1. The current on each gun is independent of the current on the other guns, the contents of the image and the position within the image.
2. The current on each gun is independent of temporal factors (such as how long the gun has been working).

Note that the constants v_C , γ , and k_j are unknown and possibly different for each of the three guns.

2.2.6 Phosphors

The electron flux j will hit the screen at a certain rate, and the phosphors on the screen will emit a radiant flux with a certain spectral composition

$$\Phi_\lambda = j (v_s - v_0) T_m T_{s,\lambda} \eta_{e,\lambda} \left(\frac{A_p}{A_T} \right) \left(1 - \frac{t_b}{t_f} \right) \quad (2.16)$$

where

Φ_λ radiant flux , Watts,

j beam current, Amps,

T_m shadow mask transmittance,

$T_{s,\lambda}$ screen transmittance,

$\eta_{e,\lambda}$ phosphor efficiency,

$(v_s - v_0)$ voltage from cathode to screen, Volts,

(A_p/A_T) fraction of screen irradiating the flux,

$(1 - t_b/t_f)$ fraction of time the beam is blanked.

See sections A.2.4 through A.2.10

Assumptions:

1. The voltage across which the beam is accelerated is the same for all points on the screen.
2. The shadow mask transmittance is constant across the screen.
3. The glass panel has the same transmittance across the screen.
4. All phosphor dots of a certain type (i.e. red, green or blue) have the same efficiency and are the same size.
5. For a given v_{G1} , the beam current is the same for all areas of the screen.
6. The relative spectral distribution of the phosphor emissions is not affected by the level of excitation.
7. There is no effect from the thermal emission of the phosphor at the working temperature.

2.2.7 Screen Radiance

The spectral radiant exitance M_λ , resulting from the propagation of the radiant flux Φ_λ from an screen area A_p will result in a screen radiance L_λ .

$$L_\lambda = M_\lambda / \pi \text{ (watts/m}^2\text{sr nm)} \quad (2.17)$$

where

$$M_\lambda = \Phi_\lambda / A_p \text{ (watts/m}^2\text{nm)} \quad (2.18)$$

See section A.2.11

Assumptions:

1. The phosphor screen emission is Lambertian (i.e. its radiance is the same for all viewing angles).
2. The screen is homogeneous, so that M_λ is independent of the position and the size of A_p .
3. The spectral radiant exitance is the result of the summation of the radiant exitance of the three kinds of phosphors,
4. There are no interreflections from other locations on the screen.

$$M_{\lambda,\text{total}} = M_{\lambda,\text{red}} + M_{\lambda,\text{green}} + M_{\lambda,\text{blue}} \quad (2.19)$$

5. All three kinds of phosphors are equally represented on the area A_p .

2.2.8 Ambient Light

$L_{\lambda,a}$ is the spectral radiance resulting from the ambient light reflecting from the CRT faceplate (commonly referred to as flare).

$$L_{\lambda,a} = \left(T_{\lambda,g}^2 R_{\lambda,p} L'_{\lambda,a} \right) + 0.04 k L'_{\lambda,a} \quad (2.20)$$

where

$L'_{\lambda,a}$ total diffuse radiance reaching the screen,

$T_{\lambda,g}^2$ - the square of the transmittance of the glass panel,

$R_{\lambda,p}$ diffuse reflectance of the phosphor layer,

0.04 Fresnel reflectance of glass first surface,

k a constant accounting for the glass anti-reflective treatment.

Assumptions:

1. The ambient radiance is diffuse.

2. The phosphor screen is a Lambertian reflector.
3. The first surface of the glass is a specular reflector.
4. The screen is being observed at 0 degrees to the normal.
5. The refractive index of the glass is 1.5.

2.2.9 Total Radiance

The spectral radiance reaching the eye will be the combination of the radiance due to the phosphor emission, L_λ , added to that due to the screen reflectances, $L_{\lambda,a}$.

$$L_{\lambda,total} = L_\lambda + L_{\lambda,a} \quad (2.21)$$

Assumptions :

1. The radiance of different phosphors is visually integrated, and the individual elements of the screen are not visible.
2. The reflected ambient radiance can be measured separately from the emitted radiance.

2.2.10 CRT Tristimulus Values

The relative tristimulus values resulting from the CRT emission can be calculated from relative amount of total radiance from each phosphor.

$$\begin{aligned} R &= \frac{\int_0^\infty L_{\lambda,r} d\lambda}{\int_0^\infty L_{\lambda,r,max} d\lambda} \\ G &= \frac{\int_0^\infty L_{\lambda,g} d\lambda}{\int_0^\infty L_{\lambda,g,max} d\lambda} \\ B &= \frac{\int_0^\infty L_{\lambda,b} d\lambda}{\int_0^\infty L_{\lambda,b,max} d\lambda} \end{aligned}$$

See sections A.2.12 and A.2.13

2.2.11 Normalizing the Transfer Function Equation

As we show next, the normalization by the highest phosphor radiance has some interesting and powerful consequences. First, we can combine the equations in the previous sections into a single equation for the CRT spectral radiance in the dark (i.e no ambient light)

$$L_\lambda = k_j \left(a k_p \left(\Delta v \left[\frac{d'}{d'_{max}} \right] + v_{min} \right) + b - v_C \right)^\gamma \left(\frac{(v_s - v_0) T_m T_{s,\lambda} \eta_{e,\lambda}}{\pi A_T} \right) \left(1 - \frac{t_b}{t_f} \right) \quad (2.22)$$

Next, we define the new constant $k_{\lambda,t}$ as

$$k_{\lambda,t} = k_j \left(\frac{(v_s - v_0) T_m T_{s,\lambda} \eta_{e,\lambda}}{\pi A_T} \right) \left(1 - \frac{t_b}{t_f} \right) \quad (2.23)$$

which accounts for all terms in the spectral radiance expression that are constant or wavelength dependent. The subscript t of $k_{\lambda,t}$ stands for total. We now have a compact notation for the radiance:

$$L_\lambda = k_{\lambda,t} j \quad (2.24)$$

where j is the beam current. Re-expanding this expression we have

$$L_\lambda = k_{\lambda,t} (a (k_p v_d) + b - v_C)^\gamma \quad (2.25)$$

further, we can express the radiance in terms of the image digital counts

$$L_\lambda = k_{\lambda,t} \left(a \left(k_p \left(\Delta v \frac{d'}{d'_{max}} + v_{min} \right) \right) + b - v_C \right)^\gamma \quad (2.26)$$

where $d' = 0 \rightarrow d'_{max}$ is an arbitrary value. The two values to be normalized to obtain the tristimulus value are

$$L_\lambda = k_{\lambda,t} \left(a k_p \Delta v \frac{d'}{d'_{max}} + a k_p v_{min} + b - v_C \right)^\gamma \quad (2.27)$$

and the maximum radiant output

$$L_{\lambda,max} = k_{\lambda,t} \left(a k_p \Delta v \frac{d'_{max}}{d'_{max}} + a k_p v_{max} + b - v_C \right)^\gamma \quad (2.28)$$

which reduces to

$$L_{\lambda,max} = k_{\lambda,t} (a k_p \Delta v + a k_p v_{max} + b - v_C)^\gamma \quad (2.29)$$

The expression for the CRT tristimulus values will be

$$C = \frac{\int_0^\infty L_\lambda d\lambda}{\int_0^\infty L_{\lambda,\max} d\lambda} = \left(\frac{ak_p \Delta v \frac{d'}{d'_{\max}} + ak_p v_{\min} + b - v_C}{ak_p \Delta v + ak_p v_{\max} + b - v_C} \right)^\gamma \frac{\int_0^\infty k_{\lambda,t} d\lambda}{\int_0^\infty k_{\lambda,t} d\lambda} \quad (2.30)$$

or simply

$$C = \left(\frac{ak_p \Delta v \frac{d'}{d'_{\max}} + ak_p v_{\min} + b - v_C}{ak_p \Delta v + ak_p v_{\max} + b - v_C} \right)^\gamma \quad (2.31)$$

where C is any of the CRT *RGB* tristimulus values.

We can now proceed to show that expression 2.3, the simplified transfer function model presented before, is a special case of the expression for C shown above. This special case is realized when, for any given gain a , the offset b of the CRT is adjusted so that the image portions corresponding to the black video level (i.e. $d' = 0$) are on the threshold of emitting radiation. Under this condition the amplified black video level and the video amplifier offset will cancel each other, which is satisfied by the condition

$$b = v_C - ak_p v_{\min} \quad (2.32)$$

Performing the above substitution we eliminate the terms related to the signal offset

$$C = \frac{L_v}{L_{v,\max}} = \left(\frac{ak_p \Delta v \frac{d'}{d'_{\max}}}{ak_p \Delta v} \right)^\gamma \quad (2.33)$$

where, to simplify the derivation, we have measured the screen output in terms of luminance, defined as [43]

$$L_v = 683 \int_{360}^{830} V_\lambda L_\lambda d\lambda \quad (2.34)$$

where V_λ is the CIE 1924 photopic observer².

Doing the obvious eliminations we obtain

$$\frac{L_v}{L_{v,\max}} = \left(\frac{d'}{d'_{\max}} \right)^\gamma \quad (2.35)$$

or

$$L_v = L_{v,\max} \left(\frac{d'}{d'_{\max}} \right)^\gamma \quad (2.36)$$

²Notice that since we assume that phosphor constancy holds, this derivation would be equally valid if we had used L_λ instead of L_v .

which is a very useful result. Notice, again, that this is equivalent to the expression 2.3 presented before.

2.3 A Model for CRT Calibration

The formulae and assumptions derived in the previous section can serve as the basis for CRT calibration. The purpose of such a calibration is to be able to predict the state of the CRT emission for any pixel value. Thus, a calibration consists of two parts :

1. The characterization of the CRT performance and the factors affecting it.
2. The development of an algorithm or a model which will permit a larger number of states to be predicted from the characterization of a smaller number of states.

The most ineffective way of performing such a calibration would be to measure all the possible states of the CRT emission and store them in a table which can later be used for the prediction of the CRT state. The drawback of this approach should be obvious. Given that our system can assume 16.8 million different states, it would take about 194 days, making one measurement every second, to characterize the CRT. Even if such a feat would be possible, after 194 days of continuous operation the CRT phosphors would have aged considerably. Even worse, there would be no warranty that the values measured would still be characteristic of that system if conditions such as room illumination, gain and offset were changed. Clearly, part of the calibration effort is the determination of the least amount of samples that can be used for a successful characterization.

Another very important factor for the success of a calibration is its robustness to deviations from the characterization conditions. A good model for the CRT behavior would be essential in this case, since it would make possible the adaptation of the characterization data to new conditions with minor adjustments of the model parameters. A case in point is the expression :

$$C = \frac{L_v}{L_{v,max}} = \left(\frac{d'}{d'_{max}} \right)^\gamma \quad (2.37)$$

derived before. If the conditions described before were met, only two measurements would be necessary to characterize a black & white CRT:

1. $L_{v,max}$ measured at d'_{max} ,
2. L_v measured at a known value of d' .

From these two measurements the value of the gamma could be simply determined by :

$$\gamma = \frac{\ln\left(\frac{L_v}{L_{v,max}}\right)}{\ln\left(\frac{d'}{d'_{max}}\right)} \quad (2.38)$$

where \ln is the natural logarithm. If several instances of d' were measured and plotted in a log-log graph against luminance, γ would be the slope of a straight line relating d' to L_v .

2.3.1 Evaluating Gamma

As was mentioned earlier, the approach just presented is lacking a description of the effects of the gain and offset adjustments in the CRT monitor. This has lead to a considerable amount of confusion in the literature. Cowan [54, 56], for instance, correctly identified the normalized gun voltage (which is called v_D here) as being the signal that will satisfy the simple relation above, but, as becomes clear from his discussion, he considers the first grid voltage v_{G1} to be the same as the video voltage (called v_d here). A more recent example of this kind of misunderstanding is presented by Hartmann and Madden [88], who also consider the voltage in equation 2.3 to be the video voltage. As a result, both authors have stated that they could not find a simple gamma that would fit the entire CRT range, and recommended that either a two parameter fit (see equation 2.6) to the CRT response be used or that values outside the linear log-log range be discarded. While the former proposition might actually work, the second has serious drawbacks, since it would severely shrink the gamut of available colors.

Figures 2.4 and 2.5 illustrate the effect on the CRT calibration of mistaking the video

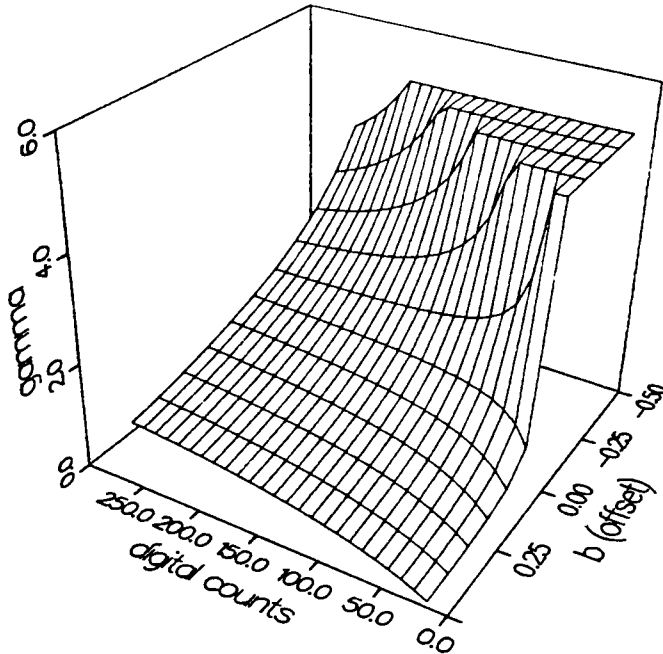


Figure 2.4: Estimating gamma for fixed gain a and different offsets b .

voltage by the gun voltage. Both graphs were obtained from the expression

$$\gamma_{estimated} = \frac{\ln \left(\left(\frac{ak_p \Delta v \frac{d'}{d'_{max}} + ak_p v_{min} + b - v_C}{ak_p \Delta v + ak_p v_{max} + b - v_C} \right)^{\gamma_{true}} \right)}{\ln \left(\frac{d'}{d'_{max}} \right)} \quad (2.39)$$

where the top expression is the true radiance ratio from our extended model and the bottom is equal to the ratio of the gun voltages in the “naive” model. Also, for both graphs, the following values were assumed :

- $L_{v,max} = 1.0$
- $d'_{max} = 255$
- $\gamma_{true} = 2.3$
- $b = b - v_C + ak_p v_{min}$ (in figure 2.4)

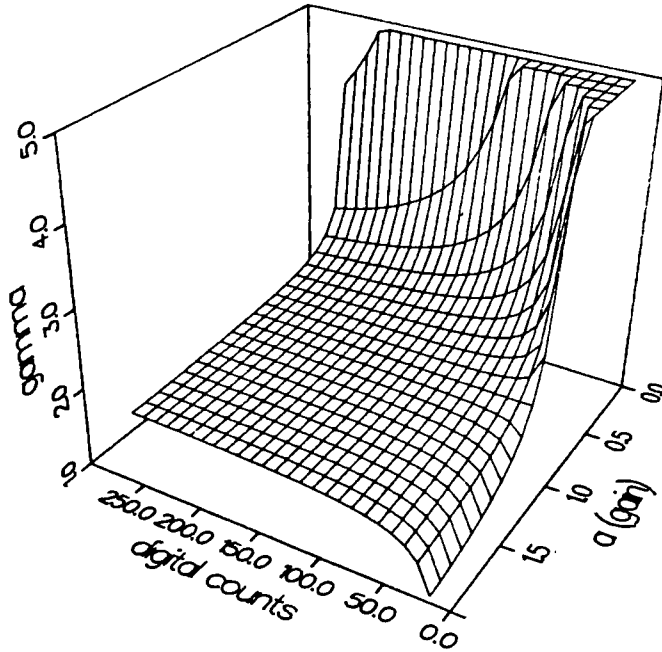


Figure 2.5: Estimating gamma for fixed offsets b and different gains a .

- $a = 1.0$ (in figure 2.5)

Notice that neither assumptions of a or b should affect the results. As a hint to the proof, notice that if the offset is equal to the cutoff voltage, the estimated gamma will be invariant with respect to the gain.

As both graphs show, deviations from the “real” gamma are to be expected for the lower digital counts (or video voltages) if the “naive” model is used. From the observations reported by Cowan (gamma estimated at 4.5 at low voltage levels and 2.5 at highest), his monitor was adjusted so that the net offset b had a negative value; in other words, it was necessary to increase significantly the video voltage before there was emission by the CRT. Hartmann and Madden, on the other hand, reported an estimated gamma that decreased as the video voltage level increased, indicating that the offset was too high (the CRT was emitting even at $d' = 0$, or 7.5 IRE).

2.3.2 Simplified Transfer Function Model

Given the above results, we must devise a way of estimating the effects of the gain and the offset terms if the CRT gamma is to be found. The normalization of the radiant output of the CRT will provide us the means of accomplishing this. First we express the normalized gun voltage as

$$\frac{v_D}{v_{D,max}} = \frac{ak_p \Delta v \frac{d'}{d'_{max}} + ak_p v_{min} + b - v_C}{ak_p \Delta v + ak_p v_{max} + b - v_C} \quad (2.40)$$

or rearranging the equation

$$\frac{v_D}{v_{D,max}} = \frac{ak_p \Delta v}{ak_p v_{max} + b - v_C} \left(\frac{d'}{d'_{max}} \right) + \frac{ak_p v_{min} + b - v_C}{ak_p v_{max} + b - v_C} \quad (2.41)$$

Two new constants are then introduced, K_1 and K_2

$$K_1 = \frac{ak_p \Delta v}{ak_p v_{max} + b - v_C} \quad (2.42)$$

and

$$K_2 = \frac{ak_p v_{min} + b - v_C}{ak_p v_{max} + b - v_C} \quad (2.43)$$

And it follows from the above definition that

$$K_1 + K_2 = 1.0 \quad (2.44)$$

Our expression for the CRT tristimulus values is then reduced to

$$C = \frac{L_v}{L_{v,max}} = \left(K_1 \left(\frac{d'}{d'_{max}} \right) + K_2 \right)^\gamma \quad (2.45)$$

where K_1 is the system gain and K_2 is the system offset. Because the beam current is zero for all driving voltages greater than the cutoff as described in equation 2.15, the complete equation will, finally, be

$$C = \begin{cases} 0, & \text{if } K_1 \left(\frac{d'}{d'_{max}} \right) + K_2 \leq 0 \\ \left(K_1 \left(\frac{d'}{d'_{max}} \right) + K_2 \right)^\gamma & \text{if } K_1 \left(\frac{d'}{d'_{max}} \right) + K_2 > 0 \end{cases} \quad (2.46)$$

Despite its simplicity, this equation will provide a much better fit to the CRT transfer function than the simple model described on section 2.1.1. Similar equations date back to Barney Oliver's³ 1949 paper on tone rendition for black and white television [145].

³Who was the founder of Hewlett-Packard's Research Laboratories.

The problem facing us now is to evaluate K_1 and K_2 . To measure a , b , v_{max} , etc., directly would be laborious and time consuming; ideally, only measurements of some function of the radiant output and d' should be necessary to characterize the CRT. A CRT calibration method will be discussed in chapter 3. The reader will find a discussion of some of the measurement related issues in the appendices.

Chapter 3

THE CALIBRATION OF A CRT

The task of calibrating a CRT consists of characterizing the CRT performance, so that we have a numerical description of the CRT state for a limited set of inputs, and the extraction of parameters from the characterization data, so that by using an appropriate model we can make predictions on the output of the CRT for any given input. The discussions in the appendices reveal several factors that influence CRT measurements and how some of them can be taken into consideration. As indicated there, the limitations imposed by the CRT performance will not only determine the measurement strategy, but also its applicability to the experimental task at hand. In the next sections, we review some practical aspects of such calibration and present the results for the calibration of a color CRT under a restricted set of conditions.

3.1 Characterization Method

The characterization method depends to a great extent on the stimulus chosen and the algorithm used to extract the CRT model parameters. A general purpose method is described here, which should be useful in most situations.

The characterization process is divided into two parts. The first concerns the characteristics that are inherent to a given CRT (e.g. phosphor constancy), while the second is

concerned with characteristics that are transitory and are affected by the CRT setup and operation (e.g. transfer functions). Most of the topics presented here are discussed at length in the appendices. Here we review some of them briefly from a more applied point of view.

3.1.1 Permanent Characteristics

A small number of the CRT properties are global or stable enough to be called permanent. They are usually not reported by the CRT manufacturers, but they are important enough to warrant careful characterization at least once before a CRT is used in visual experiments. They are presented here in the order that they should probably be evaluated.

CRT stability and latency time Before any other kind of measurement is made, it is a good idea to understand the properties of the CRT as a signal source. Some of the measurement-related issues are discussed in appendix C. The critical variables are the time it takes the CRT to stabilize (the latency time) after its state has been changed and how stable that level is. Results of the CRT stability measurements will determine the intergration time and delay needed before each measurement.

Phosphor constancy Although, a phosphor set that exhibits great deviations in chromaticity with different amounts of excitation will still be useful for a CRT display, the task of modeling and characterizing such a display will be greatly complicated. Because constancy is so desirable, and because it will be independent of the ambient conditions, angle of collection, position on the CRT image and setup, it is one of the most fundamental characteristics of a color CRT.

The measurement of phosphor constancy requires that the colorimeter or spectroradiometer used must have a large dynamic range and be as linear as possible. Absolute accuracy (with respect to the CIE or NIST) is not mandatory, since constant chromaticity or proportionality of the phosphor spectral power distribution at different levels of excitation will suffice to establish constancy. In practice, though, the results will never yield perfect constancy, nor will be free from noise. To evaluate the statistical meaningfulness of

the deviations, accurate colorimetric data will be needed.

Part of the experimental error will be due to the limited dynamic range of the phosphor itself. Another part of the experimental error will come from the lack of perfect purity common to all color CRTs (i.e. blue phosphors being excited by the green channel electron gun). Although spurious red excitation can be easily detected because of the marked peak of most red phosphors at around 635 nm, green and blue contamination will be much harder to detect due to the smooth shape of the SPDs. Also, the size and location of the beam spot with respect to the shadow mask changes with beam current and position on the screen, making it unlikely that perfect constancy can be obtained.

Thus, small deviations on phosphor constancy are to be expected. Cowan [57] has reported constancy measurements where, although by very small amounts, all three phosphors showed a decrease in colorimetric purity with higher excitations. Such a deviation probably reflects a decrease in the CRT "purity" at higher beam currents.

Except for phosphor aging, there is little reason to expect that the constancy characteristics will change for a given CRT.

Gonio properties As is reported in appendix F, the gonio properties of most color CRTs should not be a source of much concern for normal viewing angles. Still, any deviation caused by a different CRT design or extreme viewing angle will cause a change in the detected phosphor chromaticities, and the appropriate goniocolorimetric curves should be obtained for future correction. The gonio properties should remain constant throughout the life of a given CRT, since it depends mostly on the curvature of the glass faceplate, the index of refraction of the glass, and on the scattering properties of the phosphor layer, none of which is likely to change with time.

Phosphor Chromaticities Once the constancy and the dependency on viewing angle has been established, the phosphor chromaticities can be measured at any suitable level and angle. If the gonio properties are known before hand, or are of no concern, the constancy and chromaticity measurements can be made at the same time. Except for phosphor aging,

the chromaticities are unlikely to change. Notice though, that even with phosphor aging, the luminance output is more likely to change than the chromaticities. The stored chromaticity values can later be used to correct routine tristimulus value measurements by means of a 3x3 matrix. This way, less accurate colorimeters can be used for the routine characterization of the CRT.

3.1.2 Transitory characteristics

The transitory CRT characteristics are those dependent on the operation, location, and image contents. A given set of conditions will not necessarily affect the predictability of the CRT output, but will determine the model parameters used to predict the CRT output and impose limits on what kind of performance can be obtained. Here, we summarize some of them.

Setup There are two aspects of the CRT setup. The first part of the setup concerns adjusting the CRT as to obtain the proper performance. Such adjustments include

- Electrical interference A number of conditions, such as floating the CRT or the proximity of another CRT, might create an undesirable modulation on the image usually called "hum".
- Magnetic interference The position of the CRT with respect to the Earth's magnetic field and other magnetic fields will change the image position on the faceplate and affect the convergence and purity. Unless the CRT is specially shielded, adjustments made for one position of the CRT will not be retained for other positions.
- Degauss - With continuous operation, the shadow mask tends to become magnetized, often resulting in loss of purity. Many CRT monitors contain an internal degaussing coil that is activated by means of a switch or when the CRT is turned-on. Degaussing should be performed periodically and before all other adjustments and measurements.

- Purity Degaussing should resolve most of the purity problems. Further degaussing might be obtained by use of a stronger degaussing coil outside of the CRT. The remaining lack of purity might need the adjustment of the purity magnets around the CRT bottleneck. Either way, purity adjustments are rather complicated and are better performed by a trained technician.
- Convergence Unlike purity, most CRTs provide some way for the user to correct misconvergence. The adjustments can be done simply by 6 knobs, as in the case of a trinitron tube (Tek 650HR), or, in the case of a delta gun tube, might require the adjustment of as many as 45 knobs (Tek 690SR). If the CRT is well adjusted, the convergence should be fairly insensitive to the contents of the image being displayed.

The second part of the setup concerns the adjustments needed to obtain the desired image stimulus from the CRT. Such adjustments include the offset and gain of the CRT video amplifying circuit. Besides the “brightness” and “contrast” knobs commonly found in front of most CRTs, one can also adjust the gain and the offset of the individual red, green and blue channels by adjusting the “pots” inside of the CRT. Care should be exercised not to set the CRT video amplifier too far from the manufacturers specifications, since one might exceed the rating of some of the components, risking failure of the circuitry or the tube, and excessive emission of “bad” radiation.

Once the CRT is properly setup and adjusted, we can proceed with the characterization of the radiometric output.

Viewing conditions The viewing angle and the tristimulus values of the ambient light reflected from the CRT will both influence the predicted tristimulus values observed on the CRT. The viewing angle will be of little concern if it is kept fixed, and the characterization can be accomplished by either placing the detector at the observers position, or by calculating the appropriate transfer factors.

The ambient light reflected by the faceplate can be dealt with in a number of ways. For instance, with the ambient lights turned on, and the CRT turned off, the tristimulus values

of the screen reflection can be measured. The characterization would then be performed with the ambient lights turned off and, not surprisingly, the CRT turned on. Later, when predicting the combined tristimulus value, one would simply add the ambient tristimulus value to the one being emitted by the CRT itself. Another less recommended method would be to perform all measurements with the ambient lights on and then subtract a measurement obtained with the dark CRT ($d = 0$) from the rest of the data. The problem with this approach is that it will add extra noise to all measurements since the variance of the CRT and the variance of the reflected ambient light will convolve.

Screen uniformity The CRT screen uniformity is dependent on the proper adjustment of the CRT and the contents of the image being displayed. One can account for it by either characterizing the transfer function of different areas individually, or bypassing the problem with a proper choice of stimuli. All measurements should be made directly on the area to be characterized, since there will probably be no simple relationship capable of describing the output of one area with respect to another.

Load dependency Load dependency is a permanent property of the CRT, since it is determined by the regulation of the power supply and other properties of the circuitry. In practice, though, the amount of deviation that it will cause will be dependent on transitory conditions such as the image contents and the CRT setup, making it easier to characterize under the actual experimental conditions.

A number of approaches are possible for the characterization. The simplest one is probably to find the ratios between the sum of radiant output of the individual channels and the radiant output when the channels are turned on together. A method for the extraction of the meaningful parameters is outlined in appendix E. Again, a proper choice of stimuli might help reduce or solve any problems encountered.

Transfer function and White point Assuming that the phosphors chromaticities have been already determined at an earlier step, only the transfer function of each individual

channel remains to be measured. Whether or not this step is performed along with the load dependency measurements depends on the measurement strategy, the severity of the load dependency, and the algorithm used to extract the model parameters. The probable minimum requirement is that the measurement data must be enough to describe both the maximum luminous output of each channel, so that it can be matrixed with the chromaticity data, and contain enough points along each of the channels dynamic ranges to describe the characteristic curves.

In the next section we will present an experimental realization of such a characterization.

3.2 Characterizing the Transfer Functions

We present here an experimental implementation of some of the topics discussed in the previous sections. A method is presented for the characterization of the CRT transfer function along with the experimental results. In a later section we will discuss the algorithm used to extract the parameters for the model described on section 2.3.1.

3.2.1 Setup

The CRT used for this characterization was a Hewlett-Packard model 98785a, which uses a Sony made Trinitron tube similar to the Tektronix 650HR. The constancy was evaluated with a spectroradiometer between 10% and 100% of each gun maximum output and showed no systematic deviation. The chromaticity coordinates shown on table 3.1 were measured for each individual channel at 50% emission to minimize the loss of purity but still have a strong enough signal.

For the transfer function measurement, the detector used was a Minolta TV-2160 which had its linearity corrected as described in appendix C. All measurements were carried out in a darkened room. Further simplification of the setup was obtained by selecting only area 13 (see figure B.1, page 127) for calibration and surrounding it with a constant dark ($d = 0$) background.

	x	y
R	0.6175	0.3406
G	0.3040	0.5980
B	0.1441	0.0536

Table 3.1: CIE 1931 chromaticity coordinates of CRT phosphors.

3.2.2 Algorithm

The C program **crtCAL.c** in appendix J demonstrates the characterization method used. The program assumes that a suitable stimulus is on the frame buffer and that the portion of the screen to be modulated has value $d = 1$ on all three planes. The program is also setup to wait 20 seconds before each measurement, allowing the CRT to stabilize, and then to average 10 readings from the colorimeter. The program outputs Yxy data which can be redirected to a file.

First all 8 combinations of the 3 phosphor primaries (i.e. K,R,G,Y,B,M,C,W) are measured. Besides giving the intensity of the phosphor primaries, this data can later be used to estimate the amount of load dependency exhibited by the CRT. The program then steps up d from 5 to 255 in 10 digital counts increments. The advantage of increasing d_r , d_g and d_b at the same time is that it speeds up the characterization method and gives an estimate of the transfer function in a kind of “worst case” situation, where load dependency should be at its maximum. It also makes it easier to establish any eventual difference between the 3 individual transfer functions by allowing one to observe the deviations in chromaticity along a neutral scale. The strongest assumption made by this method is that the detector used has a linear response within the dynamic range tested and that its photometric scale is accurate. Since phosphor constancy holds, the individual transfer functions can be separated later using the phosphor primaries measured with the colorimeter. Notice that colorimetric accuracy is not a requirement for the separation.

3.2.3 Results

	Y	x	y	R	G	B
K	0.04	0.2993	0.4360	0.000	0.000	0.000
R	16.75	0.6470	0.3068	1.000	0.000	0.000
G	58.35	0.2940	0.6050	0.000	1.000	0.000
Y	75.20	0.4210	0.4970	0.998	1.002	0.001
B	5.79	0.1440	0.0460	0.000	0.000	1.000
M	22.50	0.2970	0.1260	0.993	0.003	0.986
C	64.00	0.2090	0.2910	-.007	1.001	0.983
W	80.85	0.2960	0.2940	0.994	1.003	0.985

Table 3.2: 8 combinations of the three CRT primaries.

Table 3.2 contains the CIE 1931 Yxy data obtained for the 8 combinations of the RGB phosphor primaries. The CRT tristimulus values, R , G and B , were obtained from the CIE tristimulus values of the red, green and blue phosphors. The matrix obtained was also used to decompose the Yxy data in table 3.3 into the respective CRT tristimulus values. Notice that because of noise and the dynamic range of the TV-2160, not all the values listed in table 3.3 will be used to calculate the transfer function parameters. The lowest values are reported only for the sake of completeness.

From table 3.2 we find that under the given conditions, the CRT showed a small amount of load dependency. The largest systematic deviations were on the order of 1.5 % deviation for the blue channel.

We now turn to the task of calculating γ , K_1 and K_2 from the CRT tristimulus values in table 3.3.

3.3 Estimating the Model Parameters

3.3.1 A Nonlinear Algorithm

The dependency of the CRT tristimulus values upon the frame buffer was expressed in equation 2.46, and is repeated here:

$$C = \begin{cases} 0, & \text{if } K_1 \left(\frac{d'}{d'_{max}} \right) + K_2 \leq 0 \\ \left(K_1 \left(\frac{d'}{d'_{max}} \right) + K_2 \right)^\gamma & \text{if } K_1 \left(\frac{d'}{d'_{max}} \right) + K_2 > 0 \end{cases}$$

where γ , K_1 and K_2 are constants, d' is the digital count at a certain pixel (or LUT entry), d'_{max} is the maximum digital count (255 in the current case) and C is the normalized CRT stimulus.

To extract the parameters, γ , K_1 and K_2 , from the experimental data we have chosen the Levenberg-Marquardt method [127]. This is a nonlinear least-squares method which interactively modifies its estimates of the model parameters until χ^2 , the figure of merit, ceases to decrease. The algorithm used here is described in detail in the book “Numerical Recipes in C” [149] (NRC), which also contains extensive discussions about this and other possible non-linear methods.

The nonlinear least-squares routines are called from the program **crtCALC.c**, which is listed in appendix K along with some of the subroutines. Because of their size, the libraries and the “include” files obtained from the NRC are not reproduced here.

The method represented by **crtCALC.c** seems to be fairly robust and has very fast execution (less than a second, total execution time, in a HP9000/350). The comments in the program should make it self-explanatory. The input is obtained from the calibration program **crtCAL.c** described before. First a matrix is built from the CIE tristimulus values of the phosphor primaries. This data is used to decompose the rest of the data into the three transfer functions, as illustrated in table 3.3. The major part of the code is devoted to practical issues, such as determining at what level the signal is strong enough to be part of the parameter estimation, and zeroing all negative tristimulus values.

d	Y	x	y	R	G	B
5	0.0325	0.2430	0.3923	0.000	0.001	0.000
15	0.0400	0.3750	0.5000	0.000	0.001	0.000
25	0.0400	0.3750	0.5000	0.000	0.001	0.000
35	0.0400	0.3750	0.5000	0.000	0.001	0.000
45	0.0300	0.4583	0.4063	0.001	0.000	0.000
55	0.0600	0.3570	0.4280	0.001	0.001	0.000
65	0.1200	0.5000	0.3750	0.004	0.001	0.000
75	0.2800	0.4930	0.3730	0.008	0.002	0.001
85	0.6700	0.4580	0.3700	0.018	0.006	0.002
95	1.3700	0.4110	0.3660	0.029	0.015	0.006
105	2.4400	0.3810	0.3530	0.046	0.027	0.015
115	3.9000	0.3610	0.3400	0.067	0.045	0.028
125	5.7950	0.3455	0.3310	0.093	0.068	0.047
135	8.1525	0.3348	0.3240	0.124	0.097	0.073
145	10.9750	0.3270	0.3183	0.161	0.132	0.105
155	14.3000	0.3208	0.3140	0.203	0.173	0.144
165	18.2000	0.3160	0.3100	0.253	0.221	0.191
175	22.7000	0.3120	0.3070	0.308	0.277	0.246
185	27.7000	0.3085	0.3040	0.370	0.338	0.310
195	33.4000	0.3060	0.3020	0.439	0.409	0.381
205	39.6500	0.3035	0.3000	0.514	0.487	0.462
215	46.5750	0.3020	0.2990	0.598	0.573	0.548
225	54.2000	0.3000	0.2970	0.689	0.668	0.650
235	62.3000	0.2980	0.2960	0.779	0.770	0.757
245	71.2500	0.2970	0.2950	0.886	0.881	0.874
255	80.8000	0.2960	0.2940	1.000	1.000	1.000

Table 3.3: CRT transfer function measured over 25 steps of d .

3.3.2 Results

	γ	K_1	K_2	X	Y	Z
R	2.4239	1.2242	-0.2244	30.3674	16.7500	2.0606
G	2.4029	1.3220	-0.3216	29.6629	58.3500	9.5624
B	2.4455	1.3622	-0.3598	15.5660	5.7900	86.6664

Table 3.4: Estimated CRT model parameters, normal setup.

The CRT model parameters estimated from the data in tables 3.2 and 3.3 are shown in table 3.4. The tristimulus values were calculated from the previously measured phosphor chromaticities (table 3.1) and the luminance measured during the experiment. Notice that, as expected,

$$K_1 + K_2 \approx 1.0$$

even though the nonlinear algorithm estimates each parameter individually.

The data in tables 3.5 and 3.6 were obtained by using all the methods previously described in this chapter, except that the “brightness” (offset) knob was set in two different positions, lower and higher than for the data shown on table 3.4. As we see in tables 3.5 and 3.6, the gamma showed only a small variation (about 5 %) while the value for K_1 and K_2 changed by as much as 40 %.

	γ	K_1	K_2	X	Y	Z
R	2.4398	1.3162	-0.3159	25.5630	14.1000	1.7346
G	2.4190	1.3545	-0.3543	24.5538	48.3000	7.9154
B	2.5003	1.3636	-0.3639	9.4095	3.5000	52.3890

Table 3.5: Estimated CRT model parameters, low brightness.

	γ	K_1	K_2	X	Y	Z
R	2.4540	1.1776	-0.1782	33.5401	18.5000	2.2758
G	2.3973	1.2123	-0.2117	32.5224	63.9750	10.4842
B	2.4758	1.2156	-0.2159	12.6222	4.6950	70.2761

Table 3.6: Estimated CRT model parameters, high brightness.

3.4 Verifying the Model

To verify how well the model could predict the CRT output, a series of measurements were made. Keeping the same setup described before, each channel was stepped from $d = 5$ all the way to $d = 255$ in steps of 20 digital counts, spanning the entire CRT gamut. In total, the CIE tristimulus values of 1331 (11^3) data points were measured with the Minolta TV-2150. The same d_r , d_g , and d_b were then used with the model to try to predict the measured tristimulus values. The chromaticities of the measured and predicted data set were corrected according to the real chromaticity values of the phosphors in table 3.1 so that an accurate estimate of ΔE_{ab}^* could be obtained. To calculate CIE 1976 L*a*b* values, the measured white point of the CRT was chosen as the reference point. The color differences between each of the predicted and measured values was calculated for each of the 1331 combinations of d_r , d_g , and d_b .

The average ΔE_{ab}^* found was 1.6 and the standard deviation was 1.4. The frequency of the resulting color differences is shown on the histogram in figure 3.1.

One aspect of the model performance that is not clarified by figure 3.1 is how meaningful are these errors compared with other systematic errors that we expect to find when using a CRT imaging system. As is reported in appendix C, most of the measurement and operation errors will be fairly small. But, because of quantization, small systematic errors may compound and result in model predictions that will be wrong by either zero or one digital count.

dE Histogram

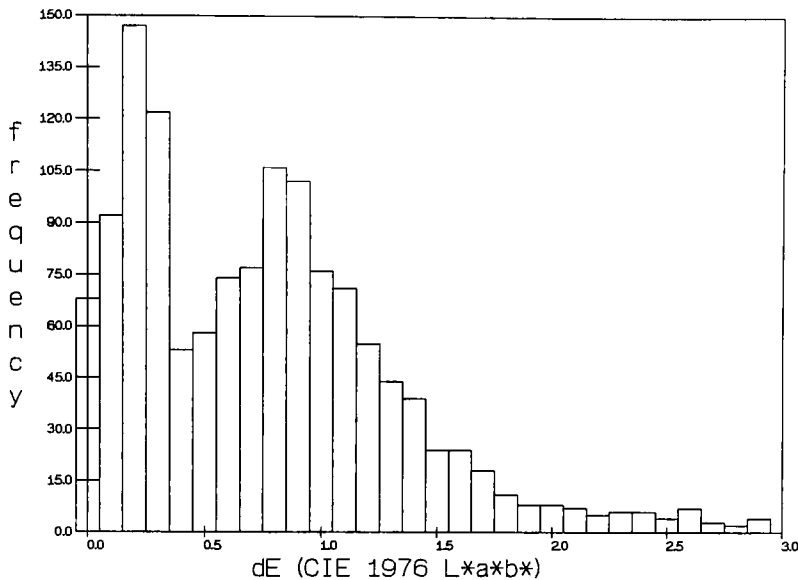


Figure 3.1: Histogram of CRT model ΔE_{ab}^* errors over entire CRT gamut.

To investigate the effect of a random 1 digital count error, another experiment was performed where the values of d_r , d_g and d_b were systematically and independently changed from 180 to 190 in 1 digital count intervals. This range was selected because it represents about 50% in the intensity of the CRT channels and in this region the transfer function is neither too flat or steep. Using the same setup as before, the colorimetric data were collected with the TV-2150. Again, the total data set contained 1331 points. From this data, an estimate was obtained of the colorimetric error expected when any of d_r , d_g or d_b were, alone or together, wrong by a single digital count. In other words, a ΔE_{ab}^* color difference was calculated between each measured point and all of its 26 closest neighbors ($d_r \pm 1$, $d_g \pm 1$ and $d_b \pm 1$).

The mean ΔE_{ab}^* obtained was 1.1 and the standard deviation was 0.3. The population obtained is depicted in figure 3.2. The similarity between the two populations, the model errors and the single digital count errors, indicate that the model performance is equivalent

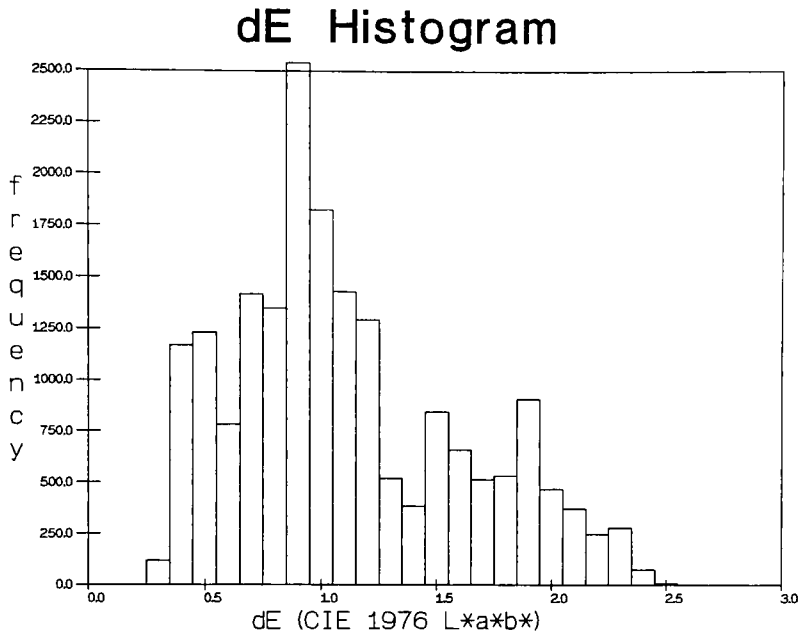


Figure 3.2: Histogram of ΔE_{ab}^* color difference due to errors of 1 digital count.

or superior to the performance of the CRT system itself.

Besides the aforementioned systematic errors, load dependency is probably one of the main factors limiting the model performance. The effect of the slight amount of load dependency found in the blue channel of the CRT tested can be visualized by comparing figure 3.1 with figure 3.3, which shows the subset of data for d_b held at zero (121 points). Under these circumstances, the mean model error reduces to 0.5 and the standard deviation to 0.1.

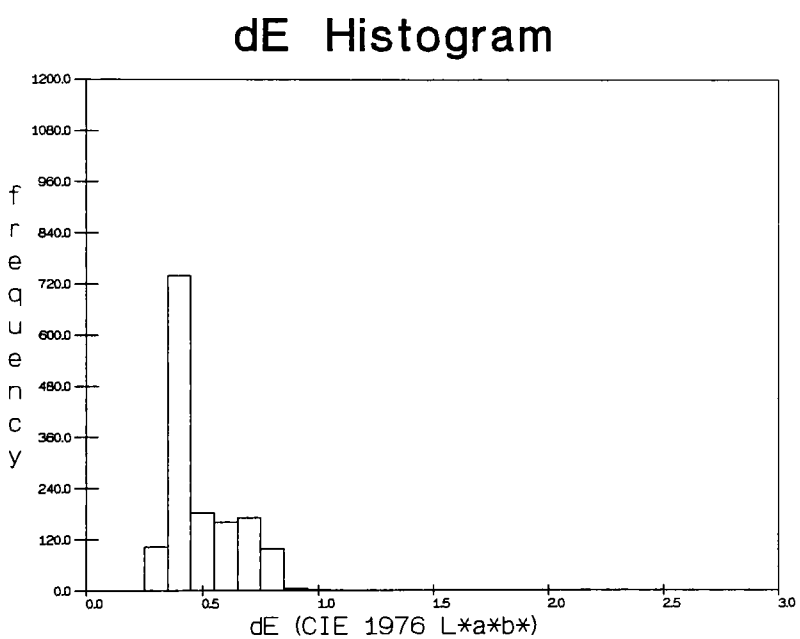


Figure 3.3: ΔE_{ab}^* model errors for only the red and green channels

Chapter 4

CONCLUSIONS

The main conclusion to be drawn from this investigation is that the relevant aspects of the CRT colorimetric performance can be accurately characterized and modeled. The model derived here might be helpful in designing experiments for color and vision research, although the actual experiment will determine the extent to which a CRT can be a substitute for some other conventional optical apparatus. Some of the limitations have been discussed in the text. The results obtained from the goniocolorimetric and repeatability measurements show that the errors that can be attributed to those factors are relatively small. Large errors in the prediction of the CRT colorimetric output will probably be due to the measurement apparatus, algorithms, load dependency and lack of uniformity.

We have seen that if CRTs are not perfect, then a careful experimental design can at least avoid some of the pitfalls. For instance, in a WYSIWYG environment, where the CRT output might have to match some other object color, the 8 bit quantization level provided by most frame buffers should be appropriate. During this investigation the average uncertainty of CIE tristimulus values for a good CRT was found to be about 1%. It follows that even if more bits per pixel are added, they might be wasted by our inability to predict and statistically differentiate them.

Another case would be that of visual threshold measurements. The average error expected when using the CRT model to predict absolute tristimulus values was found to be

about $1.5 \Delta E_{ab}^*$. Although this value is larger than most visual thresholds, the CRT is still a useful device since any specific location on the CRT will be well behaved. While we might not be able to predict the exact value of, say, a certain square area in the middle of the CRT, we can use the CRT model to make very specific predictions about what will be the *difference* between two small adjacent areas. Moreover, if the CRT is locally uniform over the test area and its immediate surround, we can use the background as an anchor point for our measurements. Under this kind of scheme the CRT model could be used for two different purposes. At the absolute level, it could be used to make sure that the test stimulus and the background are all within some tolerance. At the local level it can be used to calculate very precisely the differences between test stimuli. The normalization offered by an anchor background would relieve the model from the task of making very accurate predictions of the absolute tristimulus values. In this case more than 8 bits of quantization would surely be useful and welcome.

In several instances during this research there were indications that the model could perform as well as or better than a table of values obtained from direct measurements. The use of a model over a table offers several advantages:

- A model will consume much less storage space than a large table of numbers.
- As an option to storing too many numbers in a table, one could reduce the number of points and use interpolation to generate a larger table. This argument is equally valid for a model, and the model has the advantage of requiring less computation than most interpolation routines. If, for the sake of speed only 10 numbers were stored and linear interpolation was used in between, the errors would be considerable.
- Tables allow for faster processing time. It does not follow, though, that the data has to be stored and treated as a table. A model can be used to generate tables as well.
- A model that has basis in a physical process can have its parameters modified to reflect changes in the physical process. On the other hand, a table of numbers has to be regenerated through new measurements. Also, a model can be used to generate a

new table every time that it is needed.

- A model might not account for load dependency and other deviations, but neither will a table.

Still, the model is far from perfect and can be improved in a number of ways. We discuss some of them next.

4.1 Recommendations

One important thing that is missing from this work is the integration of all sources of errors into a single statistic. This error analysis should help determine what is the best strategy for calculating γ , K_1 and K_2 . For instance, the number of data points measured along the transfer function could be significantly reduced since that is such a smooth function. During this investigation 25 points were measured, making the estimates more robust by spreading the error among several data points. A better understanding of the sources of error could probably reduce the number of points needed to two or three.

Methods for isolating the contribution of the individual components of the model would be very useful. For example, if a and b could be either directly measured or calculated from other measurements, the CRT model could become general enough to predict intensity changes when one of the physical parameters is manipulated. For instance, one could read the data for a and b from the CRT potentiometers and convey it to the computer for predicting the transfer functions.

Another area that needs expansion is the development of the measurement techniques. The signal to noise ratio could probably be increased by an order of magnitude if proper care is taken with the synchronization and positioning of the detector. The difficulty of isolating the CRT fluctuations from the variance on the detection process will always be a limiting factor when deciding what kind of experiments can be performed by a specific system.

Other areas that are important and were bypassed in this investigation are concerned

with the spatial and temporal distribution of the CRT signal. We have only briefly mentioned the effects of the convergence and purity. To have a full description of the CRT appearance, instead of only its colorimetric properties, investigation will also be needed on the effects of flicker, spatial MTF and the development of methods for accounting for the screen lack of uniformity and load dependency.

The issue of the generality of the results reported here is also important. Although a number of devices have been tested and behaved according to predictions made by the model, this was a restricted sampling of the variety of CRT designs and manufacturers that are available in the marketplace. It would be useful to know if CRTs, as a class of devices, share the same operating characteristics. If they do, a model such as the one based on γ , K_1 and K_2 could be a satisfactory communication tool, since only a few parameters would need to be communicated. A CRT could be characterized by only twelve numbers

$$X_r \ Y_r \ Z_r \quad \gamma_r \ K_{1,r} \ K_{2,r} \ l_r$$

$$X_g \ Y_g \ Z_g \quad \gamma_g \ K_{1,g} \ K_{2,g} \ l_g$$

$$X_b \ Y_b \ Z_b \quad \gamma_b \ K_{1,b} \ K_{2,b} \ l_b$$

where l_r , l_g and l_b are the load dependency factors. A general purpose calibration procedure was outlined in chapter 3. For widespread communication of CRT attributes to be meaningful, it would be necessary to agree not only on a model, but also on both the measurement procedure and the test stimulus. Because of CRT performance variability, the specific design of the test stimulus might not be as important as having all communications refer to measurements made with the same stimulus.

In the coming years, colorimetrically calibrated CRTs are likely to find a place not only in appearance and vision laboratories, but also in the general business world. Colorimetric accuracy has not yet been needed because the CRT image is very rarely compared with something else. This situation is likely to change in the near future with the advent of better and less expensive color printing technologies. To achieve the level of functionality needed for WYSIWYG, the manufacturers of computers, CRTs and software will need

to find a way to communicate the CRT colorimetric properties. This investigation will hopefully provide some of the needed foundations.

Appendix A

DERIVATION

A.1 Computer Image Formation

A.1.1 Digital Images

A sampled image is an ordered array of numbers, and as any other discrete representation of a continuous function, it has its advantages and limitations. The clear advantage is that it can be operated upon like any other discrete function, for which mathematics offers very powerful tools. The biggest disadvantage is that the sampling operation will introduce artifacts in the function representation. Obviously, such artifacts will tend to disappear with higher resolutions, i.e., as the sampling interval becomes infinitesimal. A typical example of a sampling artifact is a periodic function that is sampled above its fundamental frequency, creating aliasing.

The sampled image is in a convenient form for processing by digital computers since these operate in a bit by bit sequential fashion. The benefit of flexibility given by such digital computers is preferred for most applications over the higher speed and resolution offered by more traditional analog systems (such as photography, optics, etc.)

Of special concern here is that the digital image uses a limited set of integers to describe both the location on the image and the state at that location. Usually the integers describing the image are stored in a special part of the computer memory called a frame or image buffer.

Besides making all pixels available at the same time, such memory is also a buffer in the sense that it lies between two processors, the computer CPU which performs operations on it and the processor which creates the display signals.

Several good texts (see for instance refs. [74] and [7]) offer descriptions of the kind of hardware discussed here. For our purposes it suffices to mention that the memory is composed of devices called dynamic random access memory (DRAM) chips, also known as VRAMs (video RAMs). Such devices are dynamic in the sense of their ability of holding information is dependent on how often they are refreshed. In the case of an image buffer this happens every time a frame of image is generated. Because the information on the image buffer is sequentially scanned and then routed to the display generator, the speed at which the computer chips can operate will be the primary factor governing the resolution of a digital image processing system (notice that this remark would not apply to a system which was writing a display viewed by some long memory system, such as a film recorder or a storage CRT). For example, if an image consisted of only 16x16 locations containing a single bit of information (i.e. a binary integer) where each pixel is displayed 60 times per second (60 Hz), the locations would have to give up information every 65 microseconds (μs). More discrete states could be added per location by adding more planes of binary data. To obtain 256 discrete levels per location one would need 8 planes of 16x16 locations ($2^8 = 256$). To keep the same display rate (60 Hz) we would have to increase the speed of the information collection operation to 8.14 μs per location.

For the case of the Number 9 512x32 image buffer (see figure A.1) used at MCSL, there are 512x512 locations, each with 32 bits of data grouped in 4 groups of 8 bits for red, green, blue and overlay data. The overlay data is mapped into the red, green and blue signals, and since it carries no additional intensity information it will be ignored hereon.

Given the previous remarks, the image position can be indexed by an ordered pair $< w, h >$, after *width* and *height*, resulting from the product of the sets \mathcal{W} and \mathcal{H} , both subsets of \mathcal{N} , the set of natural numbers, and defined as

$$\mathcal{W} = \{w : w \in \mathcal{N} \text{ and } 0 \leq w \leq 511\}$$

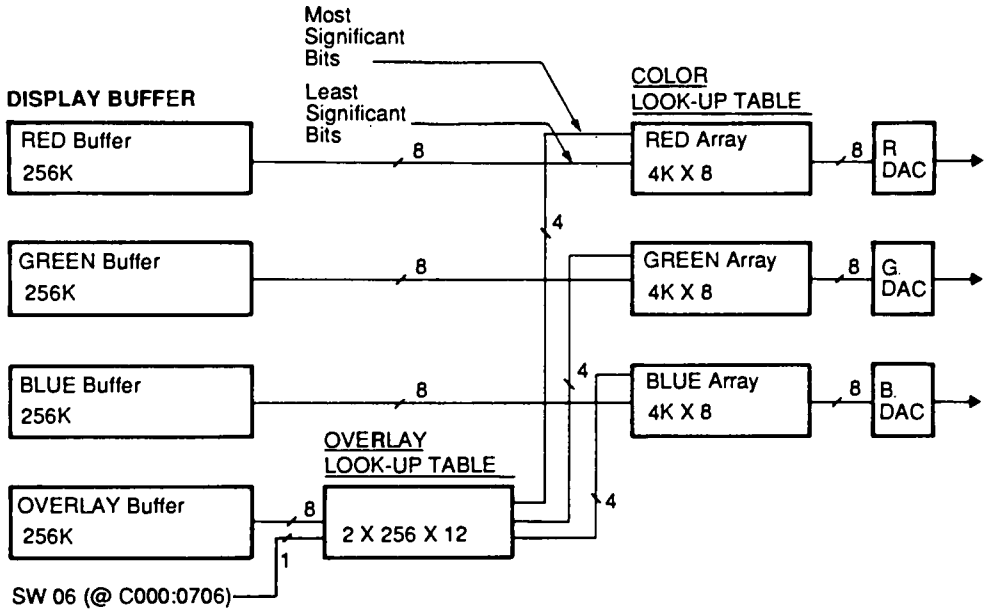


Figure A.1: Block diagram of the Number 9 512x32 graphics board.

$$\mathcal{H} = \{h : h \in \mathcal{N} \text{ and } 0 \leq h \leq 511\}$$

The image in the memory is then described by a 512×512 square matrix

$$[d_{w,h}] = \begin{bmatrix} d_{0,0} & d_{0,1} & d_{0,2} & \cdots & d_{0,511} \\ d_{1,0} & d_{1,1} & d_{1,2} & \cdots & d_{1,511} \\ d_{2,0} & d_{2,1} & d_{2,2} & \cdots & d_{2,511} \\ \cdots & \cdots & \cdots & \cdots & \cdots \\ d_{511,0} & d_{511,1} & d_{511,2} & \cdots & d_{511,511} \end{bmatrix} \quad (\text{A.1})$$

whose entries are 3×1 vectors $d_{w,h}$ of the form

$$d_{w,h} = \begin{bmatrix} d_r \\ d_g \\ d_b \end{bmatrix} \quad (\text{A.2})$$

where d_r , d_g and d_b describe the number of digital counts stored in each of the red, green and blue planes in memory location $< w, h >$. A note about the nomenclature should be made here. Unless indicated, the reader should assume that all variables that relate to the image formation have three versions, a “red” value, a “green” value and a “blue” value, corresponding to the three guns used in color CRTs which generally appear reddish, greenish and bluish. This strategy is taken to avoid the multiplication of redundant subscripts.

The values of d are expressed in digital counts, which belongs to the set \mathcal{D} , defined as

$$\mathcal{D}_n = \{d : d \in \mathcal{N} \text{ and } 0 \leq d \leq 2^{n-1}\}, \quad (\text{A.3})$$

where n is the number of bits per plane of memory. The Number 9 frame buffer has 8 bits per plane, thus on each plane $d_{w,h}$ will range from 0 to 255. The total number of discrete states that can be assigned to $d_{w,h}$ will be 2^{24} , or around 16.8 million. Notice that is **not** the number of discrete colors that can be displayed; the spacing of these colors will be very non-linear, with some falling so close that will not discernible from each other and others falling very far apart [55, 168].

Assuming that there is a different scan process happening for each color, that only 485 (for reasons to be explained later) lines are displayed per frame, and that the display is entirely refreshed once every 1/30 of a second, the scanning process would occur at 16.8 nanoseconds (ns) per pixel, or around 60 million pixels per second (pps). The stream of bits resulting from the memory scanning will be directed towards the display (video) generator and will be transformed into a luminance pattern which is scanned line by line on the face of the display (CRT in our case) forming the final visible image. But first, it will pass through a very important element for image manipulation process, the look-up-table (LUT) described next.

A.1.2 The LUT

The name of the LUT (look-up-table) gives a good indication of its use. To each incoming byte (8 bits) of data, it assigns another byte, according to rules that are defined by the programmer. Mathematically it can be described as a discrete mapping function. In some

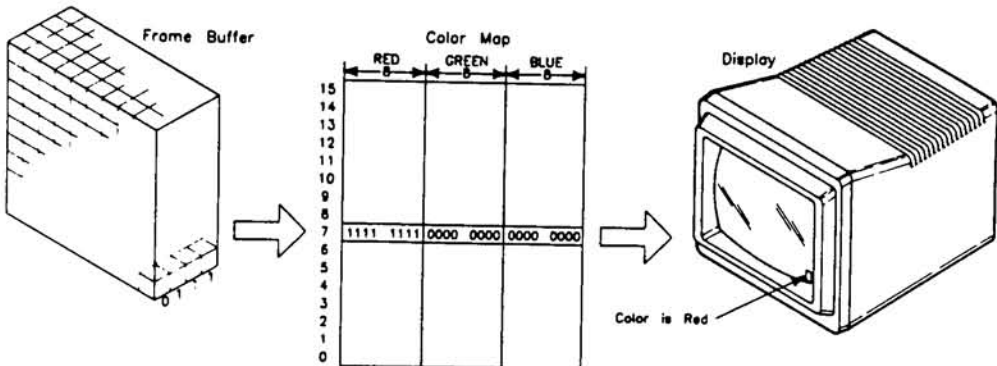


Figure A.2: A LUT where 4 bits are mapped to 24 bits.

image systems it performs as a one-to-one function [163], this being the case for systems where the number of output states on the LUT is bigger than the number of states that are recorded on the image buffer (these systems are usually advertised by saying that a palette of a number such as 256 colors out of 16.8 million are available to the user). Figure A.2 shows the block diagram of a system with a one-to-one LUT. A LUT where the number of bytes on the output corresponds to the number of bytes in the input can be a one-to-one correspondence. This last is the case for the three Number 9 LUTs, one for each of the red, green and blue channels of data. In all cases, the LUT can perform as an onto function, mapping all incoming states to a smaller set.

One of the analogs to the LUT operation on the image data is the “contrast” and “brightness” controls on common television sets. The image can be made as low contrast as to disappear, which would be an onto mapping of all input states on the LUT onto the

same output state, or the contrast could be made very high, which would again be a onto mapping by a LUT that outputs one state under a threshold and another above it. It is important to keep in mind that in the previous examples the image data has not changed (i.e. the television broadcast or the frame buffer data); instead, what has changed is just the transfer function that describes the attributes of the final image.

For our purposes we can define a function $LUT : \mathcal{D} \rightarrow \mathcal{D}$ (i.e. LUT maps members from the set \mathcal{D} into the same set, which is true for the Number 9 board, see above) which we use to redefine the image pixel values,

$$d' = LUT(d) \quad (\text{A.4})$$

A good part of the power from having a LUT in digital image processing systems is that it permits very fast control over the image transfer function. For instance, if the image contained a square filled with bytes at 234 digital counts (d) and it was decided that 123 d was suitable instead, the whole square would not have to be rewritten again, just the LUT entry corresponding to an input of 234 d would have to be modified to output 123 d' . This operation can be performed very fast, since only one byte on the computer memory has to be modified, which also indicates the suitability of the LUT for the interactive control of a specific color on the image. For most of the programs described hereon this was the approach taken. The area to be manipulated was constructed so that it was the only image element that contained a certain d level. For this reason, manipulations made on the LUT affected only the desirable areas.

One thing to keep in mind when manipulating the LUTs is that the workload on the LUT is much higher then on the image buffer DRAMs. The DRAMs are accessed only during a very short time, such as the above mentioned 16.8 ns and have the much longer display period (usually 16.66 milliseconds, ms) to wait or to be written to. On the other hand the chip that carries out the LUT operations has to process all the 512x485 pixels of image each frame, working on a frequency of at least 60 million pps. Ideally the cycle of operation on such devices should be long enough to allow it to be written to and read from on the same cycle. Depending on the quality of the device this might not be possible, and

the writing period will have to coincide with the reading; in this case some data to be read are lost. Also the cycle of the signal writing to the LUT might be much longer than the cycle of the LUT chip itself, and several pixels of data will be lost. This last is the case with the Number 9 board, and the result is many times an annoying noise on the screen, usually referred to as “snow”. The same effect can also be seen while the screen is scrolling on most IBM PCs with a color graphics adapter (CGA). One of the ways around it is to synchronize the writing period with those periods when the display signal is not visible (i.e. blanked) which happens between every line and every frame.

A.1.3 The Video Generator

The data coming out of the LUT will be directed towards the video generator, which in turn will generate the video signal by transforming image digital counts into analog voltages through a set of digital-to-analog converters (DACs) and adding to it other analog signals which control the timing of the display. The video signal will usually follow the guidelines set up by the Electronic Industries Associations (EIA). The discussion will be limited to some relevant aspects of the signal denominated RS-170 [68] that is generated by the Number 9 board.

A.1.3.1 The RS-170 Signal

Figure A.3 illustrates the basic makeup of the RS-170 signal [68, 46, 87]. This signal was originally standardized for monochrome video, and is similar to the one standardized in 1953 by the National Television Standards Committee (NTSC) for entertainment color television. The RS-170 is monochrome (only one signal amplitude is modulated) and has positive polarity. The NTSC uses an amplitude modulated luminance signal as a carrier to a higher frequency chrominance signal, and the relative levels that make up the signal are somewhat different from the RS-170. Since the signal generated by most computer-based frame buffers will not have to be encoded or broadcasted, it will not suffer from the same

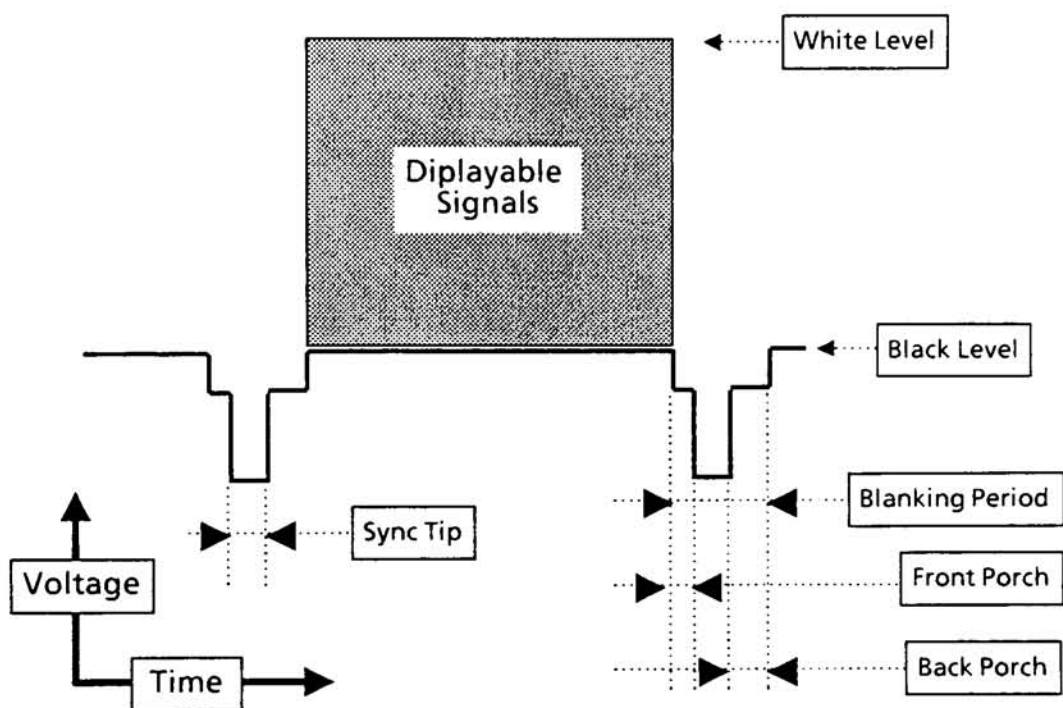


Figure A.3: Different features of the RS-170 video signal.

bandwidth limitations as commercial television¹. Thus, it can be delivered to the display device through three independent cables each with a different RS-170 signal, allowing each color signal to make use of the entire CRT bandwidth. This kind of signal is usually called “analog RGB” and it comes in two “flavors” composite and non-composite.

The composite display signal is defined as “the signal which results from combining a blanked display signal with the sync signal” [46]. The signal illustrated in figure A.3 is of this kind. The Number 9 board can generate both composite and non-composite signals. The non-composite signal needs four cables, for the red, green, blue and sync signals, while the composite signal can be transmitted over three cables, the red, green + sync and blue signals.

For the purpose of this discussion the source of the sync signal will be ignored. One of the first things that the circuitry on the CRT does is to strip the sync out of the green signal (if the sync is there, of course) and all the three video signals will look the same for the remaining circuits in the CRT.

A.1.3.2 The Frame Rate

The system proposed by the NTSC in 1953 follows what is called the 525/60 scan rate. 525 refers to the number of lines per frame, and 60 to the vertical repetition rate. It should be noticed, though, that not all 525 lines are displayed every 1/60th of a second. The system is a bit more complicated, and it is worthwhile to discuss some of the details.

The scan of horizontal lines on the CRT is performed by the horizontal deflection yoke on the electron gun assembly. This yoke is controlled by a voltage signal in the form of a sawtooth, i.e., the voltages increase slowly until they suddenly drop to a minimum and start to increase again. The increasing voltage scans the beam from left to the right of the screen smoothly and at a continuous speed; the sudden drop in voltage brings it back to the origin. Figure A.4 illustrates the path of the electron beam as it scans the CRT faceplate. A different yoke will perform the vertical scan. At the end of every line it will move the

¹The bandwidth of the NTSC signal is limited to 4.2 MHZ [8]

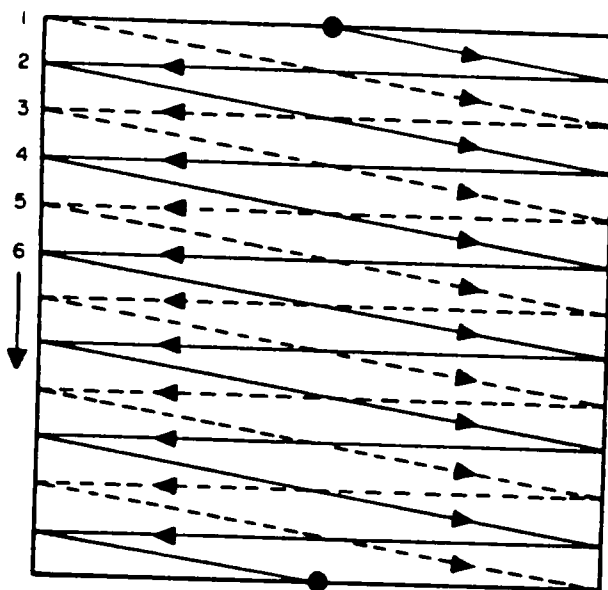


Figure A.4: Interlaced path of scanning electron beam.

electron beam down by a small amount until the bottom of the screen is reached, at this point it will swing back to the top of the screen. The two sawtooth voltages that control the fast horizontal scan and the slower vertical scan have to be very well synchronized. To time the horizontal scan a sync signal is transmitted with every line, to control the vertical scan a series of sync signals are transmitted at the end of every field.

The interlace mode of display is used to decrease the amount of visible flicker. The frame is broken into two complementary fields shown in succession. As indicated by the dashed and solid lines on figure A.4, successive fields represent the odd or the even lines of the frame. Since the effect is the same over the entire picture, the resulting frequency of the image display will be twice the repetition rate of the entire frame. This will save bandwidth and will make the image generation process less expensive. The major disadvantage is that image elements that are present in a single field will still be refreshed at the frame rate,

and might flicker. This is a problem for computer aided design (CAD), computer graphics, data display and other applications that use thin horizontal lines (i.e., one pixel thick). The problem is not as great in entertainment television since the image is much more dynamic, less sharp, and thin horizontal lines are not commonly used. The visibility of the flicker will be dependent of the color of the line and its intensity with respect to the neighborhood. The extreme case being white horizontal lines against a black background.

The synchronization signals might represent a considerable amount of the display time. On the 525/60 system only 485 lines are displayed; the remaining lines are blanked and are used by the vertical synchronization signals. Figure A.5 illustrates the form of typical synchronization pulses used.

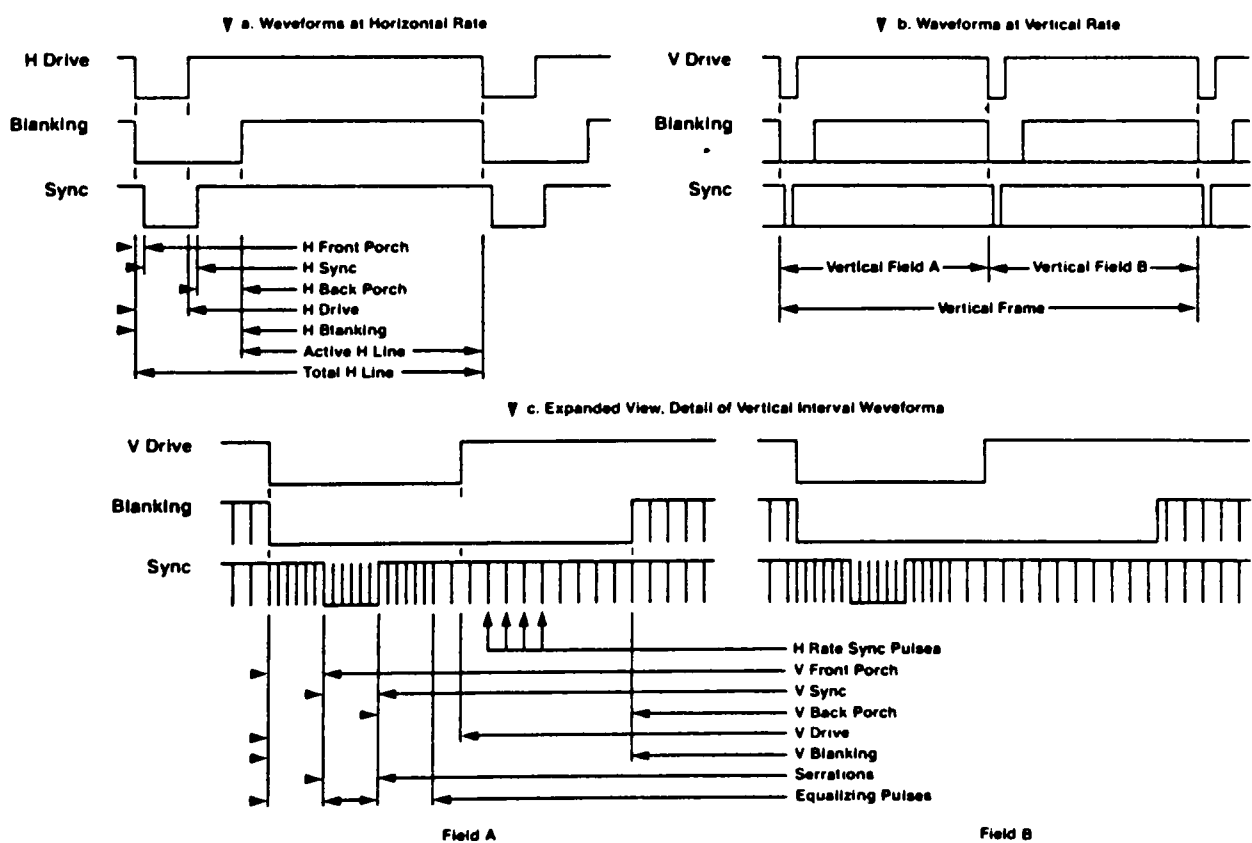


Figure A.5: Typical synchronization pulses.

Name	Description	Duration
Hf	Horizontal Frequency	15.75 KHz
H-FP	Horizontal Front Porch	24 pixels
H-SYNC	Horizontal Sync	40 pixels
H-BP	Horizontal Back Porch	48 pixels
H-BL	Horizontal Blanking	112 pixels
H-DISP	Horizontal Display Area	512 pixels
Vf	Vertical Frequency	60 Hz
V-FP	Vertical Front Porch	3 lines
V-SYNC	Vertical Sync	3 lines
V-BP	Vertical Back Porch	16 lines
V-BL	Vertical Blanking	22 lines
V-DISP	Vertical Display Area	240 lines

Table A.1: Timing of the RS-170 video signal generated by the Number 9 display buffer.

One important aspect of any raster scan video signal is that the vertical and the horizontal resolutions are governed by very different constraints. The vertical resolution is limited by the number of displayable lines, which has to be kept fixed for the synchronization of the video generator and the display. Within each line there is no limit to how much modulation can be accomplished, thus the horizontal resolution is governed by the bandpass of the equipment and not by the video signal format. Most computer generated video signals will adapt the standard television raster format, without most times strictly adhering to the strict timing specifications. For example, the Digital Equipment Corporation (DEC) uses a variant of the RS-170 signal on its VT200 series computer terminals. The odd and even fields have the same information and are not displaced, thus creating a 60 Hz image with only 240 lines. This will allow 24 lines of characters (each character 10 pixels high) with a much larger number of characters on each line (usually 80 or 132). Figure A.6 and table A.1 illustrates the timing of the RS-170 signal generated by the Number 9 board used at MCSL. Notice that about 25% of each frame is spent on the synchronization signal. This is a large figure when we consider that this time could be used to increase the resolution or the luminance of the displayed image. The fraction of time when the video signal is not blanked is simply,

$$1 - \left(\frac{t_b}{t_f} \right) \quad (\text{A.5})$$

where t_b is the amount of time per field that the signal is blanked and t_f is the time length of each field. We will return to this expression later and use it to calculate the amount of exposure of the phosphors to the electron beam.

A.1.3.3 Voltage Levels

The EIA standardized the white level of the RS-170 video signal at 100 ± 5 IRE (IRE, Institute of Radio Engineers, is a relative scale) and the blanking level at 0 ± 5 IRE. For reasons that will be clear later, it is very important to notice that the blanking level is lower than the black level, which is defined as 7.5 ± 2.5 IRE. The black level value is usually called the setup, expressed in percent and defined as the ratio between the white and black

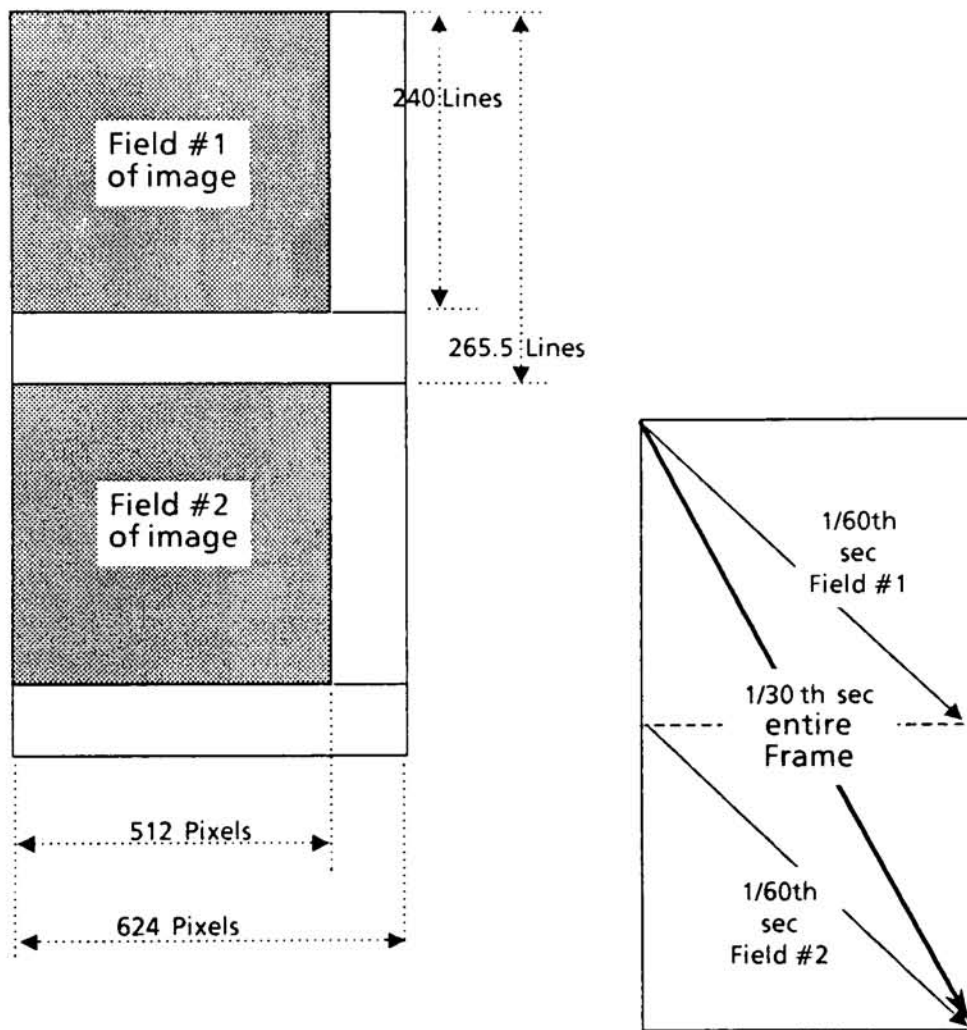


Figure A.6: Blanking and display periods of the RS-170 video signal.

levels (with the blanking level at 0). The blanking level is supposed to fall below the cutoff voltage (more about it later) to assure that when the CRT is blanked, for example during the flyback and other operations, the electron beam will not be visible. The flyback is when the electron beam moves to the beginning of the next scan line to be traced; see figure A.7. The sync level was standardized at 40 IRE nominal (i.e. absolute value). In the case of the composite signal the sync is negative from the blanking level and added to the green video, making it 140 IRE peak-to-peak (pp). Notice that no sync is added to the red and blue video signals, and they remain 100 IRE pp.

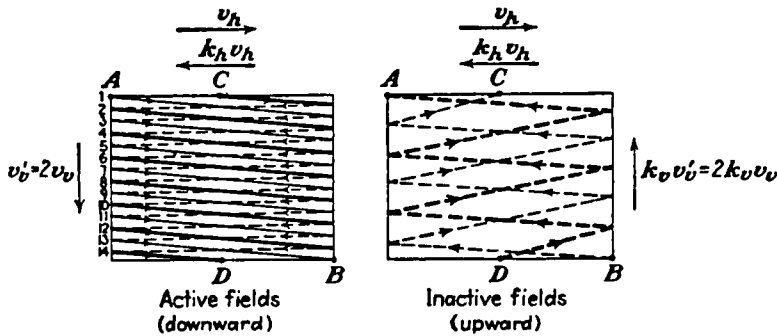


Figure A.7: Downward and upward paths of the electron beam when scanning and interlaced image.

The green composite RGB signal voltage is 1.0 volts pp including the sync, which makes the 40 IRE = 0.286 volts and 100 IRE = 0.714 volts. Nominally, these are the same voltages levels as specified for the RS-330 and RS-343 standards which the EIA has set up for high-performance and high-resolution systems. These are indicated in figure A.8.

A.1.3.4 The Effect of the Modulation Transfer Function

For a perfect system (i.e. one with no bandwidth limitations) the scanning process could be represented by a simple mapping (indicated by f) of the spatially discrete $d_{w,h}$ into time (indicated by t) resolved voltages $v(t)$, such as

$$v(t) = f(d_{g(t)}), \quad (\text{A.6})$$

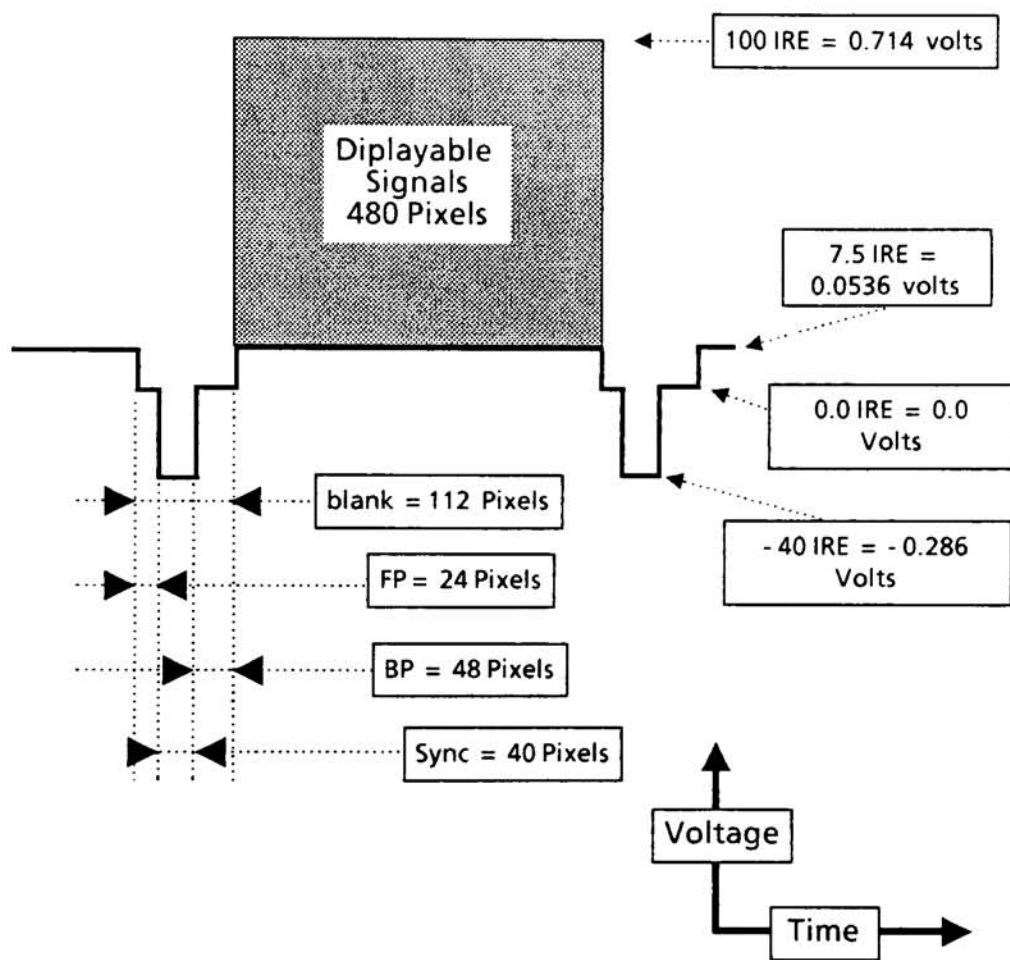


Figure A.8: Voltage values of a single line of the RS-170 signal.

where $g(t)$ indicates that the d index is a function of time. If we start at position $< 0, 0 >$ a simple rule of assignment might be

$$\begin{aligned} v(t) &= f(d_{0,0}) \\ v(t+i) &= f(d_{0,0}) \text{ while } i < \Delta t \\ v(t+\Delta t) &= f(d_{0,1}) \\ \dots &= \dots \\ v(t+n\Delta t) &= f(d_{w,h}) \end{aligned}$$

where $w + h = n$, and t is (as indicated before) around 16.8 ns.

In reality the video generator will be band-limited, having a certain raise and fall time. Thus, the video voltage will not be a simple mapping of $d_{w,h}$, and a more accurate description of $v(t)$ should take the modulation transfer function (MTF) of the video generator into account. These remarks will be true for all stages of the image formation process. The final CRT image MTF will be the result of cascading all the MTFs of the different system components.

The system MTF will have a great impact in the image appearance, since edge and surface gradients play a major role in color appearance [69, 48, 150, 170]. Sharper edges will make surfaces look more saturated and small gradients will make images look dull and of lower contrast. This will greatly increase the problem of predicting the perceived color of the CRT image, since the position of the color and its relation to its neighbors should be taken into account. If, for instance, the horizontal resolution of the CRT system is only 256 pixels, all our original 512 pixels will not be discernible and each displayed pixel will be the weighted average of at least two of the original ones. Under such conditions a pixel with 0 IRE besides another with 100 IRE could integrate to be a single pixel at 50 IRE, and predictions made on the appearance of both pixels would be wrong. Unfortunately, this is a very simplistic example. Bandwidth limitations and other artifacts stemming from the scanning process will be hard to predict and measure. Television engineers use a figure of merit for the CRT vertical resolution called the Kell factor [191], according to which a typical

television raster (525 lines/60 Hz) will only resolve 340 vertical lines (Kell Factor 0.7). For color CRTs, the microstructure of the display surface (which will be discussed later) might introduce further limitations on the system MTF.

The problems that can arise from bandwidth limitations must be taken into account in most experiments using CRTs. Mulligan [137, 138], for instance, has proposed the use of the Floyd-Steinberg [73, 194] error-diffusion algorithm to increase the number of colors displayed on the CRT when generating low-contrast gratings. The potential problem with this approach is that the error-diffusion algorithm will transform quantization errors into high frequency noise, which, to be resolvable, might require more bandwidth from the CRT system than the original image. In this case, the limited CRT system bandwidth will be a mixed blessing. In one hand it will make the noise pattern less visible, while on the other, it might make it less predictable because we usually do not know which stage of the system has the smallest bandwidth. If error-diffusion is used on a CRT system with very few discrete states (which is a situation where this kind of algorithm is very useful) the amplitude of the noise might suffer severe distortion by the system MTF. For example, several computer manufacturers use dithering to increase the number of colors displayable. Suppose that a 4 bit system (such as the one in figure A.2) obeys equation 2.5 and that one wants to create a new color between the levels given by 2 and 3 digital counts (remember, only 8 levels can be created from 3 bits). The linear additivity hypothesis suggests that an area containing an equal number of pixels on the levels 2 and 3 will visually integrate to a new intermediate level, with a luminance corresponding to the average of the luminance from levels 2 and 3. Using the simple transfer function model on section 2.1.1, the expected output can be calculated as follows,

$$\begin{aligned}
 L(v_n) &= L_{max} v_n^\gamma \\
 L_{max} &= 100 \text{ (cd/m}^2\text{)} \\
 L(2) &= 100 \left(\frac{2}{7}\right)^{2.5} = 4.36 \text{ (cd/m}^2\text{)} \\
 L(3) &= 100 \left(\frac{3}{7}\right)^{2.5} = 12.0 \text{ (cd/m}^2\text{)}
 \end{aligned}$$

and the average will be

$$L_{mean} = \frac{L(2) + L(3)}{2} = 8.19 \text{ (cd/m}^2\text{)}$$

This result assumes that the video signal can be generated with a bandwidth large enough so that neighboring pixels do not influence each other. In a real situation the video generator is band limited and some kind of smoothing of the signal will take place. Suppose that the smoothing resulted on sequences of voltage levels 2 and 3 being averaged into a new level, say, 2.5. The displayed luminance will then be

$$L(2.5) = 100 \left(\frac{2.5}{7} \right)^{2.5} = 7.62 \text{ (cd/m}^2\text{)}$$

This is a 7% difference between the predicted value and the one obtained. The significance of this difference will depend on the situation. For general image display it will probably be acceptable, but for color appearance research it will probably be too large. Recently, Mulligan reported that for the CRT monitor he tested the video signal was band-limited at the amplifying stage [138]. He further suggested that for static images this artifact could be corrected by prefiltering the image with a suitable high-pass filter, or by using a monitor with a higher bandwidth.

Our approach here is to acknowledge the existence of such problems, and limit the use of CRTs to situations where problems of this nature will not be encountered. This should be a somewhat safe strategy, since the stimuli that are used in most color appearance experiments are usually simple, consisting mostly of homogeneous surfaces with regular shapes. Complex scenes, when used, serve only as backgrounds and thus only limited knowledge about them is required.

A.1.4 The Video Equation

With the above assumptions in mind we can rewrite equation A.6 as

$$v_d = f(d'), \quad (\text{A.7})$$

from which we have eliminated the position and time dependency. Assuming that the video generator is providing a perfect RS-170 signal we can describe the signal reaching the CRT by

$$v_d = 0.66 \left[\frac{d'}{255} \right] + 0.054 \quad (\text{volts}) \quad (\text{A.8})$$

or in IRE units,

$$v_d = 92.5 \left[\frac{d'}{255} \right] + 7.5 \quad (\text{IRE}) \quad (\text{A.9})$$

where 7.5 IRE is the value of the “black”, also called the “setup”. Thus v_d will assume values between 0.714 and 0.054 volts for values of d' ranging 0 to 255, in a 8 bit system.

For the remainder of the text we will use the more general form

$$v_d = \Delta v \left[\frac{d'}{d'_{max}} \right] + v_{min} \quad (\text{A.10})$$

where $d'_{max} = 2^N - 1$, as defined by equation A.3, and

$$\Delta v = v_{max} - v_{min} \quad (\text{A.11})$$

where v_{max} is the voltage of the white level and likewise v_{min} is the voltage of the black level.

A.2 The Cathode Ray Tube Display

A CRT monitor can be divided functionally into two parts, the electronic circuit that will process the signals and drive the CRT, and the CRT itself. Figure A.9 illustrates some the circuitry commonly found in RGB composite color CRT displays. Different displays will have additional circuits. Television displays will have a tuner so that the radio signals from the TV broadcast can be picked up and turned into analog video. Systems using computer generated TTL (transistor-transistor logic) signals will place the video generator inside the CRT instead of in the computer.

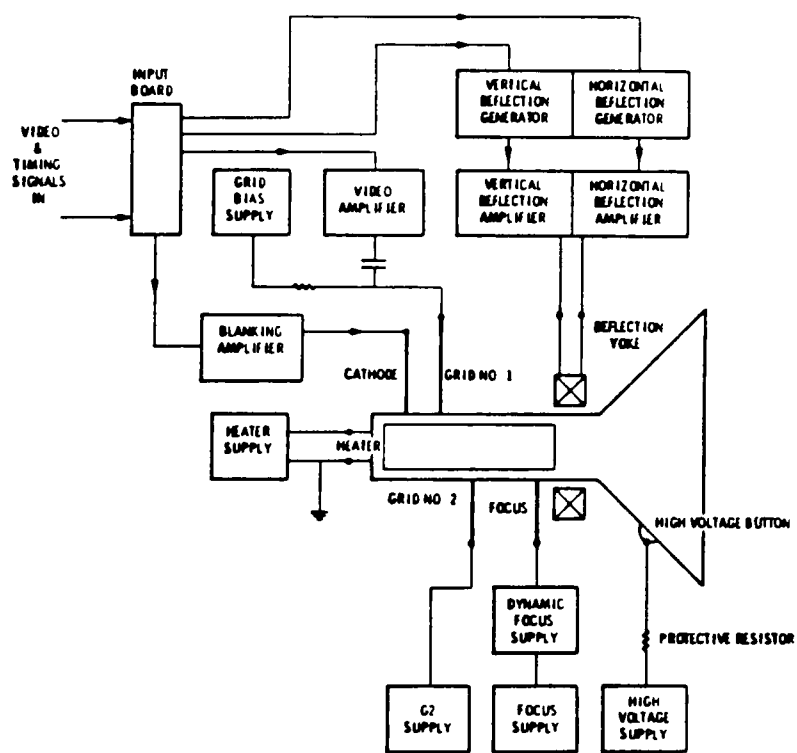


Figure A.9: Typical CRT circuit.

A.2.1 The Video Amplifier

Figure A.10 exemplifies the system at MCSL. The video voltage v_d will leave the video generator, pass through a set of cables and finally enter the circuit driving the CRT. At the CRT the video voltages will still be the same v_d if no distortions are introduced by the cables. If the cables used are too long they will present some resistance to the current, and if they are not well shielded the voltages might suffer phase distortions because of RF interference. Assuming that the values entering the CRT are different from those that left the video generator we can express v_d as

$$v_d = k_p \left(\Delta v \left[\frac{d'}{d'_{max}} \right] + v_{min} \right) \quad (\text{A.12})$$

where k_p is accounting for the loss on the electrical path.

The video amplifier will amplify the voltages so that they can drive the control grid (**G1**) on the electron gun. More about the electron gun will be said later; for the moment, it is important to know that the voltages which were originally in the range of 0.054 to 0.714 volts will be amplified to nominal values of more than 100 volts. This amplification is accomplished by the video amplifier, which is part of the circuitry driving a CRT monitor. The two main parameters for the amplification are the gain a and the voltage bias b . These two parameters are sometimes under control of the user through the “contrast” and “brightness” controls found in almost all CRT monitors. For a given video voltage v_d , the amplified voltage v_{G1} reaching the control grid can be described as²

$$v_{G1} = a k_p v_d + b \quad (\text{A.13})$$

²The reader should keep in mind that equation A.13 is applicable to each of the CRT's red, green and blue channels. The individual expressions are :

$$\begin{aligned} v_{r,G1} &= a_r k_{r,p} v_{r,d} + b_r, \\ v_{g,G1} &= a_g k_{g,p} v_{g,d} + b_g, \\ v_{b,G1} &= a_b k_{b,p} v_{b,d} + b_b \end{aligned}$$

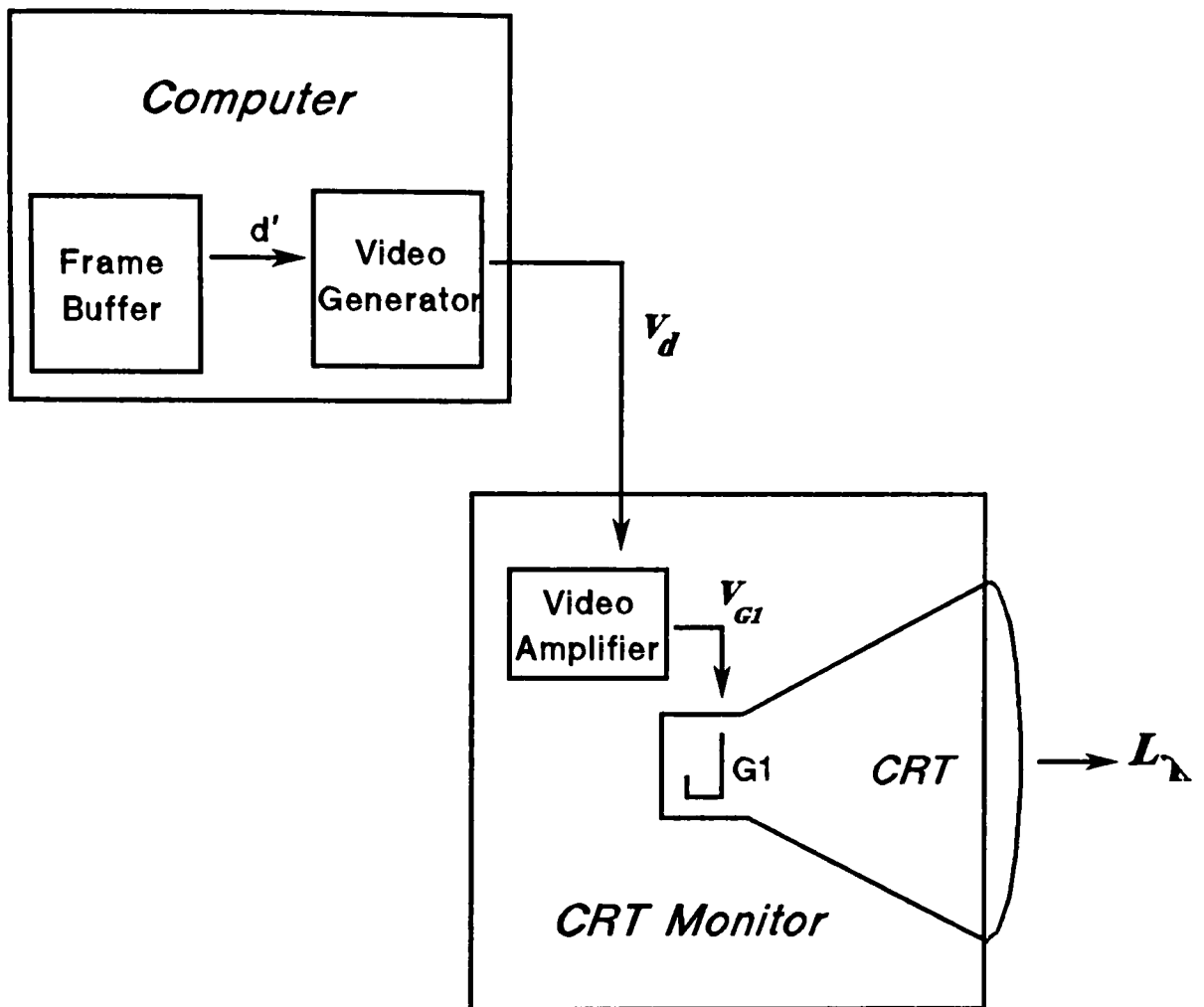


Figure A.10: The video generator and the video amplifier.

In the color CRT we have three different amplifying circuits, one for each video signal. The respective gains and biases are set so that a neutral white and a neutral gray scale are obtained for equal values of v_r , v_g and v_b . This “neutral” gray is usually around the same correlated color temperature (CCT) as the CIE illuminant D65, with black and white CRTs having a CCT as high as 9500K. The amplifying circuitry is designed so that at this setting there will be the same amount of amplification in the three circuits, with other parameters also optimized for this CCT. The two knobs controlling “contrast” and “brightness” available to the user will control the three gains and biases at once, with individual control of each available inside the CRT (as in the Barco CD 33HR), or through a side door (as in the TEK 650 HR), or a sliding drawer (as in the TEK 690 SR).

A.2.2 The Cathode Ray Tube

CRTs, as most electro-optical devices, can be quite complicated. This is compounded by the problem that the commercial success of CRT-based displays have prompted the proliferation of available designs and technologies. Figure A.11 illustrates this point. Many different kinds of tubes exist, such as beam indexed, banana, storage, penetration, multigun, flat screen, Aiken, Garbor, etc. Of interest to us is only the shadow mask color CRT. This is the most successful color CRT, and the one that we will find in most TV and computer monitors.

Another point about the scope of this discussion should be made here. A deterministic model for predicting the CRT output from a limited set of parameters is useful to the extent that the so-called *limited set of parameters* stays limited. This discussion will not cover many important aspects of the CRT electron guns, even though they could improve the model performance. This task is left to those better prepared to deal with the complexities of the CRT electro-optical design.

A cathode ray tube can be divided into five regions (figure A.12) :

I Beam forming region

II Focusing region

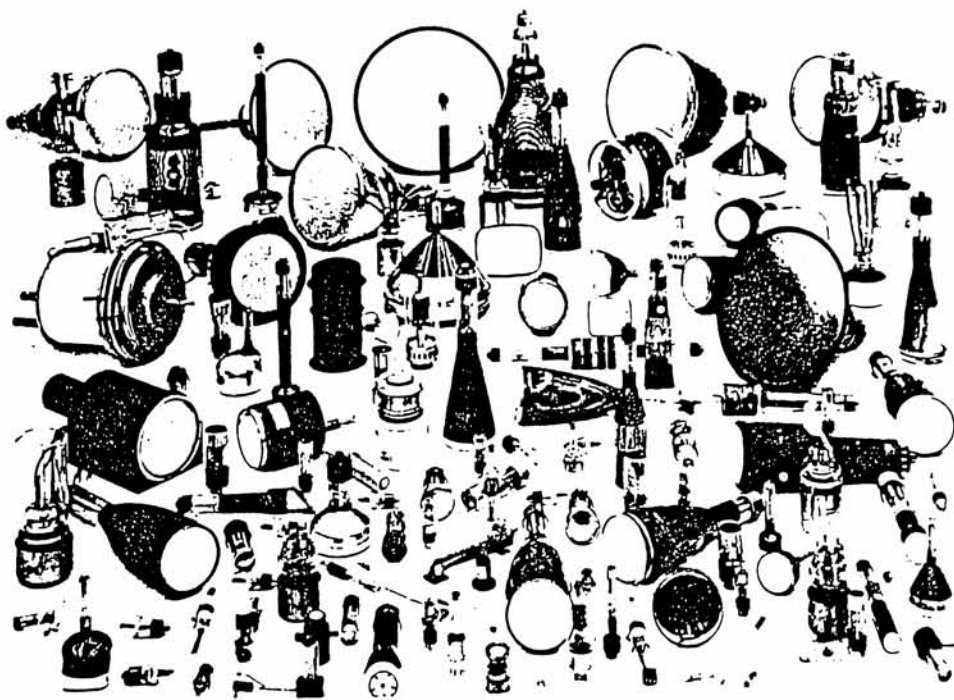


Figure A.11: Some of the different kinds of CRT available.

III Deflection region

IV Drift region

V Phosphor screen region.

This division follows that made by Lehrer [118], with the fifth region added in this thesis. The beam forming region will furnish a modulated flux of electrons that is focused into a beam and deflected by the CRT deflection yoke. This deflected electron beam will be accelerated through very high potentials, usually 25 kV from the cathode, at the ground, to the screen anode, called the Ultor. At the screen it will strike the phosphors, which will be excited and emit visible radiation when decaying from the excited state to the ground. The focusing and deflection operations are not relevant to our discussion here. We assume that

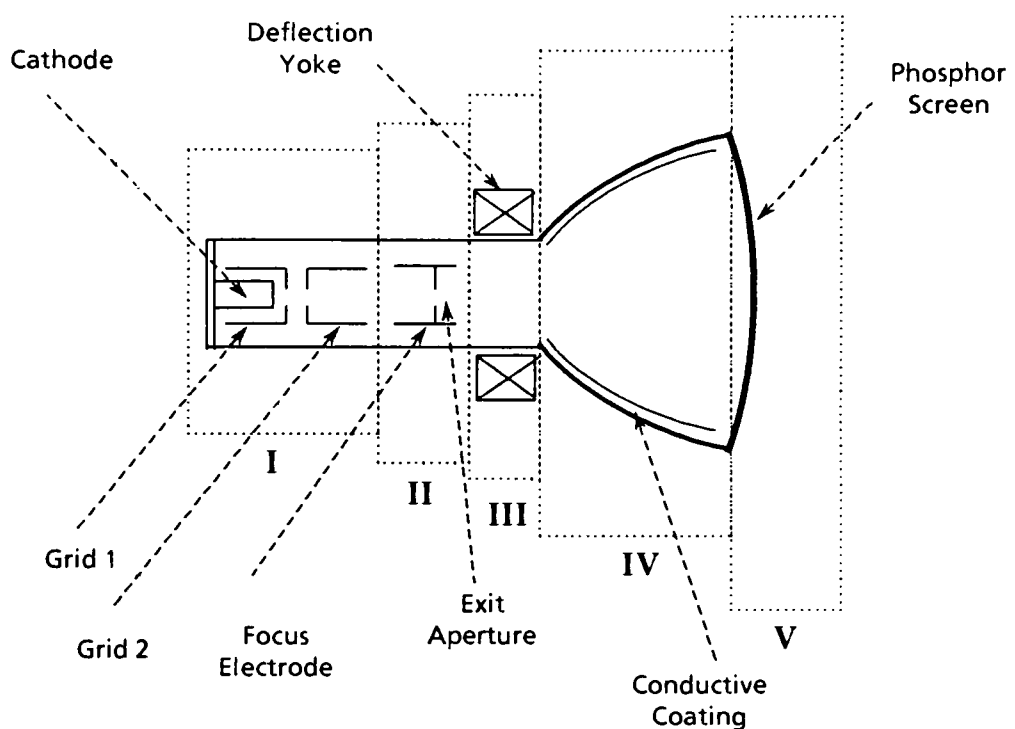


Figure A.12: The CRT divided into five regions.

they will not significantly affect the intensity of the beam reaching the phosphors. Thus, for the purpose of predicting the screen radiance from a given modulating voltage v_{G1} , we concentrate on the electron gun (region I) and the phosphor screen (region V).

A.2.3 The Electron Gun

Figure A.2.3 illustrates three of the different types of electron guns that are commonly used. Although they differ in the specific voltage potential and function of some parts, they all share some of the same basic design elements.

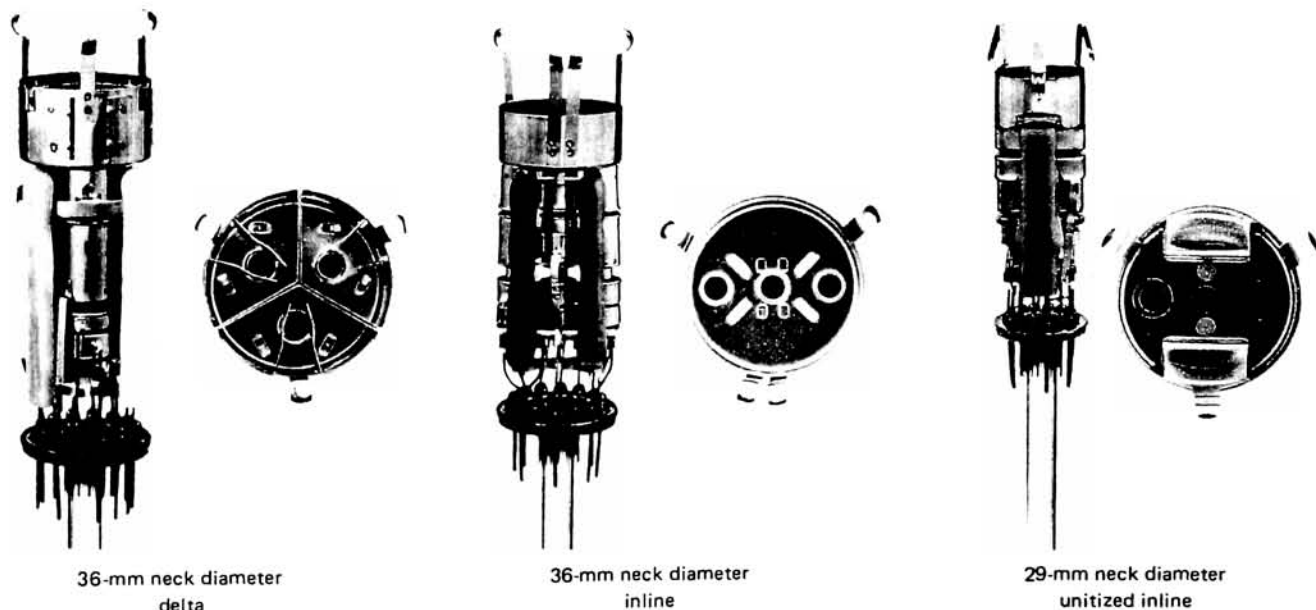


Figure A.13: Electron guns commonly used in shadow mask tubes.

Within the electron gun, the cathode is the provider of the flux of electrons that will be shaped into a beam and strike the screen phosphors. The cathode is composed of a heater

and an envelope containing some thermionic substance, such as barium-strontium oxides (oxide cathode) or some other barium compound (dispenser cathode) which emits electrons when heated. These electrons will be strongly attracted towards the higher potential of the screen, gaining through this acceleration the energy to excite the phosphors. Figure A.14 illustrate the voltage potentials typical of an electron gun used by Sony Trinitron CRTs.

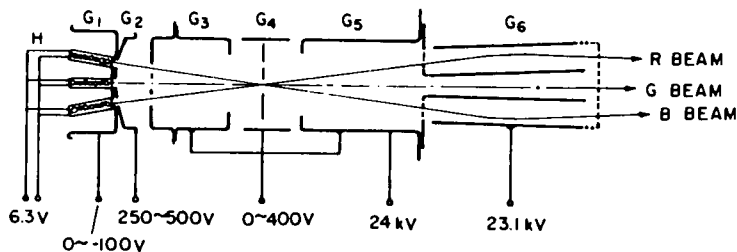


Figure A.14: In-line gun with single main-focus lens.

As we see, all the voltages except the G1 are positive with respect to the cathode, which is usually at the ground.

The first anode (G2) will be at a positive potential with respect to the cathode and will attract the electrons. To modulate the flux of electrons passing through G2 a control grid, G1, is placed between G2 and the cathode, at a negative potential with respect to the cathode. This will have the effect of repelling the negative charges of the electrons and decreasing the intensity of the electron beam. Figure A.15 illustrates the kind of arrangement common to two kinds of electron gun structures, the triode and the tetrode; our discussion should apply to both.

The relationship between the voltage bias on G1 and the beam intensity is very non-linear, as illustrated in figure A.16. It is this relation that gives rise to the non-linearity of the CRT transfer function and the exponent usually called "gamma" (represented in

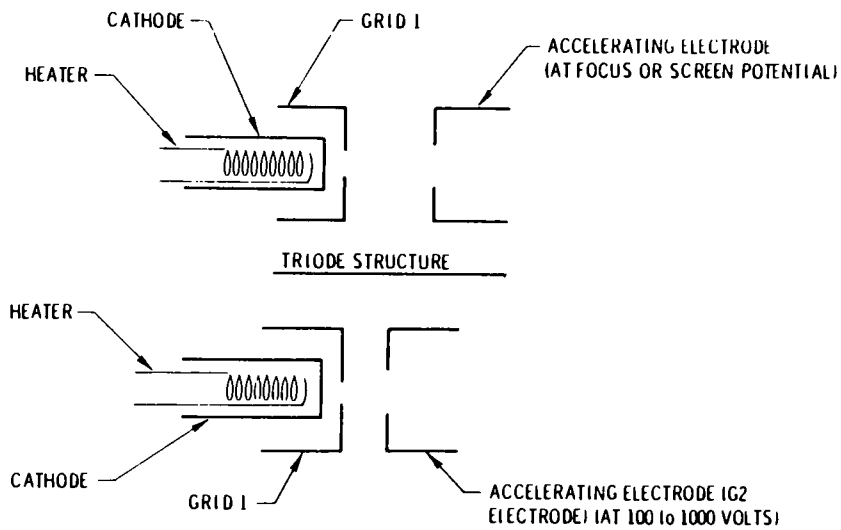


Figure A.15: Triode and tetrode structures.

equations by the greek letter γ).

One important voltage of G1 is the voltage at which the beam current reaches zero, called the cutoff voltage. The determination of this voltage is very important for the parametric characterization of the CRT performance. As it was mentioned, the voltage controlling G1 is v_{G1} , which resulted from the amplification by the video amplifier of the video signal v_d . If we call v_C the cutoff voltage we can express the voltage modulating the CRT display as a positive valued voltage called the driving voltage, or voltage above cutoff,

$$v_D = v_{G1} - v_C \quad (\text{A.14})$$

where v_D is the driving voltage and v_{G1} is the actual grid voltage. The usefulness of this definition will be clear shortly, but some drawbacks of this approach should be pointed out. The main problem is that the cutoff voltage is not a sharp boundary as the name seems to indicate. Instead, as indicated by Poole [148]:

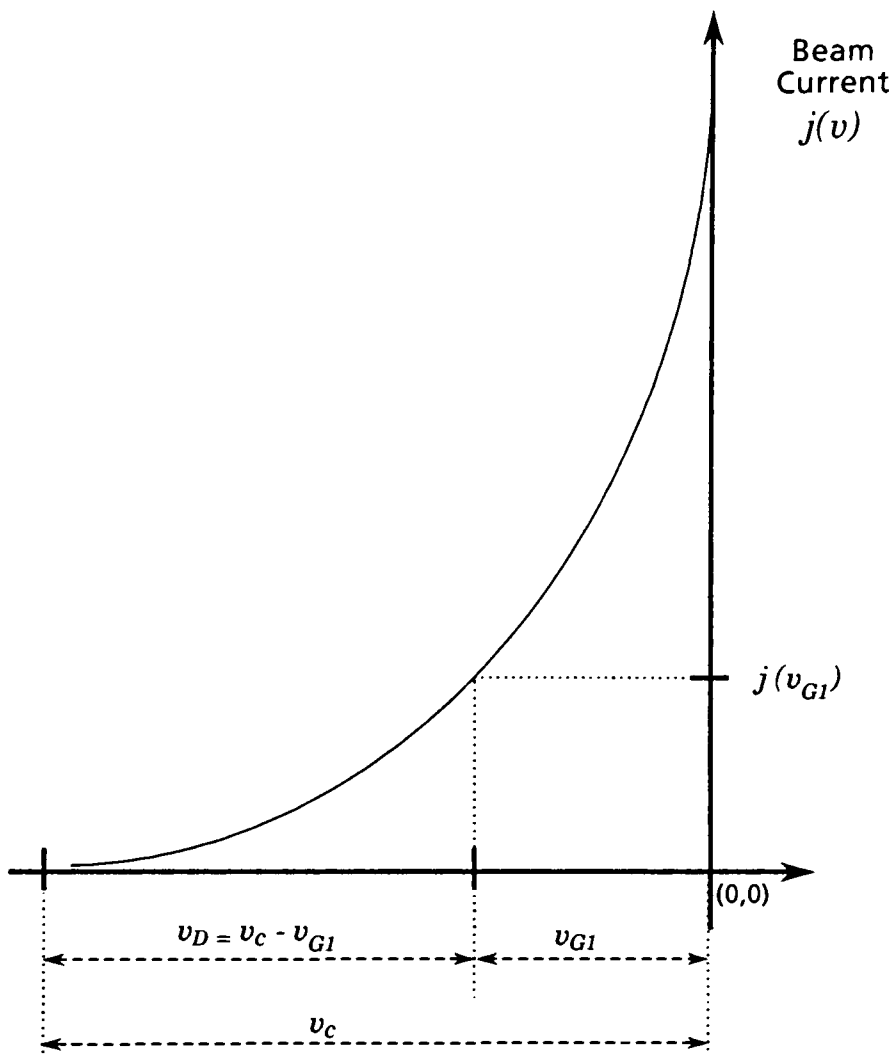


Figure A.16: The relationship between the voltage v_{G1} and the beam current.

The average velocity of the emitted electron is a function of the temperature of the cathode, and has been determined by the kinetic theory of gases to be equal to :

$$v_0 = \frac{\sqrt{2kT}}{m}$$

where v_0 is the initial velocity in centimeters per second, T is temperature in degrees Kelvin. m is electron mass, and k is Boltzman's constant. This is the average value; however, the electrons will typically have a spread of velocities from zero to twice this value.

This greatly complicates the definition of a cutoff voltage. Moss [136] recognized this, and proposed that for practical purposes the visual cutoff is accurate enough:

However ...[the velocity of the electrons] ...is Maxwellian and has no sharp maximum, so we might expect that no finite negative grid potential can completely suppress emission. Mathematically this is probably true, but for all practical purposes a "reasonably" sharp cutoff voltage is found to exist. With a triode having a cutoff around say 100 V, different observers might disagree by about ± 1 V on the exact value, if visual fluorescence of a focused spot were observed and an estimate made of the grid bias just necessary to extinguish the beam.

The importance of the cutoff voltage is that it is part of what Moss calls "the basis of a very useful engineering formula, although entirely empirical" [136]. This formula relates the beam current j leaving the cathode in a triode to v_D by:³

$$j = k_j v_D^\gamma \quad (\text{A.15})$$

³ Actually, the formula presented by Moss [136] is $j = k_j v_D^\gamma v_c^{\gamma-1.5}$. To simplify the derivation throughout the remainder of this thesis we have combined the constant term $v_c^{\gamma-1.5}$ in the above formula with k_j . This is justified since within the normal operating range of most color CRTs the cutoff voltage v_c and the gamma γ are constants determined solely by the design and other properties of the CRT, irrespective of the operating conditions or the signal being displayed.

Under the conditions that Moss determined the validity of this relation, the value of γ was 3.5. However, as Lehrer [118] points out, because of the gun design the common values will be much lower, around 2.1 or 2.2.

It should be noticed that in order to attract electrons the combination of anodes in the gun and in the tube must present a positive potential with respect to the cathode. At the cutoff the positive potentials of the Ultor and the other grids will be balanced by the negative potential of the first grid. If v_{G1} decreases even further the net potential of the tube will be negative, and no electron beam will form. Thus a more precise formula for the beam current will be

$$j = \begin{cases} 0, & \text{if } v_{G1} - v_C \leq 0 \\ k_j v_D^\gamma, & \text{if } v_{G1} - v_C > 0 \end{cases} \quad (\text{A.16})$$

For sake of simplicity we will use the original Moss' formula presented in equation A.15 for most of the following derivation. We will return to the above formula at the end of this chapter, in section 2.3.

We can expand the equation A.15 to include v_d ,

$$\begin{aligned} j &= k_j (v_{G1} - v_C)^\gamma \\ j &= k_j (a k_p v_d + b - v_C)^\gamma \end{aligned} \quad (\text{A.17})$$

and further expand to include d' ,

$$j = k_j \left(a k_p (\Delta v \left[\frac{d'}{d'_{max}} \right] + v_{min}) + b - v_C \right)^\gamma \quad (\text{A.18})$$

A.2.4 Phosphor Screen

The final destination of the electron beam is the phosphor screen, where the power of the beam will be converted into a radiant flux by the phosphors. The phosphors that comprise the screen are inorganic crystals that contain small amounts of impurities called the activators. When excited by the electron beam, such substances will go to an excited state, and when decaying to the ground state will emit visible electromagnetic radiation. This phenomena is called cathodoluminescence, and belongs to a class called luminescence, defined by Grum [80] as

... the phenomenon of the emission by matter of electromagnetic radiation that for certain wavelengths or restricted regions of the spectrum is in excess of that due to the thermal radiation from the material at the same temperature.

For a certain phosphor emitting a spectral power distribution (SPD), $S(\lambda)$, the total power emitted will be Φ_e , defined as

$$\Phi_e = \int_0^{\infty} S(\lambda) + \varepsilon M(\lambda, t) d\lambda$$

where $M(\lambda, t)$ is the radiant exitance of the blackbody at the temperature of the phosphor, t , and ε is the thermal emissivity of the phosphor. At the operating temperature of most phosphors $\varepsilon M(\lambda, t)$ is exceedingly small and can be safely ignored. With this approximation, the expression for total power emitted is simply,

$$\Phi_e = \int_0^{\infty} S(\lambda) d\lambda \quad (\text{A.19})$$

Several kinds of phosphor exist that will exhibit cathodoluminescence. Figure A.17, from reference [118], illustrates some of the ones in current use (WTDS means World Phosphor Type Designation System). Some of the principal criteria for evaluating the usefulness of a certain phosphor are the efficiency, the linearity of the response, the decay time and the “color” of the phosphor. We will discuss several of these parameters next.

A.2.5 The Energy Conversion

The relationship between the beam current j and the control grid voltage v_{G1} has been discussed before and shown to approximately conform to a power law with the exponent γ . Fortunately, the relation between beam current j and the radiant energy flux Φ_e emitted by common CRT phosphors is mostly linear. In other words, the radiant power emitted by the phosphor is proportional to the power of the beam striking the phosphor, which in turn is proportional to the beam current and the voltage across which the beam was accelerated. An early form relating the two was proposed by Lenard [72] and has the form

$$\Phi_e = k_f j (v_b - v_0) \quad (\text{A.20})$$

New WTDS Designation	Old P No.	Composition	Peak wavelength, nanometers	Decay time to 10% level	Color		Applications
					Fi	Ph	
GJ	P1	Zn ₂ SiO ₄ :Mn	525	.24 ms	YG	YG	High brightness projection
GL	P2	ZnS:Cu	543	35 to 100 μ sec	YG	YG	Scope tubes
WW	P4	ZnS:Ag + ZnS-CdS:Ag	440 565	25 μ sec 60 μ sec	W W	W	Black and white
BJ	P5	Ca WO ₄	430	25 μ sec	B	B	Photo recording
GM	P7	ZnS:Ag + ZnS-CdS:Ag	440 560	40 to 60 μ sec 6.4 sec	B UV	YG UV	Long persistence radar, scopes
BE	P11	ZnS:Ag	460	25 to 80 μ sec	B	B	Photo recording
AA	P16	Ca ₂ Mg ₂ O ₇ :Ce	385	.1 μ sec	UV	UV	Flying spot scanners, photo recording
KA	P20	ZnS:CdS:Ag	520-560	.05 to 2 msec	Y to YG	Y to YG	High efficiency, P-4 yellow component
X	P22B	ZnS:Ag	440	25 μ sec	B	B	Color TV
X	P22G	ZnS:CdS:Ag	530	60 μ sec	YG	YG	Color TV
X	P22R	Y ₂ O ₂ S:Eu	627	.9 ms	R	R	Color TV
GH	P31	ZnS:Cu	522	40 μ sec	G	G	High efficiency, scopes
GR	P39	Zn ₂ SiO ₄ :Mn:As	525	150 ms	YB	YG	Long persistence, low frame rate displays
GY	P43	Gd ₂ O ₂ S:Tb	544	1 ms	G	G	High brightness, spectral filter displays
GX	P44	La ₂ O ₂ S:Tb	540-545	1 ms	G	G	High brightness, spectral filter displays
WB	P45	Y ₂ O ₂ S:Tb	5450	2 ms	W	W	High brightness
VA	P49	YVO ₄ :Eu + Zn ₂ SiO ₄ :Mn	615 to 619 525	9 ms 24 ms	OR YG	OR YG	Penetration color, simulators
KJ	P53	YAGaG:Tb	543	7 ms	YG	YG	High brightness at low speeds

Figure A.17: List of selected phosphors.

where k_f is a constant, v_b is the beam voltage and v_0 is the voltage drop across the phosphor screen, also called "dead" voltage. This was modified by Nottingham to

$$\Phi_e = k_f j (v_s - v_0)^n \quad (\text{A.21})$$

where n is a constant, usually around 2.0, and the change in the subscript of v indicates that the voltage is measured at the fluorescent screen. Several reasons exist for this exponent on the $(v_s - v_0)^n$ term. The "dead" voltage v_0 is usually a loss in the anode potential due to the aluminized backing (discussed in more detail soon) which the electron beam has to penetrate to excite the phosphors. Although Lenard's equation accounts for this drop in potential, it does not account for the fact that an aluminized backing will reflect back light that would otherwise be lost into the tube. Since in CRTs the beam is modulated by changing the control grid voltage v_{G1} and not v_s (which would change the beam focus) the value of $(v_s - v_0)^n$ will stay constant. The constant k_f includes the efficiency of the energy

conversion, the transmittance of the face plate, and other losses to be discussed next.

A.2.6 Phosphor Efficiency

One very important characteristic of the phosphor is its efficiency. Grum [80] defined cathodoluminescence efficiency as “the ratio of the emitted power to the power of the electron beam falling on the phosphor.” The following passage is from Poole [148]:

Not all of the beam’s energy will be used for light output. Besides heat and quencher center recombinations, the incident electron can also lose energy in other ways. Backscattering, or the loss of incident electrons by re-emission, is one important effect. The radiation resulting from the change in momentum of the incident electron while scattering is called bremsstrahlung. This also results in the emission of a photon, but the wavelength is much too long to be visible. If an aluminized backing is used on the phosphor, more energy will be lost by penetration of this material. Actually two losses are present – backscattering and penetration loss. Other factors which contribute to loss in beam energy without corresponding light output are the production of secondary electrons and Compton scattering. In addition, a number of the emitted photons are lost by internal scattering, reflection, and absorption in the phosphor. It can therefore be seen that quite a number of effects limit the efficiency of the phosphor.

The power density of the beam, p , reaching the phosphor will be

$$p = j(v_s - v_0) \text{ (watts)} \quad (\text{A.22})$$

The energetic efficiency η_e of the phosphor will then be

$$\eta_e = \frac{\Phi_e}{p} \quad (\text{A.23})$$

which is expressed as a fraction or in percent (%). Expanding the above we have

$$\eta_e = \frac{k_f j (v_s - v_0)^n}{j (v_s - v_0)} = k_f (v_s - v_0)^{n-1} \quad (\text{A.24})$$

which shows that efficiency should increase with the screen potential. The relevancy of the value obtained for η_e will be dependent on the application. If for a certain phosphor η_e is very high, but all the power of the emission is concentrated on the infrared (IR), this phosphor would have little use for visual displays. A figure with more merit for CRTs is the luminous efficiency η_v , which takes into account the eye sensitivity to the emitted SPD. This is done by calculating the luminous flux Φ_v resulting from $S(\lambda)$, which is accomplished by weighting it by the spectral luminous efficiency function $V(\lambda)$ of the average human observer [201]

$$\Phi_v = 683 \int_{380nm}^{830nm} S(\lambda)V(\lambda)d\lambda \text{ (lumens)} \quad (\text{A.25})$$

thus obtaining a photometric value for Φ_v . The η_v of the phosphor is then expressed for a certain area as the ratio between the luminous flux Φ_v and p , the power density of the excitation

$$\eta_v = \frac{\Phi_v}{p} \text{ (lumens/watt)} \quad (\text{A.26})$$

Ideally all three phosphors should have the same “color matching” efficiency [181], so that a white can be achieved for equal amounts of beam current on the three guns. As Morrel [135] states:

Unit current ratio is desirable for two reasons. First, it would then be easier to match drive characteristics of the three guns to obtain a non-varying white color temperature as a function of beam current or brightness. Second, brightness would be enhanced since each gun could then be used up to its capability of supplying current limited only “spot blooming” instead of the limitation being set by the gun that is used for the weak phosphor.

The color of the “white” that should be used to balance the guns is a subject open to discussion. In a 1968 article Hirsch [92] stated that in early color television the CRT manufacturers would set the white at 9300 K because of the earlier black and white practice, and because this way the “brightness” of the image could be increased despite the small dynamic range of the red phosphor (to be discussed next). With the more efficient red

phosphors the 6500 K white recommended by the NTSC should have become the standard, but the CRT manufacturers are slow to change their practices. A more complicated, and important, aspect of this problem is to determine why the normalization at 6500 K works at all [123]. It is not intuitive why a scene under tungsten illumination (around 2800 K) has to be color corrected to 6500 K to look natural in a television set viewed under the same tungsten illumination.

A.2.7 Deviations from Linearity

Expression A.21 on page A.2.5 will fit most of the useful range of the phosphor, except at very high beam currents, when the phosphor becomes saturated and the relationship is no longer linear. There are several reasons for this occurrence. In a color CRT the phosphor dots are made up of small phosphor crystals (called grains) dispersed in a binder and deposited by a photomicrolithographic process on the inner face of a glass panel, called the face plate. The size of the phosphor grains will have an important effect in the screen brightness. Coarser grains will scatter more light, decreasing the image resolution because of the internal spread of light (usually called “halation”, see figure A.18) and will require a larger amount of binder, thereby decreasing the efficiency and luminance.

On the other hand, larger grains will have a larger number of excitation sites, increasing the probability that the energy of the electron will be converted into radiant energy. This is very similar to what happens in silver halide photography. The ability to capture electrons, or photons, increases linearly with the grain diameter (the projected area) while the number of sites that can trap these electrons increases with the square of the diameter (the volume of the grain). Because the number of sites will increase faster than the exposed area, larger grains are more efficient. One of the important consequences of this behavior is that it limits the maximum luminous radiance that can be achieved on high resolution screens. To be homogeneous, the smaller dot size will require smaller phosphor particles, making the screen less efficient, easier to saturate and less luminous.

On top of the phosphor layer (facing the interior of the tube), an aluminum layer with

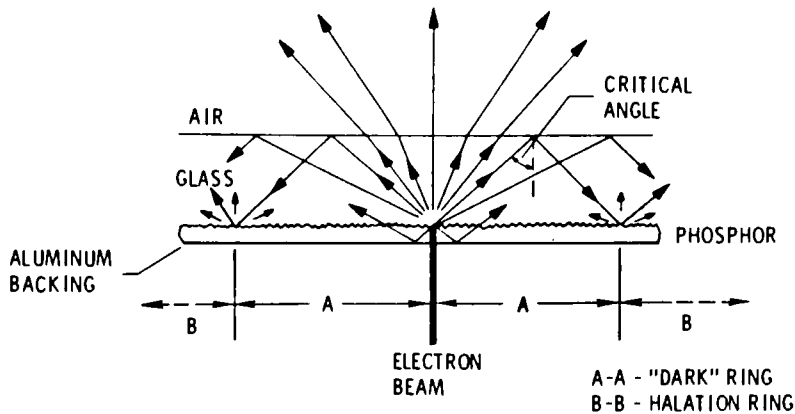


Figure A.18: Internal reflections on the phosphor screen.

conductive properties is also deposited. This aluminized backing is needed to disperse the electrons from secondary emission. If such electrons stay around the phosphor they will lower the anode potential and reduce the radiance from the screen. Besides secondary emission, the screen might also become saturated because the electrons are not being absorbed at a high enough rate. This would be the case with too frequent scans or phosphors with excessively long persistence.

Another function of the aluminized backing is to prevent heat saturation. Small increases in temperature might actually make the phosphors more efficient ([180], p.619), since less energy from the electron beam will be necessary to send it to the excited state. But at very high temperatures the phosphors will saturate and might actually be damaged by the heat. Notice that heat dissipation is also important to avoid very large gradients in the glass face-plate, since the strain from the localized thermal expansion could break the glass.

Another factor limiting the linearity is that at very high currents the beam will tend to defocus, an effect usually called “blooming”. The spread of the electron beam happens because there is a limit, called the space charge limit [115], to how much repelling charges such as electrons can be concentrated. The combined effect of phosphor saturation and beam spread will set the operational limits for a CRT. As the CRT ages the phosphors

become less efficient, either because of the destruction of the phosphors by the electron beam or by contamination to ions produced within the tube. Thus older CRTs will tend to bloom at screen luminances much lower than originally. If the CRT was used for a fixed kind of display, like the bank's ATM machines, the pattern of degradation can be quite visible.

A.2.8 Phosphor Decay and Dwell Time

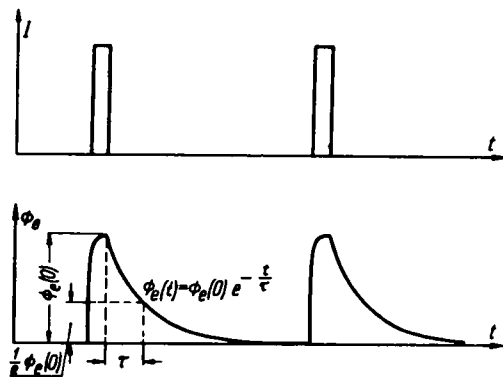


Figure A.19: Temporal profile of exciting electron pulse and phosphor decay.

Since luminescence is triggered by external sources it should also be expected that its duration is dependent on the duration of the external stimuli. With fluorescence, the excited electrons will decay directly from the excited state to the ground state, making it a very short lived phenomena, usually in the order of 10^{-8} seconds. With phosphorescence, the radiant energy results from the decay of the electrons from an intermediate state of excitation called the triplet state. Depending on the length of this decay phosphors are classified as having short, medium or long persistence. To have very long persistence two layers of phosphors are used, one absorbs the electrons and emits UV radiation, the other

(closer to the glass) absorbs UV and emits visible radiation. In general, the phosphor decay follows an exponential decay, which can be expressed as [98]

$$\Phi(t) = \Phi(0) \frac{e^{-t}}{\tau} \quad (\text{A.27})$$

where $\Phi(0)$ is the peak radiant flux from phosphor, and τ is the time it takes the phosphor to decay to 10% of $\Phi(0)$ (see values listed on table A.17). Long persistence phosphors follow a hyperbolic relation

$$\Phi(t) = \Phi(0) \frac{\beta^\alpha}{(\beta + t)^\alpha} \quad (\text{A.28})$$

where α and β are constants characteristic of a given phosphor.

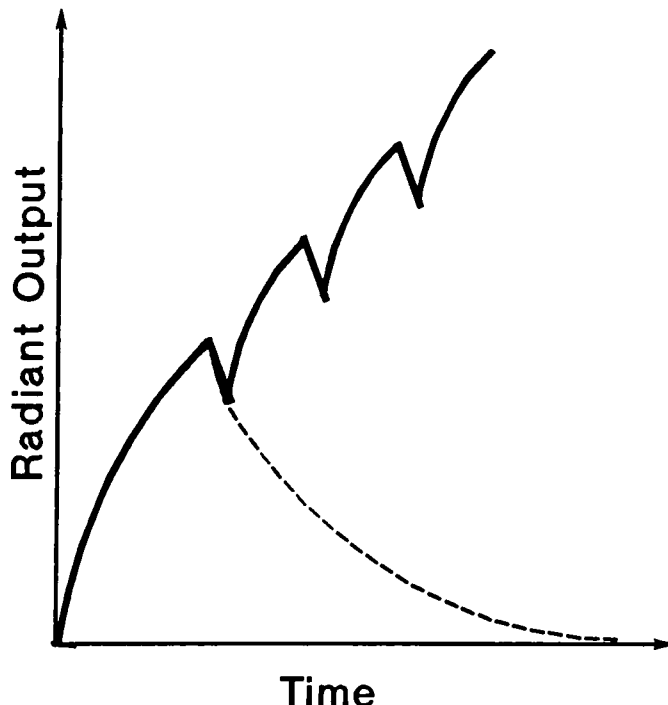


Figure A.20: Luminance buildup with repeated excitation.

For a raster scan display the decay characteristics of a set of phosphors will have mixed consequences. If the scan period is shorter than the phosphor decay time, there will be a period, counting from the start of the excitation, during which the screen response will

build up. The phosphor will be excited again before it decays completely (see figure A.20), and the resulting stabilized emission will have an offset (the carry over from previous scans) and a fluctuation from the present scan.

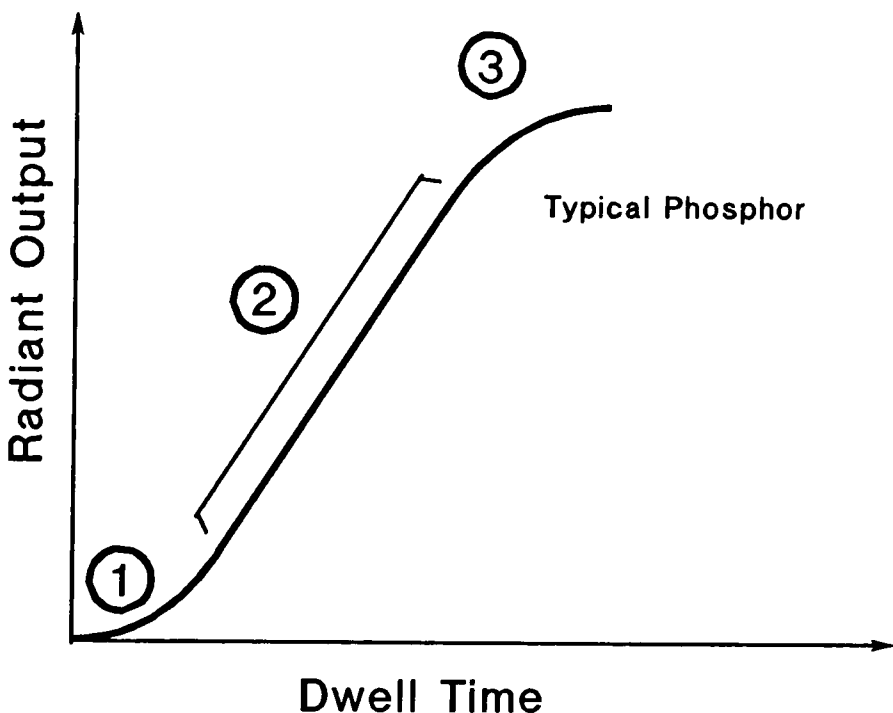


Figure A.21: Relation between the dwell time and phosphor output.

Depending on the phosphor, the frequency of the scan, and the beam intensity, the screen will saturate at different levels of radiance. This can be understood in view of the points raised above concerning phosphor saturation and efficiency. Figure A.21 illustrates the dependency of the phosphor output on the dwell time, which is the time of the exposure of the phosphor to the electron beam. In portion 1 of the curve the efficiency is increasing. The time of exposure is very small and a significant portion of the electrons is lost by backscattering, and other processes. Probably at this stage the temperature is still too low to allow the phosphor to easily pass to the excited stage, nor are all the excitation centers being occupied. In part 2 of the curve, the increase in the radiant output is linear

with respect to increases in the dwell time. This kind of behavior obeys what is called the Bunsen-Roscoe law [83], which states that the result from a photochemical reaction is a product of the total time exposure involved and the total energy of the exposure. This law, also called the reciprocity law, is usually summarized as [80]

$$H(\Delta t) = \int_t^{t+\Delta t} E_p dt \quad (\text{A.29})$$

where $H(\Delta t)$ is the photon (electron) exposure during the period Δt , and E_p is the photon irradiance, or in our case the electron flux. If E_p is independent of time, we have the familiar equation $H = E \Delta t$ (or $E = It$ as is often, mistakenly, presented in the photographic literature). Part 3 of the curve corresponds to the saturation stage, discussed already in detail. In this portion increases in the dwell time do not have a correspondent increase in the phosphor output since all the exposure can not be efficiently converted into radiant energy.

For a given CRT with total image area A_T , a smaller area A_p will be exposed to the electron beam during only a fraction of each frame period. This fraction is

$$\frac{A_p}{A_T} \left(1 - \frac{t_b}{t_f}\right) \quad (\text{A.30})$$

where the expression $\left(1 - \frac{t_b}{t_f}\right)$ is the fraction of each frame that is not blanked (equation A.5, section A.1.3.2). Assuming that over area A_p the electron beam current j is constant, the amount of power being transferred to the phosphors is simply

$$p = j (v_s - v_0) T_m \frac{A_p}{A_T} \left(1 - \frac{t_b}{t_f}\right) \quad (\text{A.31})$$

where T_m is the transmittance of the shadow mask, to be discussed in more detail on section A.3.1. If, moreover, we can assume that this exposure is within the linear range of the phosphor response (region 2 on figure A.21), the total radiant flux will be

$$\Phi_e = k_f \eta_e j T_m (v_s - v_0) \frac{A_p}{A_T} \left(1 - \frac{t_b}{t_f}\right) \quad (\text{A.32})$$

On section A.2.11 we will further expand this formula by expanding the spectral terms and thus eliminating the need for k_f .

A.2.9 Flicker

Another very important consequence of the phosphor decay is what is called flicker. The intermittent nature of the screen emission might cause the observer to see a flashing image, with strong modulation over short periods of time. Flicker can be very annoying and distracting. For the image to appear stable over time there are two solutions either the repetition rate or the length of each exposure have to be increased. On motion pictures this is accomplished by showing each frame (recorded at 24 frames per second, fps) twice by means of a shutter with, usually, four sections. The resulting image is modulate at 48 fps and the flicker is not as noticeable. With CRTs there are several ways of reducing flicker :

- Phosphors with longer persistence.
- Increased scanning rates.
- Interlacing of frames.

The application of the CRT display will govern the kind of solution used, usually a combination of the three. The interlacing of frames is similar to what is done in motion pictures. An entire frame with n lines is divided into two fields with $\frac{1}{2}n$ lines, where each field represent every other line of the original frame. Since each field contains half of the information of the original frame it can be transmitted twice as fast with the same bandwidth, reducing the apparent flicker. This technique is standard in the NTSC system, with each field being show at 60 Hz, and the entire frame at 30 Hz. Many computer generated displays are interlaced, because it reduces the price of the components. The problem is that the static quality of most computer generated images might make the flicker visible. Several applications such as CAD, character generation and business graphics, will use thin lines over a dark background. If a line consists of a single horizontal row of pixels it will be scanned on the CRT at 30 Hz, with the flicker becoming very visible depending on the color and the intensity of the line. Wider or blurry horizontal lines will tend not to flicker since they will contain portions that are refreshed at the field rate. To avoid flicker and the consequent visual fatigue, computer displays have recently departed further from

the traditional video rates by presenting non-interlaced images at field rates as high as 80 Hz.

As was mentioned, if the repetition rate is too high for a certain phosphor it will saturate more easily. On the other hand, if it is too low the display will flicker. Even if the repetition rate of the scan and the decay time are matched the combination might not be suitable. If the decay is long and the repetition slow the display might be suitable for the display images containing small time transients, such as radars, oscilloscopes and some kinds of engineering drafting and medical images. On the other hand, a long persistence display will not be suitable for the display of fast moving objects, such as pictorial films and most interactive computer usage (such as graphic animation and data entry). For such displays, a faster scan rate and faster decaying phosphor are needed. This short persistence display could obviously substitute a longer persistence display for any task, but the data would have to be generated faster, increasing the cost of the hardware with no tangible benefit.

The figure of merit when evaluating the amount of flicker is the critical fusion frequency, also called critical flicker frequency (CFF) [193, 70, 102]. It can be loosely defined as the highest repetition frequency at which temporal modulation is noticeable (or alternatively as the lowest frequency at which modulation is not noticeable). The problem with this definition is that the temporal response of the visual system is very dependent on the temporal profile, edges, color, luminance and location of the stimuli. If a stimulus has sharp edges it will flicker even at higher frequencies, because the involuntary movements (saccades) that the eye performs to keep the retina from saturating [155, 116, 202] will be out of phase with the borders, creating a visible beat pattern. The temporal profile, color and intensity will change the CFF because the three cone systems have different response and regeneration times. Finally, higher CFFs are found on the perifovea and periphery of the retina, where the number of rods and cones decreases and the cortical magnification factor increases [164, 200]. This has evolutionary advantages (detection of moving targets) but presents problems in an environment which surrounds one with CRTs (such as in a flight simulator or a modern cockpit).

For most color appearance experiments, flicker might represent a problem. Because the three cone systems have slightly different reaction times, the perceived color will change for large transients. This kind of effect is especially visible in the Benham, or Fechner, disks, which consist of concentric stripes of different lengths that will elicit very unsaturated color sensations when rotated at a low speed (around 20 Hz) [16]. Vingrys [195] and associates have reported that “since the Weber fraction for human vision is typically about 2%, Roufs’ model [which predicts the visual response to temporal variations in light] predicts that an equiluminous step change from green to red would produce a detectable luminance transient due to phosphor temporal characteristics.” He concluded, though, that for the dynamic range of phosphors used in CRTs, this kind of luminance transient would be noticeable only on extreme cases, such as the already mentioned equiluminous green to red transition. One other limitation that the repetition rate might impose is on the experimentation with animals. Rodieck [134] reported that “cats, monkeys and perhaps many other small animals have cells with flicker-fusion frequencies higher than those of humans, and these cells readily synchronize their firing to the broadcast [60Hz] field rate.” He found that a field rate of 200 Hz would be needed on his experiments with cats.

Despite the above, color matching and related experiments should not be severely affected by the CRT flicker. For most matching experiments the test stimuli is viewed by the fovea, the temporal modulation is quite slow, and there is no evidence of color shifts at or near the CFF.

A.2.10 Composition of the Phosphors

The red phosphor used in early television sets was notorious for being inefficient. A beam current ratio of 2:1:1 would be needed for achieving a white. Besides that, the phosphor would bloom at moderate currents and would not have the desired SPD constancy. The result was that highlights or strong reds on the television image would desaturate, turn orange and “bleed” into the adjacent areas. This situation was remedied by the introduction of the YVO₄:Eu (europium-activated yttrium orthovanadate) by Levine and Palila [120]

from the GTE laboratories in 1963.

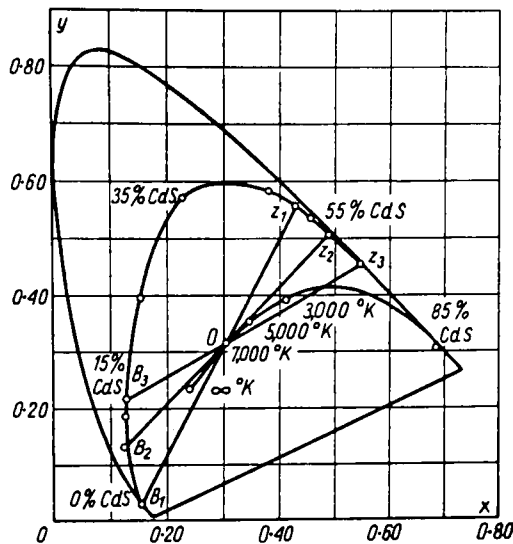


Figure A.22: Chromaticities of different compositions of $(\text{ZnS},\text{CdS}):\text{Ag}$ phosphors.

The so called all-sulfide phosphor system was used originally in color CRTs. Combinations of ZnS (zinc sulfide) or CdS (cadmium sulfide) with Ag (silver) as an activator, will yield a broad range of dominant wavelengths, going from blue to red through green as the proportion of Cd in the mixture increases (see figure A.22).

This phosphor set comprised a ZnS:Ag blue phosphor, a $(\text{ZnS},\text{CdS}):\text{Ag}$ green phosphor and with a higher amount of Cd, a $(\text{ZnS},\text{CdS}):\text{Ag}$ red phosphor. The emission spectra from such phosphors is broad (more than 40 nm half-width) and gaussian like, which limits their maximum colorimetric purity (see figures A.27 and A.28). To achieve the desired purity the emission of the red phosphor had to be corrected by a didymium glass filter incorporated to the face plate.

Figure A.23 illustrates the developments in phosphor composition that have taken place. The more efficient phosphors also brought a smaller color gamut as is shown on table A.24 and illustrated in figure A.25.

The YVO₄:Eu phosphor presented several advantages over the old ZnS,CdS:Ag formula-

Red:	<ol style="list-style-type: none"> 1. Cadmium borate : manganese 2. Zinc orthophosphate : manganese 3. Zinc selenide : copper 4. Zinc cadmium selenide : copper 5. Zinc cadmium sulfide : silver 6. Yttrium orthovanadate : europium 7. Yttrium orthovanadate : bismuth : europium 8. Yttrium oxysulfide : europium 9. Yttrium oxide : europium (limited use) 10. Gadolinium oxide : europium (limited use)
Green:	<ol style="list-style-type: none"> 1. Zinc orthosilicate : manganese (low conc.) 2. Zinc orthosilicate : manganese (high conc.) 3. Zinc aluminate : manganese 4. Zinc cadmium sulfide : silver 5. Zinc cadmium sulfide : copper : aluminum
Blue:	<ol style="list-style-type: none"> 1. Calcium magnesium silicate : titanium 2. Zinc sulfide : silver 3. Zinc sulfide : magnesium

Figure A.23: Phosphors and activators listed in chronological order of commercial use.

tion. As figure A.26 illustrates, the SPD of a modern red phosphor is quite peaked, resulting in an increase in the colorimetric purity. The rare earth phosphors are also more efficient and do not bloom or change their SPD as much as the sulfide red phosphor at high beam currents. On the practical side, this type of phosphor is also easier to work with, since it does not absorb in the UV as the sulfide phosphor does, making the photo-fabrication of the screen easier.

A.2.11 Screen Radiance

We expand our analysis to the description of the spectral distribution of the energy emitted by the CRT by noting that the only terms with wavelength dependency are the phosphor efficiency, $\eta_{e,\lambda}$, and the face-plate transmittance, $T_{s,\lambda}$. Summarizing the results thus far, a more complete formula for the spectral flux irradiating from an area A_p on the phosphor

Phosphor Set	Date Used (Approx.)	Red		Green		Blue	
		x	y	x	y	x	y
NTSC	(1953)	.670	.330	.210	.710	.140	.080
54	1954	.674	.326	.218	.712	.146	.052
61	1961	.663	.337	.285	.600	.155	.060
64	1964	.650	.325	.260	.600	.157	.047
69	1969	.628	.337	.300	.600	.150	.068
70	1970	.640	.335	.330	.590	.150	.070
71	1971	.623	.342	.326	.591	.155	.067
72-1	1972/3	.638	.334	.324	.591	.149	.074
72-2	1972/3	.625	.339	.337	.574	.151	.070
72-3	1972/3	.618	.339	.316	.592	.153	.074
Tek 690 5R	1982	.656	.320	.313	.598	.145	.063
Barco CD33hr	1983	.640	.334	.307	.589	.141	.057
Tek650 HR	1986	.664	.305	.287	.606	.143	.049

Figure A.24: Chronological evolution of phosphors chromaticities.

screen will be:

$$\Phi_\lambda = j (v_s - v_0) T_m T_{s,\lambda} \eta_{e,\lambda} \left(\frac{A_p}{A_T} \right) \left(1 - \frac{t_b}{t_f} \right) \quad (\text{A.33})$$

The terms in the equation are :

- Φ_λ radiant flux , Watts,
- j - beam current, Amps,
- T_m shadow mask transmittance,
- $T_{s,\lambda}$ screen transmittance,
- $\eta_{e,\lambda}$ phosphor efficiency,
- $(v_s - v_0)$ voltage from cathode to screen, Volts,
- (A_p/A_T) fraction of screen irradiating the flux,
- $(1 - t_b/t_f)$ fraction of time the beam is blanked.

CIE 1931 – 2 Degree Observer

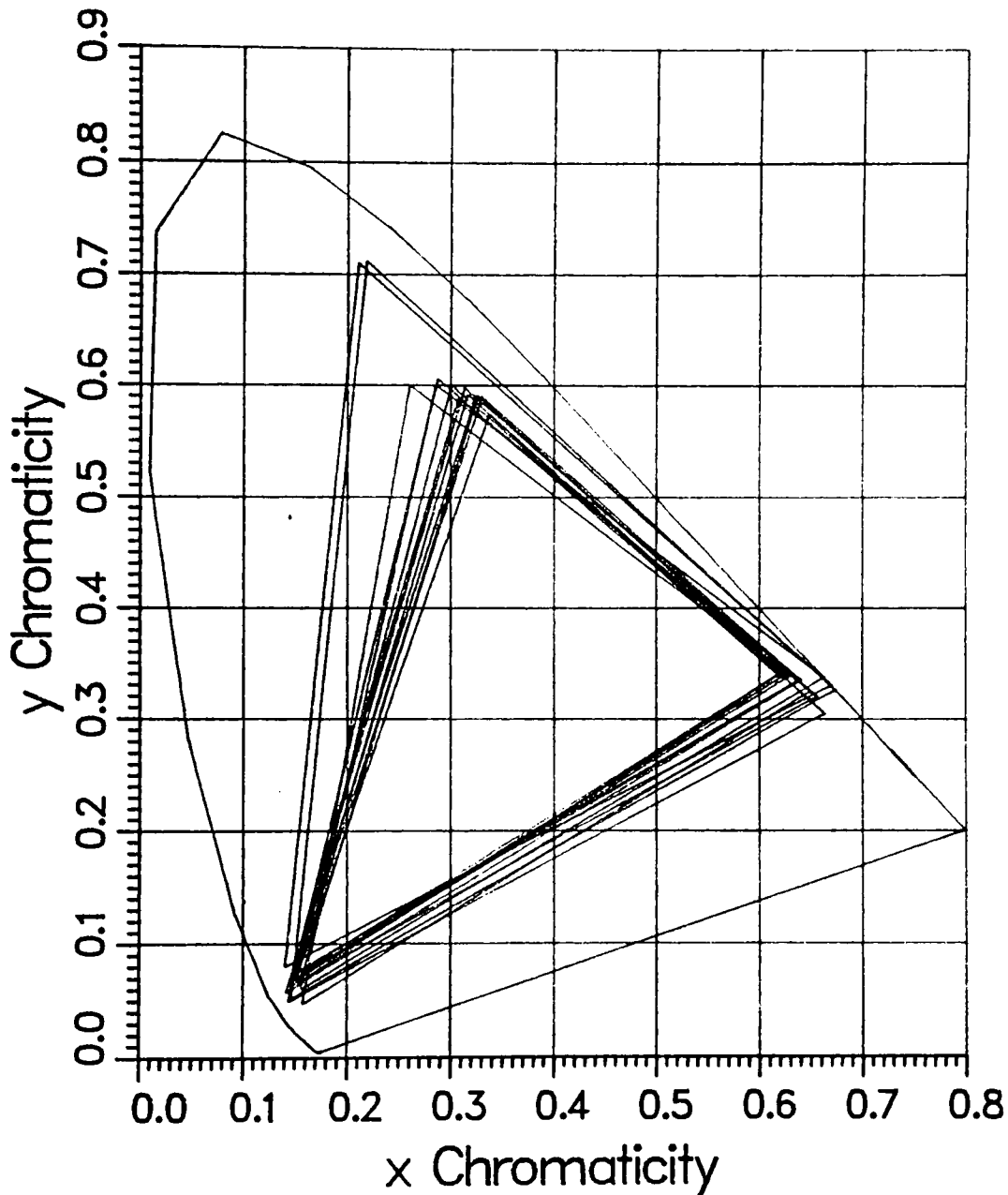


Figure A.25: Data from the previous table plotted on the CIE 1931 chromaticity diagram.

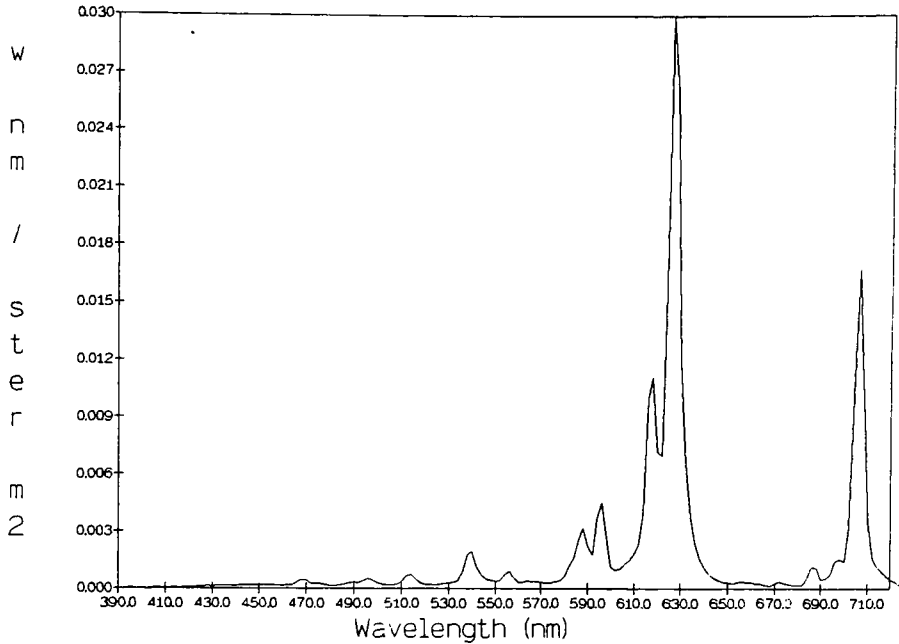


Figure A.26: SPD of Tektronix 690 SR red phosphor.

The spectral radiant exitance of a certain area element is defined as [80]

$$M_\lambda = d\Phi_\lambda / dA \text{ (watts/m}^2 \text{ nm)} \quad (\text{A.34})$$

or, if we assume a uniform screen,

$$M_\lambda = \Phi_\lambda / A_p \quad (\text{A.35})$$

and we can rewrite A.33 as

$$M_\lambda = j(v_s - v_0) T_m T_{s,\lambda} \eta_{e,\lambda} \left(\frac{1}{A_T} \right) \left(1 - \frac{t_b}{t_f} \right) \quad (\text{A.36})$$

If we further assume that the phosphor screen is Lambertian, i.e. emits radiation equally in all directions, we can calculate the spectral radiance L_λ of the screen from the simple relationship :

$$L_\lambda = M_\lambda / \pi \text{ (watts/m}^2 \text{ nm sr)} \quad (\text{A.37})$$

This relationship is easily derivable from the definition of radiance [14].

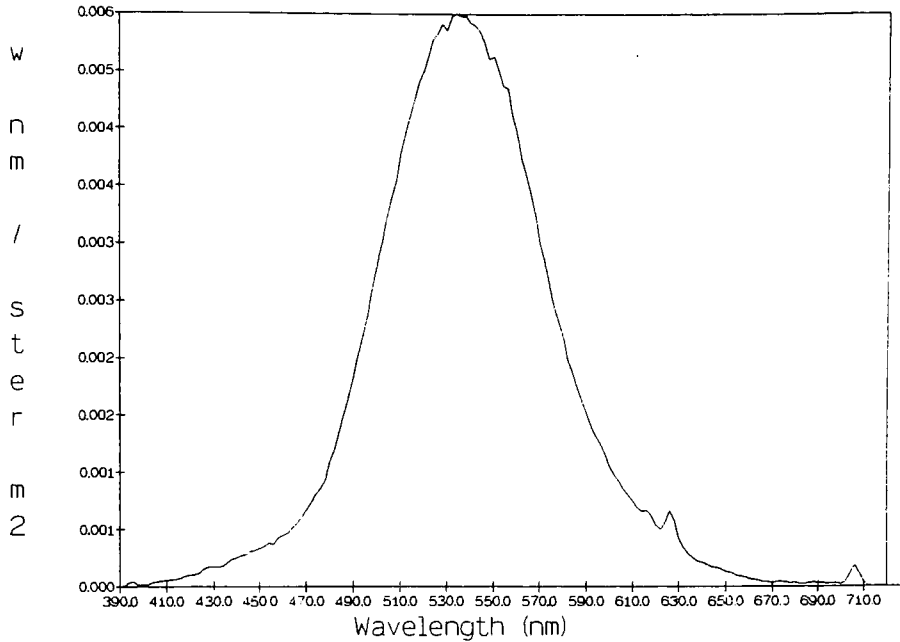


Figure A.27: SPD of Tektronix 690 SR green phosphor.

We can now express the spectral radiance from the CRT faceplate as

$$L_\lambda = j(v_s - v_0) T_m T_{s,\lambda} \eta_{e,\lambda} \left(\frac{1}{\pi A_T} \right) \left(1 - \frac{t_b}{t_f} \right) \quad (\text{A.38})$$

By rearranging the variables and introducing the expression for the beam current derived before (A.18), we have finally arrived at an expression for the absolute value of the spectral radiance from a CRT as a function of digital counts:

$$L_\lambda = k_j \left(a k_p \left(\Delta v \left[\frac{d'}{d'_{max}} \right] + v_{min} \right) + b - v_C \right)^\gamma \left(\frac{(v_s - v_0) T_m T_{s,\lambda} \eta_{e,\lambda}}{\pi A_T} \right) \left(1 - \frac{t_b}{t_f} \right) \quad (\text{A.39})$$

A.2.12 Phosphor Constancy

The SPD of the phosphor, as that of most luminescent materials, depends mostly on the phosphor composition, determining which kind of transitions will occur when the phosphors are excited. Ideally, different levels of excitation will only result in different amounts of the

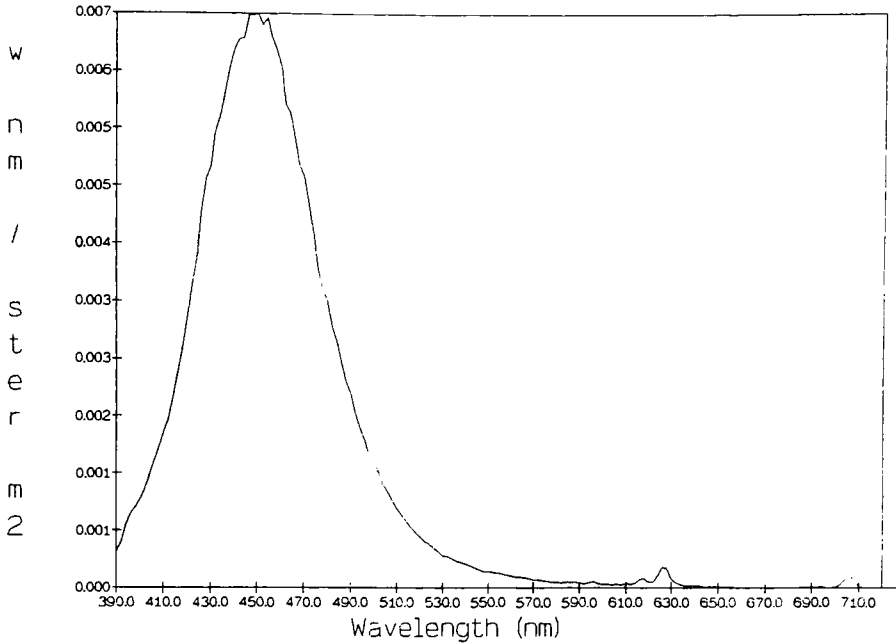


Figure A.28: SPD of Tektronix 690 SR blue phosphor.

same transitions taking place, i.e., the relative shape of the SPD should be independent of the level of excitation. If the spectral radiant flux of a certain phosphor is $\Phi_\lambda(\lambda, j)$, where j is the beam current and λ the wavelength, we expect that

$$\frac{\Phi_\lambda(\lambda_1, j_1)}{\Phi_\lambda(\lambda_1, j_2)} = \frac{\Phi_\lambda(\lambda_2, j_1)}{\Phi_\lambda(\lambda_2, j_2)} = \frac{\Phi_\lambda(\lambda_3, j_1)}{\Phi_\lambda(\lambda_3, j_2)} = \dots \text{etc.} \quad (\text{A.40})$$

which indicates that for any two values of j , the ratio of the resulting radiant fluxes will be constant for all wavelengths. It follows that

$$\Phi_\lambda(\lambda, j_2) = C \Phi_\lambda(\lambda, j_1) \quad (\text{A.41})$$

where C is the proportionality constant. This concept, known as phosphor constancy, is a very important characteristic of CRT phosphors because it will make possible their color synthesis to be treated as a purely additive system (more about it later).

From equation A.33 we know that Φ_λ is related to the beam current j by the expression

$$\Phi_\lambda = j(v_s - v_0) T_m T_{s,\lambda} \eta_{e,\lambda} \left(\frac{A_p}{A_T} \right) \left(1 - \frac{t_b}{t_f} \right)$$

It follows that for any fixed area on a specific CRT, and a fixed set of measurement conditions, the ratio of the radiant fluxes for two different beam currents will be equal to the ratio of the beam currents :

$$\frac{\Phi_\lambda(\lambda, j_1)}{\Phi_\lambda(\lambda, j_2)} = \frac{j_1}{j_2} \quad (\text{A.42})$$

substituting equation A.41 we have

$$\frac{j_1}{j_2} = C \quad (\text{A.43})$$

It also follows that if the proportionality of the SPD at different levels (as expressed on A.42 above) holds, it should also hold for the total radiant flux,

$$C = \frac{\Phi_{e,1}}{\Phi_{e,2}} = \frac{\int_0^\infty \Phi_\lambda(\lambda, j_1) d\lambda}{\int_0^\infty \Phi_\lambda(\lambda, j_2) d\lambda} = C \quad (\text{A.44})$$

even if the spectrum is truncated or modulated by the use of a filter with spectral transmittance T_λ ,

$$C = \frac{\int_0^\infty T_\lambda \Phi_\lambda(\lambda, j_1) d\lambda}{\int_0^\infty T_\lambda \Phi_\lambda(\lambda, j_2) d\lambda} = C \quad (\text{A.45})$$

The importance of this result is that to predict the SPD of a well-behaved phosphor at any beam current $j_{predict}$, all we need is the SPD obtained for an arbitrary beam current $j_{measured}$ and the ratio C of the beam currents $C = \frac{j_{predict}}{j_{measured}}$:

$$\Phi_\lambda(\lambda, j_{predict}) = C \Phi_\lambda(\lambda, j_{measured}) \quad (\text{A.46})$$

This assumption will play a crucial role in a later section, when we describe the CRT as an additive imaging system.

A.2.13 RGB CRT Tristimulus Values

A special case of equation A.45 is when $j_{measured}$ is equal to the maximum beam current, or j_{max} . Under such conditions C will assume values between 0 and 1, and we call it the **CRT stimulus value**. Similarly we define the scalars R , G and B as the **CRT tristimulus values**:

$$R = \frac{j_r}{j_{r,max}} \quad (\text{A.47})$$

$$G = \frac{j_g}{j_{g,max}} \quad (\text{A.48})$$

$$B = \frac{j_b}{j_{b,max}} \quad (\text{A.49})$$

or, alternatively,

$$R = \frac{\int_0^\infty T_\lambda L_{\lambda,r} d\lambda}{\int_0^\infty T_\lambda L_{\lambda,r,max} d\lambda} \quad (\text{A.50})$$

$$G = \frac{\int_0^\infty T_\lambda L_{\lambda,g} d\lambda}{\int_0^\infty T_\lambda L_{\lambda,g,max} d\lambda} \quad (\text{A.51})$$

$$B = \frac{\int_0^\infty T_\lambda L_{\lambda,b} d\lambda}{\int_0^\infty T_\lambda L_{\lambda,b,max} d\lambda} \quad (\text{A.52})$$

where the letters R , G and B are chosen after the reddish, greenish and bluish appearance of most color CRT phosphors.

If we optically mix the radiation from phosphors of the three different SPDs by, for instance, positioning many of them side by side and using a large detector aperture, their integrated SPD will be the sum of the individual SPDs:

$$L_\lambda(\lambda) = L_{\lambda,r}(\lambda, j_r) + L_{\lambda,g}(\lambda, j_g) + L_{\lambda,b}(\lambda, j_b) \quad (\text{A.53})$$

or

$$L_\lambda(\lambda) = R L_{\lambda,r}(\lambda, j_{r,max}) + G L_{\lambda,g}(\lambda, j_{g,max}) + B L_{\lambda,b}(\lambda, j_{b,max}) \quad (\text{A.54})$$

A.3 The CRT Color

At normal viewing distances the image displayed on a color CRT appears to be homogeneous. Areas of solid color have no noticeable texture, except for that in the displayed image itself. However, if some water droplets are sprinkled on the CRT faceplate it will reveal an underlying microstructure. Depending on the kind of CRT being viewed, a pattern of colored dots, rectangles or stripes might become visible, with dark spaces separating them. Two other noticeable things are that the arrangement of the colored elements is regular and that it contains less colors than the CRT is able to display. This is common to several other color imaging systems, such as printing and certain kinds of color photography.

This kind of color synthesis, where a large number of colors are created by the spatial summation of a limited set of primary colors, is one of the oldest means of generating color images. The spatial summation will yield a truly additive system if the radiant power from neighboring image elements is added creating a new spectral power distribution, as in equation A.54 presented before.

In his comprehensive review of color cinematography, Cornell-Clyne [47] described several early photographic processes that used additive color mixing, some of them with the elements arranged side by side in some sort of mosaic, or array. Such processes included the very first color reproduction systems, such as one described by Louis Ducos Duharon, the Autochrome from A. Lumiere, the Dufaycolor and the early 16 mm Kodacolor film. Additive color photographic systems are still in wide use by companies such as Polaroid, which has introduced products such as the Polavision super-8 film and the Polaroid CS film for 35 mm cameras, which are arranged like the already mentioned Kodacolor 16 mm film.

A.3.1 CRT Color Mosaic

There are basically three kinds of additive color mosaics used in modern color CRTs (figures A.29 and A.30) :

- Hexagonal array, circular phosphor dots.
- Hexagonal array, rectangular phosphor dots.
- Linear array, striped phosphors.

The discussion that follows will present some aspects of each different arrangement.

The three electron beams that are exciting the phosphors have to be selectively masked from certain portions of the screen, so that the beam from the electron gun only hits red phosphors, the green beam only hits green phosphors, and so forth. This is accomplished by means of a metal mask, called the shadow mask, placed between the gun assembly and the phosphor screen. The shadow mask is usually made of a thin sheet of aluminum stretched

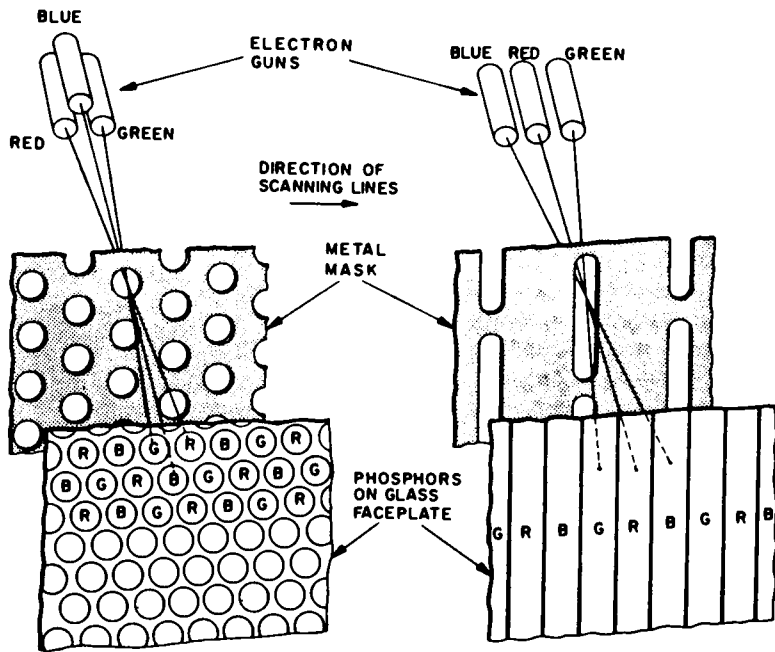


Figure A.29: Delta and precision-in-line arrangements.

on a frame and secured parallel to the face of the glass panel by a small (3 or 4) number of glass studs (see figure A.31).

The shadow mask will absorb a great portion of the electron beam, limiting the efficiency for the conversion of the power of the beam into radiant power. This is one of the main reasons why monochrome CRTs can achieve much higher luminances than a color CRT. Some monochrome CRTs used on military and aerospace applications can achieve luminances as high as $35,000 \text{ cd/m}^2$ (nits) while high resolution color CRTs used in computer graphics are usually limited to 100 cd/m^2 . The power lost in the mask is transformed into heat, which might cause the shadow mask to deform, making the electron beams excite the wrong phosphor. This condition is called a loss of purity, and should not be confused with a loss of colorimetric purity. In a CRT a loss of purity will result if, instead of a white,

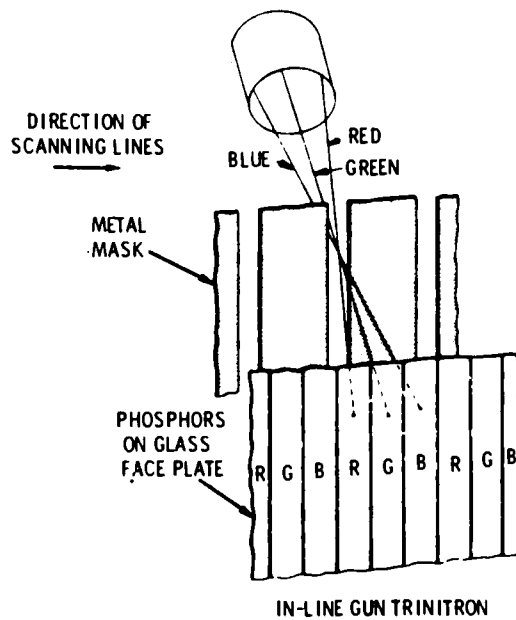


Figure A.30: In-line gun. Trinitron arrangement.

a red is displayed because all the electrons were directed towards the red phosphor. In colorimetric terms this red would have more purity than the original white since it would lie closer to the spectrum locus. To avoid the deformation of the shadow mask some special techniques are used, including the use of bimetal joints which will move the mask closer to the screen when heated (see figure A.32). Since the expansion coefficient of the glass panel and the mask are different, and since the heating might have large gradients, deformation will usually occur at the highest screen luminances.

The discreteness of the phosphor dots will limit the maximum resolution that can be attainable. Even if a very thin electron beam is used to write to the phosphors, no spatial modulation finer than the discrete phosphor "elements" could be displayed. As we will see later, any of the CRT displayable colors can be potentially achieved by a single triad of

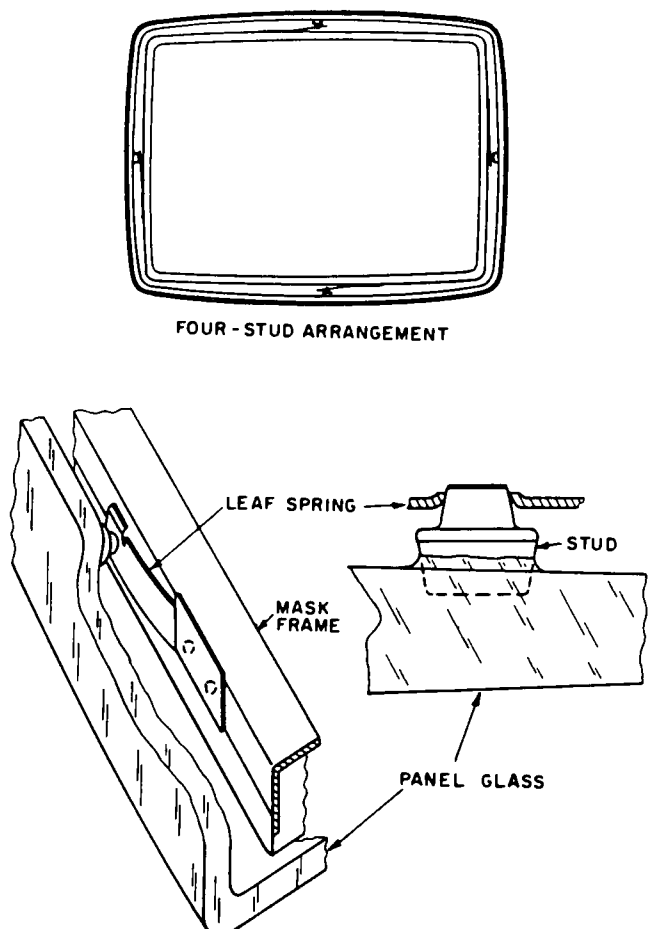


Figure A.31: Four-stud leaf-spring arrangement to secure the shadow mask.

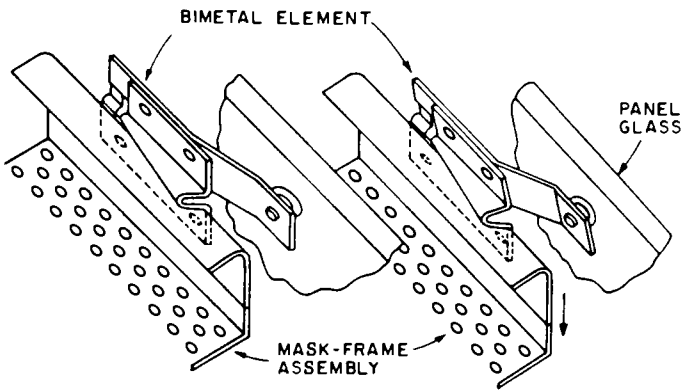


Figure A.32: Bimetal element to compensate for mask expansion when heated.

phosphors, thus the resolution element on a color CRT could be the phosphor triad. Because of technical limitations this is not possible, nor desirable. First, one has to consider that the beam is not a cylinder, but has a gaussian cross section, second, even if cylindrical beam was achievable, it would greatly amplify the sensitivity of the output to beam landing errors, creating undesirable Moire patterns, or aliasing [156, 141].

A.3.1.1 Hexagonal array, circular phosphor dots

This is the oldest kind of arrangement (figure A.29) and is still used in most delta-gun CRTs. The phosphor elements are arranged so that each color element is surrounded by elements of the two other colors (i.e. each red dot is surrounded by three green and three blue dots, etc.) Horizontally the phosphors are in the traditional red, green and blue sequence. A combination of 3 neighboring dots of different colors makes up a “dot triad”. The distance between two dots of the same kind in neighboring triads is called the dot pitch, and its value ranges from 0.21 mm in high resolution monitors to 0.5 mm, or more, in low resolution color CRTs (the dot pitch in the Tektronix 690SR color CRT is 0.43 mm.) With this kind of

arrangement as much as 80% of the energy coming from the electron beam gets trapped by the shadow mask, so that to achieve higher luminous output higher beam currents are required, which in turn will heat up the shadow masking creating physical distortion which will result in loss of purity, making the screen less homogeneous in radiant output.

A.3.1.2 Linear array, striped phosphors

This kind of arrangement (figure A.30) is used by Sony in the Trinitron picture tubes. The phosphors are arranged as stripes that run from top to bottom of the CRT face plate and are ordered in the familiar red, green and blue sequence. The shadow mask is a series of fine metal stripes which will block much less of the electron beam and increase the efficiency of the CRT (up to 60% of the electron beam reaches the phosphors.) Also, the phosphors use the space much more efficiently, with little dead space between the stripes. This kind of CRT also has better properties when the temperature of the mask gets higher, since the distortions will occur in only one direction. To support the shadow mask, the Trinitron CRT uses a couple of very thin wires running in the horizontal. In a Trinitron tube such as the Tektronix 650HR, the horizontal wires can become visible when a homogeneous field is displayed. The stripe pitch of this kind of CRT is usually 0.4 mm.

A.3.1.3 Hexagonal array, rectangular phosphor dots

This is a compromise between the two arrangements described above (see figure A.29). A shadow mask made up with slots directs the electron beams towards a striped phosphor screen, creating rectangular phosphor dots. It has the advantage of a better mask support than the Trinitron and higher mask transmittance than the circular dot CRTs. This kind of screen is common in commercial television sets with the precision in line (PIL) gun arrangement (see figure A.2.3).

A.3.2 Additive Color Synthesis

From experimentation [201], we know that additive color mixtures and color matches will follow certain basic laws of algebra. For a set of four color stimuli, called here \mathcal{A} , \mathcal{B} , \mathcal{C} and \mathcal{D} , each having a certain spectral power distribution, such laws are:

Symmetry

$$\text{If } \mathcal{A} \equiv \mathcal{B} \text{ then } \mathcal{B} \equiv \mathcal{A} \quad (\text{A.55})$$

Transitivity

$$\text{If } \mathcal{A} \equiv \mathcal{B} \text{ and } \mathcal{B} \equiv \mathcal{C} \text{ then } \mathcal{A} \equiv \mathcal{C} \quad (\text{A.56})$$

Proportionality

$$\text{If } \mathcal{A} \equiv \mathcal{B} \text{ then } k\mathcal{A} \equiv k\mathcal{B} \quad (\text{A.57})$$

Additivity

$$\text{If } \mathcal{A} \equiv \mathcal{B} \text{ and } \mathcal{C} \equiv \mathcal{D} \text{ then } \mathcal{A} + \mathcal{C} \equiv \mathcal{B} + \mathcal{D} \text{ and } \mathcal{A} + \mathcal{D} \equiv \mathcal{B} + \mathcal{C} \quad (\text{A.58})$$

where k is a scalar, the operator \equiv means that the colors visually match and the $+$ operator denotes the additive color mixture.

Additive color synthesis takes advantage of two of the principal precepts of color science, which are the Young-Helmholtz [203, 89] trichromatic theory and Grassmann's Laws [79]. The first states that any color sensation can be explained as the result of three different stimulations on the eye, each proportional to the amount of energy available on the region of the spectrum where each of three kinds of color receptors are sensitive. Grassmann hypothesized that the inverse is also true - a certain color sensation, evoked by stimulation of the eye to any light, can be reduced to the addition of at the most three lights of different spectral composition, if such lights conform to the requirement of being *primaries* (by which is usually meant that no one primary can be obtained by combination of other two).

Bartleson [4] has summarized Grassmann's laws as follows:

- Three independent variables are necessary and sufficient for specifying a color match.

- Stimuli evoking the same color appearance produce identical results in additive color mixtures, regardless of their spectral compositions.
- If one component of a color mixture changes, the color of the mixture changes in a corresponding manner.

The principle that any number of lights of different spectral composition can visually match, if all other conditions are the same, is what is called metamerism. Together, these assumptions form what Wyszecki and Stiles [201] have called the “trichromatic generalization”, which can be expressed as :

$$\mathcal{C} \equiv R\mathcal{R} + G\mathcal{G} + B\mathcal{B} \quad (\text{A.59})$$

where \mathcal{C} is a color to be matched, R , G and B are scalars usually called tristimulus values and the stimuli \mathcal{R} , \mathcal{G} and \mathcal{B} will be a set of unity vectors called the primaries. Of course, this last will only be true if \mathcal{R} , \mathcal{G} and \mathcal{B} satisfy the requirement that

$$R\mathcal{R} + G\mathcal{G} + B\mathcal{B} \equiv 0 \quad (\text{A.60})$$

has as its only solution the trivial case, where all tristimulus values have zero value. A metameric match is then expressed as an equality :

$$\mathcal{D}_1 \equiv \mathcal{D}_2 \quad (\text{A.61})$$

$$\mathcal{D}_1 \equiv R_1\mathcal{R}_1 + G_1\mathcal{G}_1 + B_1\mathcal{B}_1 \quad (\text{A.62})$$

$$\mathcal{D}_2 \equiv R_2\mathcal{R}_2 + G_2\mathcal{G}_2 + B_2\mathcal{B}_2 \quad (\text{A.63})$$

from what follows that

$$R_1\mathcal{R}_1 + G_1\mathcal{G}_1 + B_1\mathcal{B}_1 \equiv R_2\mathcal{R}_2 + G_2\mathcal{G}_2 + B_2\mathcal{B}_2 \quad (\text{A.64})$$

Grassmann's laws have been tested and found to be valid within a wide range of conditions. The major deviations found are:

- An intrusion from the rod system on the cone system responses, indicating that color vision might be tetrachromatic.

- The relative responses from the individual color channels will change as the light intensity changes, causing shifts in hue and saturation.

Both cases amount to a failure of the proportionality law :

$$\mathcal{C} \equiv R\mathcal{R} + G\mathcal{G} + B\mathcal{B}, \quad (\text{A.65})$$

is true, but

$$k\mathcal{C} \neq kR\mathcal{R} + kG\mathcal{G} + kB\mathcal{B}, \quad (\text{A.66})$$

Trezzona [192] has found that the addition of a fourth primary stimuli will keep the color match stable across all levels of intensities. Also, Cornsweet [49] pointed out that changes in the appearance of a color as the level of stimulation changes (as are in evidence in the Bezold-Bruke hue shift) should not be surprising in view of the non-linearity of the neural processes that make up our visual system.

Despite these failures, Grassmann's laws will still provide the means of fabricating the metameric color matches that are essential to color reproduction. The main reason is that even though rod intrusion and other effects might introduce hue shifts and other deviations from strict additivity, Grassmann's laws are still valid if the level of stimulation is kept constant. Because the dynamic range of most color reproduction systems is very small compared to the that of the eye, deviations from strict additivity, when found, tend to be negligible.

One of the powerful consequences of Grassmann's laws is that it allows us to change the primaries without changing the matches. This operation can be equated with a change of basis in linear algebra.

Let $(\mathcal{R}, \mathcal{G}, \mathcal{B})$ and $(\mathcal{D}, \mathcal{E}, \mathcal{F})$ be two different triplet of primaries. From Grassmann's laws we know that we can express each element of a triplet as a function of the other triplet.

$$\begin{aligned}\mathcal{D} &\equiv R_1\mathcal{R} + G_1\mathcal{G} + B_1\mathcal{B} \\ \mathcal{E} &\equiv R_2\mathcal{R} + G_2\mathcal{G} + B_2\mathcal{B} \\ \mathcal{F} &\equiv R_3\mathcal{R} + G_3\mathcal{G} + B_3\mathcal{B}\end{aligned}$$

and conversely,

$$\begin{aligned}\mathcal{R} &\equiv D_1\mathcal{D} + E_1\mathcal{E} + F_1\mathcal{F} \\ \mathcal{G} &\equiv D_2\mathcal{D} + E_2\mathcal{E} + F_2\mathcal{F} \\ \mathcal{B} &\equiv D_3\mathcal{D} + E_3\mathcal{E} + F_3\mathcal{F}\end{aligned}$$

A certain color \mathcal{P} could be expressed as a metameric match to either set of primaries:

$$\mathcal{P} \equiv R_4\mathcal{R} + G_4\mathcal{G} + B_4\mathcal{B} \quad (\text{A.67})$$

or

$$\mathcal{P} \equiv D_4\mathcal{D} + E_4\mathcal{E} + F_4\mathcal{F} \quad (\text{A.68})$$

By substituting the primaries of any one of the expression above by the other basis we have, for example,

$$\mathcal{P} \equiv D_4(R_1\mathcal{R} + G_1\mathcal{G} + B_1\mathcal{B}) + E_4(R_2\mathcal{R} + G_2\mathcal{G} + B_2\mathcal{B}) + F_4(R_3\mathcal{R} + G_3\mathcal{G} + B_3\mathcal{B}) \quad (\text{A.69})$$

by rearranging the equation we have

$$\mathcal{P} \equiv (D_4R_1 + E_4R_2 + F_4R_3)\mathcal{R} + (D_4G_1 + E_4G_2 + F_4G_3)\mathcal{G} + (D_4B_1 + E_4B_2 + F_4B_3)\mathcal{B} \quad (\text{A.70})$$

Thus the following equalities are established

$$R_4 = D_4R_1 + E_4R_2 + F_4R_3 \quad (\text{A.71})$$

$$G_4 = D_4G_1 + E_4G_2 + F_4G_3 \quad (\text{A.72})$$

$$B_4 = D_4B_1 + E_4B_2 + F_4B_3 \quad (\text{A.73})$$

Expressing it in matrix form we have,

$$\begin{bmatrix} R_4 \\ G_4 \\ B_4 \end{bmatrix} = \begin{bmatrix} R_1 & R_2 & R_3 \\ G_1 & G_2 & G_3 \\ B_1 & B_2 & B_3 \end{bmatrix} \begin{bmatrix} D_4 \\ E_4 \\ F_4 \end{bmatrix} \quad (\text{A.74})$$

This is a very powerful result. It frees us to choose any suitable set of primaries and express color matches with respect to it. The translation of tristimulus values from one set of primaries to tristimulus values based on any other set of primaries is straightforward, as long as we know how the primaries of one tristimulus basis can be expressed in terms of the other. One important corollary of Grassmann's laws is that we can express the primaries as color matching functions, which describe how much of each of our selected primaries we need to match some spectral power distribution. Spectral matching functions are usually represented by a lowercase letter with a bar on top, e.g. \bar{r}_λ .

In view of what has been discussed above, the question of what is the *actual* human spectral sensitivity function has no relevance. Instead we ask ourselves "what is the most convenient spectral matching functions to use". This kind of question was very much in the mind of the scientists at the 1931 CIE meeting when the 2 degree observer [45] was standardized. Starting with the experimental data collected by Guild and Wright [75] the CIE proposed spectral matching functions which have two very powerful characteristics:

- All three spectral matching functions, \bar{x}_λ , \bar{y}_λ , \bar{z}_λ are positive on its entire domain. This made the implementation easier in a world where calculations were still made by hand operated machines.
- One of the three matching functions, \bar{y}_λ , is equal to the photometric observer, V_λ , standardized by the CIE in 1924. The decision to express all the luminance signal with \bar{y}_λ has proved to be very useful. When the NTSC system came to age in 1953, it had a road map to follow in the encoding of the color signal.

To calculate the scalar amounts (i.e. the tristimulus values) of the three CIE primaries resulting from the spectral radiance coming from a CRT towards the eye (of the hypothetical standard observer) we can proceed as follows [3, 43, 44]

Let :

- L_λ be the spectral radiance expressed in (watts/m² nm sr).
- \bar{x}_λ , \bar{y}_λ , \bar{z}_λ be the three CIE spectral matching functions.

- K_m be 683 lumens/watt⁴
- X, Y, Z be the CIE tristimulus values.

They are all related by the following formulas.

$$X = K_m \int_{\lambda_1}^{\lambda_2} L_\lambda \bar{x}_\lambda d\lambda \quad (\text{A.75})$$

$$Y = K_m \int_{\lambda_1}^{\lambda_2} L_\lambda \bar{y}_\lambda d\lambda \quad (\text{A.76})$$

$$Z = K_m \int_{\lambda_1}^{\lambda_2} L_\lambda \bar{z}_\lambda d\lambda \quad (\text{A.77})$$

where λ_1 and λ_2 are the integration limits (usually 400 to 700 nm, although $\bar{x}_\lambda, \bar{y}_\lambda$ and \bar{z}_λ are defined from 360 to 830 nm).

Although not perfect, the CIE 1931 standard observer has proven very useful and long-lasting. The foremost reason being that within its scope it establishes a nominal color scale. By specifying that two colors have the same tristimulus value we secure that both will have the same appearance (they will match) to the average human observer when viewed the same way.

Once the CIE tristimulus values have been obtained from the color sample being measured, any number of linear operations can be applied to it without changing the basic

⁴When measuring absolute tristimulus values K_m is the maximum luminous efficacy defined as 683 [lumens/watt] [44]. If the spectral power is L_λ , measured in [watts /m² nm sr], the tristimulus value Y will be called the absolute luminance, expressed in candelas per meter square [cd/m²]. When measuring relative tristimulus K_m is substituted by 100/ $Y_{(\text{ref. white})}$ and L_λ is replaced by $S_\lambda R_\lambda$, where R_λ is the spectral reflectance of the object under consideration and S_λ is the spectral power distribution of the light reaching the object. Relative tristimulus values are used more often when measuring the color of reflective objects. In this case K is obtained from the luminance of a perfect lambertian reflector viewed under the same light source as the sample under consideration. It serves as a normalization factor so that $Y_{(\text{object})}$ will always be between 0 and 100 for non-fluorescent materials. Notice that, in general, this practice makes no sense for the measurement of CRTs since there are no reflectances modulating the light and the only light source under consideration is the CRT. Because of the normalization, relative tristimulus values have no units. Unless noted, all CIE tristimulus value measurements described in this thesis are in absolute units.

property that visual matches for the standard observer are numerical matches of the transformed tristimulus values.

Imagine for instance that we want to display specific XYZ tristimulus values on an additive system such as a color CRT. To find out what are the *RGB* CRT tristimulus values (defined on section A.2.13) necessary to match the desired CIE tristimulus values (assuming that the tristimulus values can be matched) we must first determine what is the CIE tristimulus values emitted by each phosphor. By measuring the red phosphor at full emission (i.e. $R = 1$ when $j_r = j_{r,max}$) we obtain:

$$(X_{r,max}, Y_{r,max}, Z_{r,max}) \quad (\text{A.78})$$

If we repeat the process with the green and blue phosphors we obtain:

$$(X_{g,max}, Y_{g,max}, Z_{g,max}) \quad (\text{A.79})$$

and

$$(X_{b,max}, Y_{b,max}, Z_{b,max}) \quad (\text{A.80})$$

Imagine now that a white is displayed when we have the maximum emission of the red, green and blue phosphors at the same time. Because the system is additive, it follows that the amount of X tristimulus value in the white will be the addition of the $X_{r,max}$, $X_{g,max}$ and $X_{b,max}$, and so forth for the Y and Z tristimulus values. The same reasoning will apply to any other color: The X tristimulus value is the sum of the X tristimulus value of all the three phosphors, and so forth for the Y and Z tristimulus values.

Assuming that phosphor constancy holds, we can then express the resulting CIE tristimulus values in matrix form:

$$\begin{bmatrix} X \\ Y \\ Z \end{bmatrix} = \begin{bmatrix} X_{r,max} & X_{g,max} & X_{b,max} \\ Y_{r,max} & Y_{g,max} & Y_{b,max} \\ Z_{r,max} & Z_{g,max} & Z_{b,max} \end{bmatrix} \begin{bmatrix} R \\ G \\ B \end{bmatrix} \quad (\text{A.81})$$

where the CRT tristimulus values R , G , and B will range between 0.0 and 1.0 (see definition on section A.2.13 on page 104). We are now in possession of the means to predict the CIE

tristimulus values from the normalized amounts of *R*, *G*, and *B* intensities. Under these conditions we can call *R*, *G*, and *B* the CRT tristimulus values, and by inverting the 3x3 matrix above we can predict what CRT tristimulus values will be necessary to obtain certain CIE tristimulus values.

$$\begin{bmatrix} R \\ G \\ B \end{bmatrix} = \begin{bmatrix} X_{r,max} & X_{g,max} & X_{b,max} \\ Y_{r,max} & Y_{g,max} & Y_{b,max} \\ Z_{r,max} & Z_{g,max} & Z_{b,max} \end{bmatrix}^{-1} \begin{bmatrix} X \\ Y \\ Z \end{bmatrix} \quad (\text{A.82})$$

In the case of a color CRT controlled by a frame-buffer the values of the CRT tristimulus values can be calculated from equations A.47 and A.18. We will review this calculation again in section 2.2.

Since the “metameric” properties of the standard observer are preserved across linear transforms, we are free to express colorimetric data in any suitable tristimulus basis. The approach used by the NTSC in the development of color television was, for a given set of CRT phosphors chromaticities and white point, to determine what spectral matching functions for the TV camera (\bar{r}_λ , \bar{g}_λ and \bar{b}_λ) would be the best linear approximation to the CIE (\bar{x}_λ , \bar{y}_λ and \bar{z}_λ) spectral matching functions. Another 3x3 transformation that was developed by the NTSC was the decomposition of XYZ (or the camera RGB) into YIQ [27, 99], which roughly corresponds to the principal components decomposition of the signals that are processed by the human color vision system [28, 29]. Such decomposition was used for the transmission of the signal since it allowed the bandwidth to be allocated according to the signal contribution of each band, while keeping the most descriptive principal component, the luminance *Y* signal, compatible with the black and white television sets.

The CIE system of colorimetry offers a powerful but incomplete description of color appearance. The two major limitations are :

- Tristimulus values only describes equality of colors, i.e. matches. If colors do not have the same tristimulus values nothing can be said about the magnitude of the mismatch, or the direction of the mismatch.

- Color matches are strictly valid only under the conditions they were established. Things that will, with different degrees of sensitivity, affect color matches are:
 - Variables associated to the light source:
 - * Spectral power distribution
 - * Illumination/collection geometry [154]
 - * Luminance
 - Variables associated to the samples:
 - * Spectral reflectance/transmittance
 - * Texture (for object colors)
 - * Goniospectrophotometric properties (e.g. gloss for object colors) [10]
 - Variables associated to the observer:
 - * Spectral sensitivity of the observer
 - * Position of samples in the visual field
 - * Age of observer
 - * Visual “history” of the observer
 - * State of the observer
 - * Size of samples
 - * Proximity of samples
 - * Intensity of the visible radiation
 - * Temporal behavior of the source/sample
 - * Background surrounding the samples

As the above list demonstrates, an appearance measurement is not completely specified by a simple triplet of numbers since absolute appearance has many more degrees of freedom. In fact, it has an undetermined number of degrees of freedom, and by convention (and because the effect of many of the above mentioned variables has not been quantified as yet)

a few of these have become accepted as an integral part of the colorimetric specification. They are:

- The tristimulus values data
- The observer used
- The geometry of the measurement/observation
- The illuminant or source used (for object colors)

For example, the colorimetric specification for a piece of white paper could be expressed as “ $Y = 80.0, x = 0.340, y = 0.304$, CIE 2 degree observer, D65 illuminant, 45/0 geometry”. Notice that in this case Y is the relative luminance. A CRT measurement could be expressed by simply stating the observer, the absolute tristimulus values, and the position and angle of observation. These last two parameters are needed since there are no widely accepted standards for CRT measurement geometry.

We have reached the boundary between the CRT signal and perception. To get this far we obtained a description of the CRT image as a simple point by point mapping from the frame buffer d to a CIE color space. To advance further in our description of the image would require the description of its appearance, and there would be no simple relation between radiant intensity and the perceptual attributes being analyzed. This remains a task for future color appearance research using color CRTs.

Appendix B

Experimental Techniques

B.1 Introduction

The major purpose of the experiments and calculations that will be described hereon was the characterization of the CRT behavior, aimed at determining the suitability of color CRTs for color appearance research. As we have already discussed, the researcher in color vision and appearance will require from a CRT a kind of performance very different from many other disciplines that have traditionally used the color CRT. Because the intensive use of CRTs in this kind of research is a relatively new advent [18], there is a large void in the literature in what concerns the description of some of its fundamental characteristics. For instance, there is abundant literature on the measurement and correction of misconvergence, which is a major manufacturing problem that has obviously detrimental effects on the quality of the image. On the other hand, one will find very few references on some other spatial properties of the color CRT, such as the change in luminance across the screen. This change in focus has prompted the author to carry out many of the experiments described in this thesis.

The investigation was not as extensive as one would have wished. The number of questions to be answered was very large, and some discrimination was needed when selecting what topics to investigate. Some subjects are only briefly mentioned and others completely ignored, such as the problems of visibility of flicker, misconvergence, calculation of tristim-

ulus values, spectroradiometry, and the CRT MTF. In a nutshell, the aim of this work is to provide a description of the CRT tristimulus values, *R*, *G* and *B*.

The decision on what to investigate was based on the idea that most color appearance experiments will consist of homogeneous stimuli (like rectangles or circles) surrounded by either a simple or a complex adapting field. This kind of setup is currently used in studies of color constancy, chromatic adaptation and color image reproduction. For the typical CRT-based experiment, the temporal transitions of the color image will occur slowly, probably under control of the test subject, and the viewing conditions are under strict control. This control will allow the elimination of many artifacts. For instance, the load will change slowly enough to allow thermal equilibrium in almost all conditions, and by moving the observer away from the CRT the problems due to the misconvergence and the MTF can be minimized. Notice, though, that different kinds of investigation will tend to stress different properties of the CRT. Much of vision research has been devoted to investigating phenomena such a flicker or contrast sensitivity. The experiments will typically use fast time and spatial transients displayed on the CRT in the form of moving or stationary gratings. For such experiments, the understanding of the raise and fall times of the phosphors, as well as the temporal MTF of the entire CRT apparatus will be critical. Such topics will be scarcely mentioned here since they will not be as critical for the envisioned color appearance experiments.

B.2 Apparatus

What follows is a brief description of the resources used during this investigation. Detailed descriptions on the performance of some of the different pieces will be part of later discussions.

B.2.1 Location

The entire investigation was carried out in one of the research darkrooms of the Munsell Color Science Laboratory (MCSL) in the Center for Imaging Science (CIS) in the College of Graphic-Arts and Photography of the Rochester Institute of Technology. This room was

air-conditioned throughout the year and darkened during all critical measurements.

B.2.2 Computers

The principal computers used during this investigation were of the IBM/PC type, including one IBM/PC AT, one IBM/PC XT and a Xerox 6035. For heavier computations and modeling the institute's VAXes were used. For simpler computations and record-keeping a DEC PRO350 was used. The thesis was initially typed in a Xerox Documenter (6065) system and completed in a Hewlett-Packard 9000/350 workstation.

B.2.3 Software

The bulk of the CRT control and test software was developed in Turbo-Pascal [13, 66] running under DOS in the PC type of computers. The listings are too large and numerous to be included with this text, but are available from the author. Computations were also made in FORTRAN under VAX/VMS and C under HP-UX. Several plots were prepared using S2020 and DISSPLA. Illustrations were also prepared with the Xerox Documenter running Viewpoint software and on the HP-UX workstation using Drawing Gallery. This text was prepared with L^AT_EX [114].

B.2.4 Video Generator

The video signal was generated by a Number 9 512 x 32 frame buffer installed on a IBM/PC type of computer. This board has already been discussed in some detail in section A.1.3. The signal followed the EIA RS-170 format at 15.75 KHz horizontal frequency (Hf), giving 512 x 480 displayable pixels.

B.2.5 CRTs

During the investigation the following CRTs were used at least once:

- Tektronix model 690SR. 19 inch, delta gun, 15.75 KHz Hf.

- Tektronix mode 650HR. 12 inch, trinitron, 15.75 KHz Hf.
- Barco CD33HR. 12 inch, delta gun, 15.75 KHZ Hf.
- DEC VR241A. 12 inch, delta gun, 15.75 KHz Hf.
- DEC VR201A. 10 inch, black and white, 31.5 KHz Hf. (960 x 240 pixels)
- Sony PVM-12710. 10 inch, trinitron, 15.75 KHz Hf.
- HP 98785A, 12 inch, trinitron, 31.5 KHz Hf. (1028 X 768 pixels)

The choice between monitors was dependent on what was being characterized. For instance, the load dependency measurements described in section E were made on the Barco CD33HR because this monitor presented the largest deviations from linearity. The measurements on the uniformity and repeatability were performed on the high-quality Tektronix 690SR since in that case, the interest was on understanding the ultimate limitations of CRT systems.

B.2.6 Detectors

A number of the different detectors available at MCSL were used at different stages of the investigation. Although not all results are reported here, they are listed to illustrate the scope of the measurements.

- Tracor Northern TN710, fast array spectroradiometer. Single grating monochromator imaging directly into a CCD with 512 channels, sampling from \approx 240 to 890 nanometers in \approx 1.3 nanometers intervals. For a discussion of this instrument and the measurement of CRTs and other pulsating light sources the reader should refer to Farrel [71].
- Gamma Scientific 2000, telecolorimeter. A photomultiplier (PMT) instrument with a built-in filter turret. Connected to a chart-recorder it was used mostly for monitoring and stability measurements.

- Photo-Research PR703A/PC, array spectroradiometer. Single grating monochromator with a 256 photo-diode array detector with ≈ 2 nm bandpass. Two lenses were used, the MS-70 (macro) and MS-55 (macro-zoom). For an extensive discussion on the characterization of this instrument the reader should refer to Daust [60] and Rodriguez [159].
- Minolta TV-2160 Color Analyzer II. A filter colorimeter designed for CRT measurements. Despite the poor accuracy, this instrument was very useful and extensively used for relative measurements, where only the CRT tristimulus values are of interest. Its characteristics will be discussed later on.

B.2.7 Measurement Instruments

The measurement instrumentation consisted of a number of pieces, including oscilloscopes, voltmeters, chart-recorders, wave-function generators, and smaller pieces of hardware, all obtained from CIS. These apparatus were used mainly to characterize and monitor the video signal at different phases of the image formation process.

To aid in the radiation measurements, optical hardware such as lenses, benches, prisms, mirrors, light sources, integrating spheres and support parts such as rods and holders was obtained from MCSL and the optical laboratory of CIS.

B.3 Procedures

Each kind of measurement required a different kind of set-up and procedure. Somethings, though, were kept constant throughout the investigation.

B.3.1 CRT Areas

For many measurements the CRT image was divided into 25 portions, as illustrated in figure B.1. This was made by creating in the frame buffer an image with 25 areas of equal size and assigning to each one a different d level. By manipulating the LUT, the resulting

1	2	3	4	5
6	7	8	9	10
11	12	13	14	15
16	17	18	19	20
21	22	23	24	25

Figure B.1: 25 different areas used on many measurements.

d' of each area could be manipulated independently, allowing, for instance, one area to be emitting while all others were dark, or to do measurements of one area while the other changed in value.

B.3.2 Data Collection

Two of the detectors where interfaced to the IBM/PCs, the TV-2160 and the PR703A/PC. We will discuss the performance of the instruments later, while some of the generic details of the operation are discussed next.

B.3.2.1 PR703A/PC

The Photo-Research instrument is provided with two kinds of software. The "Spectra" software is a display oriented, menu driven interface to the instrument, providing both

graphical display of the data and numerical descriptions of the principal features, such as CIE 1931 chromaticity, luminance in cd/m^2 and color temperature in Kelvins. The other piece of software is a “toolkit” which allows extensive control of the instrument. It takes a command language approach to the interface, and it achieves independency from the programming language by an ingenious use of the RAM drive provided by DOS (drive D:) and a memory resident device driver under the name “PHOTO:”. Again, for a complete description of the instrument the reader should refer to Daoust [60]. Upon completion of a measurement, the software calculated the meaningful metrics and placed them in files in drive D:, along with a report on the instrument set-up and status. Different pieces of data were used in different experiments, including the corrected spectral data itself and the calculated luminance and chromaticities.

B.3.2.2 TV-2160

The Minolta instrument is provided without any software or cables. It comes with a port for serial communication at 4800 baud. The connector used, pin assignments and cabling required are quite unusual, but once one is able to establish the correct arrangement they will provide a one-way transmission of the colorimetric data. The transmission has to be initiated by pressing a key (marked, for no apparent reason, “F”) on the front of the instrument. The rate of transmission is about one data packet (Yxy or RGB) each 0.5 second, but the instrument will stop transmitting if the measurement goes out of range. Software was written to carry out the interface with the Minolta through the serial port and to perform a number of operations on the data. The instrument allows the choice of luminance expressed either in footlamberts or cd/m^2 and the later was used. Through the front panel it also provides the choice of simple CIE 1931 Yxy or RGB data calculated according to a white point that can be measured and stored in memory. All data collected was in the form of Yxy , since the RGB was calibration and device specific. The RGB mode was used only when comparing CRTs or performing some simple monitoring.

B.3.3 Placement of the TV-2160 Probe

To ensure repeatability on the positioning of TV-2160 probe, the probe was mounted on a Oriel stainless steel rod and pressed against the CRT faceplate by a spring loaded sample holder. This sample holder was originally part of an old Kollmorgen KCS40 spectrophotometer, and when held against the CRT body by a couple of wrenches, it provided a very convenient and sturdy support. The probe could be dismounted and mounted back without any statistically significant change of the measurement values. The standard deviations of measurements made after 10 replacements of the probe were the same as when the measurements were made without replacing the probe.

Appendix C

Tristimulus Measurements

C.1 Introduction

The basic performance requirements made on any colorimeter, such as the Minolta TV-2160, are:

- Accuracy
 - Spectral sensitivity matching the desired observer (e.g. CIE 1931).
 - Linear photometric scale.
- Precision
 - Repeatability.
 - Stability.

C.1.1 Precision

The need for stability and repeatability should be obvious. We would like the instrument to always report the same value for a given input, and we would like the instrument fluctuations to be nil or small around that value. Deviations from either condition will result in noise and a larger number of samples will have to be acquired to have the desired confidence in the

data. Precision is a characteristic of the instrument and its design, and little can be done about it besides trying to minimize the conditions leading to the undesirable fluctuations (e.g. by cooling a detector) and accounting for the precision when interpreting the data. When making measurements from a CRT the noise from the colorimeter will be confounded with the noise from the CRT, and it will be difficult to resolve where is the source of noise. For this reason the precision of the measurements will be discussed in a separate section.

C.1.2 Accuracy

Accuracy is somewhat independent of the instrument. Although all instruments have a limited operational range and stability, within the useful range of the instrument we can achieve some desirable degree of accuracy by carefully calibrating and characterizing it. High accuracy is usually harder to achieve than precision, since to determine accuracy one has to compare instruments (unless the original standard is available, which is hardly ever the case) and each time one instrument is used to calibrate another their variances will add [19]. In our present case we can increase the accuracy of the TV-2160 by carefully calibrating the photometric scale and substituting the requirement of the spectral sensitivity matching the desired CIE observer by requiring only the ability to separate the red, green and blue phosphor emissions. The accurate colorimetric data can be obtained by linearly transforming the TV-2160 uncorrected XYZ values to the correct XYZ by means of a 3x3 matrix. If phosphor constancy holds, a single 3x3 matrix will suffice over the entire range of emissions. If phosphor constancy does not hold, different 3x3 matrices will have to be calculated over the appropriate ranges. In the later case the correction might become such an involved process that one should just as well consider using a more complex and accurate instrument.

If phosphor constancy holds, we can obtain the coefficients of the 3x3 matrix from spectroradiometric measurements, or some other accurate means. In the case where we are only interested on the CRT tristimulus values, R , G and B can be calculated directly from the TV-2160 data by using the chromaticity of the individual phosphors measured, say,

at full emission, or by using the TV-2160 in RGB. Thus, the major requirement for obtaining accurate data from the TV-2160 is linearity of the photometric scale. In appendix D the linearity calibration of the TV-2160 is presented in detail.

C.2 Repeatability

One of the factors that could severely limit the usefulness of CRTs as a tool in color appearance research is the uncertainty about the actual state of the CRT. Differences in tristimulus values in the order of 5% can translate into large perceptual differences. For instance, between a white with $Y = 100$ and a white with $Y = 95.0$ the ΔE_{ab}^* is about 2.0. If one wants to be 95% confident that any two tristimulus values displayed are 1% apart, the standard deviation on the measurement, or conversely the ability to predict tristimulus, will have to be on the order of 0.25% of these tristimulus values.

We have discussed the issues of accuracy in the previous section. We turn now to the questions concerning the stability and the repeatability of the CRT system. Lack of stability and repeatability will be encountered as noise in the measurements and operation of the system. They are clearly distinct. A system can be stable, but not repeatable. For instance, the values measured or display might be dead set, showing no fluctuations, but the same input to the system on different instances might not return the system to the same state. By the same token, a system might be repeatable, but not stable. In this case the system will always return to the the same mean state for a given input, but will fluctuate around that state. In a sense the two artifacts will have the same result, at any given instance they will reduce the confidence that one might have on the state of the system.

C.3 Integration Time, Area and Noise

Both stability and repeatability will be sources of noise in CRT systems. The major reason is that the CRT image is modulated in time, consisting of a sequence of discrete emissions by the CRT phosphors with long periods of inactivity between emissions.

Figure B.1 in section B.3.1 illustrates this point. During each 1/30 sec the CRT video generator sends the equivalent to 331,334 pixels to the CRT, 624 pixels on the horizontal and 531 in the vertical. These are “equivalent” pixels since part of them contain no image information at all, but the synchronization pulses and blanking periods for retrace. There are actually only 245,760 pixels on the displayed image, 512 in the horizontal and 480 on the vertical. If we would place a detector covering the entire CRT screen we would find out that the detector was receiving energy from the CRT screen only 74% of the time, i.e. during 24.7 msec for each frame period lasting 33.33 msec. As we have seen of section A.1.3.2 the fraction corresponds to

$$1 - \left(\frac{t_b}{t_f} \right)$$

where t_b is the amount of time per field that the signal is blanked and t_f is the time length of each field.

A detector with area A_d placed over a screen with total area A_t would be receiving radiation during $\frac{A_d}{A_t} \left(1 - \left(\frac{t_b}{t_f} \right) \right)$ seconds for every second of detection. One interesting aspect of the problem is that the shape of the area A_d will not influence the amount of signal detected, but will affect the temporal distribution of the signal detected. Figure C.1 illustrates this point. Areas A_1 , A_2 and A_3 are equal but have different shapes and orientation. The signal collected by area A_1 will consist of a short burst repeated at each frame. Since the CRT image is written from top to bottom the burst will last exactly as long as it takes the CRT to write those lines. The typical color CRT phosphors (see table A.17) will decay very fast, and the bursts will be separated by a long period without any signal. On the other hand, the phosphors will not decay completely between lines, and during the burst there will always be signal. If the CRT is not interlaced the burst will last exactly $\frac{A_d}{A_t} \left(1 - \left(\frac{t_b}{t_f} \right) \right)$ seconds, the same time fraction as the area fraction. If the CRT is interlaced, there will be two bursts, lasting each $\frac{A_d}{2A_t} \left(1 - \left(\frac{t_b}{t_f} \right) \right)$ sec. and 1/60 sec. apart.

The signal detected by area A_2 will be very different. Because the area spans the entire length of the CRT there will almost always be some signal under the detector. This time the signal will last $\frac{A_d}{A_t} \left(1 - \left(\frac{t_b}{t_f} \right) \right)$ for either the interlaced or the non-interlaced displays,

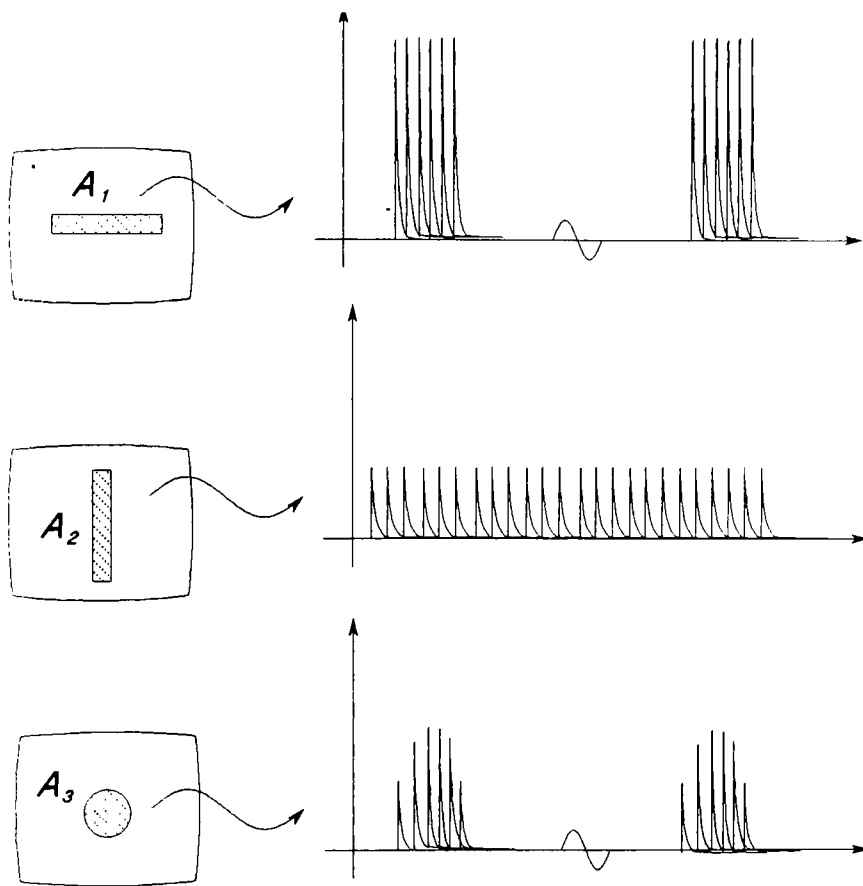


Figure C.1: The same energy, but with different temporal distributions, will be collected by the three areas.

but because the phosphors will decay almost completely in the duration of a line the signal will consist of a long trail of spikes. As we see there, length of the burst is dependent only on the vertical dimension of the area, while the amount of energy collected is dependent only on the total area.

Area A_3 , also in figure C.1, displays the typical CRT detection situation. The signal will consist of a series of small spikes at $63.5 \mu\text{sec}$ apart (15.75 KHz) resulting from the emission of each line. The trail of spikes will bundle in larger spikes lasting $\frac{A_d}{A_t} \left(1 - \left(\frac{t_b}{t_f}\right)\right)$, the fraction of the total vertical dimension occupied by the detection area, and the spikes will be repeated at each 33.33 msec on an interlaced display.

The temporal profile of the detected CRT emission might have several consequences, all related to phase differences between the CRT emission and the detection. We can divide

such problems into two classes:

- Detection of single emissions
- Integration of several emissions

The two types of problems are discussed next.

C.3.1 Detection of single emissions

A typical measurement situation will be a circular area detector covering a small fraction of the CRT faceplate. Under these conditions the CRT emission will be cyclic with the field or frame frequency, depending on whether the image is interlaced or not. The radiation emitted during a single cycle will contain high frequency noise that goes mostly undetected by the eye. The sources of this high-frequency noise include the variations in beam size, intensity and landing position, power supply filtering, the availability of emission sites on the phosphors and quantum noise.

Figure C.2 shows two typical kinds of responses. When excited by a very short signal, detector D_1 will respond very rapidly and then slowly decay. We can think of the CRT phosphor as belonging to this kind of detector. After excitation by a very fast moving electron beam the phosphor will rapidly start to emit and then decay much more slowly. Most photodetectors are of this type, including photomultipliers and silicon photodetectors. The response and decay time will determine the maximum frequency that this detector will follow. Beyond that frequency the detector will not completely decay completely, and the resulting signal will have a dc level and a fluctuation on top of it. At even higher frequency the detector might not fluctuate at all, with the output staying constant at around some dc level. This dc level can be calculated according to the property of convolutions that when two areas are convolved the area of the resulting function is equal to the product of the two areas. Thus the area under the detector pulse response can be multiplied by the area under the exciting signal and the dc level will be obtained. Measurement problems with these detectors will arise if a period of insensitivity follows the excitation. This could

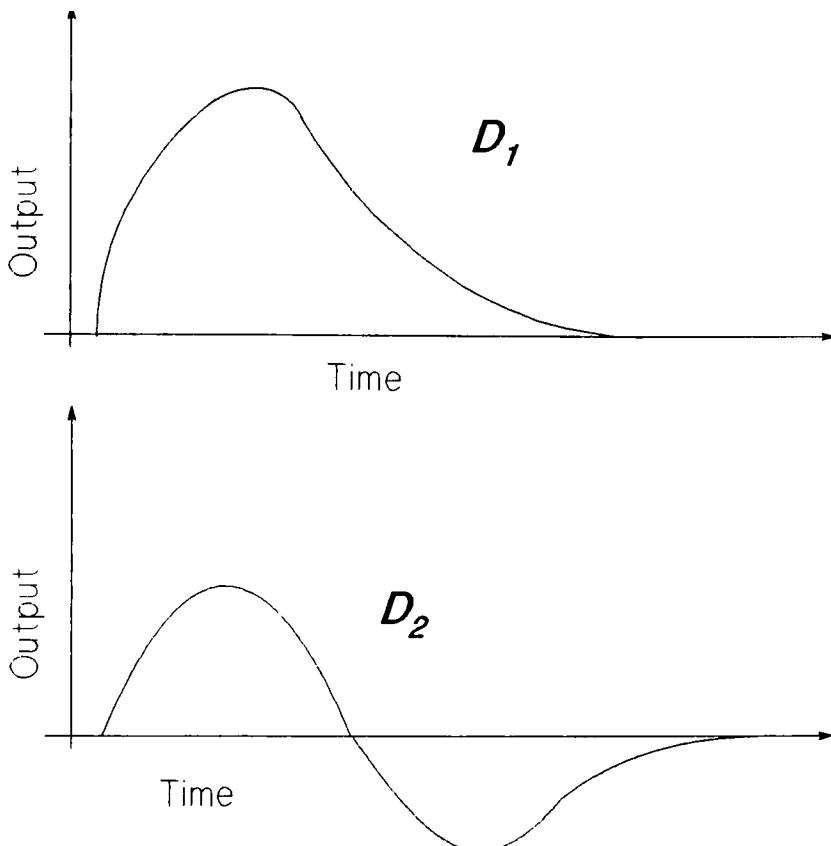


Figure C.2: Temporal responses of two different kinds of detector.

happen, for instance, if the detector response is driven by some accumulation of charge and there is a threshold for the reaction. This would be the case of someone trying to trigger an electronic flash too often. Beyond a certain frequency the triggering might start to happen when the capacitors have not built enough charge to excite the Xenon gas on the tube, and the trigger will not cause a flash.

The detector D_2 on figure C.2 shows a very similar behavior to detector D_1 , except that now the decay includes a period when the output of the detector is negative. This kind of behavior is typical of the cones in the human eye [61], while the rods behave as detector D_1 . This offers a potential problem for CRT measurements since the detector used might not detect the same amount of energy as the eye. Fortunately, the response time of the eye is quite slow, and if any artifact can be attributed to the temporal response function it is probably the increase in the flicker sensitivity at around 20 Hz [104, 100, 103]. The

fact that there are no reports in the literature concerning shifts on perceived chromaticity or brightness above 60 Hz at the typical CRT luminance (50 cd/m^2) is a good indication that as far as the eye is concerned the areas under convolution will simply multiply and we should not expect color shifts due to flicker in a regular CRT [67].

C.3.2 Integration of several emissions

Errors due to integration time will be common to almost all types of detector. The problem is two fold:

- Integration of noise.
- Synchronization of measurement.

We will discuss the two problems next.

C.3.2.1 Integration of noise

On the case where the detected signal is like that shown in figure C.3, there will be a short period of signal followed by lengthy period where only noise will be present. If the detector is sensitive enough it could extract the signal from a single spike. That will hardly ever be the case. First there are the obvious technical difficulties of accurately measuring such a small transient, and second, even if a very good detector is available there will be noise due to the fact that the spikes themselves are noisy, since there are small fluctuations in the placement and intensity of the electron beam from one scan to the other, and the limited number of photons available will make photon noise a factor [14, 80].

The best choice is, of course, to average several spikes. This brings the problem of the background noise that will also be integrated into the measurement. Part of the noise will be due to thermal or Johnson noise. Also, the signal to noise ratio increases only with the square root of the number of measurements (see [14], p. 116).

A better choice for measuring the signal might be to synchronize the measurements with the detector and only measure at the small time interval when the CRT screen is emitting.

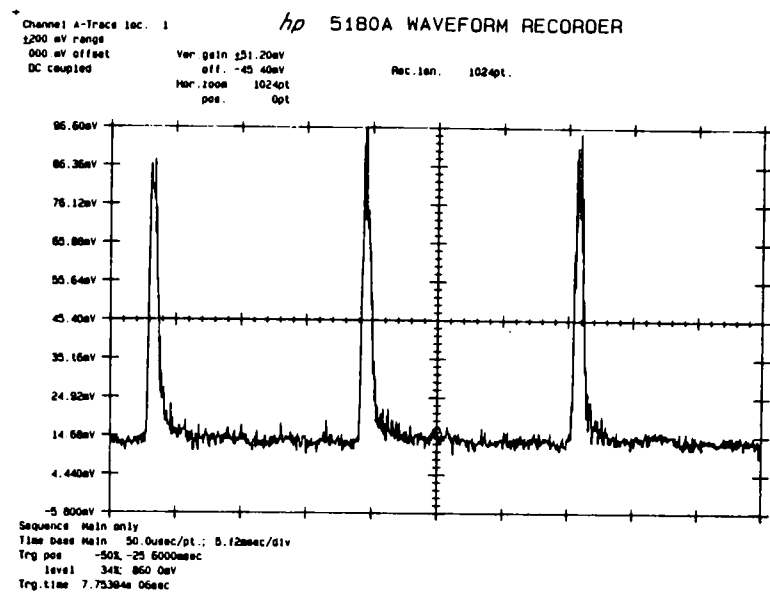


Figure C.3: Periodic signal with constant background noise.

This option is similar to the use of a lock-in amplifier, except that due to the shape of the exponential decay there will be no single harmonic carrying all the energy. The power spectrum of the CRT decay was measured with an Hewlett-Packard 3562A signal analyzer and is shown on figure C.4. The signal detector was a fast PMT. As we see there the higher harmonics due to the CRT flicker are coincident with the noise, and if a single frequency is chosen for measurement the signal might be distorted since different phosphors have different decay profiles.

C.3.2.2 Synchronization of measurement

Another class of problems resulting from the integration of the CRT emission is related to the synchronization, or lack of, between the detector and the CRT emission. Figure C.5 illustrates the problem. The detection period is T_d . Unless T has the same length as the display period times a round number, like 2/30 sec or 100/30 sec, there will be a residual left. This residual will cause a difference in phase between the detection and the emission, and the number of spikes being detected during T will fluctuate. In figure C.5 there is one spike during T_d in the first position and two spikes in the second position. It is easy to show that this fluctuation will be at maximum ± 1 spike, since if it was more than one spike the

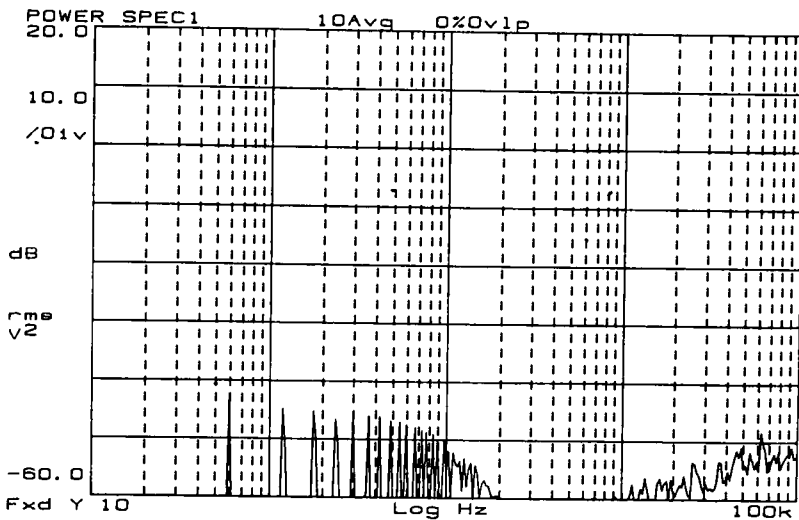


Figure C.4: Frequency spectrum of CRT signal and noise.

entire period would have increased by a round number, and the residual left will still be smaller than 1.

Another potential problem is that the detector might be taking repeated measurements, repeated at periods T_t and lasting only T_d each. Of course $T_d \leq T_t$ and unless both T_d and T_t are multiples of the display period the phase problems will appear.

One possible solution is to synchronize the measurement to the signal as has been reported by Kinameri. [108, 107] This will force at least the period T_t to be a multiple of the display period, and the T_d can be any other desired period. On the next sections we discuss how such concerns affect the measurements made with the Minolta TV-2160.

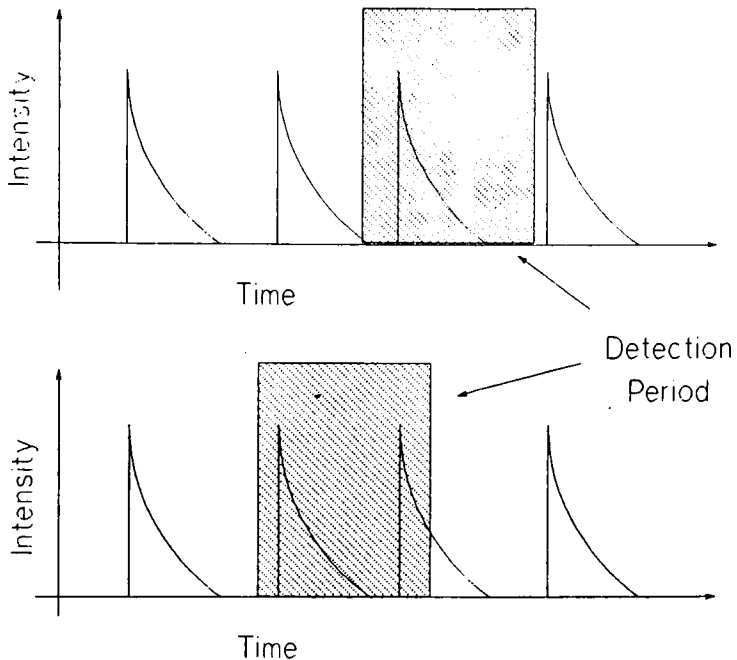


Figure C.5: Same detection period will collect different number of spikes.

C.4 Minolta Repeatability

For certain instruments, such as the Minolta TV-2160, there will be no way of triggering the device or controlling the rate of measurements. The rate at which the instrument reports data changes with the intensity of the signal, but it is usually within 0.55 ± 0.05 sec. During such a small period there will be an average of 30 spikes. Thus the fluctuations will be of $\pm 3.3\%$ and, assuming a uniform probability distribution, the standard deviation could be as large as 2% of the signal.

The actual sensitivity of the instrument to this kind of noise will depend on its strategy for sampling the data. Even though the instrument reports data at 0.5 seconds intervals, T_t and T_d might be very different. For instance, there are 4 silicon photocells on the probe, are they sampled together or in parallel? How long does the sampling of each lasts? Is there a "dead" period between samples? Is the sampling synchronized with the emissions? Since this instrument was designed specifically for the measurements of CRTs, one would believe that such things have been taken into account. One of the interesting properties of this instrument is that when the signal from the CRT changes suddenly the instruments

goes through large swings until it finally stabilizes, after about 3 seconds, or 6 reported data points. This kind of behavior could be explained, for instance, by the existence of an accumulator that gets reset if the signal change is larger than a certain threshold. This would allow integration times longer than 0.5 sec while still outputting data every 0.5 sec.

Last, but not least, one important source of noise often overlooked is quantization noise. The TV-2160 reports chromaticity only with 3 decimal places. If, for instance, the exact value was 0.2225, the output of the minolta should oscillate between 0.222 50% of the time and 0.223 the other 50% of the time. On other hand, if the signal was exactly 0.222, no variance due to quantization should occur. In practice, the situation might be a little worse, since the analog to digital converter (ADC) might have still less states. If an 8 bit ADC is used the smallest increment will be 1/256. Since the Y scale from the TV-2160 goes from 0.0 to 200, this would translate into increments of 0.78 cd/m^2 . A 10 bit ADC would give increments of 1/1024, or 0.2 cd/m^2 , which is closer to the actual behavior of the TV-2160.

To investigate some of these questions the experiments reported next were performed.

C.4.1 Experimental

During the investigation on the linearity of the TV-2160 photometric response reported in section C the standard deviations of the data were also calculated. No variance was observed, except for small fluctuations on the least significant digits of the measurements in the worst cases. The dc power supplied to the tungsten lamp was very well regulated, and no fluctuations of the lamp output would have been likely.

Another exploratory experiment was to place a chopper in front of the light source and run it at different frequencies. This time much larger variations were observed, confirming the hypothesis that the integration time might be a source of noise. At 60 Hz the variance was very similar to that of the CRT measurements that will be reported shortly. The chopper was also run at different frequencies in an attempt to identify the frequency of the TV-2160. No systematic behavior could be observed. The frequency control of the chopper was not accurate enough to permit this kind of investigation, and there was no means of

controlling the phase of the chopper. Ideally, one should be able to set the signal at a desired frequency and slowly change the phase to observe the TV-2160 response. The only meaningful observations were that at some frequencies the variance was much larger than at 60 HZ, and that at 20 Hz the readings drifted slowly and had little variance.

To numerically evaluate variance of CRT measurements, the probe of the TV-2160 was placed on area 1 of the Tek 690SR (see figure B.1) and 93 measurements were made automatically over a period of two days. The measurements were made at increments of 5 d' for whites from 25 to 255 digital counts. The colorimeter was set to the RGB mode. Enough time (about 1 minute) was allowed after each time the CRT signal level changed to permit the TV-2160 to reach equilibrium. Since the signal was always ramped-up and changed by small increments, it is assumed that the CRT was always thermally stable. The consequences of not allowing the CRT to stabilize are discussed in a later section.

C.4.2 Results

Table C.1 summarizes the principal results. The data are reported in terms of the relative CRT tristimulus values. The data were recorded in terms of RGB components since the variance of each individual channel was of interest. The variances are fairly small, about 1% in the worst cases and less than 0.2% in the better cases. This is much better than the 2% we predicted from the 0.5 seconds integration time. The standard deviations are also strongly correlated with the signal, although increasing much slower and having a small offset. This indicates that the variance is signal dependent, and probably, in view of the lack of variance in the linearity check experiment, due almost entirely to the integration time problems. At any rate, this is good news, since it indicates that for a stable system we can have 95% confidence that the signal is within 1% of the expected value.

d'	R trist. value		G trist. value		B tris. value		number of samples
	mean	std. dev.	mean	std. dev.	mean	std. dev.	
25	0.0001	0.00017	0.0014	0.00012	0.0020	0.00010	93
35	0.0009	0.00020	0.0042	0.00020	0.0056	0.00019	93
45	0.0037	0.00025	0.0096	0.00024	0.0116	0.00031	93
55	0.0091	0.00030	0.0177	0.00035	0.0205	0.00043	93
65	0.0175	0.00037	0.0289	0.00048	0.0322	0.00057	93
75	0.0288	0.00074	0.0433	0.00058	0.0471	0.00070	93
85	0.0439	0.00063	0.0610	0.00073	0.0652	0.00084	93
95	0.0622	0.00072	0.0823	0.00094	0.0867	0.00099	93
105	0.0836	0.00085	0.1065	0.00107	0.1106	0.00116	93
115	0.1101	0.00100	0.1346	0.00124	0.1388	0.00128	93
125	0.1395	0.00122	0.1667	0.00148	0.1707	0.00150	93
135	0.1721	0.00138	0.2027	0.00163	0.2059	0.00165	93
145	0.2117	0.00162	0.2422	0.00189	0.2447	0.00187	93
155	0.2543	0.00171	0.2861	0.00195	0.2889	0.00194	93
165	0.3005	0.00185	0.3353	0.00206	0.3358	0.00206	93
175	0.3542	0.00204	0.3882	0.00224	0.3892	0.00224	93
185	0.4115	0.00216	0.4461	0.00244	0.4448	0.00232	93
195	0.4754	0.00225	0.5079	0.00240	0.5055	0.00239	93
205	0.5449	0.00296	0.5735	0.00206	0.5715	0.00208	93
215	0.6120	0.00243	0.6453	0.00244	0.6404	0.00251	93
225	0.6914	0.00211	0.7202	0.00173	0.7119	0.00216	93
235	0.7780	0.00223	0.7968	0.00165	0.7887	0.00190	93
245	0.8559	0.00062	0.8766	0.00027	0.8675	0.00062	93
255	0.9549	0.00376	0.9614	0.00381	0.9526	0.00375	93

Table C.1: Uncertainty on the value of $L_{d'}$ determined by generating sequential series of d' on the Tektronix 650 HR.

As the reader might have realized, it is very hard to separate the variance due to the CRT itself from the variance due to the CRT/detector combination. Better detectors were not available during this investigation, but for the reasons already discussed, one should not expect a much better performance. If the case would be that one could devise a measurement that was free from the problems we discussed, the ultimate question would be: *How much of the noise encountered in measurements is actually meaningful for the human visual system?* How much of the variance encountered might really affect a matching experiment? The answer is probably application dependent, and will have to be determined by testing the performance of observers in a real situation.

C.5 CRT Repeatability

C.5.1 Introduction

The data reported on table C.1 was obtained under conditions that allowed the CRT to get near thermal equilibrium before each measurement. Thermal equilibrium is among the foremost factors determining the CRT repeatability in day to day operations. As any non-ideal mechanism, part of the energy that should go towards the intended task - transforming video voltages into visible radiation - will be lost as heat. Since the amount of heat is proportional to the work-load, and since the performance of most electrical components is temperature dependent, the CRT output will fluctuate with temperature changes. To describe the CRT temperature as a function of the load, the concepts of convolution and MTF are used (actually, such concepts derive from work on heat dissipation). The system will have a characteristic reaction time to changes in temperature, and for certain low frequencies the system temperature will change along with the load. If the frequency of changes is increased the CRT system might not be able to follow, and will begin to lag in time, creating a phase difference, until the frequency changes so fast that the system stays at a constant temperature with, maybe, some small fluctuations added to it. The problem is further complicated because different parts of the CRT will have different thermal

conductivities, specific heats and coefficients of expansion. Different components will be out of phase with the others and any attempt to predict the CRT behavior has probably little chance of success.

For many psychophysical experiments, such as the ones that involve some kind of matching, the load will change slowly, but one can easily imagine other experiments where an abrupt change on the CRT state would be desirable. Examples of this kind of experiment would include the study of image after-effects, flicker photometry and detection of flashing targets.

Next, we will attempt to quantify the two aspects of the CRT thermal properties that might affect color appearance experiments:

- Long term stability
- Short term repeatability

C.5.2 Long term stability

In the best of worlds the CRT would be stable and ready to use the moment we turn it on. In reality, this is hardly the case. To determine the warm-up time of the Tek 690SR and its stability after a long time of operation, the CRT was first turned off for longer than 6 hours. With the Minolta TV-2160 probe placed in position one and luminance being recorded at every minute, the CRT was turned on with a $d' = 255$ white field applied to it. The result of the first hour of operation is shown in figure C.6. On figure C.7 we display the changes in luminance during the first 6 hours of operation. Longer periods observation will show no new trends.

After being turned on the CRT output increased rapidly and was higher than the level of stabilization. The output oscillated up and down about the stabilization level with decreasing amplitude. In about 1 hour the CRT was within 1% of the mean stabilization level, which also fluctuated by about $\pm 1\%$ for the several hours of the experiment.

This behavior was typical of several CRTs measured. If the CRT was still warm from previous use, it would converge faster to a stable level. The long term fluctuations (with

a period of about one hour) was also observed on different CRTs. The reasons for these fluctuations are not clear. The fluctuations could also be caused by fluctuations of the power line.

C.5.3 Short term repeatability

A much more tangible deviation caused by the CRT “inertia” is the time it takes to settle to a level of emission after a certain level d' has been set. By connecting the Gamma Scientific telecolorimeter to the chart recorder it was observed that it takes almost five minutes for the CRT radiance to converge to a white $d' = 255$ level when we start from a stable black at $d' = 0$. As one would expect, smaller differences in levels are translated into smaller convergence times. It was also observed, that if such measurements were made on a small area, while the others remained fixed, the convergence time would change significantly (usually shorter). This kind of behavior indicates that the response time is dependent on the total load, and as discussed in section E, this kind of problem will be very hard to model.

Instead of modeling the effects of the CRT inertia, we have opted to characterize what would be the largest deviations that could be attributed to it.

C.5.3.1 Experimental

The largest deviations that can be caused by the CRT inertia would occur when the entire CRT image is quickly changing and there is no correlation between each successive level. This kind of situation could occur when a test patch is moving over an image containing a complex image. To simulate this situation a uniform random number generator was used to generate d' levels between 5 and 255 at intervals of 10 digital counts. White fields were generated at the random levels, and the mean and the standard deviations of the independent measurements at each level were calculated. Because we were interested in the combined repeatability of the detector/CRT combination, the data was recorded as Yxy since this was the typical setup of the colorimeter. A total of 2000 measurements were

made, which gives about 80 measurements per d' level. Each measurement was made by discarding the first 4 values reported by the TV-2160 and averaging the next 4. In total, the CRT stayed about 4 seconds at each level.

C.5.4 Results

As indicated in table C.2, the standard deviations obtained under these conditions are much larger than those obtained in section C.4, when the CRT was allowed to stabilize. The standard deviations amounted to about 0.5% of the means, which is very encouraging given that this is the worse possible case. Again, the standard deviation is correlated to the mean signal, except that in this case it is increasing at almost the same rate as the signal. The variance obtained is the result of the variances of the TV-2160 and the CRT itself multiplied, which indicates that the variances from the CRT inertia must be large.

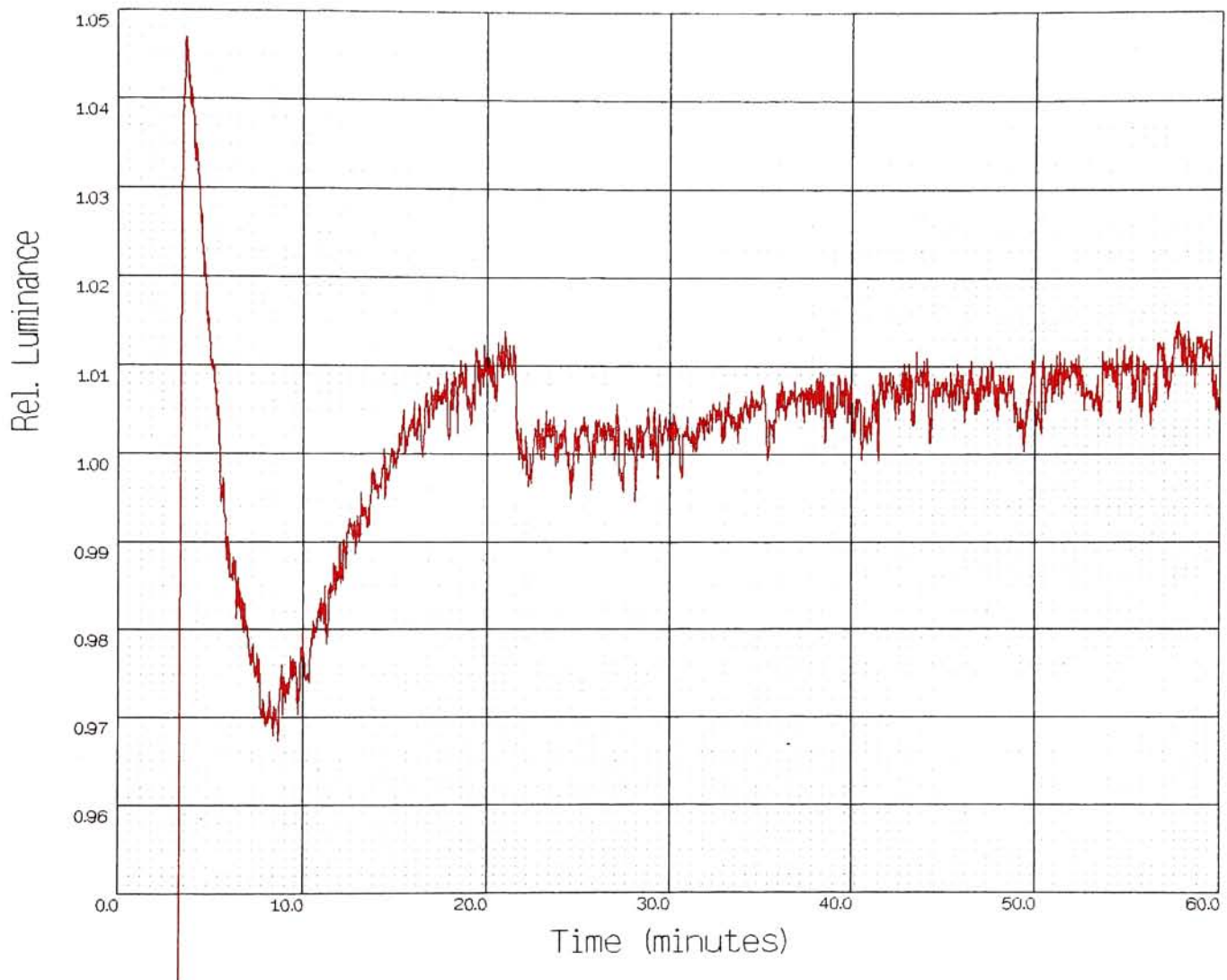


Figure C.6: Luminous output of a CRT during the first hour of operation.

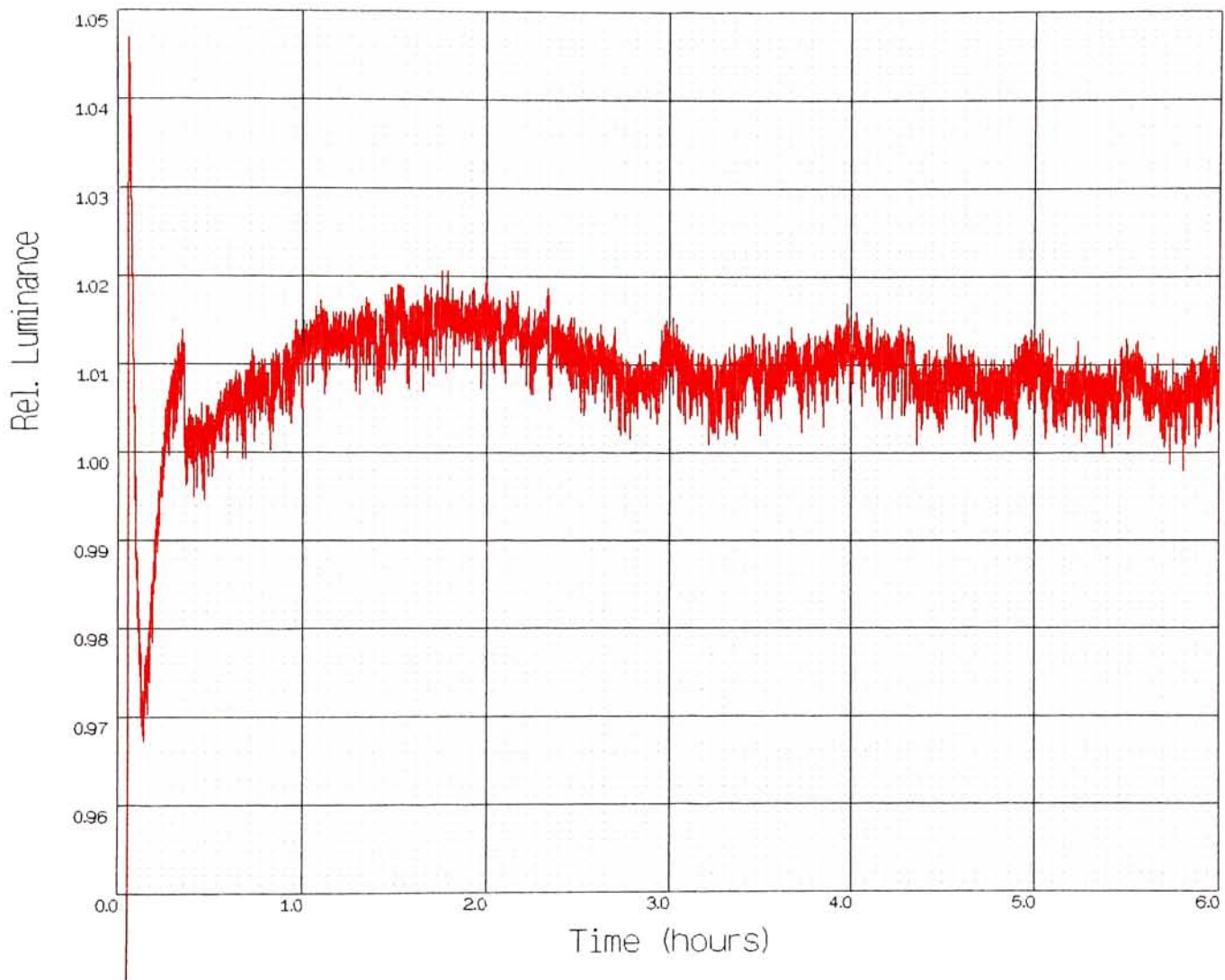


Figure C.7: Luminous output of a CRT during the first six hours of operation.

d'	Y tristimulus		x chromaticity		y chromaticity		number of samples
	mean	std. dev.	mean	std. dev.	mean	std. dev.	
25	0.0063	0.00697	0.2059	0.05477	0.1180	0.13621	102
35	0.0332	0.00446	0.2632	0.00858	0.1626	0.01505	115
45	0.1438	0.00408	0.2676	0.00213	0.1915	0.00477	119
55	0.4133	0.00725	0.2672	0.00344	0.2134	0.00293	110
65	0.8818	0.00659	0.2708	0.00143	0.2248	0.00123	110
75	1.5899	0.00815	0.2721	0.00071	0.2334	0.00067	114
85	2.5545	0.01033	0.2724	0.00038	0.2396	0.00035	102
95	3.7921	0.01366	0.2729	0.00023	0.2438	0.00025	112
105	5.3090	0.01672	0.2730	0.00017	0.2472	0.00024	138
115	7.1450	0.02082	0.2732	0.00019	0.2499	0.00014	106
125	9.2727	0.02258	0.2733	0.00022	0.2520	0.00006	118
135	11.6944	0.03612	0.2735	0.00024	0.2536	0.00023	109
145	14.4902	0.03997	0.2738	0.00017	0.2550	0.00001	99
155	17.6141	0.04315	0.2740	0.00006	0.2560	0.00000	123
165	21.1181	0.05416	0.2740	0.00001	0.2570	0.00000	110
175	24.9338	0.05909	0.2740	0.00000	0.2580	0.00000	107
185	29.1532	0.05866	0.2740	0.00000	0.2590	0.00007	115
195	33.7467	0.07381	0.2740	0.00000	0.2590	0.00004	111
205	38.6645	0.10239	0.2742	0.00027	0.2600	0.00000	123
215	43.9856	0.09117	0.2749	0.00020	0.2600	0.00002	113
225	49.6859	0.10752	0.2750	0.00000	0.2610	0.00000	122
235	55.7737	0.12981	0.2750	0.00000	0.2610	0.00000	116
245	62.2598	0.12447	0.2750	0.00000	0.2619	0.00012	110
255	69.0570	0.14517	0.2752	0.00032	0.2620	0.00000	169

Table C.2: Uncertainty on the value of $L_{d'}$ determined by generating random levels of d' on the Tektronix 650 HR.

Appendix D

Minolta Linearity Correction

D.1 Photometric Scale

A simplified equation for a radiation detection system will be like this [177],

$$S' = R A (E_s + B)(1 + q_s) + S_b + q_b \quad (\text{D.1})$$

where

S' = Detected signal, volts

R = Responsivity of the detector, volts/W (Watt)

E_s = Irradiance from signal to be detected, W/m²

B = Irradiance from background, W/m²

A = Area of detector, m²

S_b = Dark signal, volts

q_s = Signal dependent noise, $\bar{q}_s = 0$, dimensionless

q_b = Background noise, $\bar{q}_b = 0$, dimensionless

If we eliminate the noise (by averaging or filtering), the first derivative of the above

expression with respect to the irradiance will be

$$\frac{dS'}{dE} = R A \quad (\text{D.2})$$

or in other words, the gain of the signal will be proportional to the responsivity and the area of the detector. If $R A$ stay constant throughout the range of the instrument the radiometric scale is said to be linear.

In a complex instrument such as the Minolta TV-2160 most of the terms in equation D.1 will be accounted for by the internal circuitry, which will subtract the background level, as well as average and amplify the signal. If everything is done correctly, we expect the instrument to report a value $f_1(E)$ ¹, from an input E , identical to what could be obtained by other means, $f_2(E)$, from the same input.

$$\cdot \quad f_1(E) = f_2(E)$$

Unfortunately, detectors and detection circuits are not always perfectly linear. The silicon photodetectors used by the TV-2160, as most silicon photodiodes, are probably fairly linear over a wide range of inputs [30]. The difficulties arise from the need of having two or more different types of detectors, or having several of the same detectors on different circuits. Whatever is the actual arrangement of the TV-2160, one should expect non-linearities that were caused either by drift since the factory calibration, or that were never accounted for.

If the detector is not linear it will differ from the correct value by

$$\frac{f_2(E)}{f_1(E)} = \varphi(E) \quad (\text{D.3})$$

where $\varphi(E)$ is a correction factor. By comparing $f_1(E)$ with the predicted value we can obtain a table or an equation for predicting $\varphi(E)$ and use it to correct the TV-2160 signal,

$$f_2(E) = \varphi(E)f_1(E) \quad (\text{D.4})$$

Several techniques are possible for the determination of $\varphi(E)$. Any other well calibrated mean of modulating or measuring the radiation could be used. This would include,

¹The function f is used here to indicate that the instrument is reporting some value that is derived from the irradiance, but not necessarily the irradiance itself.

- Filters
- Light sources
- Other detectors

Another group of techniques commonly used is to modulate a single light source by well known and easy to measure physical method such as,

- Modulating the area of emission
- Modulating the duration of the emission
- Changing the distance from source to detector.

This last is most times the method that is easier to use and will provide the most accurate results. It uses the well known property of light sources known as the Inverse Square Law, which we will discuss next.

D.1.1 Inverse Square Law

Stated in words, the inverse square law [30] would be

The amount of flux originating from a point source which irradiates equal flux in all directions and reaching an area of fixed size and normal to the axis of propagation, will decrease with the square of the distance from the area to the point source.

This is illustrated on figure D.1. The point source is at the origin **O** and $I_\theta = I_0$, i.e. the radiant intensity (W/steradian) is the same in all directions. At distance d_1 from the origin the area A_1 is covering

$$\omega = \frac{A_1}{d_1^2} \text{ (steradians)}$$

At a greater distance, d_2 the same solid angle will cover a much larger area

$$\omega = \frac{A_2}{d_2^2}$$

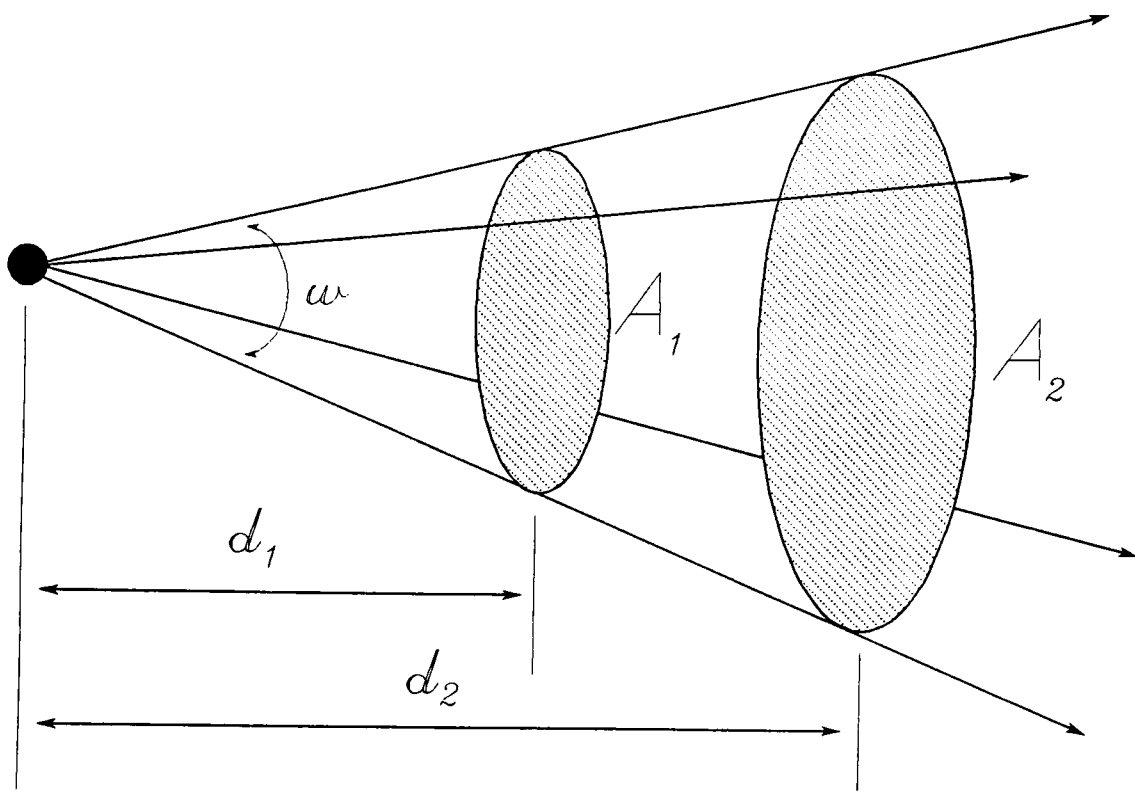


Figure D.1: Diagram illustrating the inverse square law.

and it follows that the two areas are related by

$$\frac{A_2}{A_1} = \left(\frac{d_2}{d_1} \right)^2 \quad (\text{D.5})$$

The same radiant flux Φ will be passing through both areas, and the irradiance will decrease from area A_1 to A_2 according to

$$\begin{aligned} E &= \frac{dI d\omega}{dA} \\ E_1 &= \frac{\Phi}{A_1} \\ E_2 &= \frac{\Phi}{A_2} \\ E_2 &= E_1 \frac{A_2}{A_1} \\ E_2 &= E_1 \left(\frac{d_2}{d_1} \right)^2 \end{aligned}$$

Our detector calibration can then be carried out by measuring E_1 at an arbitrary (but known) distance d_1 from the source and predicting what should be the measured value at the other positions d_2 . The ratio between the predicted value $f_2(E_2)$ and the value reported by the instrument $f_1(E_2)$ will then be the correction term $\varphi(E_2)$.

$$\frac{f_1(E_2) \varphi(E_2)}{f_2(E_1)} = \left(\frac{d_1}{d_2} \right)^2 \quad (\text{D.6})$$

and the correction factor is calculated simply as

$$\varphi(E_2) = \frac{f_2(E_1)}{f_1(E_2)} \left(\frac{d_1}{d_2} \right)^2 \quad (\text{D.7})$$

It should be noticed that $f_2(E_1)$ must be obtained with a reference instrument, since otherwise $\varphi(E_1) = 1.0$, and all results will be scaled wrong.

D.1.2 Experimental

The source of radiation was an Optronics light source. This light source contains a tungsten bulb with a fan and a large focusing mirror, which was used to focus the radiation on a aperture slit equipped with a micrometer. The radiation from this small aperture behaved

like the desired point source. To balance the tungsten source to a white more similar to the color CRTs a Wratten filter 78A was placed between the source and the aperture. The TV-2160 probe was mounted on a Oriel rod which could be slided across a precision rail. The center of the probe was aligned with the slit aperture.

Because the rail was relatively short (20 inches) 2 series of measurements had to be made:

- Detector and Wratten 78A.
- Detector, Wratten 78A, a iconel filter (ND 1.0), and a Wratten no. 96 filter (ND 0.3)

The amount of filtering was chosen to insure that the two range of measurements would meet. For each measurement the probe was placed from 13 cm to 67 cm of the aperture, with 10 measurements averaged at each 1 cm interval. The entire experiment was repeated twice, once going away from the source and another time going in the direction of the source, and the results averaged. During the measurements the room was darkened, all sources of stray light covered and the equipment covered with black velvet.

D.1.3 Results

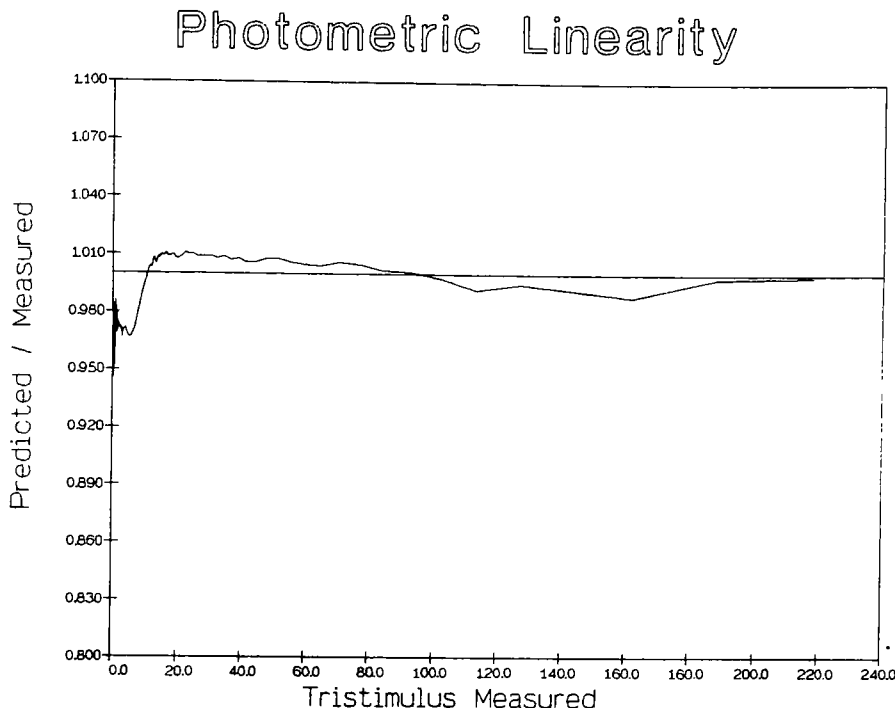
$f_2(E_1)$ was established by measuring the CIE 1931 XYZ tristimulus with a Minolta CL-100 colorimeter, which earlier experience had shown to be well calibrated. A single measurement was made at a level that coincided with the lowest levels of the high-intensity range and the highest levels of the low intensity range. This value served not only to find the correct data, but also to “glue” the two ranges together. To better illustrate this, the data are presented here:

Range of distances $13.0 \rightarrow 67.0\text{cm}$

High range $X = 244.64 \rightarrow 8.73$

$Y = 218.00 \rightarrow 8.25$

$Z = 158.27 \rightarrow 5.93$



. Figure D.2: φ , correction term for photometric linearity of the X tristimulus value.

$$\text{Low range } X = 11.76 \rightarrow 0.40$$

$$Y = 10.50 \rightarrow 0.38$$

$$Z = 6.10 \rightarrow 0.21$$

$$f_2(E_1) \quad X = 12.62$$

$$Y = 11.60$$

$$Z = 6.13$$

As we see, most of the measurements were concentrated on the low end of the photometric scale. This is unfortunate, since the top of the scale is probably more important. The difficulty was that to be able to measure the top of the photometric scale with the same intervals as at the end, the distances moved would have to be quite small, and that would be beyond the precision of the equipment used.

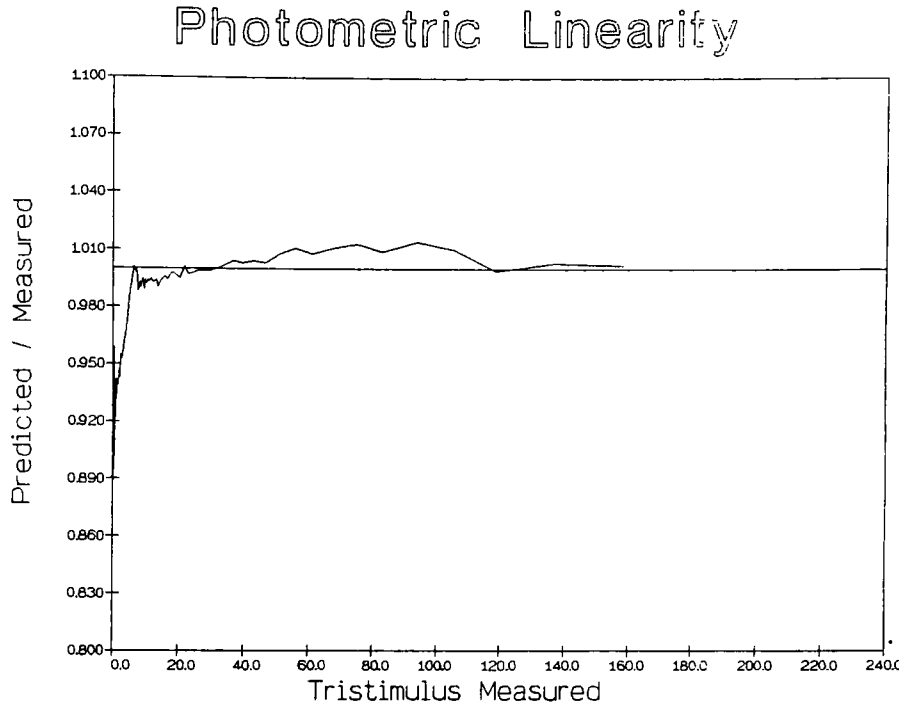


Figure D.3: φ , correction term for photometric linearity of the Y tristimulus value.

Figures D.2 thru D.4 depicts the values obtained for $\varphi(E_2)$ of the X , Y and Z tristimulus values. The deviations are in general small. Above the value of 20, the Y and Z tristimulus values stayed well within 2% of the correct value. The tristimulus value X showed a systematic deviation above 20, staying constant at about 5% more than the correct tristimulus.

Below value 10, all three tristimulus values showed a strong deviation. Figure D.5 is provided here to give a qualitative view of the same data. The three $\varphi(E_2)$ curves are shown together with the vertical axis kept, linear and the horizontal axis logarithmic. The two axes on the plot cross at the tristimulus value = 1.0 (i.e. $\log = 0.0$) and $\varphi(E_2) = 1.0$. These curves were smoothed by convolution with a square kernel. Although Minolta's manual for the TV-2160 advertises the range of the instrument as being from 3 to 200 cd/m^2 , the instrument appears very unreliable below 10 cd/m^2 . Interesting enough, the deviation is

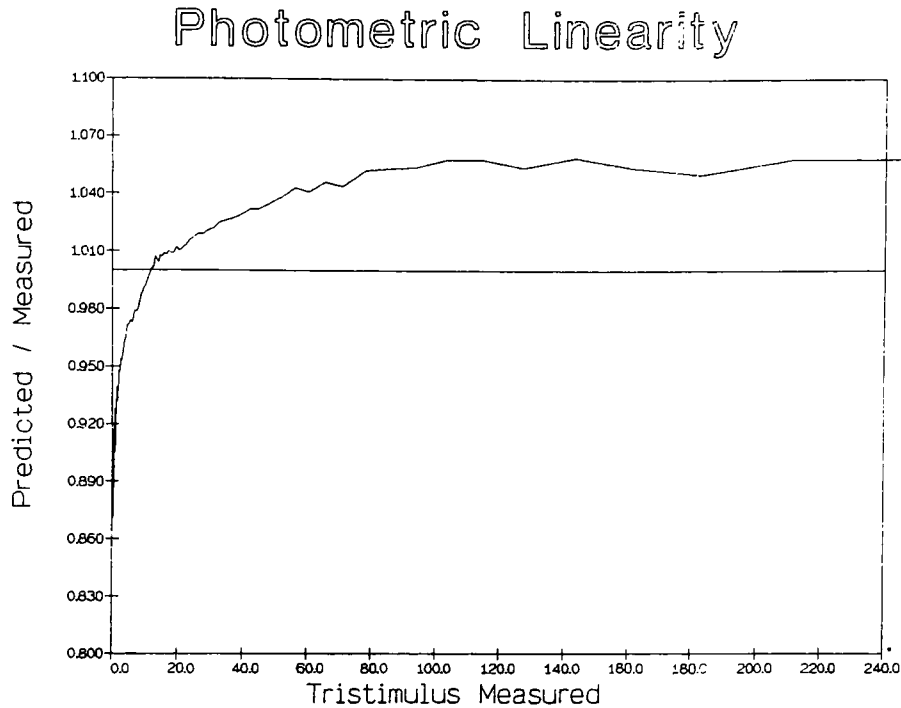


Figure D.4: φ , correction term for photometric linearity of the Z tristimulus value.

towards more sensitivity, i.e. the value reported by the TV-2160 is larger than the correct value. It may be that at these low levels the amplifying circuit changes its gain and we see a different behavior.

The smoothed data shown on figure D.5 was resampled at regular photometric intervals and later used for correcting the TV-2160 output. The measurement software loaded the data into a table and only the corrected tristimulus values were recorded.

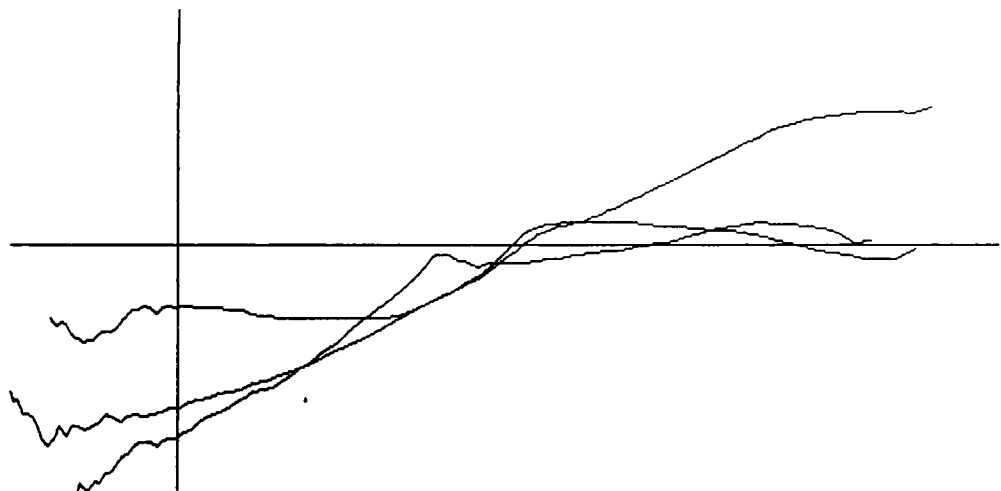


Figure D.5: All three correction terms plotted with a logarithmic horizontal axis.

Appendix E

Load Dependency

E.1 Introduction

Two crucial assumption made during the development of the CRT model in section 2.3.1 were:

- The anode voltage accelerating the electron beam is independent of the load on the CRT (equation A.21).

$$\Phi_e = k_f j (v_s - v_0)^n$$

- The operation of the CRT video amplifier is independent of the load on the CRT (equation A.13).

$$v_{G1} = k_p (a v_d + b)$$

The load is the total amount of work that is required from the CRT in a given instant to produce the image. Thus, if the image is a black field, the load will be small. Under this condition there is little signal to amplify, no electron beam to accelerate, deflect and no energy to dissipate or convert. When a white field is displayed on the CRT the situation will be very different. A large signal will have to be amplified; a larger mass of electrons will have to be deflected and accelerated from the cathode to anode, and, as one would expect, the expenditure of power will be greater. The power to perform these operations comes

from the CRT power supply. Actually, there are more than one. A high-voltage power supply is needed to raise the potential of the anode to 25 Kv or more. Throughout the CRT there are other circuits to be powered, each at its own level. For instance, the cathode heater has to be at a stable temperature to supply a constant flux of electrons; a change in the power supplied to the deflection coils might distort and change the shape of the picture; the voltage also has to be stepped up to supply the higher voltage of the second grid; and finally, all the signal processing circuitry will also have its different supply requirements. Power supplies are usually regulated to give constant voltage or constant current. The better the regulation, the more expensive and heavier the power supply will tend to be. When the workload increases above the capability of a power supply the delivered power will decrease, and again different parts of the CRT might be affected in different ways. The actual reaction is to a great extent dependent on the circuit design, and some functions might be favored over others.

From the perspective of colorimetric performance, one of the most noticeable deviations will be the decrease in the CRT output as the load increases. This deviation might be small, like $\approx 2\%$ on the Tektronix 690SR, or as large as 70% in the Barco CD33HR and the DEC VR241A. In other CRTs, like the Sony PVM-1270, the change in output with increased load is rather erratic. It will decrease at first to suddenly bounce back and overshoot the original value, indicating that some internal mechanism is trying to account for the increase in load.

The reasons behind the large deviations found on the CD33HR and the VR241A are probably rather complex. The voltage supplied to the video amplifier might decrease, bringing its operational limit down, and along with it the maximum output. Or the anode high-voltage might have dropped, or a combination of both. Cowan [57] has reported small deviations, on the order of 3% for the Tek 690SR. He called this kind of phenomena “inter-gun relationship”. We have opted instead to call it “load dependency”, since the deviations do not appear to be due to the guns, but to the load on the CRT, and because it can affect channels even when they are operated alone.

In the experiments reported next the attempt was made to characterize this load dependency, and to understand what factors will be determining it.

E.2 Additivity Failure

The additive properties of a color CRT are of paramount importance. Simply stated, we expect that it will obey Grassmann's laws [79], and that a stimuli H can be obtained by the addition of the CRT primaries,¹

$$H = R\mathcal{R} + G\mathcal{G} + B\mathcal{B} \quad (\text{E.1})$$

For this kind of additivity to hold R , G and B have to be independent; i.e. a change in any tristimulus value must not affect the other two. Additivity failure can be verified by comparing the stimulus produced when the all three channels are loaded together to the sum of the stimulus produced when each channel is loaded individually.

$$D = R\mathcal{R}$$

$$E = G\mathcal{G}$$

$$F = B\mathcal{B}$$

and a failure will be verified by

$$\frac{H}{D+E+F} \neq 1 \quad (\text{E.2})$$

Additivity is also expected within the range of each tristimulus. For instance,

$$D_1 = R_1\mathcal{R}$$

$$D_2 = R_2\mathcal{R}$$

$$D_3 = (R_1 + R_2)\mathcal{R}$$

and an additivity failure will occur if

$$\frac{D_3}{D_1 + D_2} \neq 1 \quad (\text{E.3})$$

¹We use here the $=$ sign instead of the \equiv sign since we will be describing the formulation of the color and not its appearance.

This last kind of deviation will be more difficult to observe since we do not know a priori which are the rules governing the CRT tristimulus values. When characterizing a CRT we will determine that some stimulus D_1 is obtained with a value d'_1 , to obtain D_2 we need d'_2 , and to obtain D_3 we need d'_3 . Since we do not know the relation between d' and C we must attribute to C the values measured for D and this way the failure becomes “built-in” to the data. The other kind of failure is much more obvious, since in that case there will be two or more ways of describing the relation between C and d' , and the inconsistencies in the measurements are obvious.

E.2.1 Measuring the additivity failure

The Minolta TV-2160 was used along with the Barco CD33HR for most load dependency experiments. Although another CRT, the DEC VR241, was also used in the investigation, the results are not significantly different from those of the Barco. For this experiment, the frame buffer had a constant d for all the pixels and the LUT was modified to the desired d' . To study a worst case situation, both the gain and the offset (the contrast and the brightness knobs) of the monitor was set to each maximum value. The probe of the TV-2160 was placed in the middle of the screen and 4 series of measurements were made. d' was increased from 5 to 255 in increments of 10 digital counts for all 7 combinations of the red, green and blue channels (i.e. R, G, B, C, M, Y, W). The luminance Y was the only value recorded.

Part of the resulting data is reported in table E.1. The two very noticeable features are that the transfer functions are almost linear, and that the measured white is about 50% of the predicted white. This illustrates the two forms of additivity failures that we discussed before.

At this point of the investigation the source of the additivity failure was not clear yet. It could be due to saturation of the phosphors or due to some other property of the phosphor screen. Also, it could be in the electron guns, as was implied by Cowan. [57] Two simple experiments where carried out to isolate the source of failures.

DC	Y(r)	Y(g)	Y(b)	Y(w)	Y(w)/Y(r) + Y(g) + Y(b)
25	0.30	1.80	0.20	2.60	1.13
35	0.60	3.40	0.40	4.60	1.05
45	1.10	5.50	0.70	7.10	0.97
55	1.70	8.20	0.90	10.10	0.94
65	2.60	11.30	1.30	13.10	0.86
75	3.50	14.80	1.70	16.70	0.84
85	4.50	18.40	2.20	20.30	0.81
95	5.80	22.70	2.70	23.60	0.76
105	7.00	26.80	3.20	26.90	0.73
115	8.60	31.20	3.80	30.10	0.69
125	9.90	35.70	4.40	33.00	0.66
135	11.50	40.60	5.00	36.40	0.64
145	13.00	45.20	5.60	39.10	0.61
155	14.30	49.40	6.10	41.60	0.60
165	16.00	53.30	6.70	44.10	0.58
175	17.10	56.60	7.30	46.70	0.58
185	18.80	61.20	7.80	48.70	0.55
195	20.10	63.40	8.40	50.80	0.55
205	21.30	68.20	8.70	54.20	0.55
215	22.80	71.40	9.20	56.30	0.54
225	23.70	74.50	9.80	57.20	0.53
235	25.30	77.40	10.30	58.80	0.52
245	25.90	81.20	10.60	61.30	0.52
255	27.90	84.40	11.20	63.40	0.51

Table E.1: Ratio between predicted and measured “white” luminance for the Barco CD33HR

E.2.1.1 Additivity of the phosphor screen

One possible cause for the additivity failure would be found if the CRT screen reacted differently when only one gun was exciting one area and when the three guns excited the same area. An increased number of electrons at the anode might lower its potential, or local temperature effects might distort the shadow mask, change the efficiency of the phosphors or saturate them. To investigate whether any of that was happening the following experiment was carried out.



Figure E.1: Picture of set-up for testing the screen additivity.

The large aperture of an integrating sphere from an old Perkin-Elmer instrument was placed against the Barco CD33HR. Figure E.1 illustrates the arrangement. The aperture of the sphere against the CRT was about 4 inches in diameter. On the area covered by the sphere 3 squares were generated, they are also shown in the monitor in the front, the DEC VR241. Inside the sphere a small baffle was built to avoid radiation from the CRT to reach

the measurement region directly. The Photo-Research PR703A/PC was used to make the measurements by introducing the lens on the tube that previously contained the instrument PMT and focusing on the spot protected from direct exposure to the CRT radiation. The other ports of the sphere were covered with Halon tablets (figure E.1 shows the sphere with one of the tablets removed).

The measurements consisted of substituting the individual red, green and blue squares by a single white square with the same d' values. This was done over 25 values of d' from 5 to 255 digital counts. At each level 6 measurements were carried out. First 3 measurements were made with the 3 squares exchanging position and averaging the results to account for any problem with the screen uniformity. Second, the same rotation technique was used with a single white square by placing it on each of the three square positions and averaging the results.

The radiation emitted by the 3 individual squares and by the white square showed no meaningful deviation, and it was concluded that the CRT screen was additive.

E.2.1.2 Measuring v_{G1}

If the additivity failure was due to some phenomena occurring inside of the CRT itself, say, at the guns, and not on the support circuitry, we should expect that v_{G1} will not display any deviations. For example, $v_{G1,r}$, the first grid voltage of the red gun, should always have the same value for a given video voltage² $v_{d,r}$, video amplifier gain a_r and video amplifier offset b_r . This value should be constant irrespective of the signals being fed to the other circuits.

This can be simply verified by using a oscilloscope to measure v_{G1} . The wires carrying the signal can be identified near the end of the tube. The signal is negative and ranges usually from 0 to -100 volts. The measurements were made on the red circuit by first allowing the screen to be filled by red at $d' = 255$ and then turning on the green and blue channels also at $d' = 255$.

²The linearity and load independence of the video generator are well established.

The addition of the green and blue channels resulted in a clear drop (the signal became closer to zero) on the voltage of the first grid of the red gun, indicating that some of the causes of additive failure were outside of the tube, in the amplifying circuitry.

To verify whether any part of the additive failure was due to the properties that changed inside of the tube, like a drop in the Ultor voltage, another series of experiments was performed. This time the image was divided into two halves, with the right made red at an intermediate level and the left full intensity white. The TV-2160 probe was placed on the right half, measuring the luminance of the red phosphor. By changing the left half of the image from white to black a drop in the $v_{G1,r}$ was observed with the oscilloscope. The difference from the previous experiment was that this time d'_r was increased until the original (i.e. with a black left half) $v_{G1,r}$ was restored. Luminances readings where taken at the two conditions. If the CRT had changed its properties due to a increase in load, one would expect the two luminances to be different for the same value of $v_{G1,r}$, with the luminance of the red field with a black left field being larger than the luminance of the red field with a white left field, since the load would be greater in the later case.

The measurements showed no systematic deviations when the CRT was set-up with a moderate gain and the offset was just high enough to make the black field invisible. Under these conditions the same luminance was obtained for a certain level of $v_{G1,r}$, irrespective of the condition of the left field. Only at very high levels of load, when the brightness and the contrast knobs where set to their maximum, did a certain $v_{G1,r}$ fail to produce a constant luminance. Since additivity failure was observed at both the regular and high-load CRT set-ups, it appears that most of the failure can be attributed to the CRT circuit, and only marginally to changes in the CRT properties. It was also concluded that load dependency, instead of inter-gun relationship, was a better name for this type of artifact.

E.2.2 Modeling the Additivity Failure

Let C be the expected CRT tristimulus value and C' the measured tristimulus value of a single CRT channel. We have the relation

$$\frac{C'}{C} = l \quad (\text{E.4})$$

where $l \leq 1$. The value that we measure will be smaller or equal the value one would have measured if load dependency was not present. C will create a load on the CRT that will change the value of C' and the value of the tristimulus values of the other channels. By the same token, the load on the other CRT channels will also change C .

$$\frac{C'}{C} = l_r l_g l_b \quad (\text{E.5})$$

When we display a color composed of contributions from all three channels, its tristimulus values will be

$$C' = R' + G' + B' \quad (\text{E.6})$$

or

$$C' = l_{rr} l_{rg} l_{rb} R + l_{gr} l_{gg} l_{gb} G + l_{br} l_{bg} l_{bb} B \quad (\text{E.7})$$

where l_{rr} is the loss in the red tristimulus value due to the load on the red channel, l_{rg} is the loss in the red tristimulus value due to the load on the green channel, and so on. If the loss in tristimulus value due to one channel is the same in all the other channels (i.e. $l_{rr} = l_{gr} = l_{br}$) the simplified expression will be

$$C' = l_r l_g l_b (R + G + B) \quad (\text{E.8})$$

When we measure each channel individually only the load of that channel will be influencing the measurement,

$$R' = l_r R$$

$$G' = l_g R$$

$$B' = l_b R$$

and the signal predicted by the addition of these tristimulus values will be,

$$C' = l_r R + l_g G + l_b B \quad (\text{E.9})$$

and

$$\frac{l_r l_g l_b (R + G + B)}{l_r R + l_g G + l_b B} = F \quad (\text{E.10})$$

where $1 - F$ is the fraction of the signal lost due to additivity failure.

Two interesting corollaries are the cases of a uniform white field and a uniform field made up by only two channels. The assumption to be made is that when the same tristimulus value is displayed on any channel the load will be the same. This is very plausible, since as far as the signals are concerned the CRT is color blind. This will imply that to a first approximations $C_w = R = G = B$ then $l_w = l_r = l_g = l_b$, and F for a uniform white or gray field is simply

$$\begin{aligned} F_w &= \frac{l_r l_g l_b (R + G + B)}{l_r R + l_g G + l_b B} \\ F_w &= \frac{3l_w^3 C_w}{3l_w C_w} \\ F_w &= l_w^2 \end{aligned}$$

For a uniform field made up by the additive mixture of two channels, like yellow for instance, we have

$$\begin{aligned} F_y &= \frac{l_r l_g (R + G)}{l_r R + l_g G} \\ F_y &= \frac{2l_y^2 C_y}{2l_y C_y} \\ F_y &= l_y \end{aligned}$$

The data reported in table E.1 was used to verify the model predictions. The entire data set is reported in table E.2. The results appear to confirm our model. The F found for the cyan, magenta and yellow fields was very similar, confirming that $l_{rr} = l_{gr}$ and so forth, and that the F_w is approximated by the square root of F_y , or F_y , or F_y .

DC									K1	K2	
	Y(r)	Y(g)	Y(b)	Y(y)	Y(m)	Y(c)	Y(w)	w/rgb	2w/ymc	w/rgb	k1/k2
5	0.10	0.20	0.10	0.30	0.10	0.30	0.40	1.00	1.14	1.00	1.14
15	0.10	0.70	0.10	1.00	0.30	1.00	1.20	1.33	1.04	1.15	0.90
25	0.30	1.80	0.20	2.40	0.60	2.10	2.60	1.13	1.02	1.06	0.96
35	0.60	3.40	0.40	4.30	1.10	4.00	4.60	1.05	0.98	1.02	0.96
45	1.10	5.50	0.70	6.80	1.70	6.20	7.10	0.97	0.97	0.99	0.98
55	1.70	8.20	0.90	9.70	2.50	8.70	10.10	0.94	0.97	0.97	1.00
65	2.60	11.30	1.30	13.10	3.50	11.80	13.10	0.86	0.92	0.93	0.99
75	3.50	14.80	1.70	16.90	4.70	15.10	16.70	0.84	0.91	0.91	1.00
85	4.50	18.40	2.20	20.80	5.90	18.40	20.30	0.81	0.90	0.90	1.00
95	5.80	22.70	2.70	25.00	7.30	21.90	23.60	0.76	0.87	0.87	1.00
105	7.00	26.80	3.20	28.70	8.60	25.80	26.90	0.73	0.85	0.85	1.00
115	8.60	31.20	3.80	32.90	9.90	28.60	30.10	0.69	0.84	0.83	1.01
125	9.90	35.70	4.40	36.70	11.20	31.70	33.00	0.66	0.83	0.81	1.02
135	11.50	40.60	5.00	40.80	12.40	35.10	36.40	0.64	0.82	0.80	1.03
145	13.00	45.20	5.60	43.60	13.70	38.10	39.10	0.61	0.82	0.78	1.05
155	14.30	49.40	6.10	46.60	14.70	41.20	41.60	0.60	0.81	0.77	1.05
165	16.00	53.30	6.70	50.00	16.00	43.60	44.10	0.58	0.80	0.76	1.06
175	17.10	56.60	7.30	52.60	17.10	46.30	46.70	0.58	0.81	0.76	1.06
185	18.80	61.20	7.80	56.60	17.80	48.70	48.70	0.55	0.79	0.74	1.06
195	20.10	63.40	8.40	58.40	19.10	51.10	50.80	0.55	0.79	0.74	1.06
205	21.30	68.20	8.70	62.30	19.80	53.30	54.20	0.55	0.80	0.74	1.08
215	22.80	71.40	9.20	64.20	21.30	55.50	56.30	0.54	0.80	0.74	1.08
225	23.70	74.50	9.80	67.50	22.10	58.60	57.20	0.53	0.77	0.73	1.06
235	25.30	77.40	10.30	68.80	22.60	60.90	58.80	0.52	0.77	0.72	1.07
245	25.90	81.20	10.60	71.60	23.90	62.30	61.30	0.52	0.78	0.72	1.08
255	27.90	84.40	11.20	74.60	24.50	65.00	63.40	0.51	0.77	0.72	1.08

Figure E.2: Two channel load dependency is the square of the three channel case.

E.3 Accounting for the Deviations

The good agreement between the results and the model displayed in the previous section might lead one to believe that load dependency is tractable. Unfortunately, this is far from true. As the reader might have noticed the above model is specific to uniform images, which might be of little usefulness in certain visual experiments. In many other experiments a part of the image will remain fixed (e.g. the background) while a small part (e.g. the test patch) will be modulated. In this situation a large part of the load might stay constant, and the part being modulated might have little effect on the entire load. This would be fortunate, since load dependency might be decreased; but in the other hand it will force the individual calibration of each image to be used, which is far less than desirable.

A general model for load dependency might be possible, but too many factors might have to be taken into account. For instance, the temporal MTF of the CRT will have to be

characterized. This can be explained with the help of figure B.1 in section B. Imagine that the entire CRT was at the dark level, and that only square 1 was lighted up. Would this increase in load influence all the other squares equally? The load required from the power supply can certainly change at very high frequencies, in the current example it will consist of a short burst of energy at every 1/30 seconds. If the power supply could change the delivered load very fast, the results obtained at any location on the screen would depend only on the load at that location, and the problem would be tractable. If the load supplied to the CRT changed extremely slowly, the problem could be approached by means of a histogram of the entire image and predicting the load consumption.

The actual behavior of the CRT system is somewhere in between. This can be easily verified by creating a simple image on the CRT. One can set all squares to a intermediate level, like $d' = 200$, and then set only one square to the highest level, $d' = 255$. If we do that to square 13, for example, and compare the luminance of the squares on the same line with the squares on the previous and following lines, we will see that on the Barco CD33HR and on the DEC VR241, the luminance of the squares on the lateral of square 13 will have decrease substantially. Depending on the CRT set-up this decrease might be large enough to become visible. To model such a behavior would be a very difficult task. If the image is interlaced it will have to be unfolded into two separate fields and the load increases at each line would have to be convolved with the reaction of the CRT. This would give us the instantaneous load at each pixel, which could then be corrected. The corrected image will now have a different load profile in time, and the calculations will have to be performed again and again until a stable solution is reached. Every time the image changes the entire process will have to be repeated. Thus these calculations might have to be performed 30 or 60 times a second, which is a pretty horrendous task.

Given the complexity of the task, the best solution is use CRTs which display the least amount of load dependency, or to design experiments that avoid the possible artifacts. For example, bipartite fields should be separated horizontally instead of vertically so that one field will not interfere with the other. A better CRT will usually display very little load

dependency. The cost of purchasing one is probably justified by the gains in flexibility and confidence.

Appendix F

Goniocolorimetric Properties

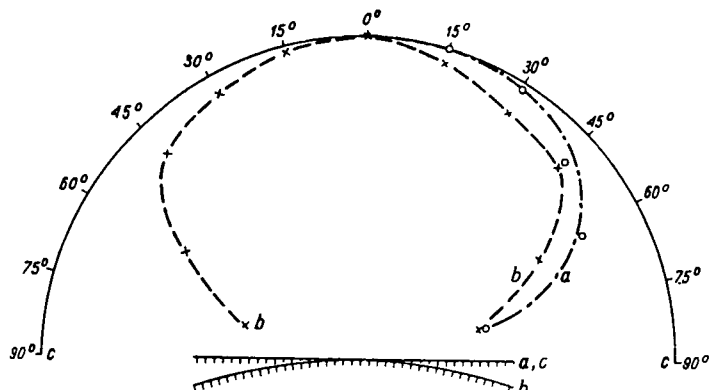
F.1 Introduction

Goniocolorimetry is concerned with the description of how the colorimetric properties of materials change when light is reflected, transmitted or emitted at different angles.

One important assumption made in section A.2.11 and commonly made for everyday CRT usage is that it behaves like a Lambertian source of radiation. Lambertian surfaces (irrespective of whether they are emitting or reflecting light) have constant appearance when viewed from different angles, and it follows that characterization of the surface properties at any angle should suffice as a description of the surface viewed from any other angle. Should the CRT behave this way, the characterization of its emission would be much simplified. Unfortunately, most materials and emitting surfaces are far from being Lambertian, and the CRT is no exception. For an extensive discussion on goniospectrophotometry the reader should consult refs. [60, 94].

Figure F.1, from ref. [98], illustrates the goniocolorimetric properties of a black and white CRT. As we see there, the radiance of the CRT decays rapidly for large angles, as is typical of most diffusing surfaces. Such deviations from Lambertian emission could be significant on color CRTs for three reasons:

- The CRT faceplate is commonly curved (see figure F.2). It is convex on delta gun



Distribution of the luminance of a picture tube screen: a — flat-screen tube, b — convex-screen tube, c — Lambert law radiation

Figure F.1: Goniophotometric curve of a black and white CRT.

CRTs, cylindrical on trinitron CRTs and flat on some other CRTs, like some models made by Zenith. On 19 inch delta gun CRTs the difference between the normal to the faceplate at the center of the screen and at the edges can be as large as 15 degrees.

- Since the CRT tends to occupy a considerable extent of the observer visual field, different parts of the CRT will be viewed at different angles (see figure F.2). For a 19 inch CRT with the observer eyes at the center of the image and normal to the CRT bezel, viewed at a distance of 15 inches (which is normal for computer graphics and workstation screens), the edges of the CRT will be viewed at angles as large as 30 degrees from the normal at the center of the faceplate.

As a result from the two above deviations combined we could expect that the CRT image will be viewed at angles as large as 45 degrees from the normal at the center of the screen.

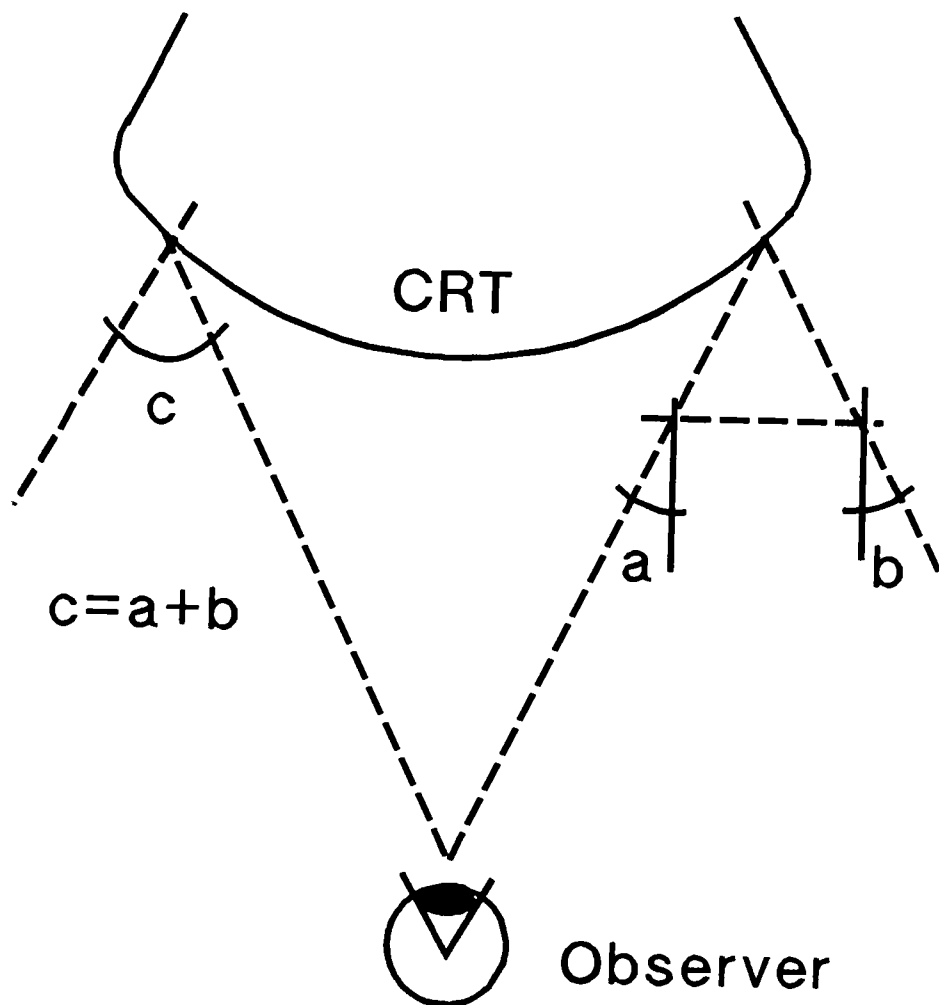


Figure F.2: Geometry of the faceplate and viewing.

- A thick glass plate covers the phosphor layer. The refraction index of any glass is dependent on wavelength (shorter wavelengths are more diffracted), and since the spectral emission of the three types of phosphor will peak at different wavelengths we can expect that the CRT's screen goniocolorimetric properties will result not only in intensity changes, but chromaticity changes as well.

By definition, the radiant intensity of Lambertian surfaces will be dependent on the cosine of the angle between the observed radiant intensity and the normal:

$$I_\theta = I_0 \cos(\theta) \quad (\text{F.1})$$

where θ is the angle measured from the normal to the surface, I_0 is the intensity along the normal and I_θ is the intensity at θ . Thus, for an infinitesimal area dA the radiance at different angles will be:

$$\begin{aligned} L &= \frac{dI_\theta}{dA \cos(\theta)} \\ L &= \frac{dI_0 \cos(\theta)}{dA \cos(\theta)} \\ L &= \frac{dI_0}{dA} \end{aligned}$$

and as we see the radiance is independent of the angle θ .

Another important result is that for a Lambertian surface the irradiance or the emittance are related to radiance simply by :

$$M = \frac{L}{\pi}$$

F.2 Experimental

To determine the goniocolorimetric properties of the Barco CD33HR a special CRT-goniocolorimeter was built as follows:

- A large bench with a central traveling stage driven by a shaft was fitted with a support plate to support the CRT (figure F.3).

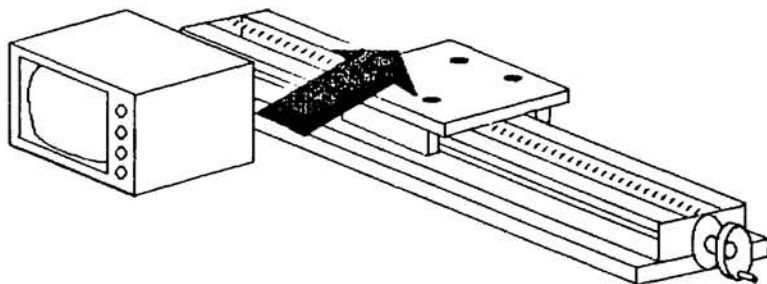


Figure F.3: Large bench to support the CRT and provide lateral movement.

- Near the center of the large bench a small triangular rail was placed perpendicular to it and a rotating stage positioned close to the CRT support plate (figure F.4). The rotating stage was lower than the CRT and the triangular rail allowed the center of rotation to be placed anywhere under the CRT faceplate. The scale on the rotating stage had marks at every degree.
- To support the detector assembly a light weight aluminum arm was fitted on the rotation stage (figure F.5). This arm and detector assemblies had to be made light since there was no clearance for using a counter-weight. The collection angles were limited to +/- 75 degrees. The detector consisted of a photographics lens (Canon FD 50mm f/1.8) positioned over the arm at around 50 cm from the axis of rotation and to collect the radiation a single optical fiber positioned at around 10 cm from the back of the lens. The iris on the lens was closed down to f/4.0 so that all radiation

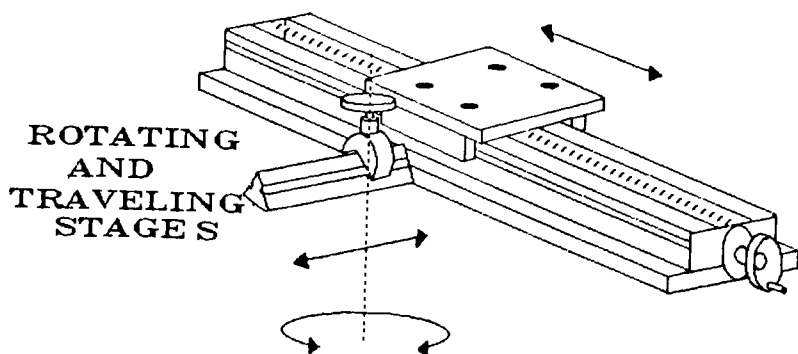


Figure F.4: A rotation stage was placed close to the bench and under the CRT faceplate.

would be well within the acceptance angle on the optical fiber and a small acceptance angle formed between the objective and the CRT screen. This was important to decrease the sensitivity to small misalignments between the fiber and the lens. The entire arm measured about 60 cm. The other end of the optical fiber was placed firmly in place with a metal bracket in front of the Photo Research PR703A/PC array spectroradiometer fitted with a macro focus lens (MS-55). The exit end of the optical fiber overfilled the measuring aperture of the PR703A/PC.

- To determine the focus and the region being detected on the CRT faceplate, a laser beam was shone through the eyepiece of the PR703A/PC into the exit end of the optical fiber. The beam was then projected onto the CRT faceplate and the proper adjustments made (figure F.6). The region of interest was selected by moving the CRT sideways along the large bench. Using the projected spot from the laser beam

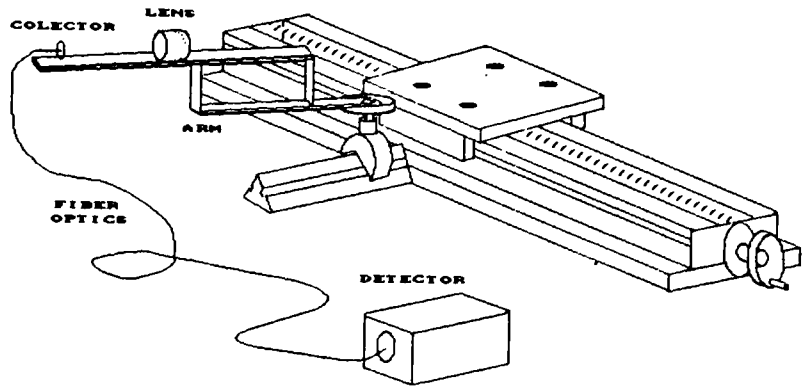


Figure F.5: A light-weight arm served as support for the detection lens and the optical fiber.

as a guide the position of the rotating stage was adjusted so at every angle the center of the spot remained on the same position.

Figure F.7 depicts the final apparatus in use. Although this apparatus was assembled only temporarily for a few measurements it proved to be rather precise and easy to operate. The repeatability of the positioning of the arm at different angles was determined by placing a white card over the center of the rotating stage and observing the shape of the projected spot both as the card stayed fixed and also when it was coupled to the arms movements. No visible deviations of the center of the projected spot were observed in either case. The shape of the projected spot was made larger (about 15 mm on apparent diameter when the beam was normal to the surface) by slightly defocusing the lens, which ensured that the microstructure of the color CRT would not be a factor in the positioning of the measuring

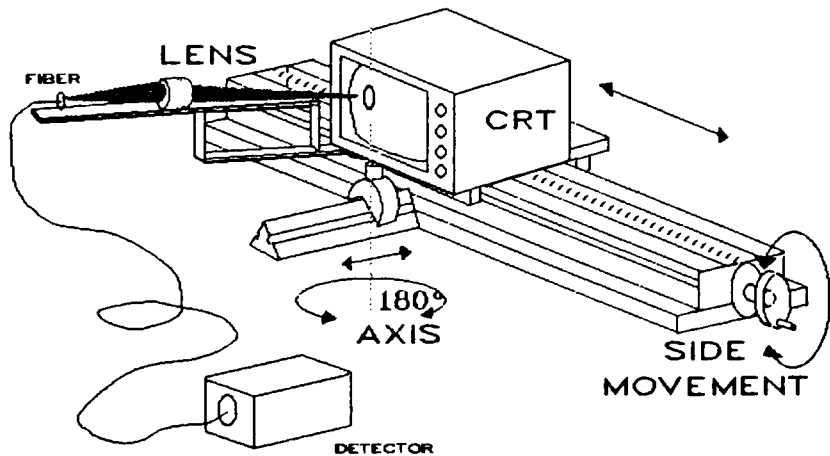


Figure F.6: CRT gonio bench assembled.

spot. Another reason for giving a gaussian-like profile to the projected spot was to weight the detected radiance at the center of the measurement area more heavily than at the edges, this way smoothing out the errors caused by the difference in the angle of detection between different regions of the "acceptance cone" (i.e. the inverse of the projected spot).

To calibrate the apparatus a near-Lambertian emitting surface was used. This source was built by Breneman for his investigations [23] at Eastman Kodak and later donated to the MCSL. Figure F.8 is a diagram of the source. The source consisted of two parts.

- A laphouse containing:
 1. A 150 watt tungsten-halogen bulb with built-in reflector.
 2. A heat absorbing filter.
 3. A fan for forced-air cooling.

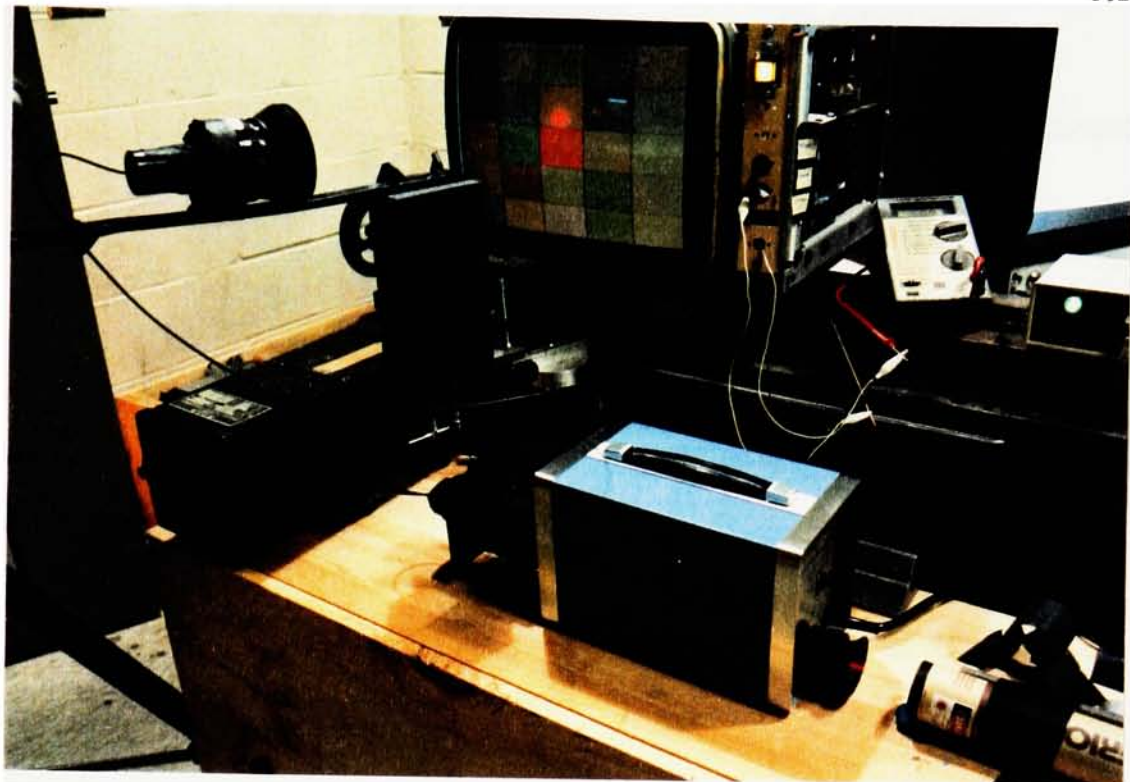


Figure F.7: Picture of apparatus in use.

- A propagation chamber containing:
 1. Opal glass diffusers on both ends.
 2. First surface mirrors covering the four lateral walls.

The effect of the first opal glass was to flood the chamber with a somewhat diffuse illumination that was reflected with great efficiency by the mirror walls, creating, from the point of view of the second opal glass at the end of the chamber, a very large diffuse surface which was further diffused by the second opal glass. The radiation being emitted by the second opal glass was assumed to be Lambertian within $+/- 70$ degrees, the angles of interest for this experiment.

By placing the emitting surface of the calibration source at the axis of rotation of the goniocolorimeter and recording Y , the luminance, at every 10 degrees the data on table I.1 was obtained. The results obtained are averages of ten different trials. A very small

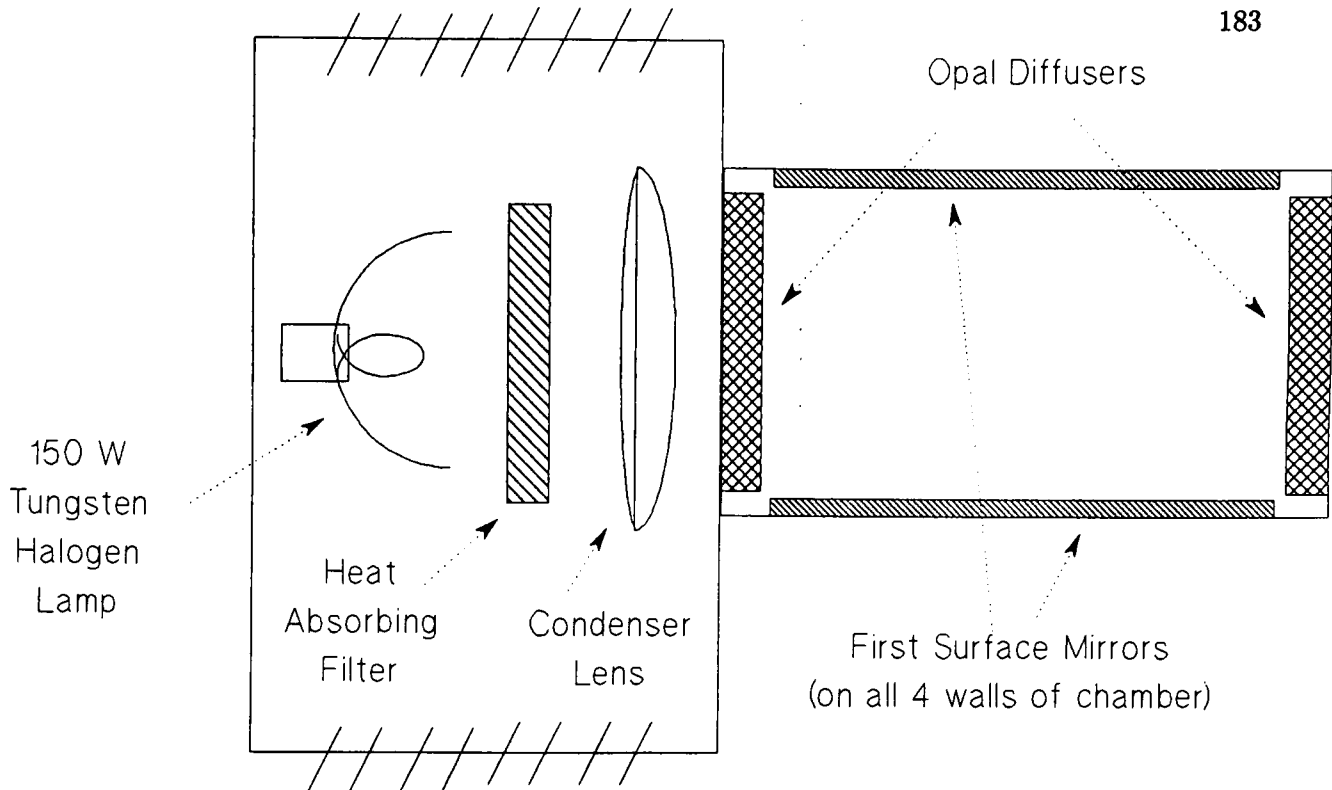


Figure F.8: Diagram of the diffuse light source.

variance was found and virtually no change in chromaticity was observed over all angles. The resulting luminance was found to be nearly constant, increasing systematically for larger angles by up to 1.36% (see figure F.9).

The increase of luminance with angle can be explained by the already mentioned difference between the angles at the edges of the acceptance cone of the detection optics. Figure F.10 illustrates this difference. If the acceptance cone has an angle α and the center of the cone will be at angle θ with the normal, then the further edge will be at angle $\theta + \frac{\alpha}{2}$ and the inner edge at angle $\theta - \frac{\alpha}{2}$. As we saw before, the radiant intensity from a point on a Lambertian surface decreases with the angle θ from the normal according to $I_\theta = I_0 \cos(\theta)$. It follows then that the inner part of the acceptance cone will be contributing to the radiant flux according to $\cos(\theta - \frac{\alpha}{2})$, while the decrease in contribution from the outer edge is only $\cos(\theta + \frac{\alpha}{2})$ which will never be small enough to compensate the increase in radiance due to

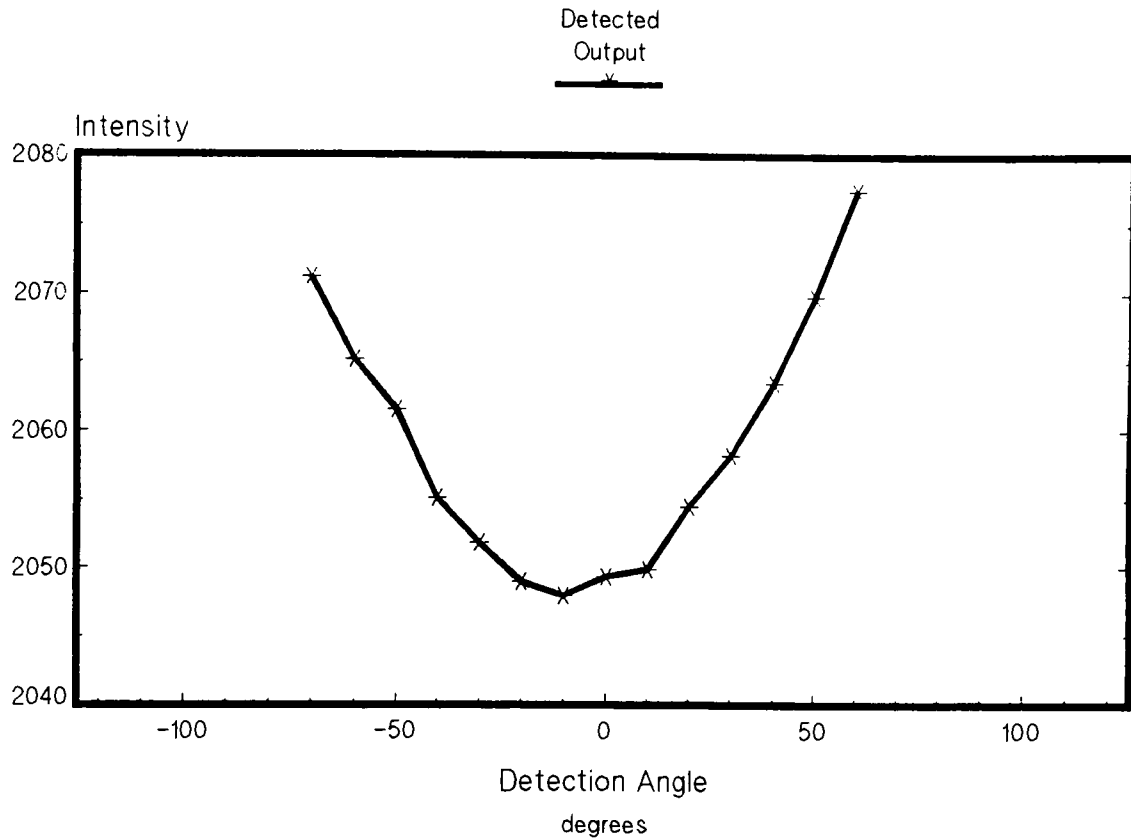


Figure F.9: The detected luminance of the near-Lambertian surface increase with angle.

$\cos(\theta - \frac{\alpha}{2})$ since it decreases faster with increasing θ . In other words,

$$\cos(\theta - \frac{\alpha}{2}) - \cos(\theta) > \cos(\theta) + \cos(\theta + \frac{\alpha}{2}) \quad (\text{F.2})$$

if $\alpha > 0$. Given that the above inequality increases with increasing α and θ we have the shape of the curve on figure F.9.

As indicated on column 2 of table I.1, the value at 0 degrees is assumed to be corrected (since at that angle $\cos(\theta + \frac{\alpha}{2}) = \cos(\theta + \frac{\alpha}{2})$), and the inverse of the deviation (column 3) from this central values was used to calculate the correction factor needed to account for the deviations introduced by α . All measurements of tristimulus values reported here have been corrected this way.

F.3 Results

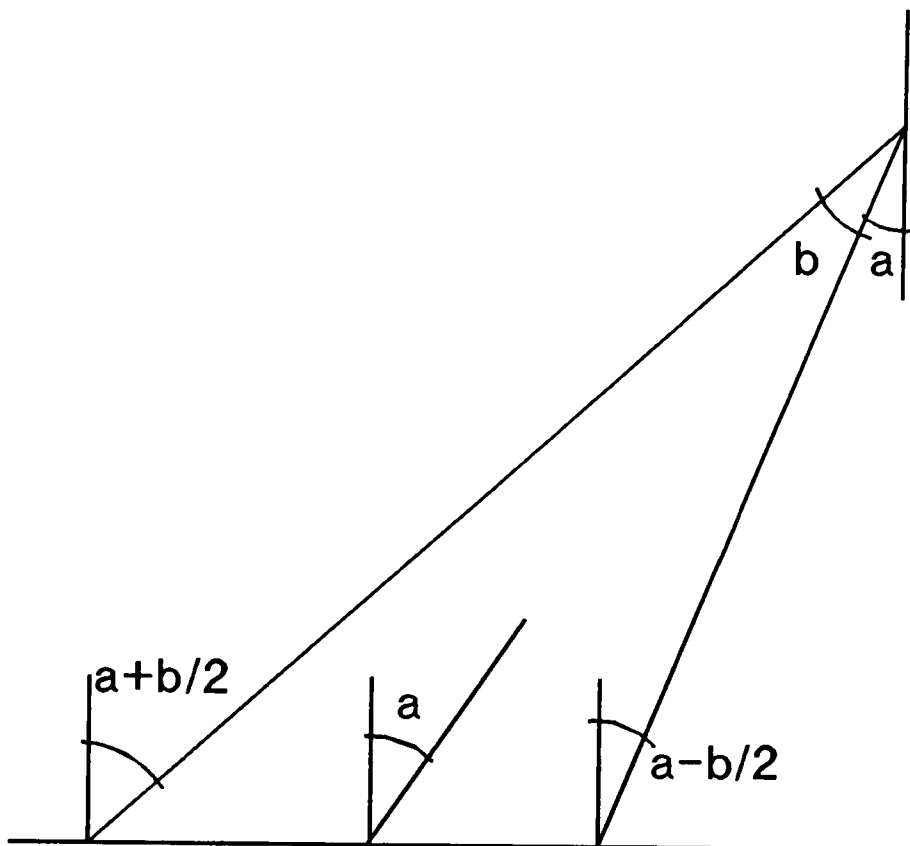


Figure F.10: Difference in collection angles at the edges of the detection cone.

Measurements were performed at areas 10, 13 and 15 of the CRT (see figure B.1, section B.3.1). In each case only the measured area was emitting and a white at $d' = 255$ was used. Ten measurements were made and averaged at each position. In the appendix, Tables I.3 through I.4 and figures F.11 through F.13 here, contains the principal results. The measurement angle refers always to the normal at the center of the CRT screen.

Somewhat surprisingly, the chromaticity remained constant at all angles and at the three positions. All tristimulus values decayed at the same rate towards the edges, indicating that the diffraction index of the glass might not be a factor for the angles and the CRT examined. Some exploratory measurements made on the Tektronix 690SR indicated behavior very similar to the Barco CD33HR¹. No measurements were made on the Tektronix 650HR, but visual inspection will show that unlike the other tubes, the trinitron tube does display a

¹In fact so similar that the results are not worth reporting here.

change in appearance at large angles.

The decay in intensity with higher angles at the center of the screen (figure F.11) is very similar to the curve from Kamler [98] (figure F.1). The curves for the edges of the screen appear to be very similar, except for being a little bit tilted due to the angle between the normal at that location and the normal at the center of the CRT.

F.4 Conclusions

The most satisfying conclusion to be drawn from the measurements is that under certain conditions the CRT tested can indeed be treated as a Lambertian surface. As seen on the previous figures, between the angles of +/- 30 degrees the CRT gonio curves for all 3 positions are very similar to that of a Lambertian surface. If the viewing arrangement is such that the observer field of view is within these limits, the CRT behavior would be indistinguishable from a Lambertian source that obeyed

$$I_\theta = k_g I_0 \cos(\theta) \quad (\text{F.3})$$

where k_g is a proportionality factor and the subscript g stands for goniocolorimetric. Thus the radiance will stay constant within the indicated limits, and it can be calculated as

$$L_\lambda = k_g \frac{M_\lambda}{\pi} \quad (\text{F.4})$$

instead of simply $L_\lambda = \frac{M_\lambda}{\pi}$, as indicated in equation A.37 before. This constant term will join the other many that are eliminated by the normalization on equation 2.30 and the model developed in section 2.3.1 will hold.

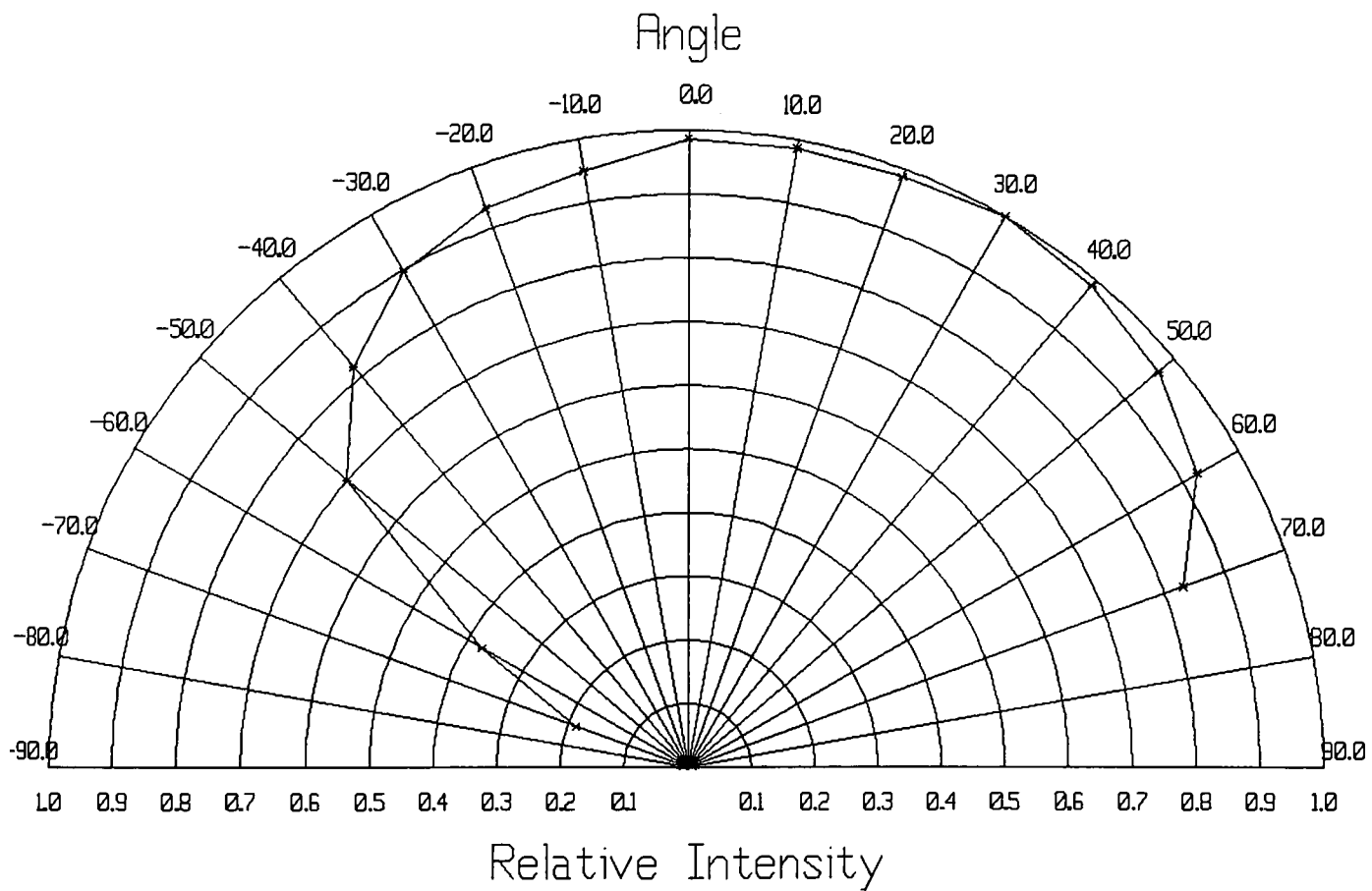


Figure F.11: Goniocolorimetric indicatrix of area 10

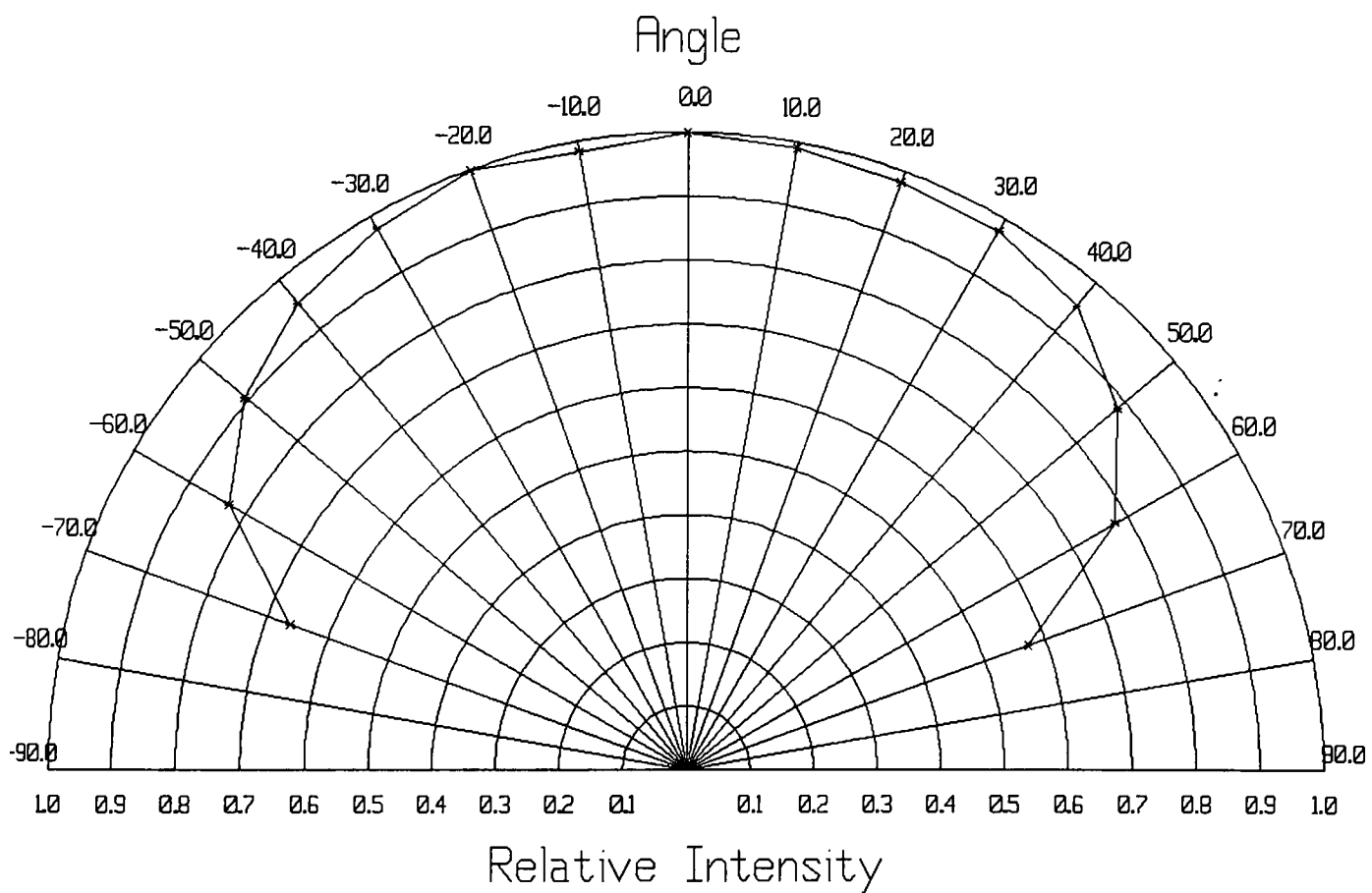


Figure F.12: Goniocolorimetric indicatrix of area 13

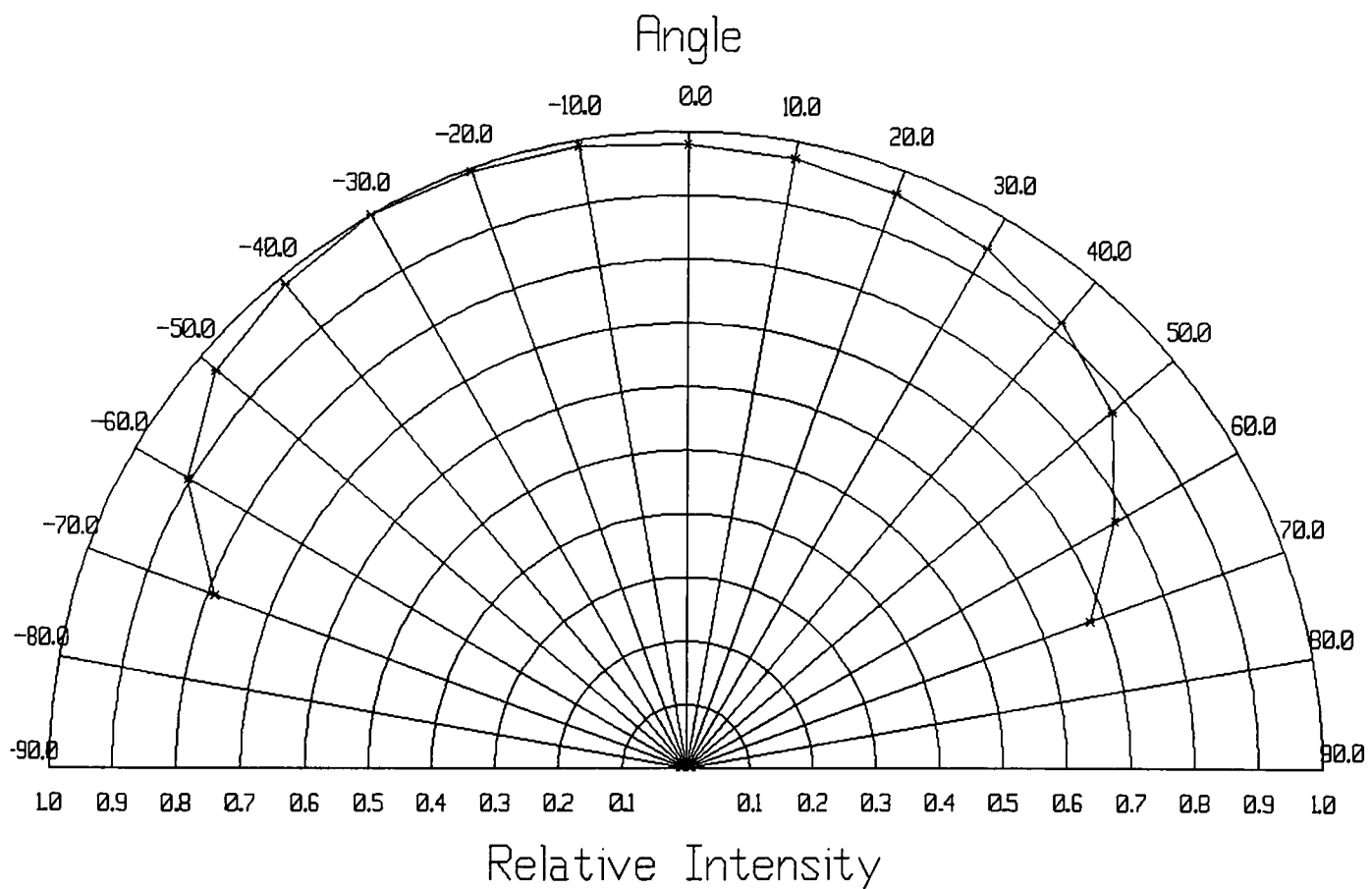


Figure F.13: Goniocolorimetric indicatrix of area 15

Appendix G

Screen Uniformity

G.1 Introduction

One characteristic of the color CRT that would be highly desirable is the uniformity of its properties across the viewing area. Such uniformity would greatly simplify the characterization and allow more confidence in the calibration. Unfortunately, most CRTs are far from being spatially uniform. The “white point” (the relative intensity of the three guns) will fluctuate across the faceplate while the maximum value of the luminance will typically decay towards the edges. Kinameri and Nonaka [107] have reported an experiment where a white field displayed on a color CRT and the faceplate scanned by a colorimeter recording measurements at every 1 cm. Their principal result is reproduced on figure G.1. The vectors represent the difference in x and y CIE 1931 chromaticity coordinates from the chromaticity coordinates of the “white point” at the center of the screen. The remarkable feature of their results is that a circular area at the center of the screen is relatively homogeneous while large deviations occur almost abruptly as we move outside of the central area. Several reasons could be proposed for this kind of behavior.

As any other electron-optical device, CRTs will suffer from optical aberrations and distortions. As seen on figures A.12 and A.4, the beam produced by the electron gun will have to be deflected from the center of the screen for the raster scan to occur. As the

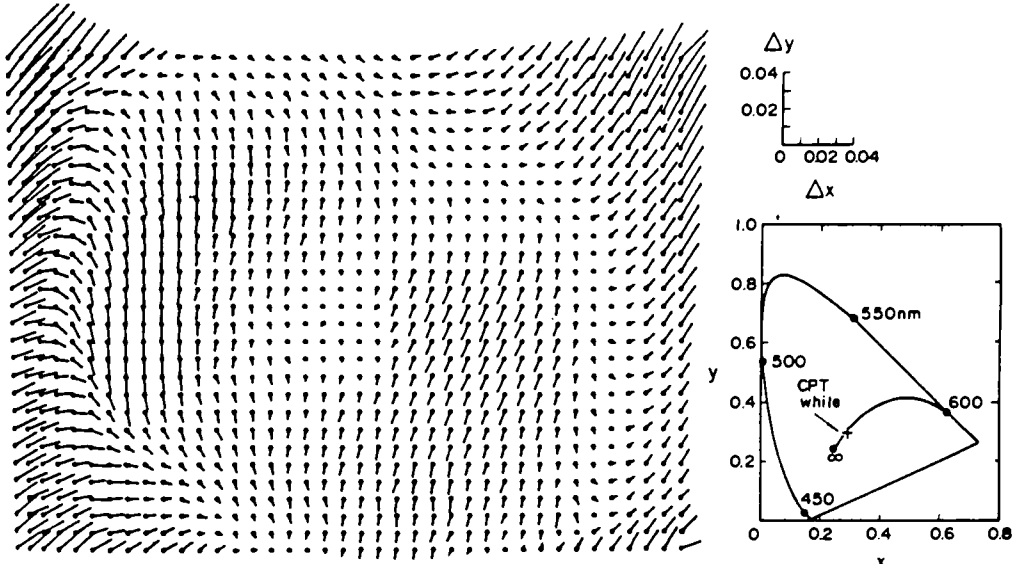


Figure G.1: Distribution of color difference vectors.

beam moves towards the edges of the screen it will be closer to the deflection coils, which tend to deviate the beam even further [95]. This extra deflection will result in the familiar pin-cushion distortion shown on figure G.2.

To counter-act this distortion magnets are placed on the bottleneck to redirect the beam. Excessive correction will cause the reverse cause of distortion to take place, the barrel distortion illustrated in figure G.2. Such distortions will modify the concentration of beam power in the distorted areas, increasing or decreasing the screen radiance depending on whether the image is being contracted or expanded.

If the magnets on the bottleneck are properly positioned the resulting image will be relatively free of geometric distortions, but the beam will have to traverse very inhomogeneous magnetic fields as it scans the faceplate. Another important factor is that to obtain a flatter screen the radial distance from the phosphor screen to the nodal point of the electro-optical focusing lens will increase as we move towards the edges. On a flatter screen the electron beam will have to travel greater distances, become defocused and hit the phosphors at angles increasingly further from the normal. As we know from geometrical optics, the

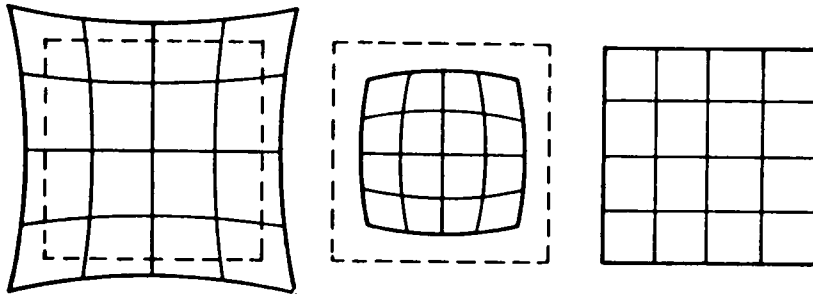


Figure G.2: Pin-cushion and barrel distortions.

intensity of the radiation emitted from a pinhole and incident on a flat surface will fall as the \cos^4 of the angle between the incident beam and the normal to the surface. The addition of the lens will reduce this rate to about \cos^2 [177]. For most CRTs the loss of focus is partially corrected by a signal (called the convergence signal) generated synchronous to the vertical and horizontal scans. This signal will change the power of the CRT lens and refocus the three electron beams as they scan the faceplate, but the resulting beams will neither be perfectly focused or free from aberrations. The compounded result from these many artifacts is that the point spread function of the CRT will grow larger towards the corners and the maximum attainable screen radiance will decrease.

While the above mentioned artifacts are an inherent property of the CRT design, another class of artifacts can be attributed mostly to the CRT manufacturing process:

- The photofabrication of the faceplate is a complex process which might cause many of the inhomogeneities [135]. The phosphors are dispersed on a photopolymer (called the sludge) which is dispersed on the faceplate and cured by UV radiation which is radiated from the bottleneck through the shadow mask. The size and concentration of the phosphors on the sludge and the thickness of the sludge across the screen are very critical. Some local inhomogeneities might arise from fluctuations in the concentration of the phosphors and the thickness of the layer.

- The alignment between the UV source during fabrication and the electron beam during operation is very critical. A slight misalignment might result in the electron beam irradiating the phosphor dots more fully in certain areas than others.
- The glass faceplate is usually tinted to increase the tube contrast and variations in the thickness of the glass might result in fluctuations in the transmittance.
- A guard-band is usually placed on the rim of the shadow mask to avoid electrons going around the mask and hitting the phosphor screen directly. The strange behavior of the CRT near its edges could be explained by the presence of some “escaped” electrons.
- The amount of power from the electron beam that is transmitted to the phosphors is dependent on the diameter of the holes in the shadow-mask. Slight fluctuations in the size of the holes will result in fluctuations in the amount of phosphor emission.

A third class of artifacts could be attributed to the operation of the CRT itself. While the inhomogeneities caused by the CRT design and fabrication are probably fixed for a certain CRT, the inhomogeneities caused by the operation will be mostly transitory and for that reason hard to characterize or correct.

- Phosphors aging and degradation might be localized because of repeated exposure, heat and ion contamination.
- The flow of charges in the CRT faceplate will depend on the conductivity of different parts of the screen as well as on the images being displayed, causing the potential of the screen to change locally.
- Local temperature differences will cause the shadow-mask to expand or contract non-uniformly.
- Exposure to magnetic fields outside of the CRT will magnetize the shadow-mask semi-permanently.

- The proximity to other CRTs, motors or any kind of strong magnetic field will also deflect the electron beams.
- The direction of the CRT with respect to the Earth's magnetic field will affect the trajectories of the electron beams.
- Convergence and purity adjustments might be lost because of thermal instability and drift during operation.
- The duty-cycle, the temperature of operation, the images displayed, the frequency of the degaussing and the CRT setup will all determine where and how much of the above defects will contribute to the inhomogeneity of the CRT display.

Given the large number of possibly detrimental artifacts that we can expect to find in the CRT image, it is almost surprising that a good image can be obtained after all. Actually, to the casual observer, much of the variations will not be noticeable since they are usually very smooth. When processing spatially distributed information (i.e. images), the human visual system behaves as a high pass filter, being somewhat insensitive to both chromatic and achromatic signals of low spatial frequency. On the other hand, such variations will be readily picked-up and amplified by most imaging systems with the typical low pass MTF, like, for instance, when we photograph the CRT and view its reduced image on a print.

As explained above, the non-uniformity of the CRT image will be the result of several somewhat independent processes, and it can be classified according to the frequency of the modulation:

Low frequency - The monotonic fall-off of the tristimulus values from a center of maximum intensity towards the edges of the CRT. Usually not visible within normal viewing distance.

Medium frequency - Local, but somewhat large, artifacts like loss of purity in certain areas. Clearly visible within normal viewing distances.

High frequency - Small artifacts that are only visible within close distance or on high frequency areas of the image, such as loss of convergence or moire patterns.

Our discussion hereon will concentrate on the characterization of the low frequency modulations. Such modulations are a characteristic intrinsic of CRT devices, and although one should not expect them to have a constant form, they will always be present. The two other kinds of modulations are results of technological problems that can be either nearly eliminated by the appropriate calibration and setup of the CRT device, or cannot be dealt with at all, since they are completely transitory.

Almost all color CRTs have controls for the degaussing of the shadow mask, and the correction of purity and convergence. Depending of the quality and purpose of the device the controls might be in the front panel, in a sliding drawer or in the interior of the CRT. On the other hand, controlling low frequency modulations is not simple, since CRT devices do not provide us with any direct means of controlling them. Although this might not represent a problem for most CRT applications (like entertainment television), it might constrain the color CRTs usefulness for color appearance research. One of the underlying assumptions that one would like to make when using a CRT for appearance research is that the stimuli displayed will not greatly differ from that prepared by conventional means, such as reflectance samples or radiance modulated by some optical apparatus. If such similarity does not hold, the advantages of using the CRT must be weighted accordingly.

In view of what was discussed above we can state our three concerns regarding the CRT uniformity as follows:

- Characterization.
- Correction.
- Specification of tolerances.

It is specially important for us to understand how a characterization performed at the center of the screen correlates to other areas of the display. To investigate such questions two series of measurements were carried out and are presented next.

G.2 Qualitative view

The first series of measurements were exploratory and designed to provide a qualitative view of the screen uniformity. Because of the difficulty of setting up the detector repeatably on the different positions only a small number of samples was obtained.

G.2.1 Experimental

The Minolta TV-2160 was used to determine the three principal CRT parameters, L_{max} , γ and K_1 on 25 different areas of the CRT. Figure B.1 illustrates how the area covered by the CRT emission was divided. The characterization was performed on the Tektronix 650 HR by placing the TV-2160 probe in close contact with the faceplate on the center of the rectangular area being modulated. The areas completely covered the probe and extended about 1 cm beyond on the top and the bottom. During the characterization only that area was modulated while the others were left dark ($d' = 0$). The parameters L_{max} , γ and K_1 were calculated using the algorithm presented on the program `crtCALC.c`, to be described later in chapter 3. For each location the characterization was repeated 3 times and the results averaged. The entire process lasted for about 6 hours with the CRT always turned on and about 4 hours of warm-up allowed with the screen at $d' = 150$. The CRT was mounted in a rack cabinet, the overall gain was set to the maximum and the offset adjusted to allow a dark black level in a completely darkened room.

G.2.2 Results

Tables H.1 through H.3 on appendix H represent the averaged results for 25 different measurements of the red, green and blue guns. This data is presented graphically in figures G.3 through G.5. The axis labeled “X position” and “Y position” correspond, respectively, to the horizontal and vertical positions on figure B.1. The z axis is relative with the values normalized between the minimum and the maximum for ease of visualization.

The assumption was made that the characteristics of the phosphors did not change across the screen. In other words, the chromaticity of each class of phosphor was the same on all

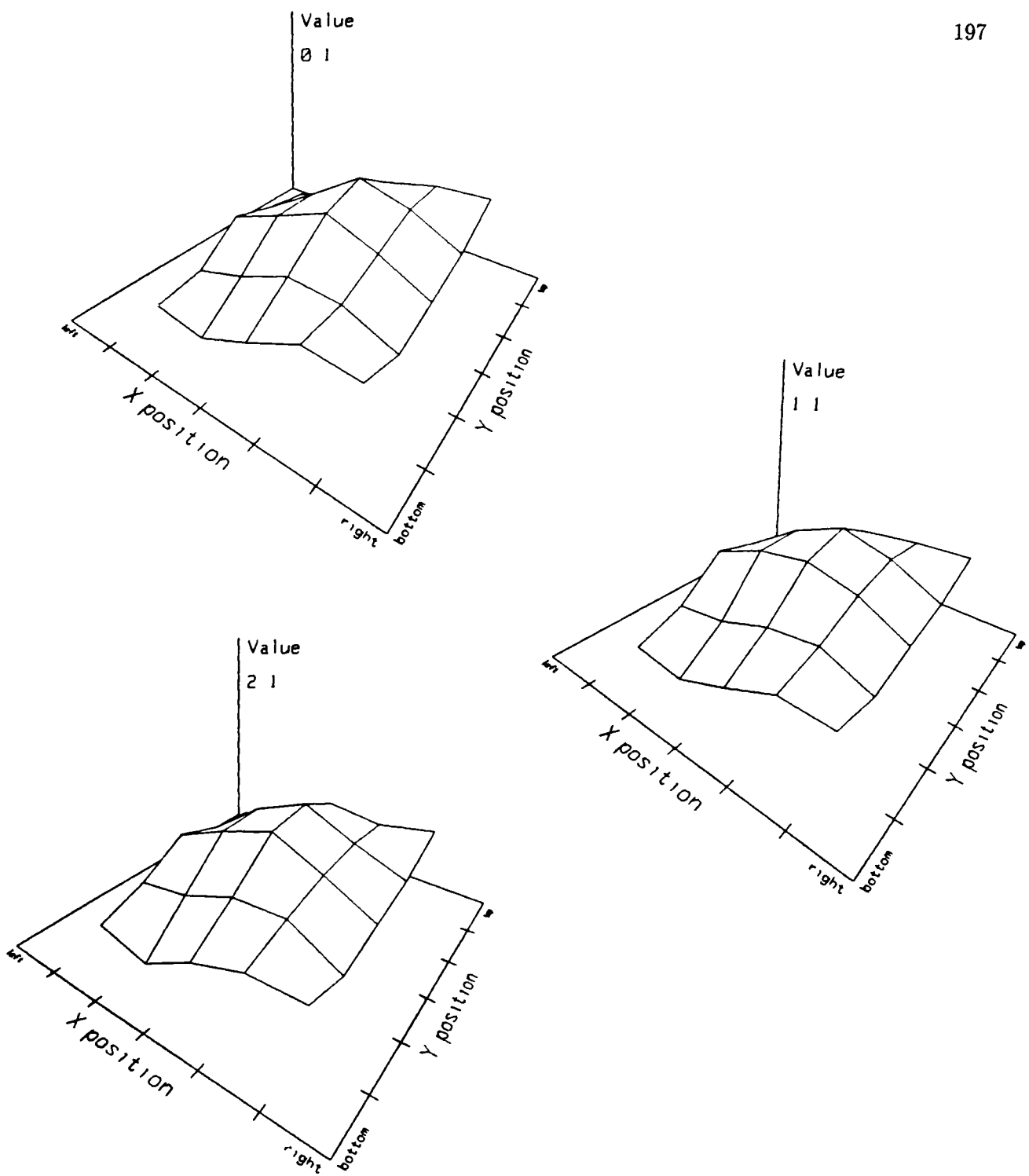


Figure G.3: Maximum screen output for the red, green and blue channels on 25 different positions on the CRT.

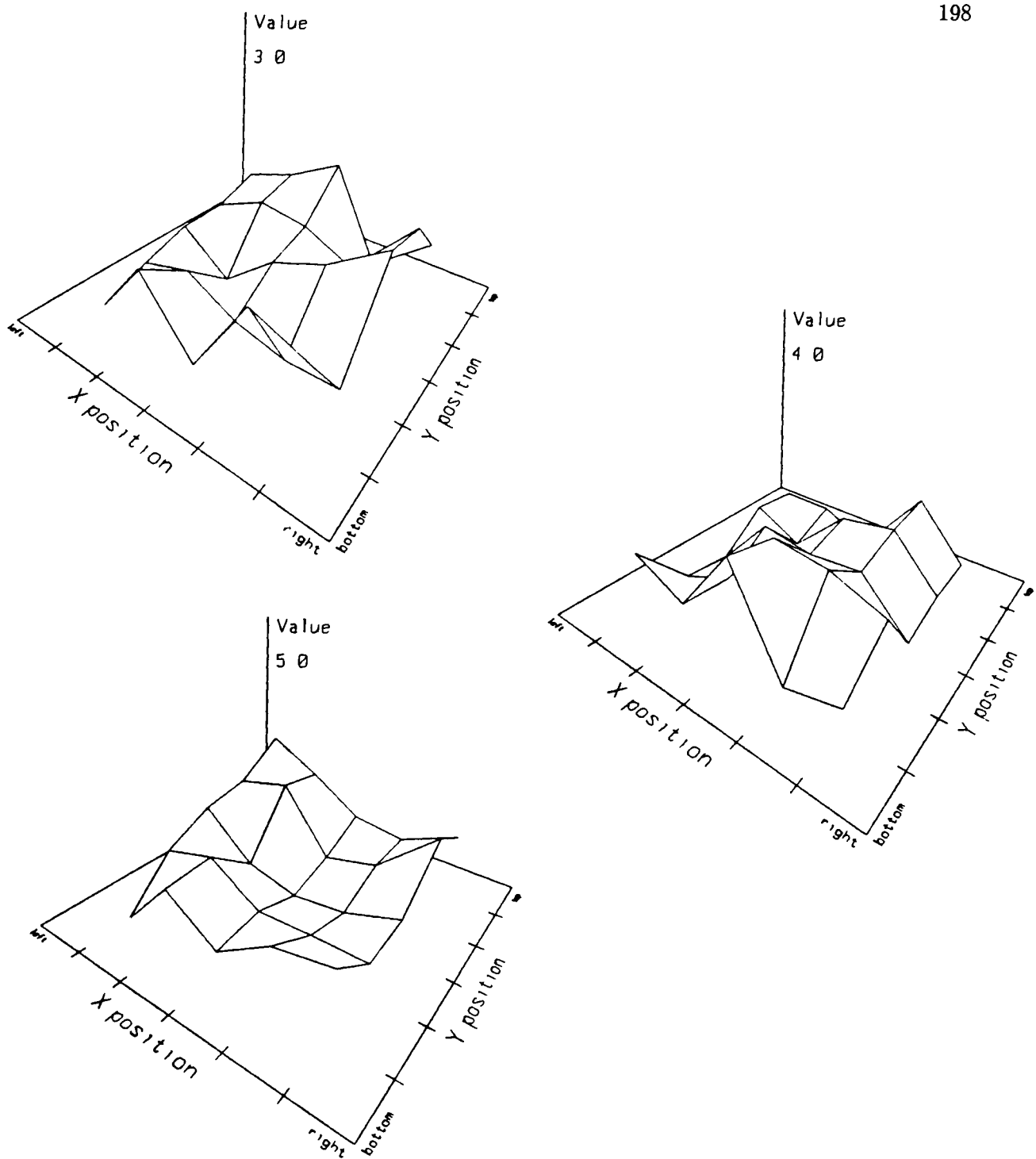


Figure G.4: Gamma (γ) of the red, green and blue channels on 25 different positions on the CRT.

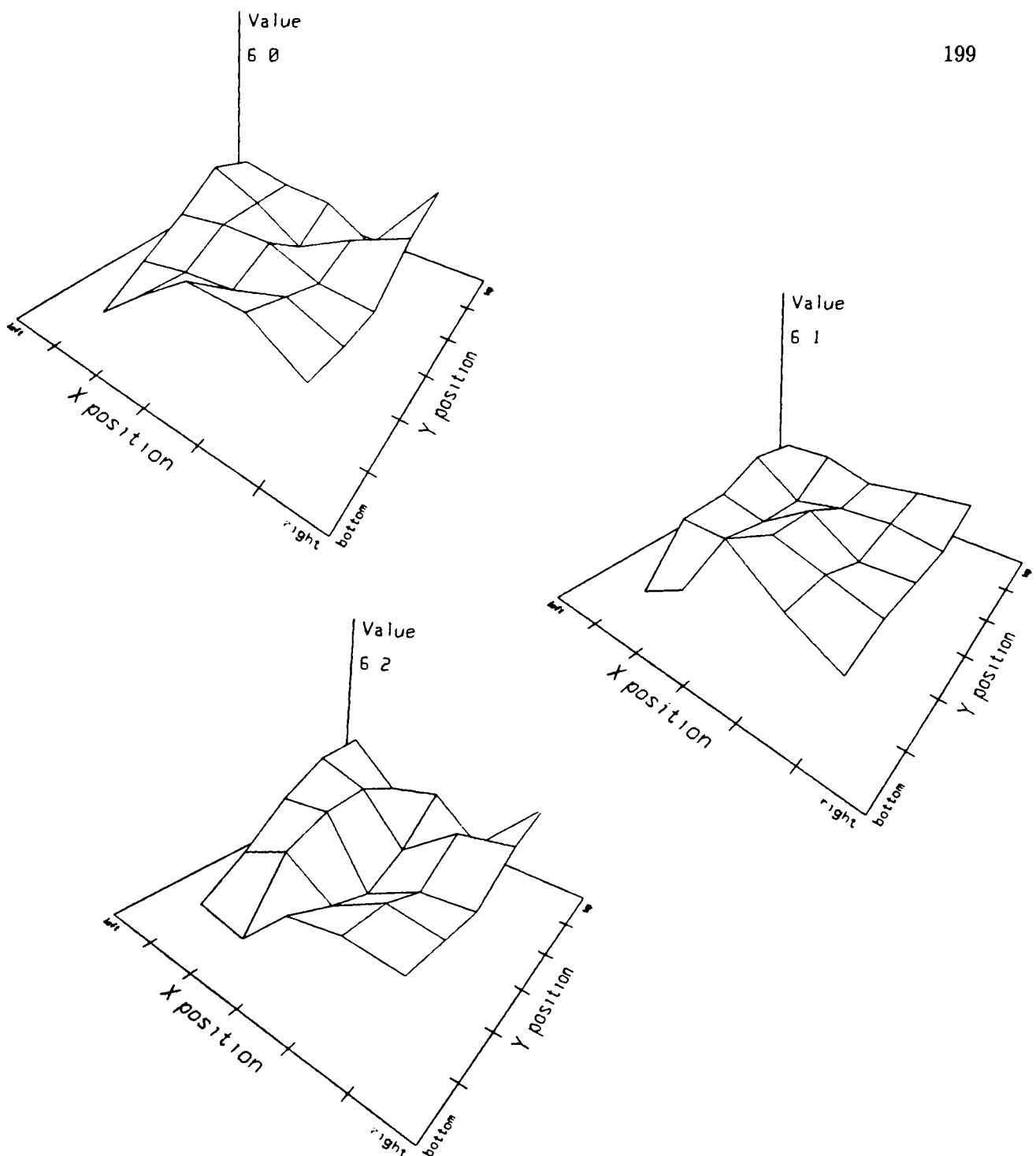


Figure G.5: The system offset (K_1) of the red, green and blue channels on 25 different positions on the CRT.

positions, so a change in the CRT tristimulus values (e.g. R increases) will increase equally all three CIE tristimulus values (X_r , Y_r and Z_r). This is probably a safe assumption, and its failure would represent only minor deviations given the size of the artifacts observed. Under this assumption the relative CRT tristimulus values can be characterized by choosing any of the three CIE tristimulus values and normalizing it for all three classes of phosphors. The Y tristimulus value was chosen for this task and is displayed in figure G.3. As we see, the screen emission peaked at area 8 and was the smallest (by 25%) on area 21 at the bottom left corner of the screen. The expected smoothness and the monotonicity of the fall-off are observed for all three CRT tristimulus. Also as expected, the three CRT tristimulus values appear to be highly correlated. The differences between R , G and B will translate into small fluctuations of the CIE tristimulus values when a uniform color is displayed on that CRT.

Figure G.4 represent the γ for each gun while figure G.5 represents the system gain K_1 . There is no apparent correlation between γ and either the position or L_{max} or K_1 . The fact that the range of values assumed by γ is small and that it varies randomly across the screen appears to indicate that it is constant and independent of position (this statement is qualified more rigorously in the next section). On the other hand, there is some form of correlation apparent between K_1 and L_{max} . As figure G.3, and figure G.5 seem to indicate, K_1 tends to increase when L_{max} decreases and tends to decrease when L_{max} increases. This could be explained by, for instance, a change on v_C for the different positions. But, unlike L_{max} , K_1 is not changing monotonically, and the correlation is stronger at the center of the screen since at the edges the tendency tends to reverse. In the next section we will explore such correlations further.

G.3 Quantitative view

G.3.1 Experimental

In order to further explore some of the above results another series of measurements was carried out. This time, to avoid the difficulties of positioning the Minolta TV-2160 detector a telespectroradiometer, the Photo Research PR703A/PC was positioned in a tripod at around 3 meters from the CRT. At that distance the measurement was made over a relatively large area (around 4 cm diameter) avoiding area related quantization errors and any goniocolorimetric problems (see section F) by measuring always near the normal. The detector was then pointed at random at the CRT, a characterization made of that area and the detector pointed again at a different area. For all characterizations the entire screen was modulated. Otherwise, the same CRT and setup described in the previous section was used.

The characterization data was obtained from the CIE tristimulus values that the driving software from Photo-Research calculates after each measurement. The integration time was pre-calculated by previously recording the relation between the measured tristimulus values and the time used by the PR703A/PC in adaptive mode to measure that tristimulus values. From the data obtained a simple best fit equation was derived and used interactively by the software. During calibration the controlling software would command the PR703A/PC to make a short measurement (around 2 sec.) and from the measured tristimulus values and the above mentioned equation find the appropriate integration time and command a second measurement with the proper integration time. This saved a great deal of time and the estimates made on the integration time proved to be fairly accurate since the approximate Y given by the spectroradiometer after 2 sec. integration was usually within 30% of the final measured value.

G.3.2 Estimating variance

Spectroradiometers are not very sensitive devices; they have to distribute the incoming radiation across several wavelengths and detectors [71]. The maximum integration time possible with the PR703A/PC is 30 sec. and all d' levels below 100 would have required longer integration times. This raised questions about the level of noise that would be present in the data and how it would affect the calculation of γ and K_1 . To help minimize these problems it was decided that the calibrations would be performed only on the green phosphor since it has a smooth gaussian shape, avoiding the photometric linearity and wavelength bandwidth problems related to the detection of the red phosphor, and also because it has peak emission where the PR703A/PC has peak sensitivity, unlike the blue phosphor.

To estimate the amount of variance presented in this measurement arrangement a series of 29 repeated calibrations were performed automatically overnight, while the measurements of different positions were performed during the next 2 days without ever changing the CRT or the rest of the apparatus (except, of course, the direction the PR703A/PC was pointing to).

Figures G.6, through G.8, along with table H.5 on appendix H contain the principal results. In the figures the data is plotted as scattergrams, with the degree of correlation r^2 and the averages and standard deviations of the two data sets printed on the right margin. In the figures *rfp* stands for *repeated fixed position* and the terminators *max*, *gamma* and K_1 have their obvious meaning. To bring it to the same order of magnitude as the other parameters the tristimulus value Y measured in cd/m^2 was divided by 100.

Most noticeable in these three figures is that the standard deviations are fairly small, about 1.23% for γ , 0.7% for K_1 and 0.3% for the intensity. The estimated values of γ and K_1 appear to be correlated. This is probably due to fact that for $K_1 > 0$ there will be values of d which equation 2.46 will predict negative values.¹ The marginal correlation found between *max* and K_1 is not strong enough to confirm any dependency, while no correlation was found between γ and *max*.

¹The calibration method is discussed in more detail on chapter 3.

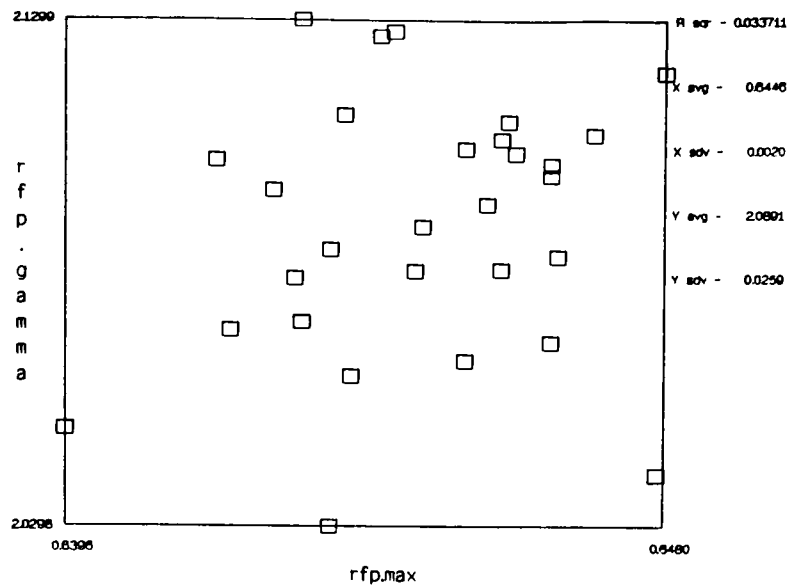


Figure G.6: Scattergram of the green channel intensity (Y_{max}) and estimated γ (gamma) for 29 repeated measurements of an area near the center of the CRT.

With the help of the above results we can analyze the results of the measurements of the random positions across the screen.

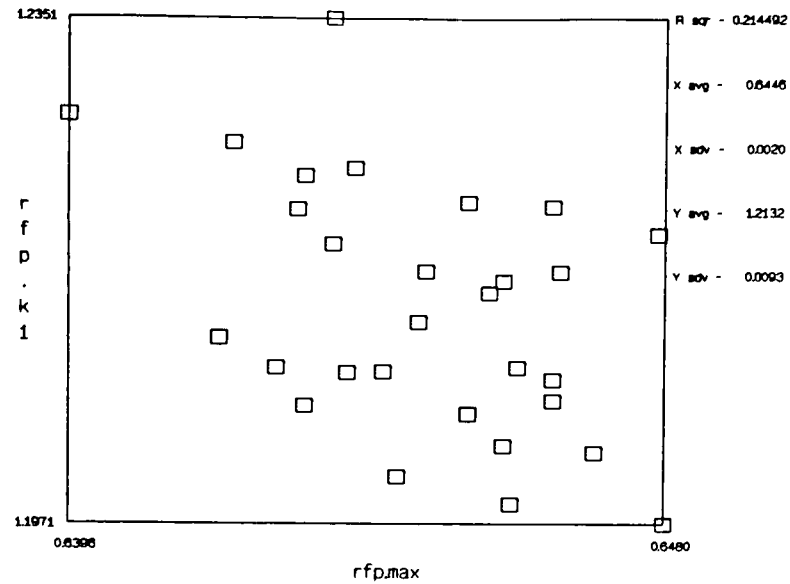


Figure G.7: Scattergram of the green channel intensity (Y_{max}) and estimated system gain (K_1) for 29 repeated measurements of an area near the center of the CRT.

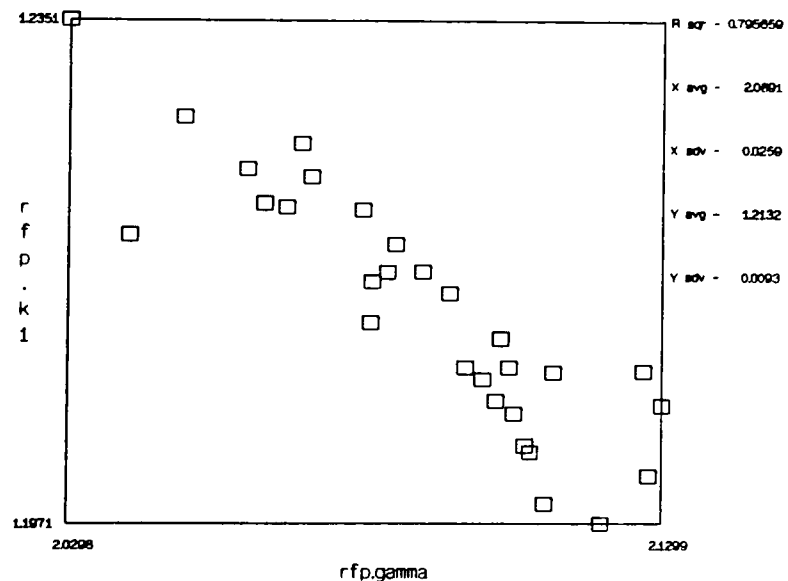


Figure G.8: Scattergram of the system gain (K_1) and estimated γ (gamma) for 29 repeated measurements of an area near the center of the CRT.

G.3.3 Results

The results from the 32 characterizations made at random positions on the CRT screen are displayed on figures G.9 through G.11 and table H.6 on appendix H. Again the same convention is used for plotting the data.

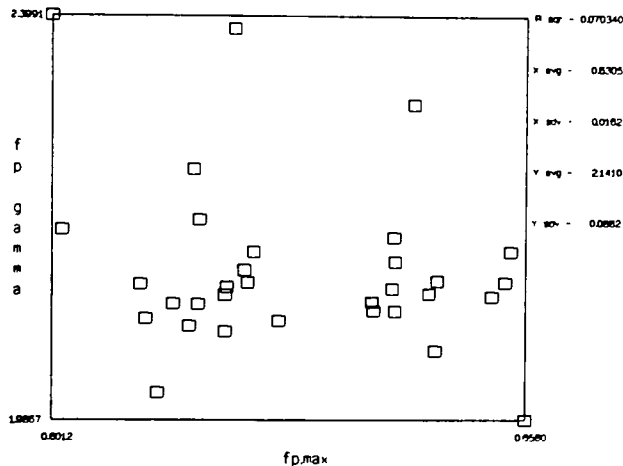


Figure G.9: Scattergram of the green channel intensity (Y_{max}) and estimated γ (gamma) for 32 measurements made on different areas of the CRT.

A high degree of correlation between γ and K_1 is again found in figure G.11. Of interest is that most of the data is clustered on the upper left corner with 3 outliers on the bottom right. The same points also appear on the two other graphs, in the top of the γ, max scattergram and in the bottom of the K_1, max scattergram. These two last graphs also appear to be inverses of each other, as one should expect from the strong correlation between K_1 and γ .

Observing the plots on figures G.9 and G.10 it is clear that, with the exception of the outliers, the values of γ and K_1 are well clustered and as indicated on figure G.12 within the 95% confidence interval (calculated as 3 standard deviations from the data obtained for the noise estimates). Given that max has variated by almost 10%, or 10 times its confidence interval, this should establish that for that CRT γ and K_1 are independent of position on the CRT screen.

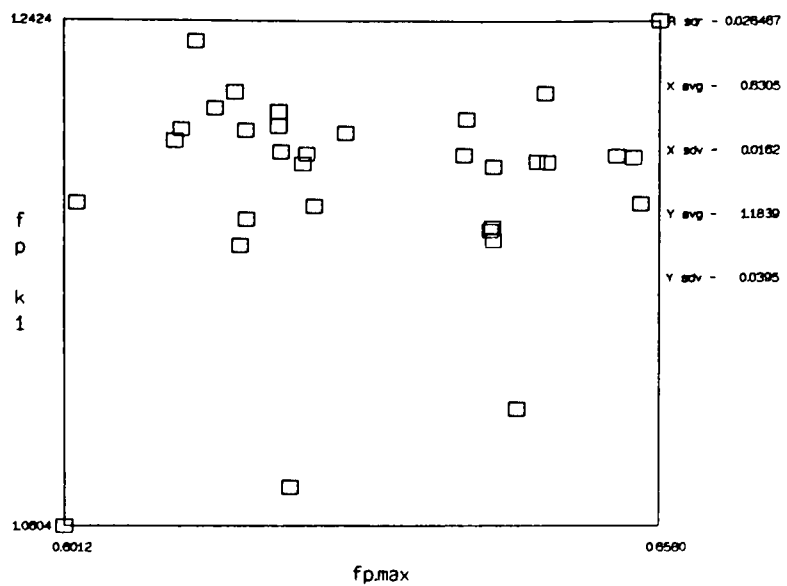


Figure G.10: Scattergram of the green channel intensity (Y_{max}) and estimated system gain (K_1) for 32 measurements made on different areas of the CRT.

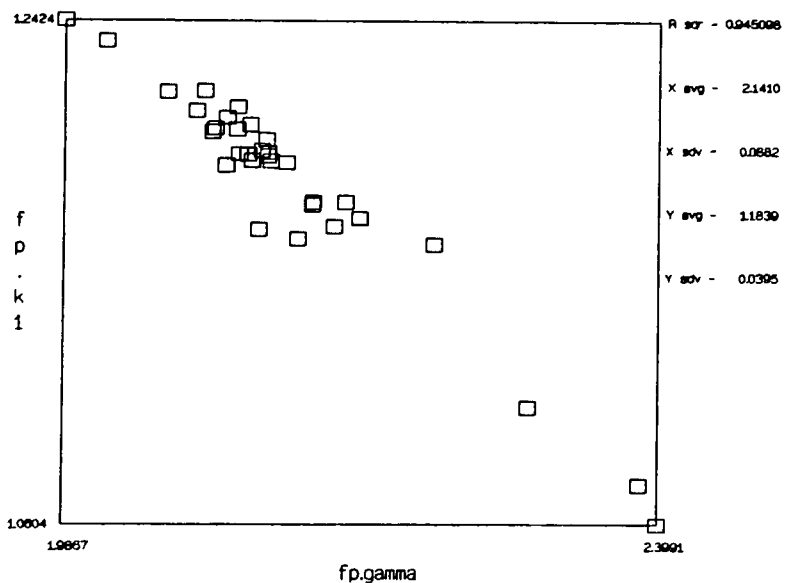


Figure G.11: Scattergram of the system gain (K_1) and estimated γ (gamma) for 32 measurements made on different areas of the CRT.

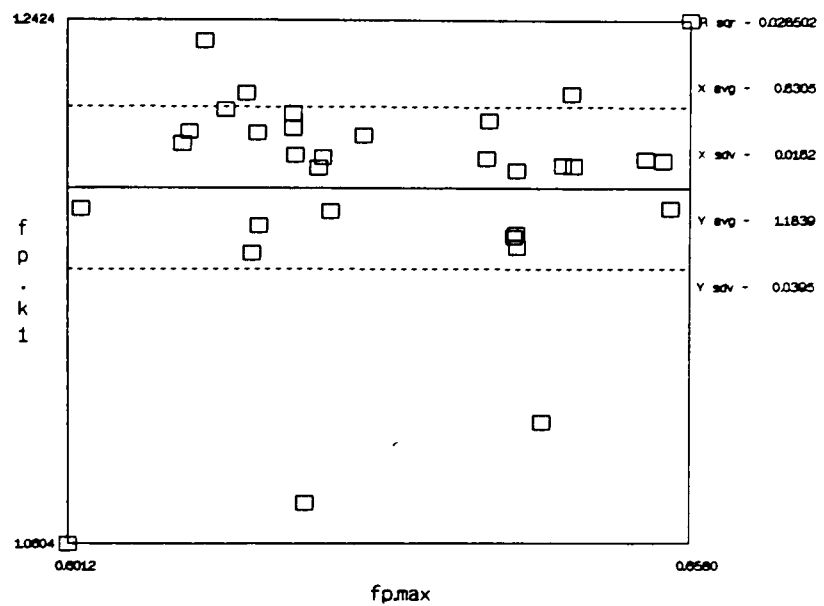
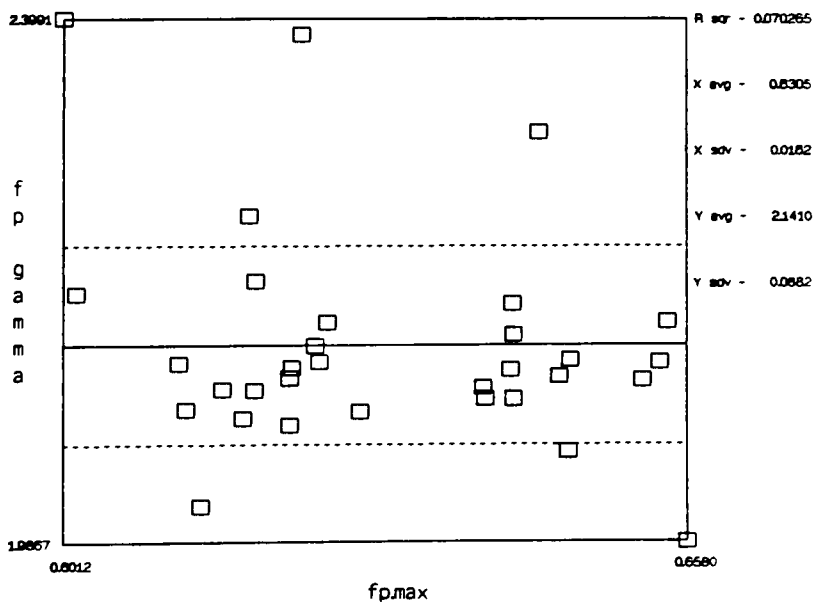


Figure G.12: Scattergrams of the green channel intensity (L_{max}) plotted against the system gain (K_1) and γ (gamma) with 95% confidence intervals



G.4 Discussion

The independence of γ and K_1 from position on the faceplate can be explained by the fact that those two parameters are governed only by the characteristics of the electron gun, the video signal and the video amplifier. As was discussed in the introduction, all the artifacts that might contribute for the lack of uniformity on the CRT image are due to phenomena that happen after the electron beam has been emitted by the cathode. As seen in equation A.39, changes on the faceplate transmittance T_s , the transmittance of the shadow mask T_m , the efficiency of the phosphor $\eta_{e,\lambda}$, the accelerating voltage $(v_s - v_0)^n$, or even loss of purity, are constant (or assumed constant once characterized) for a certain position on the screen, and will be eliminated by the normalization described in equation 2.46. Thus the only thing changing across the faceplate are the CIE tristimulus values at maximum emission, which can be expressed as a multiple of the tristimulus values at a conveniently chosen position (like the center of the CRT):

$$X(x, y) = f_X(x, y)X(0, 0) \quad (\text{G.1})$$

where X is a tristimulus, x and y are the positions on the CRT faceplate, $(0, 0)$ is at the center of the CRT and $f_X(x, y)$ is the multiplicative function for the X tristimulus.

This is a rather fortunate result. The foremost reason is that for low frequency artifacts such as the ones pictured in figure G.3, some important linear properties of the CRT are maintained across the screen. Namely, it implies that the modulation of the high spatial frequencies is maintained. Modulation here is used according to the traditional definition (see figure G.13):

$$M = \frac{a - b}{a + b} \quad (\text{G.2})$$

In other words, a sine wave grating at high frequencies with amplitudes a and b at the center of the screen will have amplitudes $f(x, y)a$ and $f(x, y)b$ elsewhere on the screen. Because $f(x, y)$ is a smooth function we can assume that it has the same value at the position of a and b , and it follows that:

$$f(0, 0) = 1.0$$

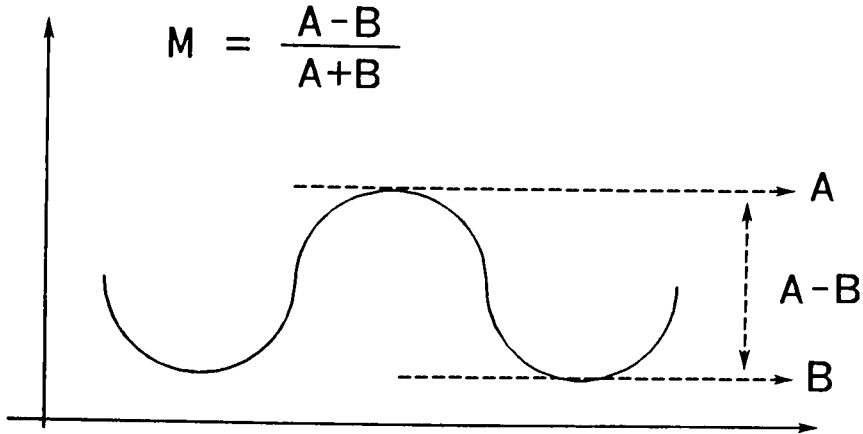


Figure G.13: Definition of modulation. $M = \frac{a-b}{a+b}$

$$\begin{aligned}
 M(0, 0) &= \frac{a - b}{a + b} \\
 M(x, y) &= \frac{a f(x, y) - b f(x, y)}{a f(x, y) + b f(x, y)} \\
 &= \frac{f(x, y) (a - b)}{f(x, y) (a + b)} \\
 &= \frac{a - b}{a + b} \\
 M(x, y) &= M(0, 0)
 \end{aligned}$$

Thus, as long as the frequency of $f(x, y)$ is large enough judgement of thresholds based on distinctness of borders [15, 97, 187, 188] will be unaffected by the position of the border on the CRT. This is specially good news for experiments involving paired comparison where the two samples are in contact with each other.

It is important to notice, though, that the above statements do not imply that any experiment can be carried out without regard to $f(x, y)$. Imagine for instance that a region of the CRT is visibly different than the others, or that the CRT image is composed of many small squares intended to be homogeneous and separated by black spaces. On either two cases $f(x, y)$ might significantly change the result of the experiments:

1. In the case where a region is visibly different than the others the $f(x, y)$ modulation will be above the threshold of the eye contrast sensitivity function (CSF) [32, 33, 34,

101]. This could be caused by either a high frequency of modulation of a low frequency modulation with a lot of power. At any rate, local adaptation as evidenced by the dip of the CSF at low frequencies will not be enough to make the pattern visible. On the case of a monochrome image, the affected area might still have the same amount of modulation, but will be placed on a different portion of the psychometric function[17], and assumptions about local linearity might not be valid anymore. The same argument would apply to the case of color, where, lets say, a step between two grays might become a step between two yellows. Although the result obtained might be applicable to that yellow border, it can not be used to describe the difference on the desired gray border.

2. In the case of the many small “homogeneous” squares over a dark background, a lot of power is generated at low frequencies because of the separations of the squares. Since it is exactly the low frequencies that are going to be distorted by the $f(x, y)$ the screen inhomogeneity can have a large impact.

There are several possible ways of accounting for $f(x, y)$ in either of the above two cases. In the case 1 the region of strong modulation should probably just be avoided. In case 2, as long as the squares are relatively small, the value of d' can be precorrected so that the square has, on average, the desired value. The main reason that correction of the individual pixels should not be attempted in a 8 bit display is because the quantization will generate modulation with high frequencies (see figure G.14), which in turn can be much more easily detected than the original artifact. In a 10 bit display it is possible to make a sparse measurement of the screen output and calculate the amount of correction for each individual pixel by interpolation.

In conclusion, we see that as long as the high frequency artifacts are corrected by adjusting the purity, convergence and degaussing the CRT, the remaining low frequencies artifacts can be accounted for or corrected by careful experimental design. In the situation where no artifacts can be observed on the CRT under the experimental viewing conditions when a homogeneous screen (i.e. constant d') is displayed and the important information

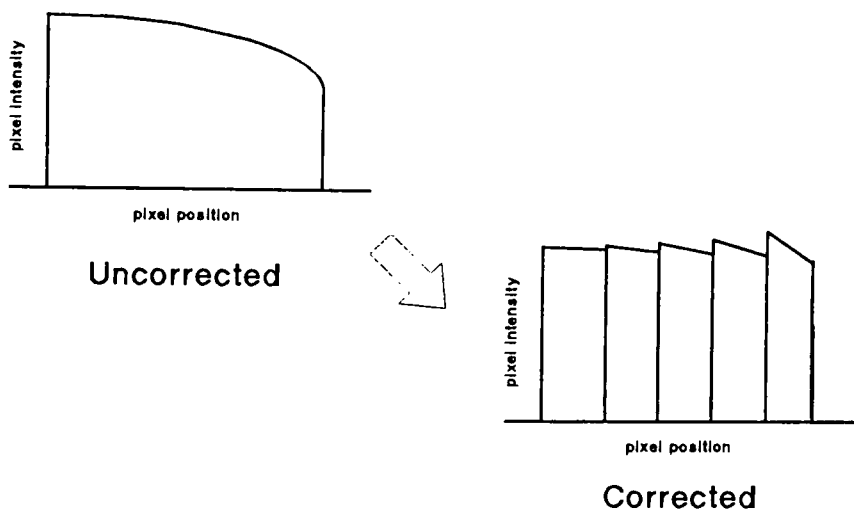


Figure G.14: Low frequency modulation and the correction by counter-modulating d' .

of the test image is at relatively high frequencies, nothing has to be done at all. This would be the case for split-field matches, paired comparisons, contrast sensitivity function measurements, etc.

Appendix H

Uniformity Measurements

Position	X	Y	Z	γ	K_1
1	30.3360	15.0300	1.7860	2.3194	1.0949
2	31.5220	15.4700	1.8040	2.3448	1.0877
3	33.0130	16.1800	1.8710	2.3878	1.0767
4	33.4670	16.4800	1.9200	2.2438	1.1101
5	33.2000	16.5800	2.0550	2.3144	1.0922
6	30.9360	15.1800	1.6580	2.2949	1.1028
7	32.9000	15.9500	1.6480	2.3290	1.0943
8	34.0320	16.7800	1.8240	2.3191	1.0976
9	33.2700	16.4500	1.7590	2.2824	1.1062
10	31.6980	15.8700	1.7770	2.3819	1.0835
11	31.0970	15.4800	1.7650	2.2924	1.1124
12	32.4010	15.9600	1.7100	2.2304	1.1262
13	33.1440	16.4760	1.8890	2.2987	1.1132
14	32.4720	16.0300	1.7400	2.3331	1.1056
15	31.0830	15.4390	1.7120	2.3917	1.0890
16	30.0050	14.6800	1.8140	2.2694	1.1232
17	30.7770	15.0800	1.8320	2.2926	1.1183
18	32.0160	15.6400	2.0380	2.2481	1.1295
19	31.6120	15.5800	1.8750	2.2275	1.1338
20	30.5850	15.0800	1.8000	2.2299	1.1319
21	29.1570	14.4900	1.9580	2.2427	1.1258
22	28.8730	14.2970	1.8360	2.3423	1.1035
23	30.1150	14.8810	1.9820	2.2336	1.1318
24	31.3910	15.5800	1.9100	2.3722	1.0965
25	31.0490	15.4800	2.0320	2.3387	1.1006

Table H.1: Variation of the basic properties of the red channel of the Tektronix 650 HR over 25 regularly spaced areas accross the screen.

Position	X	Y	Z	γ	K_1
1	19.2340	42.4300	9.5460	2.2166	1.1499
2	19.9690	43.6800	9.5280	2.2165	1.1473
3	21.1370	46.1800	10.0690	2.2014	1.1511
4	21.3170	46.8100	10.2820	2.2487	1.1390
5	21.2540	47.1500	10.5680	2.2140	1.1467
6	19.7270	43.4800	9.2780	2.2202	1.1478
7	21.2270	46.3700	9.8340	2.2039	1.1490
8	21.7210	48.2300	10.1700	2.2385	1.1425
9	21.2050	47.1800	10.1290	2.2443	1.1413
10	20.1290	45.1800	9.7750	2.2108	1.1477
11	19.9200	44.5600	9.5530	2.1962	1.1642
12	20.8350	46.3400	9.6840	2.2353	1.1534
13	21.0440	47.1660	10.0070	2.2298	1.1551
14	20.8220	46.1900	9.8200	2.2336	1.1519
15	19.7740	44.0790	9.5990	2.1991	1.1626
16	18.9240	41.3700	8.8770	2.2002	1.1703
17	19.2560	42.0400	8.9880	2.2153	1.1677
18	20.0260	43.7300	9.5800	2.2595	1.1584
19	20.1990	44.4700	9.7090	2.2554	1.1592
20	19.3270	42.7000	9.2710	2.2425	1.1608
21	18.1700	39.8600	8.7470	2.2371	1.1528
22	17.8600	39.2670	8.5210	2.2191	1.1594
23	18.8480	41.2110	9.2100	2.2669	1.1498
24	19.6310	43.4600	9.5950	2.2016	1.1644
25	19.6660	43.4800	9.9340	2.2121	1.1597

Table H.2: Variation of the basic properties of the red channel of the Tektronix 650 HR over 25 regularly spaced areas across the screen.

Position	X	Y	Z	γ	K_1
1	17.9190	6.6380	101.5150	2.2845	1.0960
2	18.6300	6.8850	104.7450	2.2552	1.1013
3	19.7290	7.2920	110.9020	2.2192	1.1063
4	19.7570	7.2100	112.0510	2.2106	1.1079
5	19.5810	7.3710	110.1320	2.2378	1.0991
6	18.0730	6.7000	102.4600	2.2504	1.1025
7	19.5500	7.2770	110.8120	2.2642	1.0962
8	20.8190	7.6040	118.1630	2.1926	1.1119
9	19.8960	7.2660	112.9310	2.2082	1.1093
10	18.7630	6.9940	106.3610	2.2672	1.0943
11	18.7250	6.9160	106.2030	2.2411	1.1114
12	19.4940	7.2560	110.5090	2.1915	1.1235
13	20.6070	7.5260	117.0060	2.1761	1.1279
14	19.6410	7.1860	111.5180	2.1840	1.1265
15	18.5800	6.7930	105.4420	2.2075	1.1202
16	17.5930	6.5050	98.9950	2.2152	1.1267
17	17.9410	6.6410	100.8740	2.2333	1.1218
18	18.8460	6.9650	105.9610	2.1947	1.1311
19	18.9040	7.0110	106.7250	2.1981	1.1302
20	17.6690	6.5700	100.0810	2.1996	1.1278
21	16.6250	6.2580	93.3520	2.1620	1.1295
22	16.2910	6.0190	91.6360	2.2301	1.1153
23	17.5590	6.4890	98.7190	2.1884	1.1280
24	18.3960	6.7980	103.4260	2.2318	1.1171
25	18.4550	6.8200	103.7530	2.2450	1.1087

Table H.3: Variation of the basic properties of the red channel of the Tektronix 650 HR over 25 regularly spaced areas accross the screen.

Position	<i>X</i>	<i>Y</i>	<i>Z</i>	<i>x</i>	<i>y</i>	ΔE_{Lab}
1	67.4890	64.0980	112.8470	0.2761	0.2622	4.3820
2	70.1210	66.0350	116.0770	0.2780	0.2618	3.8407
3	73.8790	69.6520	122.8420	0.2774	0.2615	2.4686
4	74.5410	70.5000	124.2530	0.2768	0.2618	2.0975
5	74.0350	71.1010	122.7550	0.2764	0.2654	3.5236
6	68.7360	65.3600	113.3960	0.2777	0.2641	4.2670
7	73.6770	69.5970	122.2940	0.2774	0.2621	2.4830
8	76.5720	72.6140	130.1570	0.2741	0.2599	1.1899
9	74.3710	70.8960	124.8190	0.2754	0.2625	1.9100
10	70.5900	68.0440	117.9130	0.2752	0.2652	3.9740
11	69.7420	66.9560	117.5210	0.2743	0.2634	3.4274
12	72.7300	69.5560	121.9030	0.2753	0.2633	2.4849
13	74.7950	71.1680	128.9020	0.2721	0.2589	0.0000
14	72.9350	69.4060	123.0780	0.2748	0.2615	1.6958
15	69.4370	66.3110	116.7530	0.2750	0.2626	3.3183
16	66.5220	62.5550	109.6860	0.2786	0.2620	5.6235
17	67.9740	63.7610	111.6940	0.2792	0.2619	5.2197
18	70.8880	66.3350	117.5790	0.2782	0.2603	4.0742
19	70.7150	67.0610	118.3090	0.2761	0.2619	2.8997
20	67.5810	64.3500	111.1520	0.2780	0.2647	4.8869
21	63.9520	60.6080	104.0570	0.2797	0.2651	6.9415
22	63.0240	59.5830	101.9930	0.2806	0.2653	7.6071
23	66.5220	62.5810	109.9110	0.2783	0.2618	5.5511
24	69.4180	65.8380	114.9310	0.2775	0.2632	3.8433
25	69.1700	65.7800	115.7190	0.2759	0.2624	3.5474

Table H.4: Colorimetric variations of a homogeneous white field displayed over 25 regularly spaced areas across the screen of the Tektronix 650 HR.

Sample	$Y_{green}/100$	γ	K_1
1	0.6479	2.0400	1.2189
2	0.6457	2.1065	1.2030
3	0.6396	2.0490	1.2278
4	0.6440	2.1267	1.2086
5	0.6429	2.1299	1.2060
6	0.6419	2.0686	1.2258
7	0.6417	2.1023	1.2111
8	0.6425	2.0964	1.2089
9	0.6435	2.1113	1.2085
10	0.6442	2.1276	1.2007
11	0.6429	2.0703	1.2233
12	0.6480	2.1195	1.1971
13	0.6458	2.1099	1.1986
14	0.6436	2.0596	1.2239
15	0.6433	2.0846	1.2182
16	0.6446	2.0892	1.2161
17	0.6428	2.0790	1.2208
18	0.6457	2.0806	1.2154
19	0.6452	2.0625	1.2213
20	0.6464	2.1015	1.2064
21	0.6433	2.0298	1.2351
22	0.6455	2.0937	1.2145
23	0.6445	2.0804	1.2123
24	0.6452	2.1046	1.2054
25	0.6459	2.1037	1.2089
26	0.6465	2.0832	1.2161
27	0.6464	2.0993	1.2080
28	0.6470	2.1074	1.2025
Mean	0.6446	2.0891	1.2132
Sdev	0.0020	0.0259	0.0093

Table H.5: 29 repeated calibrations performed on the green channel in a fixed position on the screen of the Tektronix 650 HR CRT.

Sample	$Y_{green}/100$	γ	K_1
1	0.6156	2.1062	1.2111
2	0.6219	2.1232	1.1955
3	0.6217	2.1151	1.2047
4	0.6240	2.1406	1.1911
5	0.6244	2.1277	1.1947
6	0.6251	2.1590	1.1758
7	0.6117	2.1265	1.1993
8	0.6123	2.0907	1.2035
9	0.6186	2.1916	1.1710
10	0.6217	2.0780	1.2099
11	0.6281	2.0889	1.2022
12	0.6418	2.1212	1.1669
13	0.6463	2.1164	1.1919
14	0.6562	2.1593	1.1767
15	0.6555	2.1276	1.1934
16	0.6539	2.1135	1.1940
17	0.6471	2.0575	1.2165
18	0.6421	2.0986	1.1900
19	0.6395	2.0989	1.2073
20	0.6580	1.9867	1.2424
21	0.6473	2.1294	1.1916
22	0.6420	2.1739	1.1681
23	0.6393	2.1076	1.1942
24	0.6421	2.1490	1.1634
60:	16.9	51.3	47.4
70:	8.4	41.0	40.8

Table H.6: Goniocolorimetric properties at 3 positions of screen.

Appendix I

Tables of Goniocolorimetric Properties

Angle	Y	Corr Factor
-70:	2071.20	0.9894
-60:	2065.18	0.9923
-50:	2061.54	0.9941
-40:	2055.12	0.9972
-30:	2051.84	0.9988
-20:	2048.99	1.0002
-10:	2047.97	1.0007
0:	2049.32	1.0000
10:	2049.93	0.9997
20:	2054.55	0.9975
30:	2058.19	0.9957
40:	2063.46	0.9932
50:	2069.78	0.9901
60:	2077.50	0.9864
70:	2051.00	0.9992

Table I.1: Goniocolorimetric properties of lambertian diffuser

angle	X	Y	Z
-70	32.76	35.41	27.81
-60	44.34	48.04	37.98
-50	50.49	54.74	43.48
-40	54.27	58.92	47.20
-30	55.56	60.54	48.39
-20	56.27	60.74	49.75
-10	56.74	61.30	50.14
0	57.24	61.86	50.38
10	56.55	60.88	50.11
20	56.72	61.79	49.53
30	55.63	60.43	48.91
40	54.32	58.94	47.42
50	51.69	56.08	45.18
60	47.25	51.28	40.97
70	37.87	41.01	32.31

Table I.2: Goniocolorimetric properties at center of screen.

angle	X	Y	Z
-60	38.75	41.70	33.72
-50	40.40	43.44	35.02
-40	41.22	44.28	35.99
-30	41.48	44.69	36.18
-20	41.18	44.08	36.02
-10	41.05	44.04	35.90
0	40.70	44.03	35.12
10	39.68	42.36	34.64
20	38.66	41.70	33.61
30	37.62	40.23	31.67
40	34.58	36.87	29.32
50	29.56	31.57	24.82
60	15.98	16.93	13.27

Table I.3: Goniocolorimetric properties at the left of screen.

angle	Y left	Y center	Y right
-70:	37.5	35.4	35.3
-60:	41.7	48.0	40.5
-50:	43.4	54.7	45.4
-40:	44.3	58.9	47.4
-30:	44.7	60.5	48.8
-20:	44.1	60.7	49.7
-10:	44.0	61.3	50.2
0:	44.0	61.9	50.6
10:	42.4	60.9	51.1
20:	41.7	61.8	51.5
30:	40.2	60.4	51.9
40:	36.9	58.9	51.4
50:	31.6	56.1	50.5
60:	16.9	51.3	47.4
70:	8.4	41.0	40.8

Table I.4: Goniocolorimetric properties at 3 positions of screen.

Appendix J

Program crtCAL.c

```

***** Program : crtcal.c *****
Description : A simple C program for color CRT characterization.
Author : Ricardo J. Motta,
         Munsell Color Science Laboratory
         Center for Imaging Science
         Rochester Institute of Technology
Created : 02-27-88
***** */

```

```

main()
{
    int d, samples, wait, plane, RGBd[3];
    float Yxy[3];

    /*-----*/
    /* Set up measurement variables */
    {
        wait = 20;      /* number of seconds to wait before measuring */
        samples = 10;   /* number of samples to average */
        plane = 1;
    }

    /*-----*/
    /* Find the phosphors chromaticity */
    {
        for (d=0 ; d<8 ; d++)
        {
            RGBd[0] = 255 * ( d & 1);           /* Set up the CRT to display */
            RGBd[1] = 255 * ( ( d & 2) >> 1); /* all 8 combinations of RGBd */
            RGBd[2] = 255 * ( ( d & 4) >> 2);
            setLUT(plane,RGBd);                /* Set the LUT entry "plane" */
            getYxydata(Yxy,wait,samples);     /* Get Yxy data from colorimeter */
            printf("%8.4f %8.6f %8.6f\n",
                   Yxy[0],Yxy[1],Yxy[2]);
        }
    }

    /*-----*/
    /* Make 25 measurements covering RGBd (5 -> 255) */
    {
        for (d=0 ; d<26 ; d++)
        {
            RGBd[0] = ((d * 10) + 5);          /* Set up the same video voltage */
            RGBd[1] = ((d * 10) + 5);          /* on all three CRT channels */
            RGBd[2] = ((d * 10) + 5);
            setLUT(plane,RGBd);                /* Set the LUT entry "plane" */
            getYxydata(Yxy,wait,samples);     /* Get Yxy data from colorimeter */
            printf("%8.4f %8.6f %8.6f\n",
                   Yxy[0],Yxy[1],Yxy[2]);
        }
    }

    exit(0);
}

```

Appendix K

Program crtCALC.c

```
*****
```

Program : crtCALC.c

Description : Will calculate the CRT vital stats = gamma, K1, K2

Author : Ricardo J. Motta,

Munsell Color Science Laboratory

Center for Imaging Science

Rochester Institute of Technology

227

```
*****
```

RGBi = CRT RGB tristimulus

XYZ = CIE tristimulus

Yxy = CIE Luminance and chromaticity

RGBd = CRT RGB digital counts

```
*****
```

```
# include <stdio.h>
```

```
#define DEBUG 0
```

```
double XCRTR, YCRTR, ZCRTR; /* Amounts of CIE tristimulus */
double XCRTG, YCRTG, ZCRTG; /* in each of the CRT primaries */
double XCRTB, YCRTB, ZCRTB;
```

```
double RCRTX, RCRTY, RCRTZ; /* Amounts of CRT tristimulus */
double GCRTX, GCRTY, GCRTZ; /* in each of the CIE primaries */
double BCRTX, BCRTY, BCRTZ;
```

```
/* MAIN PROG */
```

```
main(argc,argv)
```

```
int argc;
```

```
char *argv[];
```

```
{
```

```
/*-----*/
```

```
/* declaration of variables */
```

```
{
```

```
    int i,j, RGBd[3], nstart, nstop;
    double Yxy[30][3], RGBi[30][3], XYZ[30][3], a[9], CRTPAR[3][3];
    FILE *ifp, *ofp, *fopen();
```

```
}
```

```
/*-----*/
```

```
/* CHECK INPUT AND OPEN FILES */
```

```
{
```

```
    if (argc != 3 )
```

```
    {
```

```
        fprintf(stderr,"usage : %s infilename outfilename\n",argv[0]);
        exit(-1);
    }
```

```
    ifp = fopen(argv[1],"r");
```

```
    if (ifp == NULL)
```

```
    {
```

```
        fprintf(stderr,"*** Bad input filename : %s ***\n",argv[1]);
        exit(-1);
    }
```

```
    }
```

```
    ofp = fopen(argv[2],"w");
```

```
    if (ofp == NULL)
```

```
    {
```

```
        fprintf(stderr,"*** Bad output filename : %s ***\n",argv[2]);
        exit(-1);
    }
```

```
}
```

```
}
```

```

/*-----*/
/* INPUT THE DATA AND TRANSFORM IT FROM Yxy TO XYZ */
{
    for (i=1 ; i<8 ; i++)
    {
        fscanf(ifp,"%lf%lf%lf", &Yxy[i][0], &Yxy[i][1], &Yxy[i][2]);
        Yxy_XYZ(Yxy[i],XYZ[i]);
        for (j=0; j<3; j++)
            if (XYZ[i][j] < 0.0) XYZ[i][j] = 0.0;
    }

    XCRTR = XYZ[1][0];      YCRTR = XYZ[1][1];      ZCRTR = XYZ[1][2];
    XCRTG = XYZ[2][0];      YCRTG = XYZ[2][1];      ZCRTG = XYZ[2][2];
    XCRTB = XYZ[4][0];      YCRTB = XYZ[4][1];      ZCRTB = XYZ[4][2];
}

/*-----*/
/* CALCULATE THE XYZ -> RGBi MATRIX */
{
    a[0] = XCRTR;      a[1] = XCRTG;      a[2] = XCRTB;
    a[3] = YCRTR;      a[4] = YCRTG;      a[5] = YCRTB;
    a[6] = ZCRTR;      a[7] = ZCRTG;      a[8] = ZCRTB;

    /*** Invert the matrix */
    if (matinv(a) < 0)
    {
        fprintf(stderr,"*** Bad Matrix Inversion ***\n");
        exit(-1);
    }

    RCRTX = a[0]; RCRTY = a[1]; RCRTZ = a[2];
    GCRTX = a[3]; GCRTY = a[4]; GCRTZ = a[5];
    BCRTX = a[6]; BCRTY = a[7]; BCRTZ = a[8];
}

/*-----*/
/* TRANSFORM XYZ TO RGBi */
{
    if (DEBUG)    /*** output the RGB of the 8 combinations */
        for (i=0; i< 8; i++)
        {
            XYZ_RGBi(XYZ[i],RGBi[i]);
            fprintf(stderr,"%6.3lf %6.3lf %6.3lf\n", RGBi[i][0], RGBi[i][1], RGBi[i][2]);
        }

    /*** Input the data for the transfer function and transform it to XYZ */
    for (i=0; i< 26; i++)
    {
        fscanf(ifp,"%lf%lf%lf", &Yxy[i][0], &Yxy[i][1], &Yxy[i][2]);
        Yxy_XYZ(Yxy[i],XYZ[i]);
        for (j=0; j<3; j++)
            if (XYZ[i][j] < 0.0) XYZ[i][j] = 0.0;
        XYZ_RGBi(XYZ[i],RGBi[i]);
    }

    /*** Scale CRT tristimulus 0 -> 1 and clip at 0 */
    for (j=0; j<3; j++)
        for (i=0; i< 26; i++)
            RGBi[i][j] = (RGBi[i][j] < 0.0) ? 0.0 : RGBi[i][j]/RGBi[25][j];
}

```

```

if (DEBUG) /*** output the separated transfer functions */
for (i=0; i< 26; i++)
    fprintf(stderr,"%6.3lf %6.3lf %6.3lf\n", RGBi[i][0], RGBi[i][1], RGBi[i][2]);
}

/*-----*/
/* ESTIMATE AT WHICH DC TO START CURVE FITING */
{
    nstart = 0;
    for (j=0; j<3; j++)
    {
        for (i = 0; (RGBi[i][j] <= 0.05); i++); /* Start at 5 % */
        if (i > nstart) nstart = i;
    }

    nstop = 25;                                /* Stop at the end */
    if (DEBUG)
        fprintf(stderr," start %2d, stop %2d\n",nstart,nstop);
}

/*-----*/
/* CALCULATE GAMMA, K1, K2 */
{
    nlcrt(RGBi,CRTPAR,nstart,nstop);
}

/*-----*/
/* OUTPUT */
{
    /*** Output the XYZ tristimulus of the CRT primaries */
    fprintf(ofp,"%6.3lf %6.3lf %6.3lf\n",XCRTR, YCRTR, ZCRTR);
    fprintf(ofp,"%6.3lf %6.3lf %6.3lf\n",XCRTG, YCRTG, ZCRTG);
    fprintf(ofp,"%6.3lf %6.3lf %6.3lf\n",XCRTB, YCRTB, ZCRTB);
    /*** Output gamma, K1 and K2 for each of RGB */
    for (j=0; j<3; j++)
        fprintf(ofp,"%6.4lf %6.4lf %6.4lf\n",CRTPAR[j][0],
                CRTPAR[j][1],CRTPAR[j][2]);

    fclose(ifp);
    fclose(ofp);
}
exit(0);
}
/* END OF MAIN PROG */
*****
```

```
*****
Function : Yxy_XYZ
Description : Will transform CIE Y,x,y chromaticities into XYZ tristimulus.
*****
```

230

```
# include "/usr/local/include/ricdefs.h"
int Yxy_XYZ(Yxy,XYZ)
double *Yxy, *XYZ;
{
    double X,Y,Z,x,y,T;

    *(XYZ + 1) = Y = *Yxy;
    x = *( Yxy+1 );
    y = *( Yxy+2 );
    if ( y != 0.0 )
    {
        T = Y / y;
        *(XYZ + 0) = x * T;
        *(XYZ + 2) = T - *(XYZ + 0) - Y;
        return (0);
    }
    else return (-1);
}
```

```

*****
Function : matinv
Description : Will invert a 3 x3 matrix
*****
The values RCRTX, GCRTX, etc., must be set before the routine is called.
If the matrix inversion fails the routine returns a -1, 0 otherwise.
*****
int matinv(double *a)
{
    double m[9], detA;
    double a11,a12,a13,a21,a22,a23,a31,a32,a33;
    double m11,m12,m13,m21,m22,m23,m31,m32,m33;
    int i;

    a11 = *(a);
    a12 = *(a + 1);
    a13 = *(a + 2);
    a21 = *(a + 3);
    a22 = *(a + 4);
    a23 = *(a + 5);
    a31 = *(a + 6);
    a32 = *(a + 7);
    a33 = *(a + 8);

    detA = (a11*((a22*a33) - (a23*a32)))
        - (a12*((a21*a33) - (a23*a31)))
        + (a13*((a21*a32) - (a22*a31)));

    if ( detA != 0.0 )
    {
        *(m + 0) = ( a22*a33 - a23*a32)/detA;
        *(m + 1) = ( a13*a32 - a12*a33)/detA;
        *(m + 2) = ( a12*a23 - a13*a22)/detA;
        *(m + 3) = ( a23*a31 - a33*a21)/detA;
        *(m + 4) = ( a11*a33 - a13*a31)/detA;
        *(m + 5) = ( a13*a21 - a11*a23)/detA;
        *(m + 6) = ( a21*a32 - a22*a31)/detA;
        *(m + 7) = ( a12*a31 - a11*a32)/detA;
        *(m + 8) = ( a11*a22 - a12*a21)/detA;
        for (i = 0; i<9; i++)
            *(a + i) = *(m + i);
        return (0);
    }
    return(-1);
}

```

```
*****
Function : XYZ_RGBi
Description : Will transform CIE XYZ into RGB crt tristimulus.
*****
The values RCRTX, GCRTX, etc., must be set before the routine is called.
If the tristimulus are out of range the routine returns a -1, 0 otherwise.
*****
```

```
int XYZ_RGBi(XYZ,RGBi)
double *XYZ, *RGBi;
{
    double X, Y, Z, Ri, Gi, Bi;

    X = *(XYZ+0);
    Y = *(XYZ+1);
    Z = *(XYZ+2);

    *(RGBi+0) = Ri = (X * RCRTX) + (Y * GCRTY) + (Z * BCRTZ);
    *(RGBi+1) = Gi = (X * GCRTX) + (Y * BCRTY) + (Z * RCRTZ);
    *(RGBi+2) = Bi = (X * BCRTX) + (Y * RCRTY) + (Z * GCRTZ);

    if ( (Ri<0.0) || (Ri>1.0) ) return (-1);
    if ( (Gi<0.0) || (Gi>1.0) ) return (-1);
    if ( (Bi<0.0) || (Bi>1.0) ) return (-1);

    return(0);
}
```

```
*****
```

Function : nlcrt.c

Description : Non-linear modeling of the crt transfer function.

Reference : NRC - The Art of Scientific Computing

233

William H. Press, et al,
"Numerical Recipes in C",
Cambridge Univ. Press, 1988
QA76.73.C15N865
ISBN 0-521-35465

```
*****
```

RGBi = RGB tristimulus curve to match;

par = return for gamma, K1, K2;

nstart = starting dc index (0->25)

nstop = stoping dc index (0->25)

```
******/
```

```
#include <stdio.h>
```

```
#include "nr.h"
```

```
#include "nrutil.h"
```

```
nlcrt(RGBi,par,nstart,nstop)
```

```
double *RGBi, *par;
```

```
int nstart, nstop;
```

```
{
```

```
#define DEBUG 0
```

```
float d, *x, *a, *y, *sig, **covar, **alpha, chisq[1];
```

```
float oldchi, alamda[1], fg[1], t[3];
```

```
int i, j, ma, ndata, *lista, mfit, go;
```

```
void fcrt(), mrqmin();
```

```
/*-----*/
```

```
/* Debug check */
```

```
if (DEBUG)
```

```
{
```

```
    fprintf(stderr," Entering nlcrt\n");
```

```
    fprintf(stderr," start %2d, stop %2d\n",nstart,nstop);
```

```
    for (i=1; i<=26; i++)
```

```
        for (i=nstart+1; i<=nstop+1; i++)
```

```
        {
```

```
            for (j=1; j<=3; j++)
```

```
                t[j-1] = (float) *(RGBi + ((i-1) * 3) + j - 1);
```

```
                fprintf(stderr," * %2d - %7.4f %7.4f %7.4f\n",i,t[0],t[1],t[2]);
```

```
}
```

```
}
```

```
/*-----*/
```

```
/* Allocate matrices and vectors */
```

```
{
```

```
    /*** Allocate Data vectors */
```

```
    ndata = nstop - nstart + 1;
```

```
    x = vector(1,ndata);
```

```
    y = vector(1,ndata);
```

```
    sig = vector(1,ndata);
```

```
    /*** Allocate Parameter vectors */
```

```
    ma = 3;
```

```

a = vector(1,ma);
lista = ivector(1,ma);

/*** Allocate matrices */

covar = matrix(1,ma,1,ma);
alpha = matrix(1,ma,1,ma);
}

/*
*-----*/
/* MAIN LOOP */
{

    /*** Set up lista vector to indicate which parameters are being manipulated */
    mfit = 3;
    lista[1] = 1;
    lista[2] = 3;
    lista[3] = 2;

    for (j=1; j<=3; j++)
    {
        /*** Fill the arrays of data */
        for (i=nstart+1; i<=nstop+1; i++)
        {
            x[i-nstart] = ((i-1) * 10.0) + 5.0;
            y[i-nstart] = (float) *(RGBi + ((i-1) * 3) + j - 1);
            sig[i-nstart] = 0.02; /* Give the average stdev */
        }

        /*** Initial guesses on the value of the parameters */
        a[1] = 2.0;
        a[2] = 1.0;
        a[3] = 0.0;

        /*** STARTER */
        alamda[0] = -1.0;      /*** Initialize the delta a */
        if (DEBUG) fprintf(stderr, " %7.4lf %7.4f - %7.4f %7.4f %7.4f\n", chisq[0], alamda[0], a[1], a[2], a[3]);
        mrqmin(x,y,sig,ndata,a,ma,lista,mfit,covar,alpha,chisq,fcrt,alamda);
        if (OEBUG) fprintf(stderr, " %7.4lf %7.4f - %7.4f %7.4f %7.4f %7.4f\n", chisq[0], alamda[0], a[1], a[2], a[3]);
        oldchi = 1.0 + chisq[0];

        /*** LOOP */
        while( ((oldchi-chisq[0]) > 0.1) || (oldchi == chisq[0]) )
        {
            oldchi = chisq[0];
            mrqmin(x,y,sig,ndata,a,ma,lista,mfit,covar,alpha,chisq,fcrt,alamda);
            if (DEBUG) fprintf(stderr, " %7.4lf %7.4f - %7.4f %7.4f %7.4f %7.4f\n", chisq[0], alamda[0], a[1], a[2], a[3]);
        }

        *(par + ((j-1) * 3) + 0) = a[1];
        *(par + ((j-1) * 3) + 1) = a[2];
        *(par + ((j-1) * 3) + 2) = a[3];

    }
}

/* END OF MAIN LOOP */
/*
*-----*/

```

```
*****  
Function : fcrt.c  
Description : Will calculate RGBi from RGBd and the partial derivatives.  
This function is called by 'mrqmin()' on 'nlcrt()'  
*****  
# include <math.h>  
  
void fcrt(x,a,y,dyda,na)  
float x,a[],*y,dyda[];  
int na;  
{  
    float A1,A2,a1,a2,a3;  
  
    a1 = a[1];  
    a2 = a[2];  
    a3 = a[3];  
  
    A1 = ((a2 * ( x / 255.0)) + a3);  
    A2 = ( A1 < 0.0 ) ? 0.0 : A1;  
    *y = pow( A2 , a1);  
  
    dyda[1] = log(A1) * *y;  
    dyda[2] = x * a1 * pow(A2, a1-1.0) / 255.0;  
    dyda[3] = a1 * pow(A2, a1-1.0);  
  
}
```

Bibliography

- [1] S. Anstis, P. Cavanagh, D. Maurer, T. Lewis, D. A. I. MacLeod, and G. Mather. Computer-generated screening test for colorblindness. *Color Res. Appl.*, 11:S63–S66, 1986.
- [2] L. Arend and A. Reeves. Simultaneous color constancy. *J. Opt. Soc. Am.*, 3:1743–1751, 1986.
- [3] ASTM. Standard method for computing the colors of objects using the CIE system. Technical Report E 308-85, American Society for Testing and Materials, Philadelphia, PA, 1985.
- [4] C. J. Bartleson. Colorimetry. In F. Grum, editor, *Optical Radiation Measurements*, volume 2. Academic Press, 1980.
- [5] C. J. Bartleson and E. J. Breneman. Brightness perception in complex fields. *J. Opt. Soc. Am.*, 57:953–957, 1967.
- [6] C. J. Bartleson and E. J. Breneman. Brightness reproduction in the photographic process. *Photogr. Sci. Eng.*, 11:254–262, 1967.
- [7] G. A. Baxes. *Digital Image Processing - A Practical Primer*. Prentice-Hall, New Jersey, 1984.
- [8] K. B. Benson, editor. *Television Engineering Handbook*. McGraw-Hill, New York, 1986.

- [9] S. M. Berman, D. S. Greenhouse, I. L. Bailey, and A. Bradley. Experimental studies relating environmental lighting and flicker to visual fatigue in VDT operators. In *CIE Proceedings, 20th Session, Amsterdam*, pages D312/1–D312/5, Bureau Central de la CIE, Paris, France, 1983. Comission International d'Eclairage.
- [10] F. W. Billmeyer, Jr. and F. X. D. O'Donnell. Visual gloss scaling and multidimensional scaling analysis of painted specimens. *Color Res. Appl.*, 12:315–326, 1987.
- [11] F. J. Bingley. Colorimetry in color television. *Proc. IRE*, 41:838–851, 1953.
- [12] F. J. Bingley. Colorimetry in color television part II and part III. *Proc. IRE*, 42:48–57, 1954.
- [13] Borland. Turbo-Pascal Compiler, 1983. Version 3.0.
- [14] R. W. Boyd. *Radiometry and the Detection of Optical Radiation*. John Wiley, New York, 1983.
- [15] R. M. Boynton. Ten years of research with the Minimally Distinct Border. In J. Krauskopf J. C. Armington and B. R. Wooten, editors, *Visual Psychophysics and Physiology*. Academic Press, 1978.
- [16] R. M. Boynton. *Human Color Vision*. Holt, Rinehart and Winston, New York, 1979.
- [17] R. M. Boynton. Psychophysics. In C. J. Bartleson and F. Grum, editors, *Visual Measurements*. Academic Press, 1984.
- [18] R. M. Boynton. Color vision. *Ann. Rev. Psychol.*, 39:69–100, 1988.
- [19] R. N. Bracewell. *The Fourier Transform and Its Applications*. McGraw-Hill, New York, 2nd edition, 1978.
- [20] D. Brainard. Calibration of a computer controlled color monitor. *Color Res. Appl.*, 14:23–34, 1989.

- [21] R. C. Brainard, A. N. Netravali, and D. E. Pearson. Predictive coding of composite NTSC color television signals. *J. Soc. Motion Pict. Telev. Eng.*, pages 245–252, 1982.
- [22] E. J. Breneman. Dependence of luminance required for constant brightness upon chromaticity and chromatic adaptation. *J. Opt. Soc. Am.*, 48:228–232, 1958.
- [23] E. J. Breneman. Corresponding chromaticities for different states of adaptation to complex visual fields. *J. Opt. Soc. Am. A*, 4:1115–1128, 1987.
- [24] W. E. Bretl. Colorimetric performance of non-standard television receiver with customer adjustment. *IEEE Trans Consum Electron*, CE-25:100–110, 1979.
- [25] M. H. Brill and N. Panken. From softcopy to hardcopy on a desert island. *Color Res. Appl.*, 13:127–129, 1988.
- [26] P. Brou, T. R. Sciascia, L. Linden, and J. Y. Lettvin. The colors of things. *Sci. Am.*, 255:84–91, 1986.
- [27] G. H. Brown. The choice of axes and bandwidths for the chrominance signals in NTSC color television. *Proc. IRE*, 42:58–59, 1954.
- [28] G. Buchsbaum. Color signal coding: Color vision and color television. *Color Res. Appl.*, 12:266–269, 1987.
- [29] G. Buchsbaum and A. Gottschalk. Trichromacy, opponent colours coding and optimum colour information transmission in the retina. *Proc. R. Soc. Lond.*, B 220:89–113, 1983.
- [30] W. Budde. Physical detectors of optical radiation. In F. Grum and C. J. Bartleson, editors, *Optical Radiation Measurements*, volume 4. Academic Press, 1983.
- [31] S. A. Burns, V. C. Smith, J. Pokorny, and A. E. Elsner. Brightness of equal luminance lights. *J. Opt. Soc. Am.*, 72:1225–1231, 1982.
- [32] F. W. Campbell. The human eye as an optical filter. *Proc. IEEE*, 56:1009–1014, 1968.

- [33] F. W. Campbell and J. J. Kulikowski. Orientation selectivity of the human visual system. *J. Physiol. (London)*, 187:437–445, 1966.
- [34] F. W. Campbell and J. G. Robson. Applications of fourier analysis to the visibility of gratings. *J. Physiol. (London)*, 197:551–566, 1968.
- [35] C. R. Carlson and J. R. Bergen. Perceptual considerations for high definition television systems. *J. Soc. Motion Pict. Telev. Eng.*, pages 1121–1126, 1984.
- [36] R. C. Carter and E. C. Carter. High-contrast sets of colors. *Appl Opt*, 21:2936–2939, 1982.
- [37] R. C. Carter and E. C. Carter. CIE L*u*v* color difference equations for self-luminous displays. *Color Res. Appl.*, 8:252–253, 1983.
- [38] E. Catmull. A tutorial on compensation tables. *Comput Graphics*, 13:1–7, 1979.
- [39] A. Chapanis and R. M. Halsey. Luminance of equally bright colors. *J. Opt. Soc. Am.*, 45:1–6, 1955.
- [40] G. M. Chioran, K. L. Sellers, S. C. Benes, M. Lubow, S. J. Dain, and P. E. King Smith. Color mixture thresholds measured on a color television – a new method for analysis, classification and diagnosis of optic nerve disease. *Doc. Ophthalmol.*, 61:119–135, 1986.
- [41] CIE. Colors of light signals. Publication No. 2.2, Comission International d'Eclairage, Bureau Central de la CIE, Paris, 1977.
- [42] CIE. Vision and the visual display work station. Publication No. 60, Comission International d'Eclairage, Bureau Central de la CIE, Paris, 1984.
- [43] CIE. Colorimetric observers. Publication Standard CIE S002, Comission International d'Eclairage, Central Bureau of the CIE, Austria, Vienna, 1986.
- [44] CIE. Colorimetry, official recommendations of the CIE. Publication No.15.2, Comision International d'Eclairage, Central Bureau of the CIE, Austria, Vienna, 1986.

- [45] CIE. Colorimetry, official recommendations of the CIE. Publication No.15, Comission International d'Eclairage, Bureau Central de la CIE, Vienna, 1987.
- [46] Conrac Corporation. Conrac Division. *Raster graphics handbook*. Van Nostrand Reinhold, New York, 1985.
- [47] A. Cornell-Clyne. *Colour Cinematography*. Chapman & Hall, London, 1951.
- [48] T. N. Cornsweet. *Visual Perception*. Academic Press, 1970.
- [49] T. N. Cornsweet. The Bezold-Brücke effect and its complement, hue constancy. In J. Krauskopf J. C. Armington and B. R. Wooten, editors, *Visual Psychophysics and Physiology*. Academic Press, 1978.
- [50] W. De Corte. High contrast sets of colours for colour CRT under various conditions of illumination. *Displays*, 3:89–99, 1982.
- [51] W. De Corte. Finding appropriate colors for color displays. *Color Res. Appl.*, 11:56–61, 1986.
- [52] W. De Corte. Ergonomically optimal crt colours for nonfixed ambient illumination conditions. *Color Res. Appl.*, 13:327–331, 1989.
- [53] W. B. Cowan. The specification of heterochromatic brightness. In J. J. Rennilson, editor, *Colorimetry of Self-Luminous Displays*. Joint ISCC & SID Informal Symp, 1982.
- [54] W. B. Cowan. CIE calibration of video monitors. Technical report, National Research Council of Canada, 1983.
- [55] W. B. Cowan. Discreteness artifacts in raster based display systems. In J. D. Mollon and L. T. Sharpe, editors, *Colour Vision: Physiology and Psychophysics*, pages 166–172. Academic Press, 1983.

- [56] W. B. Cowan. An inexpensive scheme for calibration of a colour monitor in terms of CIE standard coordinates. *Comput Graphics*, 17:315–321, 1983.
- [57] W. B. Cowan and N. Rowell. On the gun independence and phosphor constancy of colour video monitors. *Color Res. Appl.*, 11:S34–S38, 1986.
- [58] W. J. Cromie. Testing the vision of infants. *The MIT Report*, 27(6):8–9, 1989.
- [59] C. L. Crouch and R. L. Vincent. Disability and discomfort glare fields studies under low luminance conditions. In *CIE Proceedings, 20th Session, Amsterdam*, pages D502/1-D502/6, Bureau Central de la CIE, Paris, France, 1983. Comission Internationale d'Eclairage.
- [60] D. J. O. Daoost. Development of a photometric primary standard for reflectance goniospectrophometry. Master's thesis, Center for Imaging Science - Rochester Institute of Technology, Rochester, NY, 1987.
- [61] H. Davson. *Physiology of the Eye*. Academic Press, New York, 4 edition, 1980.
- [62] L. E. DeMarsh. Color reproduction in color television. In M. Pearson, editor, *Optimum Reproduction of Color*, pages 69–97. Inter-Soc Color Council, 1971.
- [63] L. E. DeMarsh. Color rendition in television. *IEEE Trans Consum Elec*, pages 149–157, 1977.
- [64] D. Denham. High performance colour displays for computer graphics. *Computer Graphics Forum*, 5:57–63, 1986.
- [65] E. Dubois, M. S. Sabri, and J. Y. Ouellet. Three-dimensional spectrum and processing of digital NTSC color signals. *J. Soc. Motion Pict. Telev. Eng.*, pages 372–378, 1982.
- [66] J. Duntemann. *Complete Turbo Pascal*. Scott, Foresman and Co., Glenview, Illinois, 1987.

- [67] R. A. Easton, J. Markin, and A. Sobel. Subjective brightness of a very-short-persistence television display compared to one with standard persistence. *J. Opt. Soc. Am.*, 57:957–962, 1967.
- [68] EIA. Electrical performance standards - monochrome television studio facilities. Standard EIA-170, Electronic Industries Association, Engineering Department, Washington, D.C., 1957.
- [69] R. M. Evans. *An Introduction to Color*. Wiley, New York, 1948.
- [70] J. E. Farrel, B. L. Benson, and C. R. Haynie. Predicting flicker threshold for video display terminals. *Proc. SID*, 28:449–453, 1987.
- [71] K. W. Farrel. Investigation of the accuracy of array radiometry for measuring pulsed radiation sources. Master's thesis, Center for Imaging Science Rochester Institute of Technology, Rochester, NY, 1987.
- [72] D. G. Fink. *Principles of Television Engineering*. McGraw-Hill, New York, 1940.
- [73] R. W. Floyd and L. Steinberg. An adaptive algorithm for spatial greyscale. *Proc. SID*, 17/2:75–77, 1976.
- [74] J. D. Foley and A. VanDam. *Fundamentals of Interactive Computer Graphics*. Addison-Wesley Publishing Co., Reading, MA, 1982.
- [75] G. A. Fry. Amalgamation of the Wright and Guild color-mixture data. *Color Res. Appl.*, 13:50–54, 1988.
- [76] T. Fuchida, W. B. Cowan, and G. Wyszecki. Matching large color differences with achromatic and chromatic surrounds. *Color Res. Appl.*, 10:92–97, 1985.
- [77] E. M. Granger. *Specification of Color Image Quality*. PhD thesis, University of Rochester, 1975.

- [78] E. M. Granger and J. C. Heurtley. Visual chromaticity-transfer function. *J. Opt. Soc. Am.*, 63:1173–1172, 1973.
- [79] H. Grassmann. Zur theorie der farbenmischung. *Poggendorf' Ann. Phys.*, 89:69, 1853.
- [80] F. Grum and R. Becherer, editors. *Radiometry*, volume 1 of *Optical Radiation Measurements*. Academic Press, 1982.
- [81] G. Guekos and R. Ulmi. Room illumination and CRT flicker in display terminals. *CIE Review*, pages 6–11, 1983.
- [82] R. Hall. Color reproduction and illumination models. In D. F. Rogers and R. A. Earnshaw, editors, *Techniques for Computer Graphics*, pages 195–238. Springer-Verlag, New York, 1987.
- [83] J. F. Hamilton. Reciprocity law failure and the intermittency effect. In T. H. James, editor, *The Theory of the Photographic Process*, page 133. Macmillan, 4th edition, 1977.
- [84] A. E. Hardy. The performance of color-television picture-tube phosphor screens. *IEEE Trans. BTR*, BTR-11(2):33–37, 1965.
- [85] L. D. Harmon. The recognition of faces. In R. Held, editor, *Image, Object and Illusion - Readings from Scientific American*, pages 102–112. W. H. Freeman, 1974.
- [86] L. C. Harrop. Color television and viewing conditions. *IEEE Trans. Broadcast*, 16:1–2, 1970.
- [87] J. H. Harshbarger. Standardization of the television raster for non-broadcast applications. *J. Soc. Motion Pict. Telev. Eng.*, pages 797–807, 1982.
- [88] W. T. Hartmann and T. E. Madden. Prediction of display colorimetry from digital video signals. *J. Imaging Tech.*, 13:103–108, 1987.
- [89] H. Von Helmholtz. *Handbuch der Physiologischen Optik*. Voss, Hamburg, 1866.

- [90] S. Herman. Design of television color rendition. *J. Soc. Motion Pict. Telev. Eng.*, 84:267–273, 1975.
- [91] C. H. Hirsch. A study of the need for color controls on color TV receivers in a color TV system operating perfectly. *IEEE Trans. BTR*, BTR-10(3):71–96, 1964.
- [92] C. H. Hirsch. The chromaticity of reference white in color television. *J. Soc. Motion Pict. Telev. Eng.*, 77:702–713, 1968.
- [93] R. W. G. Hunt and L. M. Winter. Colour adaptation on picture viewing situations. *J. Phot. Sci.*, 23:112–115, 1975.
- [94] R. S. Hunter. *The Measurement of Appearance*. John Wiley, New York, 1975.
- [95] R. G. E. Hutter. The deflection of electron beams. In B. Kazan, editor, *Advances in Image Pickup and Display*. Academic Press, 1974.
- [96] J. R. Joblove and D. P. Greenberg. Color spaces for computer graphics. *Comput Graphics*, 12:20–25, 1978.
- [97] P. K. Kaiser and R. M. Boynton. Role of the blue mechanism in wavelength discrimination. *Vision Research*, 25:523–529, 1985.
- [98] J. Kamler. *Luminescent screens: photometry and colorimetry*. Iliffe, London, 1969.
- [99] R. D. Kell and A. C. Schroeder. Optimum utilization of the radio frequency channel for color television. *RCA Review*, 14:133–143, 1953.
- [100] D. H. Kelly. Adaptation effects on spatial-temporal sine-wave thresholds. *Vsion Res.*, 12:89–101, 1972.
- [101] D. H. Kelly. Visual contrast sensitivity. *Optica Acta*, 24:107–129, 1977.
- [102] D. H. Kelly. Spatiotemporal variation of chromatic and achromatic contrast thresholds. *J. Opt. Soc. Am.*, 73:742–750, 1983.

- [103] D. H. Kelly. Retinal inhomogeneity. I. spatiotemporal contrast sensitivity. *J. Opt. Soc. Am. A*, 1:107–113, 1984.
- [104] D. H. Kelly. Spatial and temporal aspects of red/green opponency. *Proc. SPIE*, 901:230–240, 1988.
- [105] D. H. Kelly, W. E. Evans, and C. H. Dawson. Software-based display system for visual experiments. *J. Opt. Soc. Am.*, 72:1757, 1982.
- [106] J. Kenney. Careful color matching makes hardcopy output conform to CRT display. *Computer Technology Review*, pages 167–175, 1985.
- [107] K. Kinameri and M. Nonaka. Measurements of white uniformity of color picture tubes. *Appl. Optics*, 13:1270–1272, 1974.
- [108] K. Kinameri and M. Nonaka. Spectroradiometric measurement of color television picture tubes. In *CIE Compte Rendu - 19th Session*, pages P-79–08. Comission International d'Eclairage, 1979.
- [109] P. E. King-Smith, G. M. Chioran, K. L. Sellers, and S. L. Alvarez. Normal and deficient colour discrimination analysed by colour television. In J. D. Mollon and L. T. Sharpe, editors, *Colour Vision: Physiology and Psychophysics*, pages 167–172. Academic Press, 1983.
- [110] P. E. King-Smith, A. J. Vingrys, and S. C. Benes. Visual thresholds measured with color video monitors. *Color Res. Appl.*, 12:73–80, 1978.
- [111] J. S. Kinney. Brightness of colored self-luminous displays in the CIE. In J.J.Rennilson, editor, *Colorimetry of Self-Luminous Displays*. Joint ISCC & SID Informal Symp, 1982.
- [112] J. S. Kinney. Brightness of colored self-luminous displays. *Color Res. Appl.*, 8:82–89, 1983.

- [113] B. Knave and P. Wideback, editors. *Work With Display Units 86*. North-Holland, New York, 1987.
- [114] L. Lamport. *LAT_EX- A Document Preparation System*. Addison-Wesley, Reading, Massachusetts, 1986.
- [115] D. B. Langmuir. Theoretical limitations of cathode-ray tubes. *Proc. IRE*, 25(8):977–991, 1937.
- [116] J. Larimer and T. Piantanida. The impact of boundaries on color : Stabilized image studies. *Proc. SPIE*, 901:241–247, 1988.
- [117] J. Laycock and J. P. ViveasBh. Calculating the perceptability of monochrome and color displays under various illumination conditions. *Displays*, pages 88–89, 1982.
- [118] N. H. Lehrer. The challenge of the cathode-ray tube. In L. E. Tannas, editor, *Flat-Panel Displays and CRTs*, pages 138–176. Van Nostrand Reinhold, New York, 1985.
- [119] J. Leibig and K. F. Roll. Acceptable luminances reflected on VDU screens in relation to the type of contrast and illumination. In *CIE Proceedings, 20th Session, Amsterdam*, pages D313/1-D313/4, Bureau Central de la CIE, Paris, France, 1983. Comission International d'Eclairage.
- [120] A. K. Levine and F. C. Palila. YVO₄:EU, a new highly efficient phosphor for color television. *Electrochemical Technology*, 4:16–20, 1966.
- [121] B. D. Loughlin. Nonlinear amplitude relations and gamma correction. In K. McIlwain and C. Dean, editors, *Principles of Color Television*. Wiley, 1956.
- [122] H. R. Luxenberg and R. L. Kuehn, editors. *Display Systems Engineering*. McGraw-Hill, New York, 1968.
- [123] D. L. MacAdam. Perception of colors in projected and televised pictures. *J. Soc. Motion Pict. Telev. Eng.*, 1956.

- [124] J. F. Mackworth and N. H. Mackworth. Eye fixations recorded on changing visual scenes by the television eye-marker. *J. Opt. Soc. Am.*, 48:439–445, 1958.
- [125] A. Maisa. A digital color separation system based on principles of colorimetry. In *TAGA Proceedings*, pages 346–361. TAGA, 1984.
- [126] A. Maisa, R. Holub, and J. Gilbert. Requirements for soft copy proofing. Technical report, Eikonix Corp., 1984.
- [127] D. W. Marquardt. *J. Soc. Ind. Appl. Math.*, 11:431–441, 1963.
- [128] J. McCormick, G. Murch, and L. Leavitt. An experimental color monitor for vision research. In E. Schlam, editor, *Advances in Display Technology IV*, volume 457, pages 26–30. SPIE, 1984.
- [129] G. W. Meyer. *Color Calculations and Perceptual Assessment of Computer Graphic Images*. PhD thesis, Cornell University, 1986.
- [130] G. W. Meyer and D. P. Greenberg. Perceptual color spaces for computer graphics. *Comput Graphics*, 14:254–261, 1980.
- [131] G. W. Meyer and D. P. Greenberg. Colorimetry and computer graphics. Technical report, Program of Computer Graphics, Cornell University, Ithaca, New York, 1984.
- [132] G. W. Meyer and D. P. Greenberg. Color education and color synthesis in computer graphics. *Color Res. Appl.*, 11:S39–S44, 1986.
- [133] K. Miller. Accurate light measurement in aircraft cockpits. *Electro Optics*, 1983.
- [134] J. D. Mollon and L. T. Sharpe, editors. *Colour Vision: Physiology and Psychophysics*. Academic Press, 1983.
- [135] A. M. Morrel, H. B. Law, E. G. Ramberg, and E. W. Herold. *Color Television Picture Tubes*. Academic Press, 1974.

- [136] H. Moss. *Narrow Angle Electron Guns and Cathode Ray Tubes*. Academic Press, New York, 1968.
- [137] J. B. Mulligan. Minimizing quantization errors in digitally-controlled CRT displays. *Color Res. Appl.*, 11:S47–S51, 1986.
- [138] J. B. Mulligan. Halftoning method for the generation of motion stimuli. *J. Opt. Soc. Am. A*, 6:1217–1227, 1989.
- [139] G. M. Murch. Visual accommodation and convergence to multichromatic displays. *Proc Soc Inf Disp*, 24:62–72, 1983.
- [140] G. M. Murch, M. Cranford, and P. McManus. Perceived brightness and color contrast of visual displays. *Soc Inf Disp Dig*, 14:168–169, 1983.
- [141] O. Myodo, K. Kurashi, M. Karino, M. Yamanoshita, and H. Koayashi. An analytical evaluation of moire pattern for color CRT displays. *Japan Display '86*, pages 52–55, 1986.
- [142] National Television System Committee. NTSC signal specifications. *Proc. IRE*, 42:17–19, 1954.
- [143] C. B. Neal. Television colorimetry for receiver engineers. *IEEE Trans. Broadcast Telev. Receivers*, BTR-19:149–162, 1973.
- [144] H. E. J. Neugebauer. Monitoring as a means of improving color correction. *Advance Printing Sci. Technol.*, 1:145–157, 1961.
- [145] B. M. Oliver. Tone rendition in television. *Proc. IRE*, 38:1288–1300, 1950.
- [146] G. Parr and O. H. Davie. *The Cathode Ray Tube and Its Applications*. Reinhold, New York, 3rd edition, 1959.
- [147] R. A. Perez. *Electronic Display Devices*. Tab Books, Blue Ridge Summit, PA, 1988.
- [148] H. H. Poole. *Fundamentals of Display Systems*. Spartan Books, Washington, 1966.

- [149] W. H. Press, B. P. Flannery, S. A. Teukolsky, and W. T. Vetterling. *Numerical Recipes in C, The Art of Scientific Computing*. Cambridge Univeristy Press, New York, 1988.
- [150] F. Ratliff, H. K. Hartline, and W. H. Miller. Spatial and temporal aspects of retinal inhibitory interaction. *J. Opt. Soc. Am.*, 53:110–120, 1968.
- [151] J. J. Rennilson. Problems in the perception of colored self-luminous displays. In *CIE Proceedings, 20th Session, Amsterdam*, pages D106/1–D106/4, Bureau Central de la CIE, Paris, France, 1983. Comission International d'Eclairage.
- [152] C. W. Rhodes. SMPTE television video technology comitee: Report on standardization of monitor colorimetry by SMPTE. *J. Soc. Motion Pict. Telev. Eng.*, pages 1201–1202, 1982.
- [153] W. L. Rhodes. Retrospective on color printing. In *Avanced Printing of Conference Summaries, SPSE's 40th Annual Conference*, pages 71–75. SPSE, 1987.
- [154] D. C. Rich. The effect of the measuring geometry on computer color matching. *Color Res. Appl.*, 13:113–118, 1988.
- [155] L. A. Riggs, F. Ratliff, J. C. Cornsweet, and T. N. Cornsweet. The disappearance of steadily fixated visual test subjects. *J. Opt. Soc. Am.*, 43:495–501, 1953.
- [156] J. D. Robbins and D. G. Mackey. Moire pattern in color television. *IEEE Trans. Broadcast*, BTR-12:105–121, 1986.
- [157] A. R. Robertson. Guidelines for coordinate research on colour difference equations. *Color Res. Appl.*, 3:149–151, 1978.
- [158] A. R. Robertson. The future of color science. *Color Res. Appl.*, 7:16–18, 1982.
- [159] N. M. Rodriguez. Application of temporal spectral analyzer in characterizing electronic flash sources used in photographic systems. *J. Imaging Tech.*, 10:197–200, 1984.

- [160] L. R. Ronchi. Successive heterochromatic brightness matches for a LED display. *Color Res. Appl.*, 11:164–168, 1986.
- [161] L. R. Ronchi and L. di Fraia. Visual depth of focus measured for various colored displays. *Color Res. Appl.*, 11:S52–S56, 1986.
- [162] J. Rosenbaum. Semi-automatic generation of film compensation tables. *Color Res. Appl.*, 13:187–192, 1988.
- [163] K. A. Ross and C. R. B. Wright, editors. *Discrete Mathematics*. Prentice-Hall, Englewood Cliffs, NJ, 1985.
- [164] J. Rovamo and A. Ranimen. Cortical flicker frequency and M-scaling of stimulus size and retinal luminance. *Vision Research*, 24:1127–1131, 1984.
- [165] H. Sakata. Masking of chrominance pattern movement and its application to color television signal transmission. *J. Soc. Motion Pict. Telev. Eng.*, pages 552–560, 1984.
- [166] H. Sakata. Picture quality compensation system based on brightness polarity. *J. Soc. Motion Pict. Telev. Eng.*, pages 190–199, 1985.
- [167] C. L. Sanders, W. Gaw, and G. Wyszecki. Colour calibrators for monitors in television studios. *J. Soc. Motion Pict. Telev. Eng.*, 77:640–642, 1968.
- [168] B. Saunders. CIELAB spacing of digitally specifier colors on a 24-bit CRT monitor. *J. Imaging Tech.*, 13:44–47, 1987.
- [169] O. H. Schade. Optical and photoelectric analog of the eye. *J. Opt. Soc. Am.*, 61:721–739, 1956.
- [170] O. H. Schade. On the quality of color-television images and the perception of color detail. *J. Soc. Motion Pict. Telev. Eng.*, 67:801–819, 1958.
- [171] R. Schafer. High-definition television production standard – an opportunity for optimal color processing. *J. Soc. Motion Pict. Telev. Eng.*, pages 749–758, 1985.

- [172] W. F. Schreiber. Psychophysics and the improvement of television image quality. *J. Soc. Motion Pict. Telev. Eng.*, pages 717–725, 1984.
- [173] R. Sekuler and E. Levinson. The perception of moving targets. In J. M. Wolfe, editor, *The Mind's Eye - Readings from Scientific American*, pages 60–68. W. H. Freeman, 1986.
- [174] S. Sherr. *Electronic Displays*. John Wiley, New York, 1979.
- [175] L. D. Silverstein and R. M. Merrifield. Color selection and verification testing for airborne color CRT displays. In J. J. Rennilson, editor, *Colorimetry of Self-Luminous Displays*. Joint ISCC & SID Informal Symp, 1982.
- [176] C. A. Siocos. Operational adjustment of picture monitors in television studios. *J. Soc. Motion Pict. Telev. Eng.*, 1965.
- [177] P. N. Slater. *Remote Sensing - Optics and Optical Systems*. Addison-Wesley, Reading, Massachusetts, 1980.
- [178] A. R. Smith. Color gamut transform pairs. *Comput Graphics*, 12:12–19, 1978.
- [179] H. L. Snyder. Perceived color contrast as measured by achromatic contrast matching. In J. J. Rennilson, editor, *Colorimetry of Self-Luminous Displays*. Joint ISCC & SID Informal Symp, 1982.
- [180] T. Soller, M. A. Starr, and G. E. Valley, Jr., editors. *Cathode Ray Tube Displays*. Radiation Laboratory Series. McGraw-Hill, 1948.
- [181] O. J. Sovers and L. J. Bodi. Cathode-ray-tube color reproduction in relation to gaussian spectral parameters. *J. Opt. Soc. Am.*, 55:1643–1650, 1965.
- [182] C. E. Spicer. NTSC color-field identification. *J. Soc. Motion Pict. Telev. Eng.*, pages 627–633, 1982.

- [183] W. N. Spronson. *Colour Science in Television and Display Systems*. Adam Hilger, London, 1983.
- [184] M. C. Stone. Color, graphic design, and computer systems. *Color Res. Appl.*, 11:S75–S82, 1986.
- [185] M. C. Stone, W. B. Cowan, and J. C. Beatty. Color gamut mapping and the printing of digital color images. Technical Report EDL-88-1, Xerox Palo Alto Research Center, Palo Alto, California, 94304, 1988.
- [186] L. E. Tannas. *Flat-Panel Displays and CRTs*. Van Nostrand Reinhold, New York, 1985.
- [187] B. W. Tansley and R. M. Boynton. A line, not a space, represents visual distinctness of borders formed *Science*, 191:954–957, 1976.
- [188] B. W. Tansley and R. M. Boynton. Chromatic border perception: the role of red- and green-sensitive cones. *Vision Research*, 18:699–706, 1978.
- [189] J. M. Taylor and G. M. Murch. The effective use of color in visual displays: Text and graphics applications. *Color Res. Appl.*, 11:S3–S10, 1986.
- [190] K. L. Thaxton. An electronic color previewer for four-color process printing. In M. Pearson, editor, *Optimum Reproduction of Color*, pages 145–148. Inter-Soc Color Council, 1971.
- [191] G. J. Tonge. The television scanning process. *J. Soc. Motion Pict. Telev. Eng.*, pages 657–666, 1984.
- [192] P. W. Trezona. Additivity in the tetrachromatic colour matching system. *Vision Res.*, 14:1291–1303, 1974.
- [193] R. E. Turnage. The perception of flicker in CRT displays. *Soc Info Disp Dig*, 3:38–52, 1966.

- [194] R. Ulichney. *Digital Halftoning*. MIT Press, Massachusetts, 1987.
- [195] A. J. Vingrys and P. E. King-Smith. Factors in using color video monitors for assessment of visual thresholds. *Color Res. Appl.*, 11:S57–S62, 1986.
- [196] G. Wald. Blue blindness in the normal fovea. *J. Opt. Soc. Am.*, 57:1289–1301, 1967.
- [197] C. Ware and J. C. Beatty. Using colour to display structures in multidimensional discrete data. *Color Res. Appl.*, 11:S11–S14, 1986.
- [198] H. L. Waruszewski. Airborne color CRT displays. In J. J. Rennilson, editor, *Colorimetry of Self-Luminous Displays*. Joint ISCC & SID Informal Symp, 1982.
- [199] W. T. Wintringham. Color television and colorimetry. *Proc. IRE*, 39:1135, 1951.
- [200] B. R. Wooten and G. Wald. Color-vision mechanisms in the peripheral retinas of normal and dichromatic observers. *Journal of General Physiology*, 61:125–145, 1973.
- [201] G. Wyszecki and W. S. Stiles. *Color Science : Concepts and Methods, Quantitative Data and Formulae*. Wiley, 2nd. edition, 1982.
- [202] A. L. Yarbus. *Eye Movements and Vision*. Plenum Press, New York, 1967.
- [203] T. Young. On the theory of light and colours. *Phil. Trans. R. Soc. Lond.*, 92:20–71, 1802.